Advanced Model Predictive Control for Three-Dimensional Motion Control of Autonomous Underwater Vehicles

PhD Thesis

Isah Abdulrasheed Jimoh

Wind Energy and Control Centre
Department of Electronic and Electrical Engineering
University of Strathclyde, Glasgow G1 1XW, UK

April 4, 2025

Declaration

This thesis is the result of the author's original research. It has been composed by the author and has not been previously submitted for examination which has led to the award of a degree.

Abstract

The increasing demand for ocean-related activities, driven by needs such as environmental preservation, offshore renewable energy deployment, border security and weather forecasting, highlights the importance of underwater operations. With minimal human intervention, autonomous underwater vehicles (AUVs) are increasingly employed to execute missions in water bodies. Improved AUV motion reliability requires advanced controllers to cope with challenges posed by nonlinear dynamics, coupled motion, actuator limits and environmental disturbances.

This thesis aims to foster the use of Model Predictive Control (MPC) for AUV motion control, leveraging its capability to optimise the performance of both linear and nonlinear systems while accounting for system and operational constraints. Standard MPC uses the receding horizon strategy to offer inherent robustness under minor uncertainties. However, the effectiveness of AUV motion control in the marine environment can degrade under substantial ocean currents and wave disturbances. Moreover, the full-order nonlinear AUV model is complex, rendering it less appealing for MPC design due to the associated online computational cost. As a result, this thesis proposes formulating the full-order nonlinear AUV model as a linear parameter-varying (LPV) system. This makes obtaining a convex optimisation control problem possible, which can be efficiently solved using off-the-shelf solvers.

Building on the overall research goals discussed in Chapter 1, this thesis introduces the mathematical model of an AUV in Chapter 2 and highlights issues impacting its use in motion control design. Chapter 3 provides a state-of-the-art

review of advanced predictive control methods to underscore the significance of this work. This thesis proposes three main design approaches, leveraging the LPV model, to address the effects of disturbances across various motion control tasks.

The first approach resulted in two novel MPC algorithms introduced in Chapter 4, both based on velocity models that use increment variables to counteract the effects of disturbances. The first controller, LPVMPC1, is designed for dynamic positioning, while the second controller, LPVMPC2, is developed for combined dynamic positioning and trajectory tracking control of AUVs. The LPVMPC2 integrates a planning scheme to facilitate a seamless transition from the trajectory tracking task to dynamic positioning. In the LPVMPC2 design, persistent AUV operation is ensured by maintaining continuous functionality even when reference signals include unreachable positions that violate the AUV workspace constraints.

The second approach, presented in Chapter 5, utilises the tube-based method for a robust tube-based MPC (TMPC) design to achieve resilience against environmental disturbances. The TMPC employs a line-of-sight (LOS) local trajectory replanning strategy to mitigate input saturation effects, enabling the consideration of realistic magnitude and rate constraints on input signals. An optimal state-dependent feedback controller is proposed to construct time-varying tubes to ensure the perturbed AUV system remains within a tube centred around the nominal trajectory. The TMPC framework is computationally tractable as it requires the online solution of a convex quadratically constrained quadratic problem.

The third MPC approach is presented in Chapter 6, which introduces an enclosure-based LOS guidance system and a robust min-max MPC (MM-MPC) for AUV path-following. By using the vehicle's desired heading angle to generate reference linear and angular position coordinates, the need to formulate an AUV error model is bypassed. The simplicity of the LOS guidance system is then leveraged to develop a multi-objective LOS guidance system (MO-LOSGS) to ensure collision-free navigation amidst static obstacles. The MM-MPC is designed to stabilise the AUV speed for time- and energy-efficient navigation. The high computational cost that

had limited the application of MM-MPC is mitigated by developing a duality-based transformation strategy to reformulate the problem into a quadratic minimisation control problem.

All simulation validations of the developed controllers are performed using a realistic Naminow-D AUV manufactured by Mitsubishi Heavy Industries Ltd. The concluding chapter offers a summary of key research contributions to the development of advanced MPC techniques for AUV motion control and proposes potential avenues for future research.

Key Words: Model Predictive Control; Dynamic Modelling; Autonomous Underwater Vehicles; Dynamic Positioning; Trajectory Tracking; Path-Following; Robust Control; Convex Optimisation.

Acknowledgements

First and foremost, I am grateful to Allah, the Most Beneficent and Merciful, for granting me the strength to embark on and complete this PhD research. Then, I extend my appreciation to the *Petroleum Technology Development Fund* (PTDF) and the University of Strathclyde PGR Travel Fund for their generous financial support.

My deepest thanks go to my advisors, Dr. Hong Yue and Professor Michael Grimble, for their invaluable support, feedback, and suggestions throughout this journey. I am particularly grateful to Dr. Hong Yue for her belief in me and for providing the environment that allowed me to complete this work in record time. I would also like to thank Dr. David Campos-Gaona for always being willing to listen to my ideas and provide recommendations, as well as the entire Wind Energy and Control (WECC) group for their tremendous support.

I am grateful to Industrial Systems and Control Ltd for facilitating my collaboration with Mitsubishi Heavy Industries Ltd, whose underwater vehicle model served as the foundation for the simulated validation of the controllers developed in this thesis. Specifically, I would like to thank Dr. Hiroshi Uchihori from the Underwater Systems Design Section of Mitsubishi Heavy Industries Ltd for his consistently prompt and detailed responses to my inquiries. I also appreciate the valuable comments from Professor Ikuo Yamamoto during the conception of this work.

My sincere gratitude to the Marine Robotic Society (MRS) team at the University of Strathclyde for providing a platform where I was able to work in a mul-

tidisciplinary setting to design and implement an autonomous surface robot, the StrathVoyager, for the Njord 2023 competition at Trondheim City Centre, Norway.

Special thanks to my beautiful spouse, Khadijat Jimoh, and to my lovely daughter, Junaynah Efua Jimoh, for being my constant source of joy and motivation. I also acknowledge my mother and siblings, whose encouragement and feedback helped me secure funding for both my MSc and this PhD research.

Lastly, I thank the Technology and Innovation Centre (TIC), University of Strathclyde for housing amazing people and providing an environment that fosters a collaborative and supportive research culture. Retrospectively, I feel very fortunate to have met and worked with Ziwei Chen, Oyedotun Oyewole, Taimur Zaman, Abdulrahman Babagana, Muhammad Younas, Alinane Brown, Alfred Amiolemen, Kwopnan Dikwal, Raymond Yogo and Muhammad Hijaaj Tahir.

Dedicated to my family.

Contents

List of Figures

List of Figures

List of Figures

List of Tables

Nomenclature

Main variables and parameters

(x, y, z)	Translational AUV position coordinate [m]
(ϕ, θ, ψ)	Angular AUV position coordinate [rad]
(u, v, w)	Translational AUV velocities [m/s]
(u_c, v_c, w_c)	Translational ocean current velocities [m/s]
(p, q, r)	Angular AUV velocities [rad/s]
(p_c, q_c, r_c)	Angular ocean current velocities [rad/s]
(x_d, y_d, z_d)	Desired 3D translational coordinate [m]
$(\phi_d, \theta_d, \psi_d)$	Desired orientation coordinate [rad]
(p_d, q_d, r_d)	Desired angular velocities [rad/s]
(u_d, v_d, w_d)	Desired translational velocities [m/s]
$(x_{los}, y_{los}, z_{los})$	Line-of-Sight 3D coordinate [m]
V_c	Resultant ocean current speed [m/s]
$\bar{\boldsymbol{\eta}} \in \mathbb{R}^6$	Nominal AUV position vector
$\boldsymbol{\eta}' \in \mathbb{R}^3$	True AUV position vector for horizontal motion model

$\boldsymbol{\eta} \in \mathbb{R}^6$	True AUV position vector
$\boldsymbol{\nu}' \in \mathbb{R}^3$	True AUV velocity vector for horizontal motion model
$\boldsymbol{\nu} \in \mathbb{R}^6$	True AUV velocity vector
$\boldsymbol{\nu}_r \in \mathbb{R}^6$	AUV relative velocity vector
$\bar{\boldsymbol{\nu}} \in \mathbb{R}^6$	Nominal AUV velocity vector
$\mathbf{x} \in \mathbb{R}^{12}$	True AUV state vector incorporating its position and velocity vectors
$\mathbf{x}'_e \in \mathbb{R}^6$	State error vector in horizontal model-based motion
$\mathbf{x}_e \in \mathbb{R}^{12}$	State error vector in full-order model-based motion
$\boldsymbol{\xi} \in \mathbb{R}^{12}$	State vector incorporating velocity increment (Chapter 4)
$\mathbf{x}_r \in \mathbb{R}^{12}$	Reachable state vector
$\boldsymbol{\tau}' \in \mathbb{R}^3$	Control input vector for horizontal motion model
$\boldsymbol{\tau}'_d \in \mathbb{R}^3$	Desired control input vector for horizontal motion model
$\boldsymbol{\tau} \in \mathbb{R}^6$	True control input vector for the full-order AUV model
$\mathbf{v} \in \mathbb{R}^6$	Nominal control input vector
$\mathbf{z} \in \mathbb{R}^{12}$	Nominal AUV state vector
$\boldsymbol{\nu}_c \in \mathbb{R}^6$	Ocean current velocity vector
$\boldsymbol{\tau}^w \in \mathbb{R}^6$	Vector of generalised ocean wave forces and moments
$\mathbf{x}'_d \in \mathbb{R}^6$	State reference vector of the horizontal motion model
$\mathbf{x}_d \in \mathbb{R}^{12}$	State reference vector of the full-order motion model

Nomenclature

$\mathbf{y}_d \in \mathbb{R}^6$	Position reference vector
$\mathbf{y}_{d,ss} \in \mathbb{R}^6$	Docking position reference vector or constant reference position
$\mathbf{w}/\mathbf{w}_{\max} \in \mathbb{R}^{12}$	Lumped disturbance term/disturbance upper bound
k/T_s	Time index/sampling period [s]
$\mathbf{u}_{\max}/\boldsymbol{\delta}_{\max} \in \mathbb{R}^6$	Input/input increment vector upper bound
$\mathbf{x}_{\max} \in \mathbb{R}^{12}$	State vector upper bound
$N, N_1/N_u$	Prediction/control horizon
$\mathbf{U} \in \mathbb{R}^{6N_u}$	Predicted input sequence over the control horizon. Represents a sequence of input forces and moments except in Chapter 6 where it is the sequence of velocity increments.
$\mathbf{V} \in \mathbb{R}^{6N}$	Predicted nominal input sequence over the control horizon
$\mathbf{X}_d \in \mathbb{R}^{12N}$	Predicted state reference over the prediction horizon
$\mathbf{Y} \in \mathbb{R}^{6N}$	Predicted output sequence over the prediction horizon
$\mathbf{Y}_d \in \mathbb{R}^{6N}$	Predicted output reference over the prediction horizon
$\Delta\mathbf{U} \in \mathbb{R}^{6N_u}$	Predicted input increment sequence over the control horizon
$\Delta\mathbf{Y} \in \mathbb{R}^{6N}$	Predicted output increment sequence over the prediction horizon
ρ_c	Radius of the circle of acceptance [m] (Chapter 6)
ρ_s	Radius of the sphere of acceptance [m] (Chapter 6)
R_a	User-defined spherical error limit which defines the sphere of acceptance [m] (Chapter 5)

α, β, γ	Scalars for guidance and control system design (Chapter 5)
$\mathbf{J}'(\boldsymbol{\eta}') \in \mathbb{R}^{3\times3}$	AUV rotation matrix for horizontal motion model
$\mathbf{J}(\boldsymbol{\eta}) \in \mathbb{R}^{6\times6}$	AUV rotation matrix
$\mathbf{M} \in \mathbb{R}^{6\times6}$	AUV's inertia matrix including rigid body and added mass components
$\mathbf{C}'(\boldsymbol{\nu}') \in \mathbb{R}^{3\times3}$	AUV Coriolis-centripetal matrix for horizontal motion model
$\mathbf{C}(\boldsymbol{\nu}) \in \mathbb{R}^{6\times6}$	AUV Coriolis-centripetal matrix
$\mathbf{D}'(\boldsymbol{\nu}') \in \mathbb{R}^{3\times3}$	Hydrodynamic damping matrix for horizontal motion model
$\mathbf{D}(\boldsymbol{\nu}) \in \mathbb{R}^{6\times6}$	Hydrodynamic damping matrix
$\mathbf{g}'(\boldsymbol{\eta}') \in \mathbb{R}^{3}$	Weight and buoyancy induced forces for horizontal motion model
$\mathbf{g}(\boldsymbol{\eta}) \in \mathbb{R}^{6}$	Vector of forces and moments due to AUV's weight and buoyancy
$\mathbf{A}_c(\mathbf{x}) \in \mathbb{R}^{12\times12}$	State-dependent continuous-time system matrix
$\mathbf{B}_c \in \mathbb{R}^{12\times6}$	Continuous-time input matrix
$\mathbf{A}(\mathbf{x}(k)) \in \mathbb{R}^{12\times12}$	State-dependent discrete-time system matrix
$\mathbf{A}_\mathbf{x}/\mathbf{A}_\mathbf{z}$	Compact form of $\mathbf{A}(\mathbf{x}(k))/\mathbf{A}(\mathbf{z}(k))$
$\mathbf{B} \in \mathbb{R}^{12\times6}$	Discrete-time input matrix
$\mathbf{H} \in \mathbb{R}^{3\times6}$	Reference coordinate selector matrix (Chapter 5)
$\mathbf{G}_x, \mathbf{G}_u/\mathbf{h}_x, \mathbf{h}_u$	Matrices/vectors that define compact sets
$\mathbf{K} \in \mathbb{R}^{6\times12}$	State-dependent feedback gain (disturbance controller)
$\Phi_K \in \mathbb{R}^{12\times12}$	Pre-stabilised system matrix *i.e.,* $\mathbf{A}_\mathbf{z} + \mathbf{BK}$

$\mathbf{Q}, \mathbf{R} \in \mathbb{R}^{6\times6}$	Weighting matrices in cost function
$\mathbf{Q}_x, \mathbf{P} \in \mathbb{R}^{12\times12}$	Weighting matrices in cost function
O_B	Body-fixed/motion reference frame
O_E	Earth-fixed/inertia reference frame
(x_b, y_b, z_b)	Centre of buoyancy coordinates [m]
(x_g, y_g, z_g)	Centre of gravity coordinates [m]
$\mathbf{I}_b \in \mathbb{R}^{3\times3}$	Moment of inertia matrix

Notations

$(\cdot)^\top$	Transpose of matrix or vector $(\cdot)$
$\otimes$	Kronecker product
$\mathbf{I/0}$	Identity/zero matrix of appropriate dimensions
$\mathbb{N}$	The set of non-negative integer
$\mathbb{R}$	The set of real numbers
$\mathbb{R}^n$	A n-dimension vector
$\mathbb{R}^{m\times n}$	A $m \times n$ matrix
$\mathcal{X}$	Compact set that defines state constraints
$\mathcal{X}_e$	Polytopic set that defines error state bounds
$\mathcal{Y}$	Compact set that defines output constraints
$\mathcal{T}$,$\mathcal{U}$	Compact sets that define input constraint
$\mathcal{Y}_r$	Compact set that defines workspace constraint

$\mathcal{W}$	Compact set that defines upper bound on disturbances
$\mathcal{Z}_K$	Polytopic set used to define state tube
$\| \mathbf{x} \|^2_{\mathbf{Q}}$	The weighted 2-norm of $\mathbf{x}$, *i.e.,* $\mathbf{x}^\top \mathbf{Q}\mathbf{x}$
$\texttt{blkdiag}(Q_1, \ldots, Q_n)$	the block diagonal matrix having the entries $Q_1, \ldots, Q_n$ in its main diagonal
$\mathbf{S}(\mathbf{a})$	The skew-symmetric matrix of vector $\mathbf{a}$ with 3 entries
$\mathcal{R}^N_{\mathcal{X}}$	The set of reachable states in N steps
$\mathcal{R}^N_{\mathcal{Y}}$	The set of reachable output in N steps

Abbreviations

ADR	Active Disturbance Rejection
AMV	Autonomous Surface Vehicle
AM	Added Mass
ASV	Autonomous Surface Vessel
AUV	Autonomous Underwater Vehicles
CB	Centre of Buoyancy
CG	Centre of Gravity
CT	Computational Time
DARE	Discrete-time Algebraic Riccati Equation
DoF	Degree-of-Freedom
DSC	Dynamic Surface Control

EAOB	Extended Active Observer
EC	Energy Consumption rate metric
EKF	Extended Kalman Filter
ESKF	Extended State Kalman Filter
ESO	Extended State Observer
FHCOCP	Finite Horizon Contained Optimal Control Problem
IAE	Integral of Absolute Error
ISMC	Integral Sliding Mode Control
LMI	Linear Matrix Inequalities
LMPC	Lyapunov Model Predictive Control
LOS	Line-of-sight
LPV	Linear Parameter-varying
LTI	Linear Time-invariant
LTV	Linear Time-varying
LWT	Linear Wave Theory
MHE	Moving Horizon Estimation
MM-MPC	Min-Max Model Predictive Control
MO-LOGS	Multi-objective Line-of-Sight Guidance System
MPC	Model predictive control
NMPC	Nonlinear Model Predictive Control

Nomenclature

NN	Neural Network
OFNMPC	Offset-free Nonlinear Model Predictive Control
PD	Proportional-Derivative
PF	Path-Following
PID	Proportional-Integral-Derivative
PNG	Proportional Navigation Guidance
QCQP	Quadratically Constrained Quadratic Problem
QP	Quadratic Problem (or Program)
RBF	Radial Basis Function
RB	Rigid Body
RL	Reinforcement Learning
RMSE	Root Mean Square Eror
ROV	Remotely Operated Vehicle
SD-DARE	State-dependent Discrete-time Algebraic Riccati Equation
SDW	Sliding Window
SMC	Sliding Mode Control
SPURV	Self-propelled Underwater Research Vehicle
STA	Super-Twisting-Algorithm
TMPC	Tube-based Model Predictive Control
TSMC	Terminal Sliding Mode Control

UARS	Unmanned Arctic Research Submersible
UUV	Unmanned Underwater Vehicles

Chapter 1

Introduction

This thesis presents research findings from an investigation into the three-dimensional (3D) motion control problem of autonomous underwater vehicles (AUVs). This chapter presents an overview of the research work performed, including the research motivation, aims and objectives, contributions to the body of knowledge and the thesis outline.

1.1 Research Context and Motivation

An AUV refers to a marine vehicle that can autonomously perform missions using onboard sensors, guidance and control systems [2]. AUVs have drawn a lot of attention in recent years from academia and industry due to their important role in decreasing the risks involved in the exploration and the exploitation of underwater resources [3]. The growing demand for underwater operations, driven by industries such as petrochemicals, military, telecommunications (underwater cables) and scientific research, has fueled enthusiasm for the design and manufacture of AUVs with greater autonomy for inspection, maintenance and repair tasks [4, 5]. The need for a high level of autonomy by AUVs to carry out desired tasks with minimum human intervention makes it important to design advanced control schemes. The advanced control strategies need to be able to achieve desired motion control objectives de-

spite AUV's high nonlinearities, coupled dynamics and environmental disturbances in the form of ocean currents and waves [6]. Furthermore, important design factors that should be considered include the limits on actuation capabilities, restricted energy supply and the environmental constraints posed by obstacles that were not accounted for during path planning.

The motion control problems can be classified into three main categories based on the nature of the set-point or reference signal [6]. *Dynamic positioning*, also known as station keeping, is a form of point stabilisation problem. It involves manoeuvring the AUV to maintain a fixed position and orientation, often in the presence of environmental disturbances. *Path-following control* refers to missions where an AUV is directed to follow a spatially constrained reference path. There is no restriction on the time taken to travel along the path, but the AUV is usually required to maintain a defined orientation. Finally, *trajectory tracking* involves guiding an AUV to track a time-parameterised reference signal. In this case, the reference imposes both spatial and temporal requirements on the AUV.

Model predictive control (MPC) is a potent optimisation-based control strategy that relies on dynamic system models, enabling the optimisation of predicted future actions while accommodating operational constraints. Historically, the use of MPC has been restricted to slow industrial processes like those prevalent in the petrochemical sector due to computational constraints. However, advancements in constrained optimal control problem (COCP) solvers, multi-core processors and field-programmable gate arrays (FGPAs) have substantially mitigated this limitation, broadening the applicability of MPC to faster systems [7]. The ability of MPC to handle nonlinearities, system constraints and optimise AUV performance has significantly bolstered its adoption in AUV motion control. The recent successful real-time implementation of MPC-based control algorithms in autonomous marine vehicles (AMVs) [8–11] strongly indicates that computational challenges may not hinder the deployment of MPC in AUVs.

Consequently, there have been significant efforts in developing MPC-based mo-

tion controllers for AUVs [12]. The doctoral thesis [13] provided novel theoretical results to enhance the application of advanced predictive controllers for AUV horizontal motion control problems by mostly relying on the inherent robustness of the MPC strategy. These controllers require additional schemes such as PID to stabilise the AUV vertical motion [6]. Moreover, standard MPC can handle small uncertainties such as model mismatch and additive disturbances to some extent. However, it has limited robustness and may not perform well in practical applications of AUVs subject to significant uncertainties and environmental disturbances [14]. This awareness has prompted the adoption of diverse disturbance handling strategies, including observer-based methods [15], the fusion of MPC and Sliding Mode Control (SMC) [16], and robust MPC strategies [17]. In [18], recent advancements in MPC for AUVs were discussed, focusing primarily on motion control within a local plane. These local plane controllers need supplementary mechanisms to manage depth, roll, and pitch motions to maintain vehicle stability. These supplementary mechanisms could include PID and LQR stabilisers [6, 19] whose performance often deteriorates under strong nonlinearities and external disturbances. Even for a well-designed LQ-based controller tracking curved trajectories, linearisation along the path is required, with restrictive assumptions on the nature of the curved path [20].

The choice of MPC for local plane motion control is due to the significant complexity associated with using a complete 6 Degree-of-Freedom (DoF) model in nonlinear MPC (NMPC) design [18]. In [21], the AUV model is simplified into horizontal and dive planes, allowing for the implementation of two linear MPC controllers and avoiding the use of traditional controllers like PID to stabilise some AUV dynamics. It is pertinent to mention that some studies [16, 22, 23] on 3D motion control also assume negligible roll and pitch motion while others [17, 24] neglect only the roll motion. The work by Zhang et al. [25] considered a full-order model but relied on the availability of accurate models, as the input forces and moments were computed using the dynamic parameters of the AUV. Another significant yet challenging aspect involves designing MPC frameworks that incorporate realistic input constraints,

where both magnitude and rate limits are enforced to prevent abrupt variations in thruster forces. Such abrupt changes are either operationally prohibited or accelerate actuator wear, thereby compromising system longevity and reliability [13, 14].

Driven by the need for computational efficiency, the development of full 6-DoF model-based controllers, mitigation of actuator saturation issues, and effective disturbance handling, this thesis seeks to advance the application of MPC-based motion controllers for AUVs operating under disturbances in 3D motion tasks. In considering the full 6-DoF AUV model, this research aims to achieve various motion control tasks without reliance on traditional controllers to stabilise any subsystem. The work attempts to develop disturbance-handling strategies to improve tracking precision and resilience under model uncertainties and environmental disturbances. Besides, the developed strategies strive to mitigate computational resource requirements by avoiding nonlinear optimisation control problems associated with standard NMPC, which is renowned for its substantially higher computational burden than its linear MPC counterpart. Additionally, the research also explores the development of predictive controllers for AUVs in uncertain environments containing obstacles. It also considers a strategy that incorporates both input and input rate constraints to reflect realistic types of control inputs. These design considerations prompted the development of research questions that became the foundation for this work, and they are outlined in the following section.

1.2 Research Questions

The following set of questions underpinned the strategy adopted in the conduct of this research.

1. How can effective and computationally efficient MPC-based motion controllers be designed without relying on traditional controllers like PID to stabilise some AUV dynamics?

2. How can the tracking accuracy of MPC-based motion controllers be enhanced under disturbances, especially for dynamic positioning that is critical for successful docking operations?

3. How can trajectory tracking and dynamic positioning be integrated to enable an AUV to transition seamlessly from executing tracking missions to safe docking?

4. Can robust predictive control be designed for a high-dimensional AUV system without prohibitive computational requirements for real-time applications?

5. How can robust optimal path-following be achieved in a time-efficient manner when tracking 3D waypoints in uncertain environments including obstacles?

1.3 Research Aim and Objectives

This research aims to promote the broader application of advanced MPC strategies to AUV motion control problems, eliminating reliance on traditional controllers such as PID, particularly in the presence of environmental disturbances and system constraints. It seeks to achieve this by developing predictive algorithms with disturbance-handling capabilities that can be efficiently implemented using off-the-shelf solvers.

This research work covers three motion control tasks, namely, dynamic positioning, trajectory tracking and path-following problems while outlining the assumptions that underpin the developed controllers. The methodology for designing the controllers is divided into three, each based on a distinct approach to managing system disturbances. The first method uses increment variables to reduce steady-state error for improved tracking performance under disturbances. The second method employs a tube-based approach to robustly track the nominal state trajectory, maintaining the real vehicle trajectory within a tube set despite the influence of disturbances.

The third method is based on the so-called min-max MPC approach, which considers the worst-case scenario under bounded disturbances. Motivated by these ideas and the research questions in Section 1.2, the objectives of this research are stated as follows:

1. The first objective of this study is to improve the positioning accuracy of AUVs during dynamic positioning tasks by introducing a velocity form prediction model to mitigate the effects of external disturbances. The task entails maintaining a predetermined position and orientation, which is particularly crucial to facilitating docking operations. Consequently, the precision of the positioning controller holds significant importance in ensuring the successful execution of such motion control tasks. The proposed method strives to enhance tracking accuracy without assuming constant disturbances, making it more suitable for real-world scenarios.

2. The second objective is to design an algorithm for combined trajectory tracking and dynamic positioning to maintain a desired position and orientation/pose during docking operations. Given that docking operations typically occur after completing motion control tasks such as trajectory tracking, ensuring the smooth transition of the vehicle to the docking task is paramount. This is particularly crucial as the endpoint of the trajectory tracking task may not exactly correspond to the docking station. This needs to be addressed by employing a temporal path planner to generate a feasible path for guiding the AUV towards the docking station. Additionally, in the trajectory tracking task, the controller should ensure continuous AUV operation even if certain parts of the reference trajectory are unreachable due to workspace constraints.

3. The third objective is to develop a computationally efficient robust tube-based control system for AUV 3D trajectory tracking subject to external disturbance and input saturation. The input saturation problem is likely to occur when input magnitude and rate limits are imposed, representing more realistic input

signals. The goal is to formulate a strategy to achieve local replanning in order to limit the tracking error experienced by the controller. The re-planned trajectory can subsequently be used to design a robust tube-based control framework that respects the input magnitude and rate limits.

4. The fourth objective is to develop a guidance system capable of achieving 3D waypoint following for the coupled AUV system without the need to create an error model, while also ensuring collision avoidance with static obstacles. The aim is to leverage the simplicity of the conventional LOS strategy to derive a position and orientation tracking problem. Using the reformulated LOS approach, a multi-objective LOS guidance system (MO-LOSGS) can be developed to achieve collision avoidance.

5. The final objective of this thesis is to develop a robust min-max MPC control system to track the reference from the MO-LOSGS for path-following control of an AUV in an uncertain environment with static obstacles. To ensure the timely and energy-efficient completion of path-following tasks, the velocity vector increment is used to formulate an objective function that minimises excessive fluctuations in the AUV's travel speed during path-following. To address the computational complexity of solving the min-max problem, a duality-based transformation technique is employed, reformulating the problem into a convex quadratic minimisation control problem.

1.4 Research Contributions

The main contributions of this thesis to motion control of AUVs are divided into two main categories. They are summarised as follows.

- *Predictive control algorithms for motion control tasks:*

1. A velocity MPC (LPVMPC1) algorithm that exploits the interdependence of the kinematic and dynamic equations of an AUV to avoid increased state

dimensions associated with traditional velocity MPC algorithms is developed for dynamic positioning of an AUV. Performance is compared to other existing MPC-based controllers.

2. A second velocity MPC algorithm (LPVMPC2) is developed, which circumvents the necessity for model augmentation, thereby preventing an increase in state dimensions. By formulating the optimisation problem to satisfy a defined reachable set, the method allows an AUV to track trajectories containing both reachable and unreachable positions, ensuring that the workspace boundary is always respected when operating in a constrained workspace. It is noteworthy that the LPVMPC2 described here is not limited to AUVs and similar systems but applies to a wide range of practical linear time-invariant and linear time-varying systems. Furthemore, a simple re-planning scheme is used to enable integrated trajectory tracking and dynamic positioning control of AUVs by facilitating a seamless transition between the two motion control tasks.

3. A Tube-based MPC (TMPC) is proposed for 3D trajectory tracking using a 6-DoF AUV model, taking into account both input magnitude and increment constraints. Determining a local linear feedback law to characterise this tube presents a challenge for the nonlinear AUV model. To address this, we propose an optimal state-dependent feedback gain to replace the conventional linear feedback law used in traditional tube-based MPC designs. This state-dependent feedback is employed for constructing time-varying tubes to ensure that the perturbed AUV system remains within a tube centred around the nominal AUV trajectory.

4. A fast robust min-max MPC (MM-MPC) strategy that minimises velocity variations in the constrained optimisation control problem is developed. This helped to ensure roughly constant AUV speeds during the path-following task, making it possible to complete the task in a considerably shorter duration, resulting in energy savings of up to 40% compared to an MPC that does not

include velocity increments in the cost function. Additionally, the computational complexity associated with solving the min-max problem is reduced by developing a duality-based transformation strategy to reformulate the problem into a convex quadratic minimisation control problem.

- *Guidance system and replanning for input saturation mitigation:*

5. A modified 3D LOS local trajectory re-planning algorithm is developed and incorporated into the TMPC to mitigate input saturation problems in trajectory tracking control of AUVs.

6. A LOS guidance system which redefines the conventional heading and depth control problems into a 3D LOS path-tracking problem is proposed. This approach circumvents the need to develop a kinematic error model. In contrast to conventional waypoint tracking methods, the proposed approach does not just track the desired heading but instead uses it to compute the desired position and orientation vector. This guidance system is combined with the MM-MPC to achieve a 3D path-following control for fully coupled AUVs.

7. A MO-LOSGS is developed by leveraging the simplicity of the reformulated LOS strategy, enabling both path-following and collision avoidance with detected obstacles.

1.5 Thesis Organisation

This thesis is organised into seven chapters. Fig. 1.1 shows a conceptual flow of the work presented in the thesis. The main content in each chapter is briefly discussed as follows.

Chapter 1 introduces the rationale behind the research and delineates its aims and objectives. In addition, it provides a concise overview of the primary contributions made by this research.

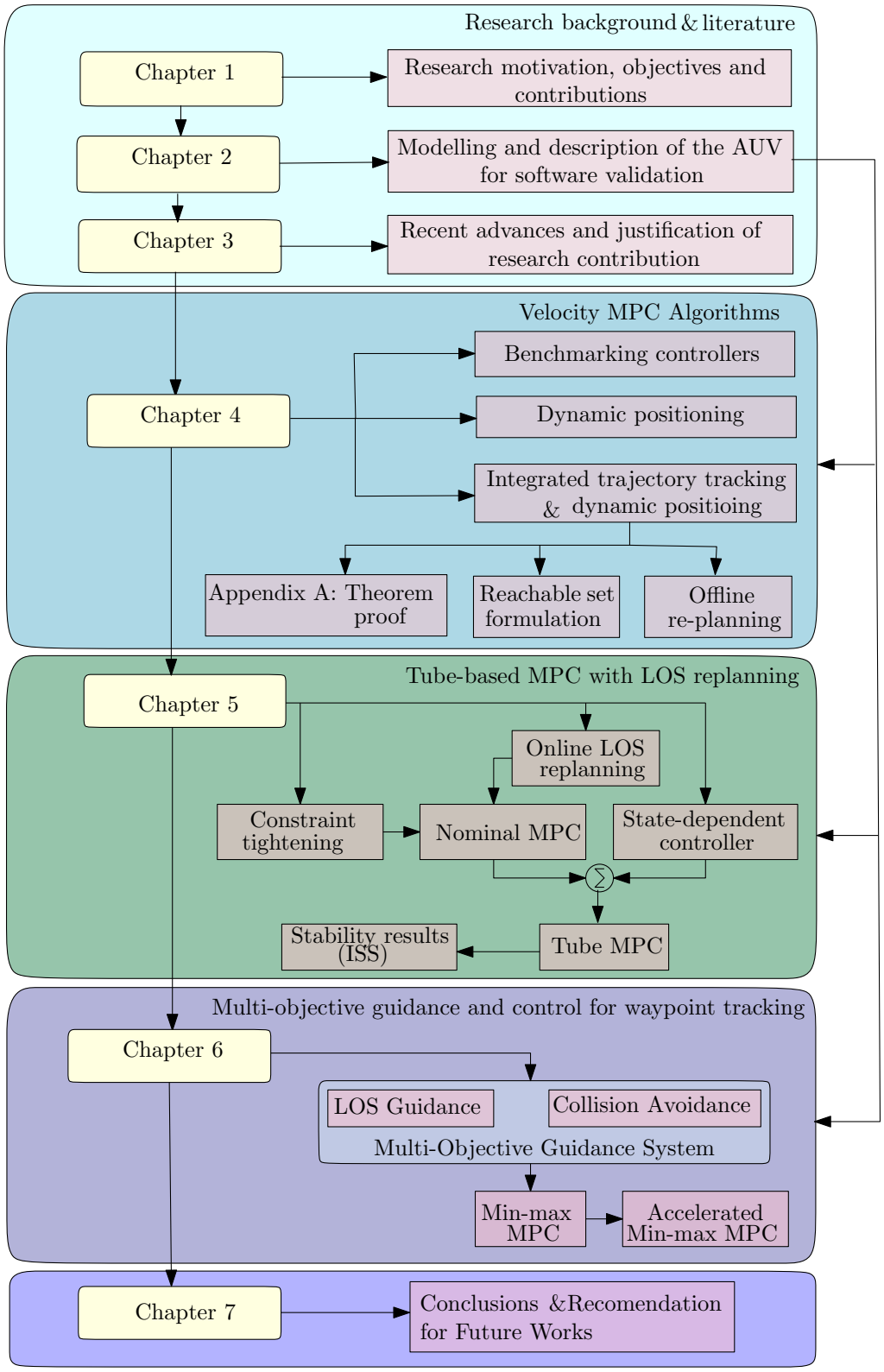

Fig. 1.1: Conceptual organisation of the thesis chapters.

Chapter 2 presents the mathematical modelling of the AUV with coupled motion and highlights assumptions that can simplify the control design model. Furthermore, it provides the realistic dynamic parameters of the Naminow-D vehicle, which are used to numerically validate the proposed control frameworks in Chapters 4–6 within the MATLAB/SIMULINK environment. It underscores crucial aspects of the vehicle model, as well as the modelling of environmental disturbances such as ocean currents and waves.

Chapter 3 contains a critical review of MPC-based motion controllers for AUVs, relying on the context provided by the AUV modelling described in Chapter 2. It begins by presenting advancements in AUV development and applications, followed by a discussion on the primary motion control tasks of an AUV. The chapter then reviews disturbance-handling methods within the MPC framework for AUV motion control, followed by an extensive discussion of key research insights. The chapter concludes by highlighting the key research gaps that this thesis has sought to address.

Chapter 4 presents two velocity form MPC frameworks. First, it outlines an MPC framework for dynamic positioning, leveraging the interdependence between the kinematic and dynamic equations of an AUV to prevent increased state dimension. The prediction model relies on the vehicle's velocity increments to mitigate disturbance effects, eliminating the need for an estimator. The second MPC framework uses both position and velocity increments, avoiding the necessity for model augmentation to maintain standard vehicle state dimensions. The scheme incorporates a switching law and an offline replanner, enabling its deployment for combined trajectory tracking and dynamic positioning.

Chapter 5 investigates trajectory tracking control for an AUV subject to input saturation and unknown environmental disturbances. A LOS method is em-

ployed to develop a local trajectory re-planner used to design a TMPC, aiming to limit the magnitude of tracking errors experienced by the trajectory tracking controller. This approach mitigates abrupt changes in velocities and control inputs. The robust constraint satisfaction and the state-dependent feedback control law used to confine the state trajectory to time-varying tubes are described.

Chapter 6 presents a guidance and MPC-based control system for path-following control of an AUV in an uncertain environment with static obstacles. A LOS-based strategy with online collision avoidance is developed for guidance by formulating a multi-objective optimisation problem. The path-following objective is achieved via a robust min-max MPC strategy. This algorithm penalises the velocity increment in the cost function rather than the actual input forces and moments to ensure timely and energy-efficient task completion. The computational efficiency of min-max MPC is improved tenfold by developing a duality-based technique to transform the problem into a convex minimisation problem.

Chapter 7 provides a summary of the research presented in this thesis and discusses potential areas for future investigation.

1.6 List of Publications

The contributions of this thesis which have either been published or submitted are listed below.

- I. A. Jimoh, H. Yue, and I. B. Küçükdemiral, "Autonomous underwater vehicle positioning control - a velocity form LPV-MPC approach," *IFAC-PapersOnLine*, vol. 56, no. 2, pp. 4388–4393, 2023, 22nd IFAC World Congress. https://doi.org/10.1016/j.ifacol.2023.10.1820.

- I. A. Jimoh and H. Yue, "Path following model predictive control of a cou-

pled autonomous underwater vehicle," *IFAC-PapersOnLine*, vol. 58, no. 20, pp. 183-188, 2024, 15th IFAC Conference on Control Applications in Marine Systems, Robotics and Vehicles CAMS 2024. https://doi.org/10.1016/j.ifacol.2024.10.052.

- I. A. Jimoh and H. Yue, 2023, "A Velocity Form Model Predictive Control of an Autonomous Underwater Vehicle" Accepted in *IEEE Journal of Oceanic Engineering,* 2024. https://doi.org/10.1109/JOE.2024.3519680.

- I. A. Jimoh, H. Yue, and M. J. Grimble, "Tube-based model predictive control of an autonomous underwater vehicle using line-of-sight re-planning," *Ocean Engineering*, vol. 314, p. 119688, 2024. https://doi.org/10.1016/j.oceaneng.2024.119688.

- I. A. Jimoh, T. Zaman, M. Syed, H. Yue, G. Burt and M. S. E. Moursi, "Tube-based linear parameter-varying model predictive control for wind energy conversion systems" in *IEEE Transactions on Sustainable Energy*, pp. 1–13, 2024. https://doi.org/10.1109/TSTE.2024.3512997.

- I. A. Jimoh, H. Yue and M. J. Grimble, "Accelerated min-max model predictive control for AUV path-following in uncertain environments", Ready for Submission, 2024.

Chapter 2

Autonomous Underwater Vehicle Modelling

In general, marine vehicles have six degrees of freedom (DoF), which encompasses translational motion in surge, sway and heave, along with angular motions involving roll, pitch and yaw. Various design considerations such as plane of motion control can influence the simplification of the mathematical model employed for control design, leading to the adoption of different assumptions.

As shown in Fig. 2.1, the position and velocity of an AUV are typically described using two reference frames, namely, the body-fixed (or motion) reference frame $\{O_B\}$ and the earth-fixed (or inertia) reference frame $\{O_E\}$. The position, velocity and input variables used in describing the model of an AUV are summarised in Table 2.1. To aid the review of existing works in the next chapter, both the full 6-DoF model and the reduced 3D motion model typically used for horizontal motion control of an AUV are described.

2.1 6-DoF Model for AUVs

The AUV motion model can be described by both kinematic and dynamic equations. The kinematic model forms the basis for the transformation from the vehicle's mo-

Table 2.1: Notations used for developing AUV model.

DoF	Position and Euler angle	Vehicle Velocities	Force/ moment	Motion Type
1	x (m)	u (m/s)	τ_X (N)	Motion in the x-axis (surge)
2	y (m)	v (m/s)	τ_Y (N)	Motion in the y-axis (sway)
3	z (m)	w (m/s)	τ_Z (N)	Motion in the z-axis (heave)
4	ϕ (rad)	p (rad/s)	τ_K (Nm)	Rotation about the x-axis (roll, heel)
5	θ (rad)	q (rad/s)	τ_M (Nm)	Rotation about the y-axis (pitch, trim)
6	ψ (rad)	r (rad/s)	τ_N (Nm)	Rotation about the z-axis (yaw, heading)

tion reference frame to the earth-fixed coordinate system. Whereas the earth-fixed reference frame is used to define the position and orientation of the vehicle, the motion reference frame is used to describe the velocities of the vehicle.

2.1.1 AUV Kinematics

The kinematics of the AUV based on Euler angles is given as [6]:

$$\dot{\boldsymbol{\eta}} = \mathbf{J}(\boldsymbol{\eta})\boldsymbol{\nu} = \begin{bmatrix} \mathbf{J_1}(\boldsymbol{\eta}) & \mathbf{0_{3\times 3}} \\ \mathbf{0_{3\times 3}} & \mathbf{J_2}(\boldsymbol{\eta}) \end{bmatrix} \begin{bmatrix} \boldsymbol{\nu}_1 \\ \boldsymbol{\nu}_2 \end{bmatrix}, \tag{2.1}$$

where

$\boldsymbol{\eta} = [x\ y\ z\ \phi\ \theta\ \psi]^\top = [\boldsymbol{\eta}_1\ \boldsymbol{\eta}_2]^\top$ denotes the position and orientation vector in the earth-fixed reference frame.

$\boldsymbol{\nu} = [u\ v\ w\ p\ q\ r]^\top = [\boldsymbol{\nu}_1\ \boldsymbol{\nu}_2]^\top$ represents the translational and angular velocities in the body-fixed reference frame.

Further, $\boldsymbol{\tau} = [\tau_X\ \tau_Y\ \tau_Z\ \tau_K\ \tau_M\ \tau_N]^\top$ is the generalised input forces and moments acting on the AUV, $\mathbf{J}_1(\boldsymbol{\eta})$ represents the rotation matrix from the body-fixed frame to the earth-fixed frame, following the $z-y-x$ rotation sequence and $\mathbf{J_2}(\boldsymbol{\eta})$ is a matrix representing the transformation of the angular velocity from the body-fixed

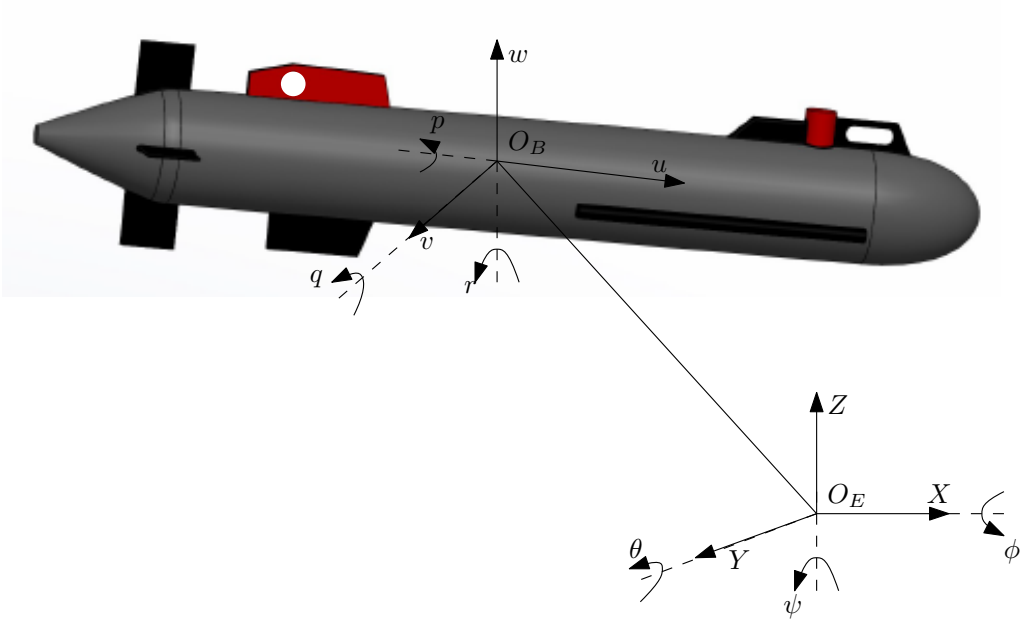

Fig. 2.1: Diagram showing the 6 DoF of an AUV with body-fixed and earth-fixed reference frames illustrated.

frame to the earth-fixed frame. The matrices are given as

$$\mathbf{J_1}(\boldsymbol{\eta}) = \begin{bmatrix} \cos\theta\cos\psi & -\sin\psi\cos\phi + \cos\psi\sin\theta\sin\phi & \cos\psi\cos\phi\sin\theta + \sin\psi\sin\phi \\ \sin\theta\cos\psi & \cos\psi\cos\phi + \sin\phi\sin\theta\sin\psi & \sin\theta\sin\psi\cos\phi - \cos\psi\sin\phi \\ -\sin\theta & \cos\theta\sin\phi & \cos\theta\cos\phi \end{bmatrix},$$

$$\mathbf{J_2}(\boldsymbol{\eta}) = \begin{bmatrix} 1 & \sin\phi\tan\theta & \cos\phi\tan\theta \\ 0 & \cos\phi & -\sin\phi \\ 0 & \sin\phi/\cos\theta & \cos\phi/\cos\theta \end{bmatrix}.$$

2.1.2 Nonlinear AUV Dynamics

The 6-DoF AUV motion dynamics that rely on the Newton-Euler equation and Quasi-Lagrange equation can be written as [6]:

$$\mathbf{M}\dot{\boldsymbol{\nu}} + \mathbf{C}(\boldsymbol{\nu})\boldsymbol{\nu} + \mathbf{D}(\boldsymbol{\nu})\boldsymbol{\nu} + \mathbf{g}(\boldsymbol{\eta}) = \boldsymbol{\tau}, \tag{2.2}$$

where each term in the dynamic model is defined below.

- $\mathbf{M} = \mathbf{M}_{\text{RB}} + \mathbf{M}_{\text{AM}} \in \mathbb{R}^{6\times 6}$ is the inertia matrix consisting of two matrices, with subscript 'RB' standing for rigid body and 'AM' for added mass components, defined explicitly as

$$\mathbf{M}_{\text{RB}} = \begin{bmatrix} m & 0 & 0 & 0 & mz_g & -my_g \\ 0 & m & 0 & -mz_g & 0 & mx_g \\ 0 & 0 & m & my_g & -mx_g & 0 \\ 0 & -mz_g & my_g & I_{xx} & 0 & 0 \\ mz_g & 0 & -mx_g & 0 & I_{yy} & 0 \\ -my_g & mx_g & 0 & 0 & 0 & I_{zz} \end{bmatrix},$$

$$\mathbf{M}_{\text{AM}} = -\begin{bmatrix} X_{\dot{u}} & 0 & 0 & 0 & 0 & 0 \\ 0 & Y_{\dot{v}} & 0 & 0 & 0 & Y_{\dot{r}} \\ 0 & 0 & Z_{\dot{w}} & 0 & Z_{\dot{q}} & 0 \\ 0 & 0 & 0 & K_{\dot{p}} & 0 & 0 \\ 0 & 0 & M_{\dot{w}} & 0 & M_{\dot{q}} & 0 \\ 0 & N_{\dot{v}} & 0 & 0 & 0 & N_{\dot{r}} \end{bmatrix},$$

  where m is the mass of the vehicle, $\mathbf{r}_g^b = [x_g \ y_g \ z_g]^\top$ is the distance vector from the origin of the body-fixed coordinate system to the centre of gravity of the AUV expressed in the same reference frame. I_{xx}, I_{yy} and I_{zz} represent the moment of inertia. The added mass matrix component $X_{\dot{u}}$, represents the hydrodynamic added force X along the x-axis due to acceleration $\dot{u}$. Similar notations are used for $y-$ and $z-$directions, on the other five acceleration terms, $\dot{v},\ \dot{w},\ \dot{p},\ \dot{q}$ and $\dot{r}$. The entries in $\mathbf{M}_{\text{RB}}$ and $\mathbf{M}_{\text{AM}}$ are typically provided in AUV specifications.

- $\mathbf{C}(\boldsymbol{\nu}) = \mathbf{C}_{\text{RB}} + \mathbf{C}_{\text{AM}} \in \mathbb{R}^{6\times 6}$ is the Coriolis-centripetal matrix with rigid body and added mass components. The rigid body component based on Lagrangian

parameterisation is given by [6]:

$$\mathbf{C_{RB}} = \begin{bmatrix} \mathbf{0}_{3\times3} & -m\mathbf{S}\left(\boldsymbol{\nu}_1\right) + m\mathbf{S}\left(\mathbf{r}_g^b\right)\mathbf{S}\left(\boldsymbol{\nu}_2\right) \\ -m\mathbf{S}\left(\boldsymbol{\nu}_1\right) - m\mathbf{S}\left(\boldsymbol{\nu}_2\right)\mathbf{S}\left(\mathbf{r}_g^b\right) & \mathbf{S}\left(\mathbf{I}_b\boldsymbol{\nu}_2\right) \end{bmatrix}, \quad (2.3)$$

in which $\mathbf{I}_b = \mathtt{diag}(I_{xx}, I_{yy}, I_{zz})$, $\boldsymbol{\nu}_1 = [u\ v\ w]^\top$ and $\boldsymbol{\nu}_2 = [p\ q\ r]^\top$.

For convenience of parameterization of the added mass component of the Coriolis-centripetal matrix, the inertia matrix is written in a block structure as

$$\mathbf{M_{AM}} = \begin{bmatrix} M_{11} & M_{12} \\ M_{21} & M_{22} \end{bmatrix}. \quad (2.4)$$

The added mass Coriolis effects based on skew-symmetrical parameterisation is written as

$$\mathbf{C_{AM}} = \begin{bmatrix} \mathbf{0}_{3\times3} & -\mathbf{S}(M_{11}\boldsymbol{\nu}_1 + M_{12}\boldsymbol{\nu}_2) \\ -\mathbf{S}(M_{11}\boldsymbol{\nu}_1 + M_{12}\boldsymbol{\nu}_2) & -\mathbf{S}(M_{21}\boldsymbol{\nu}_1 + M_{22}\boldsymbol{\nu}_2) \end{bmatrix},$$

- $\mathbf{D}(\boldsymbol{\nu}) \in \mathbb{R}^{6\times6}$ is the vehicle's hydrodynamic damping matrix. The Naminow-D AUV [1] adopted in this work employs a coupled structure and nonlinear representation of the damping effects such that $\mathbf{D}(\boldsymbol{\nu}) = -\mathbf{D}|\boldsymbol{\nu}|$, where

$$\mathbf{D} = \begin{bmatrix} X_{|u|u} & 0 & 0 & 0 & 0 & 0 \\ 0 & Y_{|v|v} & 0 & 0 & 0 & Y_{|r|r} \\ 0 & 0 & Z_{|w|w} & 0 & Z_{|q|q} & 0 \\ 0 & 0 & 0 & K_{|p|p} & 0 & 0 \\ 0 & 0 & M_{|w|w} & 0 & M_{|q|q} & 0 \\ 0 & N_{|v|v} & 0 & 0 & 0 & N_{|r|r} \end{bmatrix},$$

in which $X_{|u|u}, \cdots, N_{|r|r}$ are the nonlinear hydrodynamic coefficients and $|\boldsymbol{\nu}|$ denotes the absolute value of the velocity vector.

- The vector $\mathbf{g}(\eta) \in \mathbb{R}^{6\times 1}$ describes the forces and moments due to the AUV's weight and buoyancy as follows:

$$\mathbf{g}(\eta) = \begin{bmatrix} (W-B)\ \sin\theta \\ -(W-B)\ \cos\theta\ \sin\phi \\ -(W-B)\ \cos\theta\ \sin\phi \\ -g_y \cos\theta\ \sin\phi + g_z \cos\theta\ \cos\phi \\ g_z \sin\theta + g_x \cos\theta \cos\phi \\ -g_x \cos\theta\ \sin\phi - g_y \sin\theta \end{bmatrix},$$

  where $g_x = (x_g W - x_b B)$, $g_y = (y_g W - y_b B)$ and $g_z = (z_g W - z_b B)$. Here, the vector $[x_b\ y_b\ z_b]^\top$ denotes the centre of of buoyancy of the AUV and is assumed to coincide with the centre of gravity, while W and B are the weight and buoyancy of the AUV, respectively.

Table 2.2 summarises important properties of the AUV dynamic matrices and vectors that can be explored in control design. It is important to note that the damping matrix in many AUVs [6, 18] is often a positive definite matrix, *i.e.,* $\mathbf{D}(\boldsymbol{\nu}) \succ 0$, particularly when considering the linear component of the damping matrix. For the Naminow-D AUV, Mitsubishi Heavy Industries Ltd modelled the damping matrix as a nonlinear matrix as described above, making it a positive semi-definite matrix, *i.e.,* $\mathbf{D}(\boldsymbol{\nu}) \succeq 0$.

The use of the 6-DoF model is common when aiming for a high-fidelity simulation model for the 3D motion control of relatively large AUVs. Note that it is not uncommon to neglect [24] the effects of roll motion (*i.e.,* $p = 0$), resulting in a simplified 5-DoF model. Further simplification can be achieved depending on the AUV such that both roll p, and pitch q, motions are neglected to obtain a $4-$DoF model [22]. This represents the simplest dynamic model employed for 3D motion control tasks in the published literature.

2.2 Horizontal Motion Model: 3–DoF Model for AUVs

The 3–DoF model is obtained by neglecting roll (ϕ, p), pitch (θ, q) and depth (z) motions. In this case, the depth motion is assumed to be stabilised by some other conventional methods. The resulting 3-DoF model is applied in [26] focused on autonomous surface vehicles (ASVs) or AUV horizontal motion control.

Define $\boldsymbol{\eta}' = [x\ y\ \psi]^\top$ and $\boldsymbol{\nu}' = [u\ v\ r]^\top$, the kinematic equation in this case is given as

$$\dot{\boldsymbol{\eta}}' = \mathbf{J}'(\boldsymbol{\eta}')\boldsymbol{\nu}', \tag{2.5}$$

with

$$\mathbf{J}'(\boldsymbol{\eta}') = \begin{bmatrix} \cos\psi & -\sin\psi & 0 \\ \sin\psi & \cos\psi & 0 \\ 0 & 0 & 1 \end{bmatrix}.$$

The dynamics of the vehicle is then simplified as follows:

$$\dot{u} = \frac{1}{m_{11}}\left[m_{22}vr - X_u u - X_{u|u|}u|u| + \tau_X\right], \tag{2.6a}$$

$$\dot{v} = \frac{1}{m_{22}}\left[-m_{11}ur - Y_v v - Y_{v|v|}v|v| + \tau_Y\right], \tag{2.6b}$$

$$\dot{r} = -\frac{1}{m_{33}}\left[(m_{11} - m_{22})uv - N_r r - N_{r|r|}r|r| + \tau_N\right], \tag{2.6c}$$

where $m_{11} = m - X_{\dot{u}}$, $m_{22} = m - Y_{\dot{v}}$, and $m_{33} = I_z - N_{\dot{r}}$. The 3−DoF model can be written in the compact form

$$\dot{\mathbf{x}}' = \begin{bmatrix} \mathbf{J}'(\boldsymbol{\eta}')\boldsymbol{\nu}' \\ -\mathbf{M}'^{-1}\left(\boldsymbol{\tau} - \mathbf{C}'(\boldsymbol{\nu}') - \mathbf{D}'(\boldsymbol{\nu}') - \mathbf{g}'(\boldsymbol{\eta}')\right) \end{bmatrix} := f\left(\mathbf{x}', \tau'\right), \tag{2.7}$$

where $\dot{\mathbf{x}}' = [(\boldsymbol{\eta}')^\top\ (\boldsymbol{\nu}')^\top]^\top$, $\mathbf{M}' = \mathrm{diag}(m_{11}, m_{22}, m_{33})$, $\mathbf{C}'(\boldsymbol{\nu}') = \mathrm{diag}(X_u, Y_v, N_r)$, $\mathbf{g}'(\boldsymbol{\eta}') = \mathbf{0}$ and $\mathbf{D}'(\boldsymbol{\nu}') = \mathrm{diag}(X_{u|u|}, Y_{v|v|}, N_{r|r|})$.

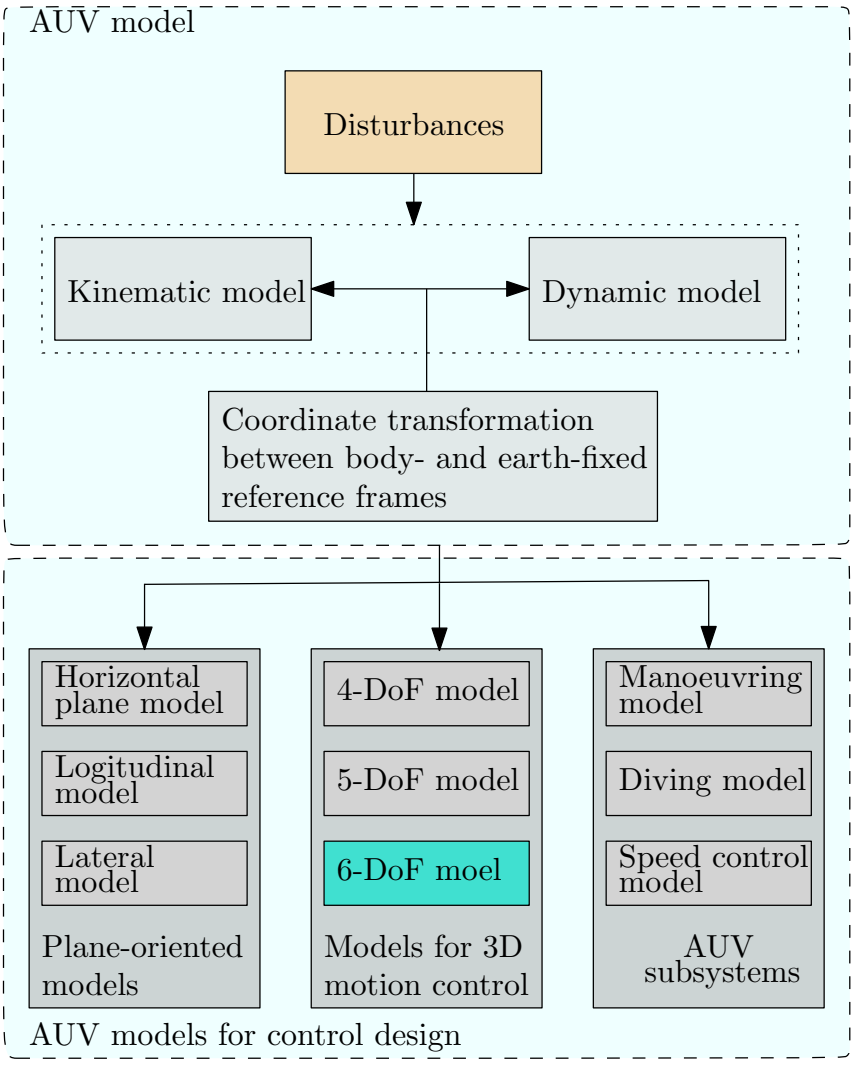

Fig. 2.2: Diagram showing the dynamical models of the AUV and subsystems.

Fig. 2.2 shows the main parts of an AUV motion model and its different forms based on vehicle characteristics or specific control objectives. This thesis focuses on 3D motion control using the nonlinear 6-DoF model of the vehicle, considering the effects of modelling errors and environmental disturbances. The described 3-DoF model is presented to aid a systematic review of the literature on motion control, including techniques for handling disturbances within MPC framework.

Table 2.2: Important properties of AUV model explored in control design.

Parameter	**Properties**	
	4-DoF model	**6-DoF model**
Rotation matrix	$\mathbf{J}(\eta)^{-1} = \mathbf{J}(\eta)^\top$	$\mathbf{J}_1(\eta_1)^{-1} = \mathbf{J}(\eta_1)^\top$, $\mathbf{J}_2(\eta_2)$ is undefined for $\theta = \pm\pi/2$
Inertia matrix	$\mathbf{M} = \mathbf{M}^\top \succ 0$	$\mathbf{M} = \mathbf{M}^\top \succ 0$
Coriolis-centripetal matrix	$\mathbf{C}(\nu) = -\mathbf{C}(\nu)^\top$	$\mathbf{C}(\nu) = -\mathbf{C}(\nu)^\top$
Damping matrix	$\mathbf{D}(\boldsymbol{\nu}) \succeq 0$	$\mathbf{D}(\boldsymbol{\nu}) \succeq 0$
Weight and buoyancy forces	$\| \mathbf{g}(\boldsymbol{\eta}) \|_\infty < \bar{g}$	$\| \mathbf{g}(\boldsymbol{\eta}) \|_\infty < \bar{g}$, $\bar{g}$ is an upper bound.

2.3 External Disturbance Modelling

The movements of AUVs can be affected by various environmental disturbances, depending on whether the AUV is operating in shallow or deep waters. These disturbances are complex and are caused by spatio-temporal fluctuations induced by the turbulent nature of the ocean. Some of the factors that impede AUV motion include tides, topographic perturbations, wind-induced waves, and current effects. The effects of waves, radiating in all directions due to external interference, and currents, directional water movements driven by wind, density variations, or gravity, have been extensively studied in the academic literature [22, 27–32]. When AUVs operate in shallow waters, they are more affected by water waves, and this effect grows as the AUV size decreases [33]. It is noted that some studies [34–36] have modelled waves as simple sinusoidal signals with defined frequencies. Although this approach may not accurately represent real ocean waves, researchers often employ it for the sake of simplicity. In this thesis, a more representative model of the wave disturbance is considered and this is presented in the next subsection.

2.3.1 Wave Model

To model the effects of ocean waves, denote $\boldsymbol{\tau}^w = [\tau_X^w \ \tau_Y^w \ \tau_Z^w \ \tau_K^w \ \tau_M^w \ \tau_N^w]^\top \in \mathbb{R}^{6\times 1}$ as the forces and moments generated by ocean waves affecting the vehicle's motion,

with superscript 'w' standing for waves. Each component of the 6 DoFs ocean wave vector $\boldsymbol{\tau}^w$, can be modelled by a second-order system [6], i.e.,

$$\begin{bmatrix} \dot{z}^w_{i,1} \\ \dot{z}^w_{i,2} \end{bmatrix} = \begin{bmatrix} 0 & 1 \\ -\omega^2_{e,i} & -2\xi_i\omega_{e,i} \end{bmatrix} \begin{bmatrix} z^w_{i,1} \\ z^w_{i,2} \end{bmatrix} + \begin{bmatrix} 0 \\ K_{w,i} \end{bmatrix} w_i, \tag{2.8}$$

$$\tau^w_i = \begin{bmatrix} 0 & 1 \end{bmatrix} \begin{bmatrix} z^w_{i,1} \\ z^w_{i,2} \end{bmatrix} + d_i, \tag{2.9}$$

where the subscript i $(= X,\ Y,\ Z,\ K,\ M,\ N)$ corresponds to the DoF of the vehicle, the amplitude of τ^w_i in the $i-$th DoF can be changed by the choice of parameter $K_{w,i}$. The term w_i is a zero-mean white process noise, ξ_i is the damping coefficient, $\omega_{e,i}$ is the frequency of encounter. It is noted that $\omega_{e,i}$ is relevant only when the vehicle is moving at a forward speed $u > 0$ m/s since it is related to peak frequency $\omega_{0,i}$ of the wave spectrum by

$$\omega_{e,i} = \left| \omega_{0,i} - \frac{\omega^2_{0,i}}{g} u\cos(\beta_i) \right|. \tag{2.10}$$

Here, β_i is the encounter angle. The term d_i in the output equation can be modelled as slowly changing bias terms (Wiener processes). It is recommended in [6] that a maximum value of $d^{\max}_i$ is applied to d_i, i.e., $|d_i| \leq d^{\max}_i$.

2.3.2 Ocean Current Model

To incorporate the influence of ocean currents, adjustments are made to the AUV 6-DOF coupled motion model (2.2). This modification involves considering the velocity component $\boldsymbol{\nu}_c = [u_c, v_c, w_c, p_c, q_c, r_c]^\top$ of the current disturbance relative to O_B. It is typical to assume that the currents are irrotational in an inertial frame of reference [1, 37–39]. This assumption of irrotational currents implies that $p_c = q_c = r_c = 0$ m/s, and for a resultant current speed V_c, the 3D irrotational

current model is formulated as [40]:

$$\boldsymbol{\nu}_c = [u_c \; v_c \; w_c \; 0 \; 0 \; 0]^\top, \tag{2.11}$$

where $u_c = V_c\cos(\alpha_c)\cos(\beta_c)$, $v_c = V_c\sin(\beta_c)$ and $w_c = V_c\sin(\alpha_c)\cos(\beta_c)$ with α_c denoting the angle of attack and β_c is the sideslip angle.

When the current speed V_c is not assumed to be stochastic, it may be modelled as a first-order Gauss-Markov process [41]

$$\dot{V}_c + \mu V_c = w^n, \tag{2.12}$$

in which $\mu \geq 0$ is a constant and w^n is white Gaussian noise and the ocean current speed is considered bounded *i.e.*, $|V_c| \leq V_{\max}$. The vehicle's relative velocity with respect to the ocean current, given as $\boldsymbol{\nu}_r = \boldsymbol{\nu} - \boldsymbol{\nu}_c$, can then be determined.

2.4 AUV Motion Model with Disturbances

The 6–DoF coupled motion model considering the ocean current and wave disturbances is given as

$$\mathbf{M}\dot{\boldsymbol{\nu}} + \mathbf{C}(\boldsymbol{\nu}_r)\boldsymbol{\nu}_r + \mathbf{D}(\boldsymbol{\nu}_r)\boldsymbol{\nu}_r + \mathbf{g}(\eta) = \boldsymbol{\tau} + \boldsymbol{\tau}^w. \tag{2.13}$$

Since the ocean current is generally constant or slowly-changing, it is assumed that the current acceleration is negligible, that is, $\dot{\boldsymbol{\nu}}_c \approx \mathbf{0}$. The nonlinear system dynamics of an AUV subject to disturbances is established as

$$\dot{\mathbf{x}} = \begin{bmatrix} \mathbf{J}(\boldsymbol{\eta})\boldsymbol{\nu}_r \\ \mathbf{M}^{-1}\left(\boldsymbol{\tau} - \mathbf{C}(\boldsymbol{\nu}_r)\boldsymbol{\nu}_r - \mathbf{D}(\boldsymbol{\nu}_r)\boldsymbol{\nu}_r - \mathbf{g}(\boldsymbol{\eta}) + \boldsymbol{\tau}^w\right) \end{bmatrix} := f\left(\mathbf{x}, \boldsymbol{\tau}\right), \tag{2.14}$$

where $\mathbf{x} = [\boldsymbol{\eta}^\top \; \boldsymbol{\nu}^\top]^\top \in \mathbb{R}^{2n}$ is the state vector and $\boldsymbol{\tau} \in \mathbb{R}^m$ denotes the control input. Here, n and m represent the number of DoF and input variables, respectively. An

AUV is said to be underactuated if $m < n$ and fully-actuated for $m = n$. A similar procedure can be used to introduce the effects of currents and waves into the horizontal motion dynamic model (2.7).

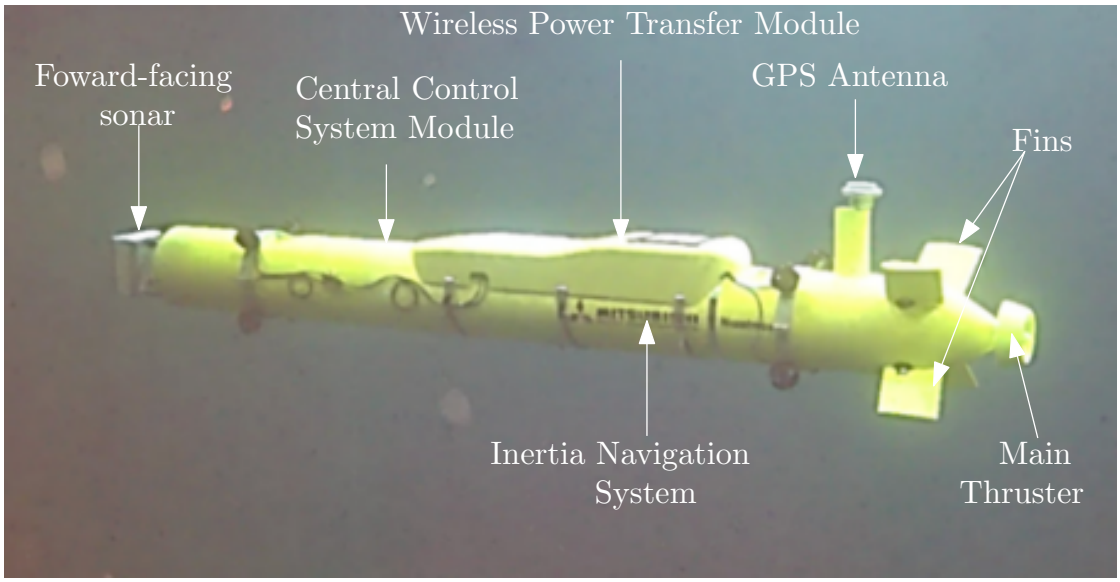

Fig. 2.3: Naminow-D AUV in a demonstration task in the sea. Adapted from [1].

The thesis focuses on the 3D motion control of AUVs employing a coupled 6-DoF model. Specifically, the research utilises the Naminow-D AUV as depicted in Fig. 2.3. This AUV prototype, developed by Mitsubishi Heavy Industries Ltd, measures 3 m in length and is a scaled version of the REMUS AUV. AUVs use various sensors to gather data, navigate and perform motion tasks efficiently. A key sensor is the sonar, which maps underwater terrain and detects obstacles to prevent collisions. Underwater acoustic positioning systems for marine applications can be categorised into Long Baseline (LBL) [100 m - 6000 m], Short Baseline (SBL) [20 m - 50 m] and Ultra-Short Baseline [USBL] [<20cm] systems [42]. The spacing between beacons in the calibrated network is called the baseline.

LBL systems use seabed-mounted transponder beacons and a vessel-mounted sonar transducer. The transducer, mounted on a ROV or AUV, sends an acoustic signal detected by the transponder [43]. SBL systems consist of three or more sonar transducers connected by wire to a central control unit. The spacing between

transducers and the mounting approach influences their accuracy. With wider spacing, such as from a large fixed platform, the performance of SBL can closely match the performance of LBL systems [42]. USBL or the super short baseline (SSBL) systems use a compact transducer array. They are typically mounted on a pole to determine the target distance via the signal run time and direction via phase shift. Thus, the technology differs from LBL and SBL, which rely on multiple distance measurements [42].

The inertial navigation system (INS) estimates the AUV's position by integrating acceleration and angular velocity data [6]. However, INS drifts over time and requires corrections from external references like Global Positioning System (GPS) or Doppler Velocity Log (DVL) data. Note that GPS provides absolute positioning but only works at or near the surface, allowing the antenna to periodically update the AUV position before submergence.

Wireless power transfer modules are increasingly used in AUVs, enabling battery recharging without physical connectors. This is especially beneficial for long-duration missions, where docking stations support continuous operation without human intervention. To maintain precise control underwater, the central control system module integrates sensor data for real-time thruster force computation and autonomous navigation. Refer to Table 2.3 for the Naminow-D AUV model parameters. In this thesis, the nonlinear AUV model (2.14) is solved using the fourth-order Runge-Kutta method, as detailed in Appendix A.

2.5 Summary

In this chapter, the kinematic and dynamic modelling of the AUV were described, encompassing both the 6-DoF and reduced 3-DoF motion control models. It is emphasised that the adoption of the 6-DoF model in this research ensures that the proposed algorithms can achieve not only 2D motion control but also 3D motions. Additionally, the modelling of environmental disturbances was presented. The

Table 2.3: Naminow-D AUV Dynamic Parameters

	Parameter	**Value**	**Units**
Model & hull parameters	m	197.8	kg
	W, B	1940, 1999	N
	x_b, y_b, z_b	$-1.378, 0, 0$	m
	I_{xx}, I_{yy}, I_{zz}	$5.8, 144, 114$	kg·m^2
Added mass coefficients	$X_{\dot{u}}, Y_{\dot{v}}, Z_{\dot{w}}$	$-6, -230, -230$	kg
	$Y_{\dot{r}}, Z_{\dot{q}}$	$28.3, -28.3$	kg·m/rad
	$M_{\dot{w}}, N_{\dot{v}}$	$-28.3, 28.3$	kg·m
	$K_{\dot{p}}, M_{\dot{q}}, N_{\dot{r}}$	$-1.31, -161, -161$	kg·m^2/rad
Hydrodynamic coefficients	$M_{\|w\|w}, N_{\|v\|v}$	$27.4, -27.4$	kg
	$Y_{\|r\|r}, Z_{\|q\|q}$	$12.3, 12.3$	kg·m/rad^2
	$X_{\|u\|u}, Y_{\|v\|v}, Z_{\|w\|w}$	$-12.7, -574, -574$	kg/m
	$K_{\|p\|p}, M_{\|q\|q}, N_{\|r\|r}$	$-0.63, -4127, -4127$	kg·m^2/rad^2

Naminow-D AUV, developed by Mitsubishi Heavy Industries, is chosen for software simulation validation of the motion controllers. To facilitate this validation, the hydrodynamic parameters of the vehicle are outlined. The next chapter presents a critical review of the literature on MPC-based motion controller design for AUVs under disturbances, providing justification for the research conducted in this thesis.

Chapter 3

Model Predictive Control of Autonomous Underwater Vehicles - A Review Perspective

3.1 Introduction

Over the past two decades, AUVs have garnered considerable attention from academia and industry for their potential to reduce risks associated with ocean exploration and resource exploitation. With advancements in computational power, optimisation algorithms, perception, and communication technologies, MPC has emerged as a crucial motion control design method due to its ability to accommodate system and environmental constraints while optimising AUV performance. This chapter explores the advancements in the design of MPC-based motion controllers for AUVs.

The remainder of this chapter is structured as follows. Section 3.2 presents an overview of the development of AUV technology and highlights some important applications. The rationale behind this review is provided in Section 3.3. Section 3.4 delves into the primary motion control tasks of an AUV. In Section 3.5, techniques for handling disturbances in MPC-based motion control design are ex-

amined, emphasising essential features related to performance and implementation. The reviewed works are critically analysed to establish a foundation for the main contributions of this thesis, which are detailed in the subsequent chapters in Section 3.6. This is followed by a summary of the key points of interest to this research in Section 3.7.

3.2 Advances in AUV Applications

The ocean, covering approximately 70% of the Earth's surface, is vital for sustaining life and requires comprehensive understanding across diverse domains [44]. Increasing demands for ocean-related activities, propelled by concerns like environmental preservation, border security, offshore renewable energy deployment, and weather forecasting, have spotlighted underwater operations. Unmanned underwater vehicles (UUVs), comprising remotely operated vehicles (ROVs) and autonomous underwater vehicles (AUVs), have emerged as indispensable tools for diverse underwater tasks. ROVs, controlled either via a tether or remotely by a human operator on the surface, excel in tasks with direct human oversight. Conversely, AUVs, self-propelled and operating autonomously or semi-autonomously, offer the capability to execute missions with minimal human intervention.

The need to advance ocean research led to the development of the first true AUV in the 1950s, known as SPURV (Self-Propelled Underwater Research Vehicle), by the Applied Physics Laboratory of the University of Washington, USA [45]. Initially designed for deepwater research, the development of the UARS (Unmanned Arctic Research Submersible) followed, dedicated to under-ice research [46]. Subsequently, various research centres across the globe, driven by different applications and uses, have developed different AUV technologies [47–56]. These vehicles were primarily developed for government use [47, 48, 57], university-based ocean-related research [53, 58], or commercial applications [50, 54, 55]. Some vehicles initially designed for research were later commercialised, such as the Odyssey-class AUVs developed by the

Massachusetts Institute of Technology (MIT), which were later offered commercially through Bluefin Robotics, now providing models like Bluefin 9, 12, 21, and HAUV [55, 59–61]. The commercialisation of Odysseys targeted offshore oil services [59].

Over the years, AUVs have seen extensive applications across various sectors, driven by the offshore industry's increasing need to explore deep and ultra-deep waters. This industry encompasses not only oil and gas but also telecommunications, offshore renewable energy infrastructure, ocean mining, sub-ice surveys, environmental monitoring, pollution monitoring and cleanup endeavours, and geo-environmental studies [62–67]. Rising defence needs have further propelled the adoption of AUV technology [68]. Advancements in electronics and energy sources have significantly transformed modern AUVs, enabling them to achieve six degrees of freedom (6 DoF) motion, higher speeds, and greater compactness, making them accessible for a wide range of applications [3, 69].

Table 3.1 outlines some important tasks performed by AUVs, highlighting various industrial applications they have been deployed to perform. Equipping AUVs with appropriate sensors, such as magnetometer sensors, enables them to localise, map, and detect irregularities in ocean power cables, as demonstrated by the REMUS 600 AUV [70]. Moreover, unconventional intervention tasks, including valve turning, plugging and unplugging connectors, and item recovery, have become feasible by integrating manipulators into traditional AUV systems [71–75]. For example, the Girona 500 from the TRIDENT project, equipped with a 3-finger arm, has been tested for retrieving black boxes, illustrating its potential for search and rescue missions [74]. Another notable example is the Girona AUV, equipped with an embedded manipulator and end-effector, capable of performing valve turning operations [71]. With such remarkable advancements achieved over the past decades, the demand for AUV technology continues to rise steadily [76–78].

Table 3.1: Applications/tasks for which AUVs have been deployed.

Sector	**Application**	**References**
Industry		
Oil and Gas	Offshore site survey	[79–81]
	Pipeline inspection, monitoring and mapping	[82–87]
	Valve turning	[71, 88]
	Chain inspection and cleaning	[88, 89]
	Structure inspection	[88–90]
	Connector plugging and unplugging	[72, 91, 92]
	Pipeline leak detection	[80, 86, 93]
	Subsea plumes tracking and monitoring due to oil and gas leaks	[94]
	Environmental monitoring and asset integrity	[95, 96]
	Pipe transportation	[97]
	Transport ROVs to docking station	[57]
Telecommunication	Structural monitoring of underwater cables	[98]
	Underwater or under-ice cable laying	[99–101]
	Detection and tracking a specific cable	[102–104]
	Inspection of underwater cables	[70, 105]
	Geophysical survey for cable route determination	[106–108]
	Search and recovery of cable	[109]
Offshore Renewable Energy	Inspection/mapping of offshore wind farm	[5, 110]
	Surveys *e.g.,* soil types and seabed features, power cables used to take power from offshore wind turbines to land	[111, 112]
	Maintenance such as cleaning of bio-fouling of offshore renewable energy structures	[113]
Scientific Research	Survey for bio-logging and general sea animal environmental studies	[114–117]
	identification of predators	[115]
	tracking of sea animals	[118–120]
	geological studies	[121–123]
	environmental effects monitoring	[124–127]

Table 3.1: Applications/tasks for which AUVs have been deployed.

Sector	**Application**	**References**
Industry		
	archaeological studies	[128–131]
Military	Surveillance	[54, 132–134]
	Mine countermeasures	[135–137]
	Search and rescue	[138–143]
	Wreckage inspection	[144–147]
	Bathymetric surveys and ocean exploration	[148–154]
	Ocean floor mapping	[133, 155–159]
	Claim maritime borders based on continental shelf data	[133, 160, 161]
	Payload delivery to seafloor	[162]
	Time critical strikes	[163]
	Anti-submarine warfare	[164–168]

3.3 Motivation for the Review

Despite the considerable advancements in AUV technology, numerous areas require further development [3, 12], particularly in the realm of designing more efficient controllers to enhance the reliability of marine vehicle motion [18]. Traditional motion control methods, such as Proportional-Integral-Derivative (PID) controllers and Linear Quadratic (LQ) control, often rely on linearisation around specific operating points or decomposition into subsystems like depth and surge [6, 20, 169]. However, these approaches may not be suitable for modern AUVs that need to track complex paths and adapt dynamically to uncertain environments. The performance of these control strategies often deteriorates significantly under external disturbances. Even for a well-designed LQ-based controller, linearisation along the path is required with restrictive assumptions regarding the path that can be tracked [20]. As a result, there has been a surge in interest in more advanced model-based control strategies in

recent years. These approaches aim to develop the capabilities of modern AUVs by incorporating models and control algorithms to achieve robust and adaptive motion control in complex environments.

One advanced model-based control approach is backstepping based on Lyapunov theory [170,171]. A drawback of backstepping approach is the requirement of an accurate mathematical AUV model which is not always available [172]. Consequently, different methods such as fuzzy logic [173], exponential observers [174] and neural networks (NNs) [175] are often deployed to estimate unknown dynamics and environmental disturbances. Another challenge often faced in backstepping strategy is the so-called complexity explosion that can arise from backstepping due to repetitive differentiations of virtual control signals. First-order filters including those augmented with hyperbolic tangent functions [176,177] and time-delay introduction [178] have been deployed to address this problem.

Sliding mode control (SMC) serves as an alternative motion control design method widely applied to AUVs because of its high robustness against parameter variations and ability to mitigate the effects of external disturbances [179]. The major setback of traditional SMC is that it is characterised by high switching gains and is heavily affected by chattering around the sliding surfaces which inevitably results from the high gains [180]. The phenomenon is undesirable because it can lead to reduced control accuracy, high heat losses in power circuits and increased mechanical wear of parts [181]. One way of addressing the chattering problem is through the use of integral SMC (ISMC) which ensures that the order of the sliding mode equation is equal to the original system's order; consequently, guaranteeing robustness throughout the entire response of the system. In the context of AUV motion control, several advanced SMC-based algorithms have been proposed *e.g.,* output feedback adaptive nonsingular terminal SMC (ANTSMC) [182], adaptive non-singular integral terminal SMC (ANITSMC) [183], globally finite-time stable tracking control (GFTSTC) [184], adaptive high-order SMC (AHSMC) [185], to mention but a few. Besides, intelligent methods including fuzzy logic, NN and Reinforcement

learning (RL) have been adopted to improve the performance of SMC-based motion controllers [186–192]. Although chattering may be reduced, its effects are often not entirely eliminated. Moreover, neither backstepping nor SMC methods offer a straightforward solution for managing opertional constraints.

MPC has also been widely used for AUV motion control. Its capability to incorporate system constraints, including environmental constraints, as well as input and state constraints, renders MPC particularly suitable for AUV applications [22]. Initially, its application was limited to slower systems due to high computational demands. However, recent advancements in computing, perception, algorithm efficiency, and communication technologies have facilitated widespread adoption across diverse application domains, and the strategy can be applied to linear, nonlinear, and time-delay systems [14]. Over the past two decades, MPC-based algorithms have become increasingly popular in AUV motion control, driven by promising experimentally validated results in Autonomous Surface Vehicles (ASVs) and AUV motion control in a local plane, as reported in various studies [8–11, 193, 194].

For autonomous marine vehicles, several reviews have been published regarding specific topics such as collision avoidance [195, 196], planning [197], dynamic positioning [198], guidance, navigation and control (GNC) systems [3, 199]. The recent review by [12], which focused on MPC applications to various motion planning and control tasks for single and multiple AUVs, is the most closely related to this review. However, the review in this chapter is distinct from [12] because its primary objective is to critically explore MPC design techniques, including assumptions related to modelling, deployed to handle the effects of unknown environmental disturbances. It aims to outline the nuances associated with design and performance and identify areas open for further investigation. This focus is motivated by the realisation that while standard MPC provides robustness to small disturbances, it lacks adequate robustness against significant disturbances [200] such as those encountered in underwater environments. The next section examines the primary motion control tasks of an AUV from the perspective of MPC-based controllers.

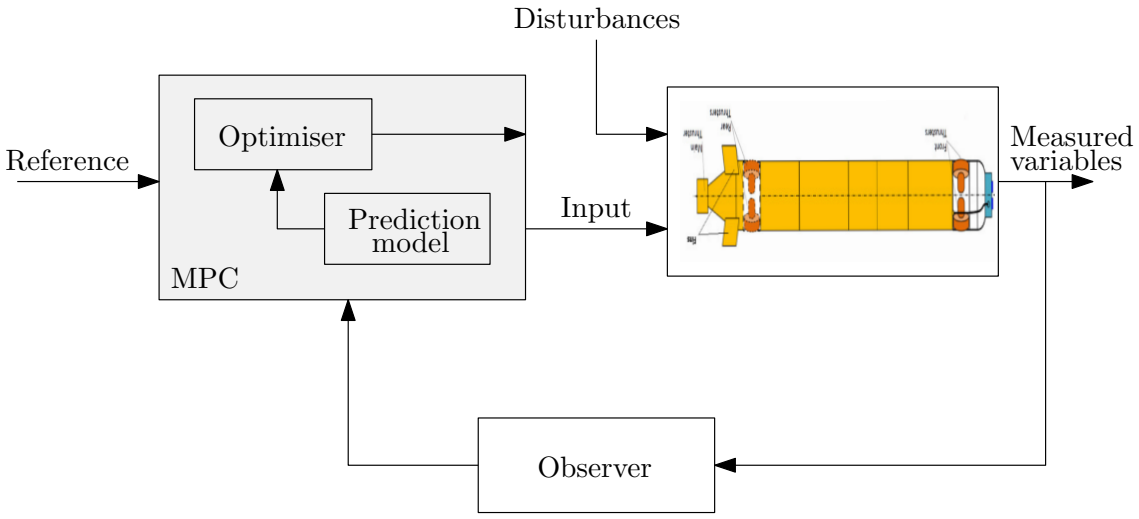

Fig. 3.1: A generic illustration of MPC application to AUV motion control.

3.4 MPC for AUV Motion Control

The primary goal of describing AUV dynamics is to achieve effective motion control of the vehicle using model-based design techniques. However, various challenges such as environmental disturbances, actuator constraints, uncertain model parameters, underactuation, and nonlinearities pose significant hurdles to developing effective motion control schemes. Motion control typically involves generating input forces and moments to achieve defined motion control objectives. In general, control problems for AUVs fall into three categories: dynamic positioning, path-following, and trajectory tracking [41, 201, 202]. Each of these control problems is crucial in different operational scenarios. This section focuses on MPC-based strategies for AUVs. Fig. 3.1 illustrates the process of applying MPC to motion control of AUVs, where the reference signal depends on the specific motion task and/or the DoFs of the model used for control design. The observer is included to generalise the illustration to cases where it is needed for state, disturbance or parameter estimation. The following subsections discusses the three primary motion control tasks and introduces the basic MPC problem that is used for their execution.

3.4.1 MPC for Dynamic Positioning

The goal of dynamic positioning is to steer the AUV to maintain a predetermined position and orientation despite the impacts of time-varying environmental disturbances [6, 203]. The variable $\boldsymbol{\eta}_d = [x_d, y_d, z_d, \phi_d, \theta_d, \psi_d]^\top$ defines the desired position and orientation of the AUV. In this task, defining the orientation of the AUV, particularly the heading angle ψ_d indicating the direction of the vehicle's movement is crucial [12]. From a control perspective, the dynamic positioning of AUVs is synonymous with point stabilisation and station keeping [12, 28]. In general, achieving dynamic positioning of AUVs poses a significant challenge. This difficulty arises not only from the complexities associated with nonlinearities, disturbances, and coupling but also due to potential nonholonomic[1] constraints on the vehicle's motion [204]. These constraints can render it impossible to achieve point stabilisation using any continuous or smooth constant state-feedback control law.

This control objective is crucial for inspection tasks, where the vehicle must maintain a specific position and orientation to allow a non-rotating onboard camera to inspect a facility or structure. Additionally, it is vital in docking scenarios, where the vehicle needs to hover around a predetermined point with a defined orientation to be captured by a remotely-operated docking station. It is worth noting that practical docking scenarios involve a combination of trajectory tracking/path-following and dynamic positioning, as the vehicle must move from its current position to a vicinity around the docking station. Moreover, dynamic positioning plays a crucial role in missions such as target reconnaissance and obstacle detection [28]. In MPC-based controller design for dynamic positioning, the objective is to compute the optimal control sequence $\mathbf{U}(k) = \{\boldsymbol{\tau}^*(k+j|k)\}, j \in [0, N-1]$, where $\boldsymbol{\tau}^*(k+j|k)$ denotes the $k+j$ prediction of the optimal input sequence at sampling instant k. The input sequence is obtained by solving a Finite Horizon Optimal Control Problem

[1] A constraint on a system which does not lead to a reduction in DoF because it only limits how certain configurations can be achieved without restraining the number of possible configurations.

(FHOCP), at every sampled instant k, as follows:

$$\begin{aligned}
\mathbf{U}(k)^* &= \arg\min_{\mathbf{U}(k)} V_{DP}(\mathbf{U}(k), \mathbf{x}(k)) \\
\text{s.t} : \mathbf{x}(k+j+1|k) &= f(\mathbf{x}(k+j|k), \boldsymbol{\tau}(k+j|k)), \\
\mathbf{x}(k+j|k) &\in \mathcal{X},\ j = 1, \ldots, N, \\
\boldsymbol{\tau}(k+j|k) &\in \mathcal{T},\ j = 0, \ldots, N-1, \\
\mathbf{x}(k|k) &= \mathbf{x}(k),
\end{aligned} \tag{3.1}$$

where N is the prediction horizon, $\mathcal{X}$ and $\mathcal{U}$ are the state and input constraint sets, respectively; and the cost function $V_{DP}(\mathbf{U}(k), \mathbf{x}(k))$ is given by

$$\begin{aligned}
V_{DP}(\mathbf{U}(k), \mathbf{x}(k)) = &\parallel \boldsymbol{\eta}_d - \boldsymbol{\eta}(k+N|k) \parallel^2_{\mathbf{P}} + \sum_{j=0}^{N-1} \parallel \boldsymbol{\eta}_d - \boldsymbol{\eta}(k+j|k) \parallel^2_{\mathbf{Q}} \\
&+ \parallel \boldsymbol{\tau}(k+j|k) \parallel^2_{\mathbf{R}},
\end{aligned}$$

in which $\boldsymbol{\eta}_d$ denotes the desired position and orientation vector, $\mathbf{Q}, \mathbf{R}$ and $\mathbf{P}$ are positive definite weighting matrices.

The vast majority of MPC applications for dynamic positioning problems are focused on horizontal motion control of AUVs or ASVs [201, 205–207]. The algorithms described in the aforementioned works may not be directly suitable for the dynamic positioning of underactuated AUVs with nonholonomic constraints. As a result, an MPC algorithm that relies on a time-varying feedback law and homogeneous system dynamics was deployed for underactuated AUVs [208]. Additionally, authors of [209–211] investigated this problem using tube-based MPC strategies for ASVs. Since the focus of the above studies is typically on the horizontal plane, separate depth controllers such as PIDs are needed in practical scenarios involving AUVs. Recent studies such as [1, 211] proposed MPC algorithms for positioning control in 3D space. These studies employed the LPV AUV model for control design to circumvent the computational complexity linked with nonlinear MPC for higher-

order systems. However, many of these studies [1, 211, 212] on dynamic positioning assume constant disturbances or overlook their effects. This is particularly due to the significant challenge of maintaining precise positioning control in the presence of persistent disturbances. Therefore, research on the dynamic positioning problem of AUVs, particularly in 3D space, remains an area ripe for further exploration.

3.4.2 MPC for Trajectory Tracking

Trajectory tracking deals with steering an AUV to track a time-parameterised path. In this motion control problem, the spatial and temporal requirement of the trajectory is defined. For studies based on 3−or 4−DoF models, the reference trajectory is typically assumed to be generated by a virtual AUV, that is, the reference state trajectory $\mathbf{x}'_d$ satisfies the nonlinear trajectory of the AUV as

$$\dot{\mathbf{x}}'_d = f(\mathbf{x}'_d, \boldsymbol{\tau}'_d), \tag{3.2}$$

with $\boldsymbol{\tau}'_d$ denoting the corresponding reference input, which may be taken as zeros for simplicity. By defining the error state as $\mathbf{x}'_e(k) = \mathbf{x}'(k) - \mathbf{x}'_d(k)$, the error dynamics of the reduced-order AUV model is given by

$$\dot{\mathbf{x}}'_e = f(\mathbf{x}'_e, \boldsymbol{\tau}'). \tag{3.3}$$

The error dynamics is then employed in the formulation of a stabilisation MPC problem. The discretised finite-horizon optimal control problem (FHOCP) is given as

$$
\begin{aligned}
\mathbf{U}(k)^* = \arg\min_{\mathbf{U}(k)} \; & V_{TT}(\mathbf{U}(k), \mathbf{x}'_e(k)) \\
\text{s.t} : \; & \mathbf{x}'_e(k+j+1|k) = f(\mathbf{x}'_e(k+j|k), \boldsymbol{\tau}'(k+j|k)), \\
& \mathbf{x}'(k+j|k) \in \mathcal{X}, \;\; j = 1, \ldots, N, \\
& \boldsymbol{\tau}'(k+j|k) \in \mathcal{T}, \;\; j = 0, \ldots, N-1, \\
& \mathbf{x}'_e(k|k) = \mathbf{x}'_e(k),
\end{aligned}
\tag{3.4}
$$

in which $\mathbf{x}'_e(k+j|k)$ denotes the error state predictions at future time step $k+j$ computed at sampling instant k, and the cost function is defined as

$$
\begin{aligned}
V_{TT}(\mathbf{U}(k), \mathbf{x}'_e(k)) = \sum_{j=0}^{N-1} & \parallel \mathbf{x}'_e(k+j|k) \parallel^2_{\mathbf{Q}} + \parallel \boldsymbol{\tau}'(k+j|k) \parallel^2_{\mathbf{R}} \\
& + \parallel \mathbf{x}'_e(k+N|k) \parallel^2_{\mathbf{P}} .
\end{aligned}
$$

However, when dealing with 3D trajectory tracking, particularly with the use of a 5- or 6-DoF model, the MPC problem is frequently framed as a tracking problem similar to that of dynamic positioning MPC problem (3.1), with the distinction that $\boldsymbol{\eta}_d = \boldsymbol{\eta}_d(k)$ *i.e.,* the reference position and orientation vector varies with time. While numerous studies [21, 22, 25, 212] on 3D trajectory tracking primarily concentrate on the translational position reference trajectory (x_d, y_d, z_d), it is crucial to acknowledge the significance of attitude, particularly the heading angle ψ_d, in practical scenarios. In such instances, one might set $p_d = q_d = 0$ while defining ψ_d to represent the desired heading direction [16].

Although the trajectory tracking control problem for fully actuated AUVs is well-understood [213], there is still scope for future investigation, especially in addressing more practical control inputs by considering input magnitude and rate constraints [13]. Furthermore, the utilisation of the 6-DoF AUV model for control design remains underexplored [18].

3.4.3 MPC for Path-Following

The path-following control objective arises in scenarios where the vehicle must execute a time-independent manoeuver along a feasible path, maintaining a specified orientation [214–216]. This means that the task imposes spatial constraints with no limits on the temporal travel along the defined path, making it possible to separately control the spatial and temporal constraints. Closely related to path-following is the *path manoeuvring* task which involves two tasks - the geometric task that enables the AUV to follow the desired path and the dynamic task that specifies the time, speed or acceleration with which the law is updated [217].

In path-following control problem, an error model of the form (3.3) is typically obtained, even for higher-order models such as the 5-DoF model based on the assumption of negligible roll motion [218]. However, in this case, the reference path $\mathbf{x}_d(s) \in \mathbb{R}^{2n}$ is parameterised by the time-independent variable $s \in \mathbb{R}$. Based on this desired path, error dynamics are derived, transforming the control problem into a regulation problem. The vehicle error dynamics are of the form:

$$\dot{\mathbf{x}}_e = f(\mathbf{x}_e, \boldsymbol{\tau}), \tag{3.5}$$

in which $\dot{\mathbf{x}}_e \in \mathcal{X} \subset \mathbb{R}^{2n}$ is formulated to include the heading and cross-track errors [218]. Generally, the MPC problem formulated for this motion control task is similar to the trajectory tracking problem (3.4). In the realm of MPC, research on this topic has predominantly focused on ASVs [219–222] or the horizontal motion control of AUVs [216, 221, 223–225]. In the 3D path-following context, authors of [226] considered a 4-DoF model of a robotic penguin propelled by median and paired fin (MPF). Their proposed approach introduces an event-triggered fuzzy linear MPC method for path-following. The event-triggered condition is used to reduce optimisation frequency. Simulation results validated the effectiveness of the scheme. In [227], an error model for a decoupled 5-DoF AUV model is developed using Lyapunov techniques, employing MPC as the kinetic controller. Subsequently, an SMC

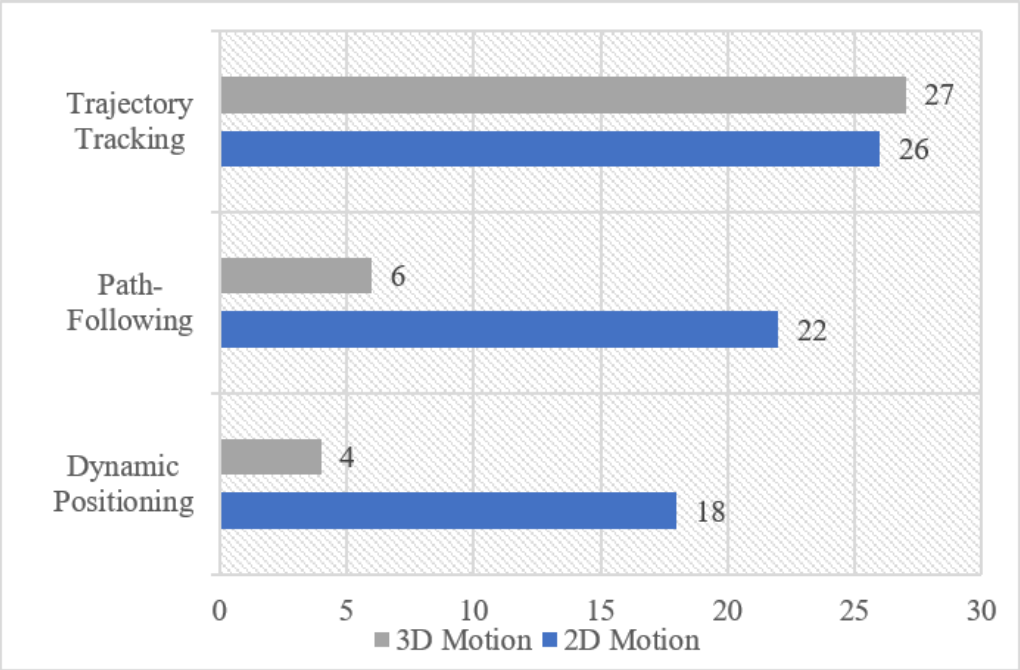

Fig. 3.2: Number of published articles on "MPC for motion control of AUVs/ASVs" indexed in the Web of Science database between 2000 and 2023.

scheme was utilised as the dynamic controller to track the reference speed computed by the MPC-based kinematic controller.

While numerous studies have explored 3D path-following control using alternative model-based control design techniques [224, 228–231], there remains a paucity of MPC-based investigations in this area. Path-following, just like dynamic positioning, in 3D space, is not widely studied under the MPC framework. In contrast, path-following has garnered considerable attention in 2D motion control over the years, as illustrated in Fig. 3.2. The figure summarises published articles indexed in the Web of Science (WOS) database between 2000 and 2023. These articles were identified using the following keywords in the titles: "autonomous underwater vehicle/AUV", "Underwater robot," "model predictive control/MPC", "autonomous marine vehicle/AMV", "remotely operated vehicle/ROV", "control", and "autonomous surface vehicle/ASV." Note that the works in Fig. 3.2 do not include those focusing on 1D motion, such as in the vertical direction. It is noted that the less amount of

work on 3D paths compared to 2D paths, especially in path-following, may be explained by the fact that it is more straightforward to formulate an error model of the form (3.3) that satisfies the dynamics of the vehicle when compared to higher-order models of marine vehicles. Therefore, this domain presents ample opportunities for future research endeavours.

3.5 Disturbance Handling in Motion Control of AUVs

AUVs are subject to model uncertainties and external disturbances caused by environmental factors such as ocean currents and waves. While nominal model parameters can be estimated through parameter and/or system identification techniques, they may still exhibit variations due to unmodeled dynamics and unpredictable environmental disturbances [6]. Handling disturbances in AUVs has been a longstanding research focus, with ongoing investigations employing a variety of techniques [232]. In the context of MPC, various methods for handling disturbances have been investigated. These can broadly be categorised into incremental variable-based MPC methods, observer-based MPC methods and robust MPC methods. In what follows, the main techniques utilised for disturbance handling are critically discussed, emphasising nuances in their design and applications.

3.5.1 Increment Variable-Based MPC Design

This approach to handling disturbances in MPC design for AUVs has garnered considerable interest in the literature. Methods in this category utilise AUV velocity increment to facilitate MPC design for AUVs operating in the presence of disturbances. The motion controllers in this category are usually designed using MPC by creating a kinematic model where the velocity increment is considered as the input signal. A MPC controller, known as the kinematic controller, is designed using this

model to compute the desired velocity of travel for the vehicle. Then, a dynamic controller, which may or may not be an MPC scheme, is used to track the desired velocity despite the effects of unknown disturbances. The link between the kinematic and dynamic controllers is illustrated in Fig. 3.3.

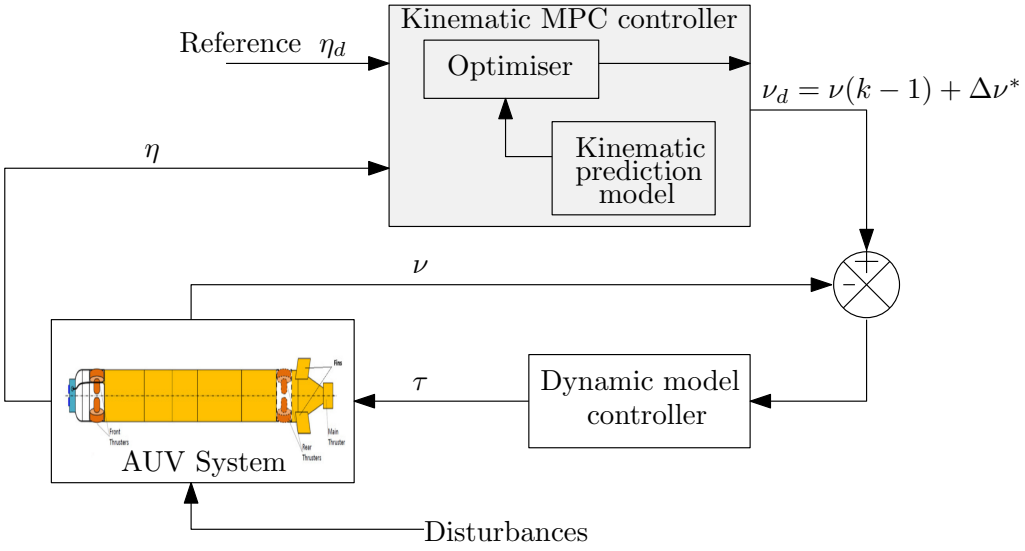

Fig. 3.3: An illustration of increment-variable MPC design strategy for disturbance handling in AUV motion control.

The work [25] proposed a LTV MPC strategy as the kinematic controller with AUV velocity increment, $\Delta\boldsymbol{\nu}$, as the input signal to be computed. Through this formulation, an efficient quadratic MPC problem can be solved online to determine the optimal velocity vector of the vehicle. Subsequently, the optimal velocity reference is used to compute the input forces and moments from the dynamic model directly. However, this approach may be overly sensitive to modelling errors and external disturbances due to its reliance on the accuracy of the dynamic model. In [24], a second dynamic controller based on an LTV MPC problem where the prediction model incorporates the increment of the input forces and moments is proposed. Unlike [25] which is based on the 6-DoF model, the approach [24] assumes a pre-stabilised roll motion and utilises a 5-DoF model. It is worth noting that the technique of augmenting state variables with input signal increment does not effectively mitigate disturbances. It is similar to the so-called *partial velocity*

form of MPC, which fails to provide offset-free control for linear time-invariant (LTI) systems in the presence of constant disturbances unless an observer is employed to estimate both states and input signals used for predictions [233]. Given that disturbances in AUVs are typically persistent and varying in time, and studies [24, 25] did not employ an observer, the performance of these methods [24, 25] can deteriorate substantially under significant disturbances.

An interesting advantage of the increment variable-based MPC design approach is its compatibility with alternative techniques for disturbance management in dynamic controller design. SMC-based methods have emerged as primary strategies for enhancing the effectiveness of disturbance mitigation, resulting in an integrated MPC-SMC framework. A significant contribution in this domain was made by [16], where the authors initially devised an error kinematic model for a 4-DoF AUV model. Subsequently, the error model is transformed into a partial velocity form, employing velocity increment as the input. The authors [16] employed SMC to compute the input forces and moments based on the optimal reference velocity computed using MPC. A similar scheme was also deployed by [23] in dynamic target tracking. The merit of these schemes over [24, 25] is that they take advantage of the robustness of SMC to modelling error and external disturbances. Nevertheless, it should be noted that SMC may lead to input chattering. To mitigate chattering, authors of [10] incorporated ISMC into an integrated NMPC-SMC framework for local plane motion control of an AUV. Therefore, the method relating to formulating the kinematic model with velocity increment as input may rely on other methods such as SMC–based techniques to mitigate disturbances.

One of the main methods used for ensuring offset-free control in LTI systems is the use of velocity form state space models in MPC design [234]. This involves formulating a prediction model by augmenting the state increment with the plant outputs and using the change in the input signal as the input to the resulting extended model. This method eliminates the need for an estimator to handle constant or slowly changing disturbances. The approach was proposed for nonlinear systems

by approximating their dynamics using quasi-LPV model [235]. This approach is yet to receive any interest in AUV motion control, particularly when navigating curved trajectories in 2D and 3D space. This lack of use can be attributed to the presence of nonlinearities and coupling effects, which make it challenging to approximate the system model using linear methods. Additionally, employing augmented models in the FHOCP increases the state dimension of the prediction model, resulting in higher computational costs and potential loss of stabilisability [236].

3.5.2 Disturbance Model-based MPC Design

Disturbance model-based MPC design encompasses strategies that incorporate modelled disturbances through various techniques to mitigate the impact of unmeasured disturbances within the MPC framework. Depending on the approach adopted for disturbance modelling, these methods are further classified into observer-based, linear wave theory-based and intelligent design methods. These classifications are elaborated upon in the following subsections.

3.5.2.1 Observation-Based MPC Design

Observation-based techniques refer to methods where estimators are utilised to directly approximate external disturbances or to reconstruct the states of the system to account for the effects of internal and external disturbances. Authors of [237] proposed an extended state observer (ESO)-based MPC strategy for 3D trajectory tracking for an underactuated 4-DoF AUV model. This scheme employs MPC to compute the reference velocity vector using the input increment technique as in [16]. The impacts of underactuation and disturbances are accounted for through a control law that uses ESO for lumped disturbance approximation [237]. Indeed, it would have been intriguing to compare the ESO-based MPC with a standard MPC controller, given the latter's advanced capabilities. In [238], a super-twisting-algorithm (STA)-based observer was used to estimate unknown disturbances, which was then

utilised in an MPC algorithm. This MPC algorithm leveraged feedback linearisation to facilitate efficient computation. Simulation results showcased the effectiveness of this strategy for horizontal motion control of an AUV.

Under the premise of constant current disturbance, authors of [211] devised an offset-free NMPC (OFNMPC) based on a 4-DoF model for docking operations wherein a disturbance model is integrated with the system dynamics and estimated utilising a Kalman filter. The study [1] proposed an LTV MPC algorithm employing an LPV Kalman filter to estimate disturbances by comparing estimated and measured states. However, assuming constant disturbances is not always practical due to the dynamic nature of the ocean environment [6]. Authors of [212] devised an MPC-based 3D trajectory tracking algorithm incorporating an Extended State Kalman Filter to estimate disturbances by augmenting system states with an integrating disturbance model. While the work [212] accounted for measurement noise, it relies on the impractical assumption of a constant ocean current disturbance.

Authors of [15] conducted a comparative study of two OFNMPC algorithms integrated with EKF and Moving Horizon Estimation (MHE) for AUV dynamic positioning control. The study revealed that the OFNMPC-EKF combination offers superior robustness in the presence of varying disturbances. The study [239] proposed the use of an extended active observer as a disturbance estimator under an NMPC framework for 3D trajectory tracking. In [240], an EKF was employed for wave disturbance estimation, serving as feedback to enhance the performance of LTV-MPC for 2D station keeping control in the xz-plane. The scheme's performance was benchmarked against a PID controller. However, one can argue that a more appropriate comparison could have been made with conventional MPC without the observer. An important point to note is that approaches relying on observers to estimate additive disturbances for correcting prediction models often assume constant disturbances, which may not always be practical in real-world scenarios.

Lyapunov-based MPC (LMPC) design is a methodology that imposes closed-loop stability for complex nonlinear systems by incorporating a Lyapunov stability

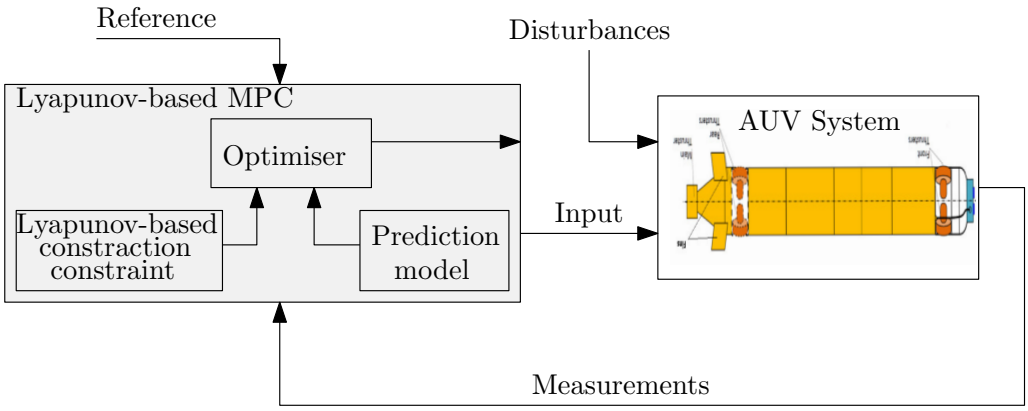

Fig. 3.4: Lyapunov-based MPC generic framework for motion control of an AUV.

contraction constraint into the NMPC problem as illustrated in Fig. 3.4. In this method, the derivative of the Lyapunov function of the MPC controller should not exceed that of the Lyapunov function of a pre-designed auxiliary controller. While this concept was first introduced by [241,242], its application to AUV motion control was pioneered by [206]. They formulated [206] a Lyapunov constraint within the MPC framework to ensure closed-loop stability for dynamic positioning control in the horizontal plane. This approach is advantageous as it avoids local linearisation to ensure stability. Subsequently, the scheme was extended to trajectory tracking in a later work [243]. However, these initial applications to AUVs did not explicitly incorporate methods for mitigating the effects of disturbances and thus relied on the inherent robustness of NMPC. Observer-based LMPC design has been employed to estimate and mitigate the impact of disturbances in the trajectory tracking of co-operative AUVs [244]. By utilising an ESO-based auxiliary controller, closed-loop stability is ensured [244]. The distributed LMPC inherits the robustness and stability features of the ESO-based controller, leveraging online optimisation to enhance performance. This observer-based LMPC approach has been extended to guarantee closed-loop stability for underactuated cooperative ASVs as well [245]. Extending these observer-based LMPC schemes to facilitate 3D motion control of AUVs is likely to receive interest from researchers in the near future.

3.5.2.2 Linear Wave Theory-Based MPC Design

Linear Wave Theory (LWT) describes a wave field in a random sea as a superposition of sinusoidal components. The authors of [246] proposed a MPC strategy that relies on LWT to approximate the fluid dynamics within a wave field. The approximated disturbances are then incorporated into the MPC future predictions to counteract the effects of wave-induced disturbances. The LWT-based wave prediction was experimentally validated using an ROV [247]. Under the assumption that the velocities of currents, waves, and wind remain constant for short periods, authors of [207] devised a mathematical model to approximate the effects of disturbances on an AUV in the horizontal plane. The unknown model parameters are estimated by minimising the least square criteria between the measured velocities and those of the disturbance model. Through performance metrics such as average mean error, RMS error, and average maximum error, the approach demonstrated superior performance compared to conventional MPC lacking disturbance predictions [207].

3.5.2.3 Intelligent MPC Design

Artificial intelligence has taken centre stage in different fields and is today closely linked with control system design. In the context of AUVs, intelligent methods such as neural networks and fuzzy logic have found extensive use as approximators for actuator faults, unknown dynamics and external disturbances in motion control under backstepping and sliding mode control frameworks [248–252]. The study [253] proposed a modification to the MPC-SMC framework from [16], using a nonsingular terminal sliding mode control (NTSMC) instead of SMC as the dynamic controller. The authors [253] then used a RBF-NN for lumped disturbance estimation to enhance the adaptiveness of the scheme. In [8], a combined reinforcement learning (RL) and system identification method was used to learn and identify modelling errors and disturbances to improve the performance of an MPC motion controller for an ASV. Experimental results demonstrated the potential of this method. It

is worth mentioning that fuzzy- and NN-based methods have been proposed for data-driven predictive control, which aims to develop predictive control strategies without relying on a mathematical model of the system. The authors of [254] proposed a predictive control using a Takagi–Sugeno (T–S) fuzzy model predictor with sliding window (SDW), omitting the need for a detailed AUV model but ignoring disturbances. In [255], the fuzzy-based predictor was extended to estimate disturbances and compensate for time delays. However, they lacked comparisons with model-based schemes for a more comprehensive assessment of their performances. In a recent study [256], the parameters of an RBF-NN model-based predictor were optimised using an adaptive sparrow search algorithm. This method compensates for disturbances by updating the neural network output layer's deviation from the desired trajectory.

3.5.3 Robust MPC Design

Due to its receding-horizon nature, standard MPC can handle small uncertainties such as model mismatch and additive disturbances to some extent. However, it has limited robustness and may not perform well in practical applications when model uncertainties or disturbance levels are high. Hence, researchers have been developing robust MPC methods to ensure good performance while robustly satisfying system constraints. See [14] for an extensive review of robust MPC techniques, namely, min-max optimisation-based approaches [257, 258], tube-based methods [259, 260], and constraint-tightening techniques [258, 261]. Robust MPC design has received considerable interest for ASV and AUV motion control under the influence of disturbances. The authors of [262] proposed a min-max NMPC for ASVs, where the worst-case scenario, based on the disturbance upper bound, is considered in the computation of the input forces and moments. However, considering the worst-case scenario is likely to result in conservative controller performance. Based on linear matrix inequalities (LMI), the authors of [216] proposed a robust MPC scheme based on H_∞

criterion to achieve path-following for AUVs in the presence of model uncertainties and environmental disturbances. The robust MPC scheme relies on a factorised Extreme Learning Machine (fELM) dynamic model for prediction. Simulation and experimental results verified the effectiveness of the proposed scheme in achieving the path-following in the horizontal plane. The following subsections explore robust strategies, tube-based and energy-optimal methods, which have received interest in the AUV control literature.

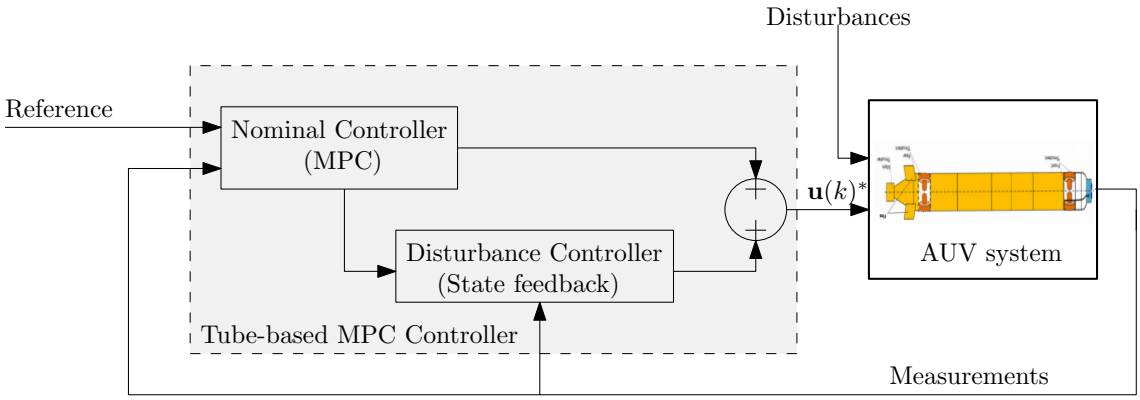

Fig. 3.5: Tubed-based MPC generic framework for motion control of an AUV.

3.5.3.1 Tube-Based MPC Design

The tube-based MPC (TMPC) is a robust control strategy aimed at confining the system's evolution within a tube surrounding a desired nominal trajectory. As shown in Fig. 3.5, TMPC typically consists of two control laws. The first is a nominal controller, which employs the nominal model for prediction in an MPC problem. The second is an auxiliary or state-feedback controller, often referred to as the disturbance controller, used to ensure that the actual trajectories of the system remain within a state tube centred along the nominal state trajectories. The size of the tube is determined by the system's dynamic constraints and the upper bound of the disturbances. A combined TMPC and ISMC approach is proposed for dynamic positioning in the horizontal plane, addressing system constraints and disturbances, including faults [263]. Given that the vehicle operates within a small

known neighbourhood, a conventional linear state feedback design is employed [263] to characterise the tubes.

However, characterising the tube with a local linear feedback gain remains challenging for nonlinear AUV trajectory tracking problems. To address this, the work [264] employed an ancillary nonlinear optimisation method to formulate an implicit control law aimed at minimising the distance between the perturbed system and the nominal system. The study [22] developed a TMPC for 3D trajectory tracking of an underactuated AUV represented by a 4-DoF model where the state feedback control law is formulated using a backstepping technique. The authors of [17] introduced a dual-loop TMPC for a 5-DoF AUV model, inspired by the input increment approach outlined in [24], to tackle model uncertainties in 3D trajectory tracking control. The dual-loop TMPC utilised a finite-time ESO to estimate dynamic system uncertainties to achieve adaptiveness under disturbances. The major drawback of this approach lies in the computational intensity required for its implementation as it relies on the sequential solving of a state-dependent discrete-time algebraic Riccati equation (SD-DARE) and two distinct constrained optimisation control problems. Additionally, the work [17] assumes negligible roll motion based on the assumption that the roll motion of the vehicle is pre-stabilised by an appropriate method. Therefore, further research is encouraged to explore TMPC for 3D motion control utilising full 6-DoF models.

3.5.3.2 Robust Energy-Optimal MPC Design

An interesting technique mostly deployed for path-following is the so-called robust energy-optimal methods. In the work [265], a robust energy-optimal LOS MPC (ELOS-MPC) was employed for surge and yaw control while PID was deployed for heave and pitch control. To account for uncertainty, the authors [265] analysed how the optimal surge speed changes when the current deviates from its nominal value. Then, minimisation of the maximum potential energy loss is performed to make the optimal surge speed robust. Simulation results demonstrated that the

scheme has the potential to provide satisfactory path-following while resulting in considerable energy savings. The authors of [21] introduced a modified technique, known as the robust energy-optimal integral LOS MPC, for achieving 3D path-following without relying on PID controllers. To ensure feasibility in the tracking problem, reference signals for sway (v) and roll (p) directions were set to zeros due to the AUV's lack of actuation in these directions. The yaw angle reference (ψ_d) was determined using the standard ILOS technique, while setpoints for surge velocity (u_d), heave velocity (w_d), and pitch angle (θ_d) were obtained from an optimisation problem. This problem, designed to robustly account for uncertainties, aimed at minimising energy consumption. The scheme concurrently solves two MPC problems to track (u_d, ϕ_d) and (w_d, θ_d), respectively [21]. It is noted that the scheme relies on an EKF to estimate model uncertainties and constant ocean currents that are used in robust reference computation. However, it is essential to note that this scheme's development relies on the assumption that surge, heave, pitch and yaw dynamics remain in a steady state, which may not hold true for arbitrary 3D motion. Moreover, assuming a constant current is impractical due to the time-varying nature of environmental disturbances in the ocean environment.

The next section discusses key points from the review of various disturbance-handling techniques, highlights research gaps and outlines their implications for future research.

3.6 Discussions and Research Outlook

This chapter has offered a critical review of applications and MPC-based motion control strategies of AUVs, emphasising design intricacies and techniques for handling disturbances. It acknowledges that while the receding horizon principle inherently provides robustness for standard MPC against relatively small uncertainties, the complex mix of model uncertainties and environmental disturbances encountered by AUVs in underwater environments necessitate the incorporation of more advanced

methods to effectively mitigate disturbances in MPC applications for AUVs. Developing MPC-based motion controllers for 3D problems is inherently complex due to the requirement of using higher-order models, which leads to solving computationally intensive optimal control problems online. Controllers for AUVs based on MPC have mainly focused on planar motions, with those targeting 3D motion relying on simplified AUV models. The strategies for handling disturbances in MPC-based motion controllers were categorised into three main subheadings: increment variable-based methods, observation-based methods and robust methods. It is important to note that not all algorithms neatly fit into one specific category, as some approaches may incorporate elements from multiple strategies. This is illustrated in Fig. 3.6, where certain algorithms exhibit characteristics that span across various disturbance management strategies.

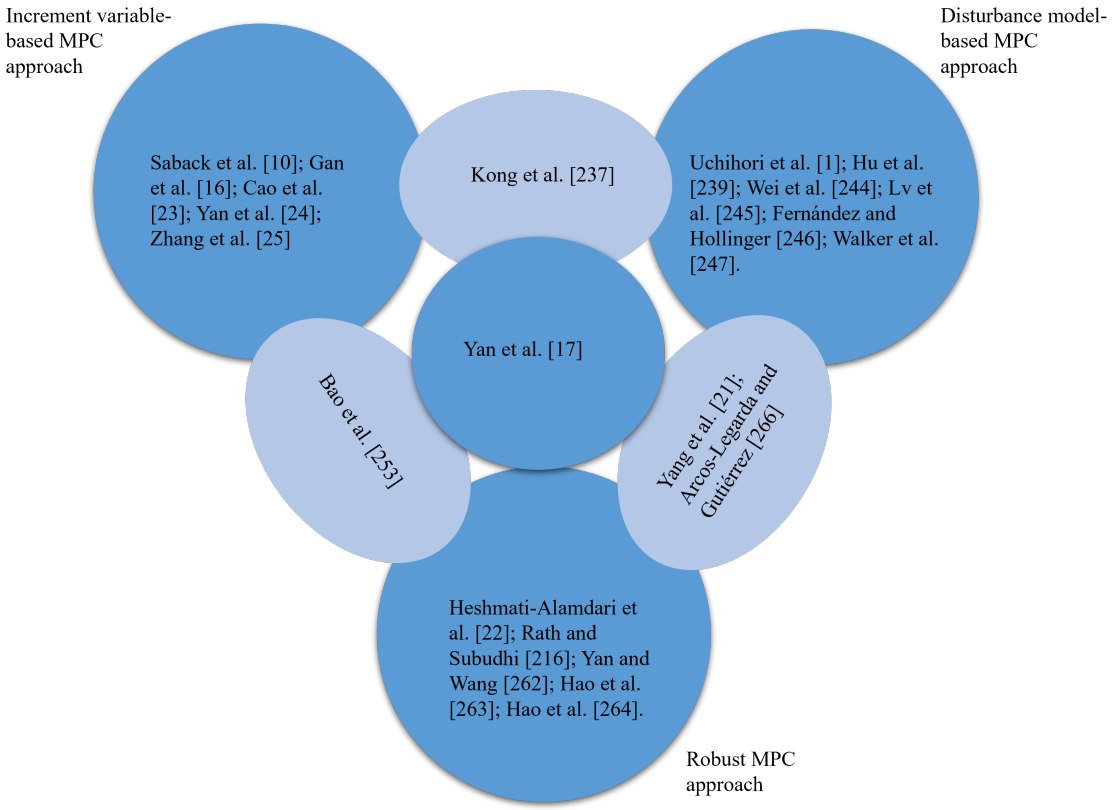

Fig. 3.6: Selected papers used to exemplify the interconnectedness among various techniques for managing disturbances in AUV motion control.

In the AUV literature, the increment variable-based method has relied on the so-called *partial velocity form* where a virtual input (AUV velocity) increment is augmented with the state vector. It is noted that this method on its own does not adequately mitigate the effects of disturbances and as such requires the design of approaches such as SMC-based techniques to ensure robustness against disturbances and model uncertainties. In MPC literature, an alternative increment variable-based MPC is known as the *velocity form* MPC. The velocity form, which appears to have seen no applications in AUV 2D or 3D motion control, involves utilising the increments of both states and inputs to construct a prediction model, aimed at mitigating the effects of disturbances. The advantage of the so-called velocity form MPC stems from the fact that it does not require a separate observer to mitigate the effects of disturbances. While this technique was traditionally applied to LTI systems [234], the work by [235] developed a velocity form MPC for nonlinear systems by using quasi-LPV models for predictions. A major drawback of this method and other velocity form MPC algorithms is the requirement for model augmentation, which has made this approach less appealing because it can potentially increase computational burden due to increased state dimension. Hence, the development of velocity MPC algorithms for AUVs remains an ongoing research challenge, particularly algorithms capable of bypassing the need for model augmentation.

Observation-based techniques, utilising estimators like Kalman filtering-based methods, MHE, or intelligent tools such as NN and fuzzy logic, are commonly employed for disturbance rejection in AUV motion control. These methods are popular because they can be integrated into different MPC formulations. In MPC design, where disturbances are assumed additive, the estimators are used to compensate for the unknown disturbances [1, 211, 239, 240]. A drawback of these methods is that they mostly rely on the impractical assumption of constant disturbances. In robust control, estimators allow adaptability by adjusting disturbance bounds based on the prevailing operating conditions [17, 266]. Thus, the observation of uncertainties is expected to continue to play an important role in control design. This includes

mitigating disturbances in nominal MPC design and reducing the conservatism associated with robust strategies, such as the min-max approach, which considers the worst-case scenario.

The robust TMPC approach has garnered increased interest in AUV motion control, and this trend is expected to continue due to its ability to achieve effective trajectory tracking, often with theoretical stability guarantees under disturbances. However, tracking curved trajectories is challenging as it is difficult to obtain a linear stabilising feedback controller to characterise the state and input tubes. To address this in horizontal motion control, the work [264] proposed a technique that requires solving two nonlinear optimisation problems, which may pose challenges for deployment in real applications due to computational complexity. The 3D trajectory tracking approach proposed by [17] based on a 5-DoF model involves sequentially solving two quadratic optimisation problems and an SD-DARE. Moreover, there is a lack of research using the 6-DoF model, which would eliminate the need for an additional method to pre-stabilise roll motion. Hence, this research area presents ample opportunities for future investigation and development.

In the context of path-following control, robust energy-optimal methods have been introduced to enhance robustness in MPC design through the computation of robust optimal reference signals [21, 265]. Further exploration is warranted in this area to develop schemes that consider time-varying disturbances. The study of coupled AUVs with up to 6-DoF remains an open challenge, particularly for waypoint-following. Indeed, disturbance handling has received more attention in the context of trajectory tracking and dynamic positioning compared to path-following from an MPC perspective. So, studies may seek to advance the deployment of MPC in this area, particularly for 3D path-following control.

In the domain of min-max MPC design for AUV motion control, there is still considerable potential for exploration. Min-max MPC design is appealing for its ability to ensure robust satisfaction of system constraints. While the work by [262] provided an NMPC algorithm for horizontal motion control, further research can

focus on the development of quasi or relaxed min-max MPC algorithms [267–269]. These avenues offer promising opportunities for investigation, especially considering the growing interest in approaches where the AUV model may be formulated as an LTV system. Hence, avoiding the need for obtaining a nonlinear optimisation control problem. For the AUV horizontal model, researchers may consider formulating the system as a LPV system with the yaw angle as the parameter. Furthermore, limited attention has been given to the use of higher-order models in min-max MPC in AUV control problems, and this area warrants further investigation as it provides a relatively straightforward approach to robustly satisfy system constraints.

Indeed, the increasing role of data-driven methods in AUV motion control cannot be overlooked. Traditionally, designing MPC-based motion controllers involves a two-stage process: system identification followed by controller design [12]. However, due to the complex nature of AUV systems, including cross-coupling, hydrodynamic forces, nonlinearities, and disturbances, developing accurate mathematical models is challenging. Data-driven MPC strategies, such as those proposed by [216, 254, 255], offer a promising solution by leveraging input-output data obtained from AUVs, thereby bypassing the need for extensive system identification. Given the rapid advancements in computing, artificial intelligence and the potential impact of data-driven control methods on advanced motion control, it is evident that future research will persist in advancing this research domain. The author argues that enhancing mathematical models with intelligent techniques will likely gain greater industry acceptance, at least in the near future, as mathematical models offer a clearer understanding of system behaviour compared to relying solely on input-output data.

3.7 Summary

This chapter provides an overview of MPC-based motion controller design for unmanned marine vehicles, with a specific focus on disturbance-handling strategies. It reviews state-of-the-art design strategies for MPC-based motion controllers, cat-

egorising them into increment variable-based approaches, observation-based approaches, and robust MPC-based approaches. The review highlights the strengths and weaknesses of various strategies, along with subtleties related to the design, implementation and performance. Despite the advancement of various techniques for disturbance handling in MPC-based motion controllers for AUVs, the pursuit of safer disturbance handling methods within MPC algorithms, especially for 3D motion control applications, remains ongoing.

Section 3.6 explores potential areas for research aimed at enhancing the performance of AUVs in the presence of environmental disturbances. The survey underscores the necessity for research endeavours aimed at addressing the key issues highlighted by the research questions of this thesis as outlined in the first chapter. Some of the identified key issues that motivated the research carried out in this thesis are listed below.

- The limitations of MPC-based algorithms that rely on partial velocity form MPC and disturbance estimation for the dynamic positioning of AUVs subject to time-varying environmental disturbances.

- Existing works have not employed velocity MPC for AUV motion control in either 2D or 3D motion control. This may be due to the need for model augmentation, which can increase computational cost and negatively affect model properties.

- Although tube-based MPC is well recognised for its advantages in the AUV literature, none of the studies have employed the full-order model for control design. Furthermore, the computational cost of existing strategies for reduced-order models may be prohibitive for real-time implementation.

- While MPC controllers for AUVs typically account for input constraints, they rarely address input rate constraints, thereby overlooking potential saturation issues in practical applications.

- The requirement of efficient energy utilisation during path-following control of marine vehicles where the reference path is not subject to time constraints.

In the subsequent chapters, this work aims to address the research gaps identified above in the realm of 3D motion control using 6-DoF design models, as described in Chapter 2.

Chapter 4

Velocity Form MPC for Dynamic Positioning and Trajectory Tracking of an Autonomous Underwater Vehicle

4.1 Introduction

The operational duration of an AUV is limited by the internal battery which typically acts as the sole energy source. Remotely operated docking stations have been developed to avoid frequent launching and recovery tasks of the vehicle, enabling charging and data upload to be performed underwater [40]. For AUVs with underwater docking stations, it is necessary to steer the vehicle during underwater operations through desired trajectories which may be curved before returning to the docking point where the vehicle needs to maintain a defined constant position for docking. In the literature [26,28,270], the trajectory tracking and dynamic positioning problems are often studied separately because it is challenging to provide good performance in both curved and constant reference signal tracking by AUVs subject

to disturbances. In the AUV context, tracking constant reference signals is known as dynamic positioning which is closely related to point stabilisation [28]. Many studies [25, 271] on AUV control have been dedicated to trajectory tracking tasks without necessarily considering how the proposed controllers would perform when tracking piece-wise constant signals under persistent disturbances such as ocean currents. The need to consider the effects of both ocean currents and waves adds complexity to the controller design.

This chapter is divided into two main parts. In the first part, the dynamic positioning control of an AUV is considered for docking operations in the presence of varying tidal currents. The AUV model is described by a dynamic model and a kinematic model, both formulated as LPV systems. A *velocity form* LPVMPC1 scheme is proposed, in which the AUV dynamic model is used for the states and the kinematic model is used for the output. The interdependence of the AUV kinematic model and dynamic model is exploited to avoid increased state dimension. This complete velocity form controller design enables the cancellation of disturbance effects through the use of the AUV's velocity vector increment for predicting the future evolution of the system.

The second part of the chapter considers combined trajectory tracking and dynamic positioning. This is achieved by proposing an alternative velocity form LPVMPC2 strategy that can effectively steer AUVs along 3D trajectories that may be curved, and also provide effective tracking of piece-wise constant reference signals required to maintain a desired position and orientation as in underwater docking operations. The second controller uses the increment in AUV position and velocity vectors without requiring model augmentation.

The main contributions of this chapter are described in the following points.

1. A LPVMPC1 algorithm is developed that uses the interdependence between the kinematic and dynamic equations of an AUV to formulate a *velocity form* prediction model. The model depends on the AUV velocity increment to cancel

disturbances, enabling effective dynamic positioning control.

2. A combined trajectory tracking and dynamic positioning controller is developed. In conventional velocity form MPC algorithms [234,235,272], augmented models are used which can lead to increased computational requirements due to increased state dimensions. This challenge is reported [236] to be a limiting factor for the wide use of velocity form MPC algorithm to high-order systems. The developed novel velocity LPVMPC2 algorithm does not require model augmentation. Here, both increments in position and velocity variables are employed in the prediction model to mitigate disturbances. The velocity form LPVMPC2 problem is formulated to ensure closed-loop asymptotic stability through the imposition of terminal state constraints.

3. To smoothly transition from 3D trajectory tracking to dynamic positioning and avoid jump discontinuity, a time parameterization of the transition path is proposed. This helps mitigate abrupt changes in input forces and velocities during the transition phase.

4. The developed LPVMPC2 scheme can cope with tracking reachable references and also trajectories including unreachable points. For AUVs operating in a constrained workspace, this feature can be used to ensure the AUV remains within the workspace boundaries that define the set of reachable output references.

The remainder of this chapter is structured as follows. Section 4.2 outlines the proposed velocity form LPVMPC algorithm for dynamic positioning control of AUVs. In Section 4.3, the alternate velocity MPC strategy is developed for combined trajectory tracking and dynamic positioning. Concluding remarks are provided in Section 4.4.

4.2 AUV Positioning Control - a Velocity Form LPVMPC Approach

This section presents the development of a velocity LPVMPC strategy, denoted LPVMPC1, for dynamic positioning control of an AUV by exploiting the interdependence of the dynamic and kinematic models.

4.2.1 A Systematic Synthesis of the Velocity Form Prediction Model

In [25], a predictive control algorithm based on partial velocity model was developed for AUV path tracking, in which $\boldsymbol{\eta}(k)$ was taken as the state vector and $\boldsymbol{\nu}(k)$ as the virtual control input to be computed such that $\boldsymbol{\eta}(k)$ follows a time-parameterised desired reference, $\boldsymbol{\eta}_d(k)$. Consequently, the velocity given as $\boldsymbol{\nu}(k) = \boldsymbol{\Delta\nu}(k)+\boldsymbol{\nu}(k-1)$, was augmented with the kinematic equation to formulate the prediction model. With this approach, the effects of disturbance can be mitigated only when an observer is used to estimate the control signal employed in the augmented state prediction model [233]. As a result, the complete velocity form MPC design approach, which is well-known for attenuating disturbance effects [234, 235, 273], is considered in this chapter.

In the design of the positioning controller, the effects of tidal currents are considered. Tidal current (2.11) is simulated using a V_c as the resultant speed with variations in the current disturbances caused by the time-dependent angle of attack $\alpha_c(t)$ and side slip $\beta_c(t)$. Since the assumption of a zero mean disturbance is not always practical, a constant offset term is introduced into the current disturbance

to obtain:

$$\boldsymbol{\nu}_c = \begin{bmatrix} V_c\cos(\alpha_c(t))\cos(\beta_c(t)) + d_x \\ V_c\sin(\beta_c(t)) + d_y \\ V_c\sin(\alpha_c(t))\cos(\beta_c) + d_z \\ 0 \\ 0 \\ 0 \end{bmatrix}. \tag{4.1}$$

To allow controller design without an observer, the motion dynamic model is used rather than the kinematic model as a basis for controller design. The developed complete velocity form of the predictive model minimises the impact of model mismatch as well as constant-type/slowly-varying disturbances via the use of increments in the AUV's velocities.

Since the ocean current is unknown to the controller, the model in (2.14) is used solely for the vehicle's motion simulation. As a result, the discretised kinematic and dynamic equations used for controller design are not based on $\boldsymbol{\nu}_r$ but $\boldsymbol{\nu}$ as follows.

$$\boldsymbol{\eta}(k+1) = \boldsymbol{\eta}(k) + \mathbf{J}(\boldsymbol{\nu}(k))T_s\boldsymbol{\nu}(k), \tag{4.2}$$

$$\begin{aligned} \boldsymbol{\nu}(k+1) = &\left(\mathbf{I} - \mathbf{M}^{-1}(\mathbf{C}(\boldsymbol{\nu}(k)) + \mathbf{D}(\boldsymbol{\nu}(k)))T_s\right)\boldsymbol{\nu}(k) \\ &+ \mathbf{M}^{-1}\boldsymbol{\tau}(k)T_s - \mathbf{M}^{-\mathbf{1}}\mathbf{g}(\boldsymbol{\eta})T_s, \end{aligned} \tag{4.3}$$

where T_s is the sampling time, $\mathbf{I} \in \mathbb{R}^{6\times 6}$ is the identity matrix of appropriate dimension. This LPV model in (4.2)-(4.3) is used for controller design while the nonlinear model (2.14) is used for AUV motion simulation.

Using the motion dynamic model in (4.3) as the transient state model and the kinematic model in (4.2) as the output, the following LPV discrete-time state space model is established by setting $\mathbf{g}(\boldsymbol{\eta}) = \mathbf{0}$ for the AUV.

$$\boldsymbol{\nu}(k+1) = \mathbf{E}(k)\boldsymbol{\nu}(k) + \mathbf{F}\boldsymbol{\tau}(k), \tag{4.4}$$

$$\mathbf{y}(k+1) = \mathbf{H}(k)\boldsymbol{\nu}(k) + \mathbf{y}(k), \tag{4.5}$$

in which $\mathbf{E}(k) = \mathbf{I} - \mathbf{M}^{-1}(\mathbf{C}(\boldsymbol{\nu}(k)) + \mathbf{D}(\boldsymbol{\nu}(k)))T_s$, $\mathbf{F} = \mathbf{M}^{-1}T_s$, $\mathbf{H}(k) = \mathbf{J}(\boldsymbol{\eta}(k))T_s$ and the output, $\mathbf{y}(k)$, is the vehicle position and pose vector.

To reduce steady-state error due to disturbances in the control scheme, consider the impact of the unknown ocean current on the AUV velocity as $\boldsymbol{\nu}(k) = \boldsymbol{\nu}_r(k) + \boldsymbol{\nu}_c(k)$. Hence, the vehicle velocity increment is defined as

$$\boldsymbol{\Delta\nu}(k) = \boldsymbol{\Delta\nu}_r(k) + \boldsymbol{\Delta\nu}_c(k), \tag{4.6}$$

where $\boldsymbol{\Delta\nu}(k) = \boldsymbol{\nu}(k) - \boldsymbol{\nu}(k-1)$, $\boldsymbol{\Delta\nu}_r(k) = \boldsymbol{\nu}_r(k) - \boldsymbol{\nu}_r(k-1)$ and $\boldsymbol{\Delta\nu}_c(k) = \boldsymbol{\nu}_c(k) - \boldsymbol{\nu}_c(k-1)$. By using the vehicle's velocity increment in (4.6), the effect of the slowly-varying component of the unknown ocean current $\boldsymbol{\nu}_c(k)$ can be minimised and the constant offset term can be cancelled.

The following velocity form model is written from the LPV model in (4.4) - (4.5).

$$\boldsymbol{\xi}(k+1) = \tilde{\mathbf{A}}(k)\boldsymbol{\xi}(k) + \tilde{\mathbf{B}}\boldsymbol{\Delta\tau}(k) + \tilde{\mathbf{D}}\boldsymbol{\Delta}\mathbf{y}(k), \tag{4.7}$$

$$\mathbf{y}(k) = \tilde{\mathbf{G}}\boldsymbol{\xi}(k). \tag{4.8}$$

Here, $\boldsymbol{\xi}(k) = [\boldsymbol{\Delta\nu}^\top(k)\ \mathbf{y}^\top(k)]^\top$ is the augmented state vector, $\boldsymbol{\Delta}\mathbf{y}(k) = \mathbf{y}(k) - \mathbf{y}(k-1)$, $\boldsymbol{\Delta\tau}(k) = \boldsymbol{\tau}(k) - \boldsymbol{\tau}(k-1)$, and

$$\tilde{\mathbf{A}}(k) = \begin{bmatrix} \mathbf{E}(k) & \mathbf{0} \\ \mathbf{H}(k) & \mathbf{I} \end{bmatrix}, \tilde{\mathbf{B}} = \begin{bmatrix} \mathbf{F} \\ \mathbf{0} \end{bmatrix}, \tilde{\mathbf{D}} = \begin{bmatrix} \mathbf{0} \\ \mathbf{I} \end{bmatrix}, \tilde{\mathbf{G}} = \begin{bmatrix} \mathbf{0} & \mathbf{I} \end{bmatrix}. \tag{4.9}$$

For all $j = 1, \ldots, N$, $\boldsymbol{\xi}(k+j|k)$ denotes the j-th prediction of $\boldsymbol{\xi}$, at time k. To avoid the computational burden associated with the update of the LPV model in each prediction instant [274], the following assumption is made.

Assumption 1. *At each sampling instant,* $\tilde{\mathbf{A}}(k+j|k) = \tilde{\mathbf{A}}(k|k) = \tilde{\mathbf{A}}(k)$ *for all* $j = 1, \ldots, N$.

Based on Assumption 1, the output prediction using (4.7)-(4.8) gives

$$\mathbf{Y}(k) = \mathbf{A}_p(k)\boldsymbol{\xi}(k) + \mathbf{B}_p(k)\Delta\mathbf{U}(k) + \mathbf{D}_p(k)\boldsymbol{\Delta}\mathbf{Y}(k), \tag{4.10}$$

in which

$$\mathbf{Y}(k) = \begin{bmatrix} \mathbf{y}(k+1|k) \\ \mathbf{y}(k+2|k) \\ \vdots \\ \mathbf{y}(k+N|k) \end{bmatrix}, \ \Delta\mathbf{Y}(k) = \begin{bmatrix} \boldsymbol{\Delta}\mathbf{y}(k|k) \\ \boldsymbol{\Delta}\mathbf{y}(k+1|k) \\ \vdots \\ \boldsymbol{\Delta}\mathbf{y}(k+N-1|k) \end{bmatrix},$$

$$\mathbf{A}_p(k) = \begin{bmatrix} \tilde{\mathbf{G}}\tilde{\mathbf{A}}(k) \\ \tilde{\mathbf{G}}\tilde{\mathbf{A}}(k)^2 \\ \vdots \\ \tilde{\mathbf{G}}\tilde{\mathbf{A}}(k)^N \end{bmatrix}, \ \Delta\mathbf{U}(k) = \begin{bmatrix} \boldsymbol{\Delta}\boldsymbol{\tau}(k|k) \\ \boldsymbol{\Delta}\boldsymbol{\tau}(k+1|k) \\ \vdots \\ \boldsymbol{\Delta}\boldsymbol{\tau}(k+N_u-1|k) \end{bmatrix},$$

$$\mathbf{B}_p(k) = \begin{bmatrix} \tilde{\mathbf{G}}\tilde{\mathbf{B}} & \mathbf{0} & \cdots & \mathbf{0} \\ \tilde{\mathbf{G}}\tilde{\mathbf{A}}(k)\tilde{\mathbf{B}} & \tilde{\mathbf{G}}\tilde{\mathbf{B}} & \cdots & \mathbf{0} \\ \vdots & \vdots & \ddots & \vdots \\ \tilde{\mathbf{G}}\tilde{\mathbf{A}}(k)^{N-1}\tilde{\mathbf{B}} & \tilde{\mathbf{G}}\tilde{\mathbf{A}}(k)^{N-2}\tilde{\mathbf{B}} & \cdots & \tilde{\mathbf{G}}\tilde{\mathbf{A}}(k)^{N-N_u}\tilde{\mathbf{B}} \end{bmatrix},$$

$$\mathbf{D}_p(k) = \begin{bmatrix} \tilde{\mathbf{G}}\tilde{\mathbf{D}} & \mathbf{0} & \cdots & \mathbf{0} \\ \tilde{\mathbf{G}}\tilde{\mathbf{A}}(k)\tilde{\mathbf{D}} & \tilde{\mathbf{G}}\tilde{\mathbf{D}} & \cdots & \mathbf{0} \\ \vdots & \vdots & \ddots & \vdots \\ \tilde{\mathbf{G}}\tilde{\mathbf{A}}(k)^{N-1}\tilde{\mathbf{D}} & \tilde{\mathbf{G}}\tilde{\mathbf{A}}(k)^{N-2}\tilde{\mathbf{D}} & \cdots & \tilde{\mathbf{G}}\tilde{\mathbf{D}} \end{bmatrix}.$$

Here, N_u is the control horizon for MPC, $1 \leq N_u \leq N$. Since constant output increment $\Delta\mathbf{y}(k)$ is known in every time step, define $\boldsymbol{\Delta}\mathbf{y}(k+j|k) = \boldsymbol{\Delta}\mathbf{y}(k)$ for all $j = 1, \ldots, N$, which means that $\Delta\mathbf{Y}(k) = \mathbf{1}_{N\times 1} \otimes \Delta\mathbf{y}(k)$.

Remark 1. *It is noted that $\tilde{\mathbf{A}}(k)$ is the only time-varying matrix in the velocity predictive model (4.7)-(4.8) that needs to be computed at each time k to enable the output prediction over horizon N.*

4.2.2 Velocity Form LPVMPC1 Algorithm

Take $\Delta\mathbf{U}(k) = \begin{bmatrix}\Delta\boldsymbol{\tau}(k|k)^\top & \cdots & \Delta\boldsymbol{\tau}(k|k+N_u-1)^\top\end{bmatrix}^\top$ as the vector of the decision variables at time k, the FHOCP for the AUV to follow a desired position $\mathbf{y}_d(k)$ is formulated as follows.

$$\begin{aligned}\Delta\mathbf{U}^*(k) = \arg\min_{\boldsymbol{\Delta\tau}(k+i|k)} & \parallel \mathbf{y}(k+N|k) - \mathbf{y}_d(k+N|k) \parallel^2_{\mathbf{P}} \\ & + \sum_{j=1}^{N-1} \parallel \mathbf{y}(k+j|k) - \mathbf{y}_d(k+j|k) \parallel^2_{\mathbf{Q}} + \sum_{i=0}^{N_u-1} \parallel \Delta\boldsymbol{\tau}(k+i|k) \parallel^2_{\mathbf{R}} \\ & \text{s.t. (4.7) \& (4.8)}, \\ & \mathbf{y}_{\min} \leq \mathbf{y}(k) \leq \mathbf{y}_{\max},\end{aligned} \tag{4.11}$$

where $\mathbf{P}, \mathbf{Q} \succeq \mathbf{0} \in \mathbb{R}^{6\times6}$ and $\mathbf{R} \succ \mathbf{0} \in \mathbb{R}^{6\times6}$. The two terms $\mathbf{y}_{\max}$ and $\mathbf{y}_{\min}$ define the maximum and minimum bounds on the position and orientation/pose output by incorporating the constraint on the pitch angle $|\theta| < \pi/2$ and the AUV depth $z \leq 0$ m.

The MPC problem can be written in a more compact form by making the following definitions:

$$\tilde{\mathbf{R}} = \texttt{blkdiag}(\mathbf{R}, \ldots, \mathbf{R}),$$

$$\tilde{\mathbf{Q}} = \texttt{blkdiag}(\mathbf{Q}, \ldots, \mathbf{Q}, \mathbf{P}),$$

$$\mathbf{Y}_d(k) = \begin{bmatrix}\mathbf{y}_d(k+1|k)^\top & \ldots & \mathbf{y}_d(k+N|k)^\top\end{bmatrix}^\top.$$

The resulting quadratic program (QP) to be solved at each sampling time is written as

$$\begin{aligned}\Delta\mathbf{U}^*(k) = \arg\min\ & \frac{1}{2}\Delta\mathbf{U}(k)^\top\boldsymbol{\Pi}(k)\Delta\mathbf{U}(k) + \mathbf{f}(k)^\top\Delta\mathbf{U}(k) \\ \text{s.t.}\quad & \boldsymbol{\Gamma}\Delta\mathbf{U}(k) \leq \mathbf{b},\end{aligned} \tag{4.12}$$

where

$$\boldsymbol{\Pi}(k) = 2(\mathbf{B}_p(k)^\top\tilde{\mathbf{Q}}\mathbf{B}_p(k) + \tilde{\mathbf{R}}),$$

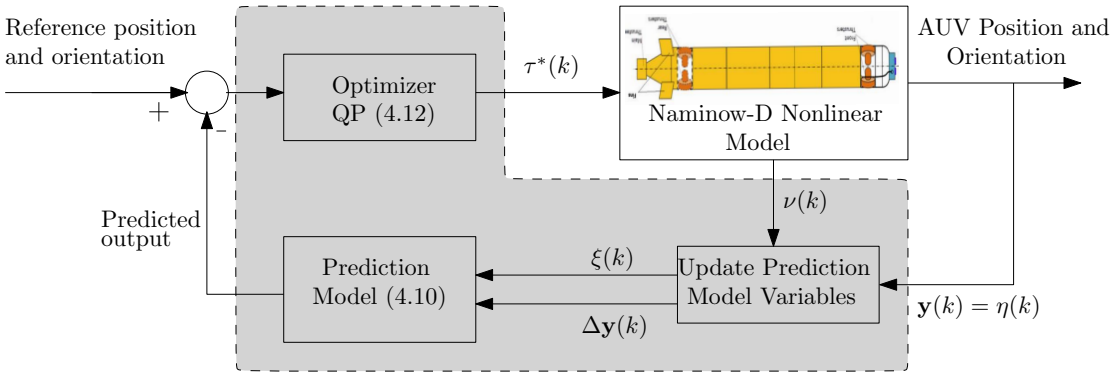

Fig. 4.1: Proposed LPVMPC1 control system configuration.

$$\mathbf{f}(k) = 2\mathbf{B}_p(k)^\top \tilde{\mathbf{Q}}(\mathbf{A}_p(k)\boldsymbol{\xi}(k) + \mathbf{D}_p(k)\boldsymbol{\Delta}\mathbf{y}_p(k) - \mathbf{Y}_\mathbf{d}(k)),$$

$$\boldsymbol{\Gamma} = \begin{bmatrix} \mathbf{B}_p(k) \\ -\mathbf{B}_p(k) \end{bmatrix}, \mathbf{b} = \begin{bmatrix} \mathbf{Y}_{\max} - \mathbf{A}_p(k)\boldsymbol{\xi}(k) - \mathbf{D}_p(k)\Delta\mathbf{Y}(k) \\ -\mathbf{Y}_{\min} + \mathbf{A}_p(k)\boldsymbol{\xi}(k) + \mathbf{D}_p(k)\Delta\mathbf{Y}(k) \end{bmatrix},$$

$$\mathbf{Y}_{\max} = \mathbf{1}_{N\times 1} \otimes \mathbf{y}_{\max}, \ \mathbf{Y}_{\min} = \mathbf{1}_{N\times 1} \otimes \mathbf{y}_{\min}.$$

where $\otimes$ denotes the Kronecker product. Based on the receding horizon principle, $\boldsymbol{\Delta\tau}^*(k) = \boldsymbol{\Delta\tau}^*(k|k)$, and the forces and moments applied to the vehicle at each time step is

$$\boldsymbol{\tau}^*(k) = \boldsymbol{\Delta\tau}^*(k) + \boldsymbol{\tau}(k-1). \tag{4.13}$$

The proposed velocity form LPVMPC control system configuration is shown in Fig. 4.1. The control strategy implementation steps are summarised in Algorithm 1.

4.2.3 Benchmark Controllers

The benchmark algorithm is the original predictive controller jointly developed by Industrial Systems & Control Ltd and Mitsubishi Heavy Industries Ltd for the dynamic positioning of the Naminow-D AUV [1]. Recall the definition of the state vector $\mathbf{x} := [\boldsymbol{\eta}^\top \ \boldsymbol{\nu}^\top]^\top \in \mathbb{R}^{12}$ in (2.14), the continuous-time nonlinear dynamic model (2.14) of the AUV can be written in state-dependent form as:

$$\dot{\mathbf{x}} = \mathbf{A}_c(\mathbf{x})\mathbf{x} + \mathbf{B}_c\boldsymbol{\tau} + \mathbf{D}_c\mathbf{g}(\boldsymbol{\eta}) + \mathbf{B}_c\boldsymbol{\tau}^w, \tag{4.14}$$

Algorithm 1: Velocity form LPVMPC1 algorithm

Input: Set up $\mathbf{Q}$, $\mathbf{R}$, N, N_u, and the desired output trajectory $\mathbf{y}_d(k)$.

$k \leftarrow 0$
Get the measurements of current position $\boldsymbol{\eta}(k)$ and velocities $\boldsymbol{\nu}(k)$.
repeat
  Compute the augmented state $\mathbf{x}(k)$ and the output increment $\boldsymbol{\Delta}\mathbf{y}(k)$.
  Determine $\mathbf{E}(k)$ and $\mathbf{H}(k)$ to update $\tilde{\mathbf{A}}(k)$.
  Calculate the model prediction using (4.7) and (4.10).
  Solve the optimisation problem in (4.12) to find $\Delta\mathbf{U}^*(k)$.
  Take the first element of $\Delta\mathbf{U}^*(k)$ as $\boldsymbol{\Delta\tau}^*(k) = \boldsymbol{\Delta\tau}^*(k|k)$.
  Calculate the optimal forces and torques vector $\boldsymbol{\tau}(k)^*$ using (4.13).
  Implement $\boldsymbol{\tau}^*(k)$ for one sampling period.
  Update the state measurement as $\mathbf{x}(k+1)$.
  $k \leftarrow k+1$
until end

in which

$$\mathbf{A}_c(\mathbf{x}) = \begin{bmatrix} \mathbf{0} & \mathbf{J}(\boldsymbol{\eta}) \\ \mathbf{0} & -\mathbf{M}^{-1}(\mathbf{C}(\boldsymbol{\nu}) + \mathbf{D}(\boldsymbol{\nu})) \end{bmatrix},$$

$$\mathbf{B}_c = \begin{bmatrix} \mathbf{0} \\ \mathbf{M}^{-1} \end{bmatrix}, \mathbf{D}_c = \begin{bmatrix} \mathbf{0} \\ -\mathbf{M}^{-1} \end{bmatrix}.$$

Here, $\mathbf{0} \in \mathbb{R}^{6\times6}$ is the zero matrix. Since wave-induced disturbances are neglected due to their minimal effects in deep underwater conditions [6], the model is expressed as:

$$\dot{\mathbf{x}} = \mathbf{A}_c(\mathbf{x})\mathbf{x} + \mathbf{B}_c\boldsymbol{\tau} + \mathbf{w}, \tag{4.15}$$

where $\mathbf{w}$ is the system disturbance due to model mismatch and environmental disturbance due to ocean currents. By using the sampling period T_s, the discrete-time state space model for control design is obtained as:

$$\mathbf{x}(k+1) = \mathbf{A}_\mathbf{x}\mathbf{x}(k) + \mathbf{B}\boldsymbol{\tau}(k) + \mathbf{w}(k), \tag{4.16}$$

$$\mathbf{y}(k) = \mathbf{G}\mathbf{x}(k), \tag{4.17}$$

where $\mathbf{A_x} = \mathbf{A}(\mathbf{x}(k))$ for compactness and the matrices in (4.16) and (4.17) are given by

$$\mathbf{A_x} = \begin{bmatrix} \mathbf{I} & \mathbf{J}(\boldsymbol{\eta}(k))T_s \\ \mathbf{0} & \mathbf{I} - \mathbf{M}^{-1}(\mathbf{C}(\boldsymbol{\nu}(k)) + \mathbf{D}(\boldsymbol{\nu}(k)))T_s \end{bmatrix}, \tag{4.18}$$

$$\mathbf{B} = \begin{bmatrix} \mathbf{0} \\ \mathbf{M}^{-1}T_s \end{bmatrix}, \mathbf{G} = \begin{bmatrix} \mathbf{I} & \mathbf{0} \end{bmatrix}, \tag{4.19}$$

where $\mathbf{I} \in \mathbb{R}^{6\times6}$ is an identity matrix. To counter the impact of ocean currents, the unknown disturbance $\mathbf{w}(k)$ in (4.16) was estimated using the Kalman filtering technique to improve the accuracy of the prediction model [1]. This benchmark algorithm was proposed under the assumption that the tidal current disturbance is bounded and constant. In addition to the benchmark controller, the algorithm based on the increment variable-based MPC in [25], which adopts the partial velocity form strategy, is also employed for comparison to the proposed algorithm.

4.2.4 Simulation Results

4.2.4.1 Simulation Set-up

The simulation study considers the positioning control of the Naminow-D AUV. The model parameters of the AUV are given in Table 2.3. The task is to drive the AUV to the docking position, where it can be caught by remote operation. The AUV model, the control algorithms and operating conditions are developed in `MATLAB` environment. To implement the controllers, the `quadprog` solver is used to solve the formulated QP. The transformation matrix $\mathbf{J}(\boldsymbol{\eta})$ is the standard 6 DoF transformation matrix with $|\theta| \leq 2\pi/5$ rad. The ocean current speed is $V_c = 0.2$ m/s with $\alpha_c = 0.002t$, $\beta_c(t) = (3\pi/20)t$ and the offset terms are $d_x = 0.2$ m/s, $d_y = 0.2$ m/s and $d_z = 0.15$ m/s.

The initial position and orientation of the AUV is given by $\mathbf{y}(0) = [0\ 0\ 0\ 0\ 0\ 0]^\top$. Despite the effects of time-varying tidal currents, the control objective is to position

the AUV as close as possible to $\mathbf{y}_d(0) = [0.5\ 0.5\ 0\ 0\ 0\ 0]^\top$. The proposed complete velocity form LPVMPC1, Algorithm 1, is denoted as MPC1, the benchmark controller in [1] is denoted as MPC2, and the partial velocity form LPVMPC method in [25] is denoted as MPC3. The manually tuned parameters for the three controllers are listed in Table 4.1. While the three controllers use the same control and prediction horizons, the weighting matrices differ significantly because the algorithms are fundamentally different in design. Overall, the tuned controller parameters are selected to minimise the AUV's position and orientation tracking errors as much as possible.

Table 4.1: Controllers turning parameters.

Parameter	**Symbol**	MPC1	MPC2	MPC3
Prediction horizon	N	20	20	20
Control horizon	N_u	2	2	2
Control weights	$\mathbf{R}$	$2 \times 10^{-3}\mathbf{I}$	$2 \times 10^{-3}\mathbf{I}$	$20\mathbf{I}$
Output weights	$\mathbf{Q}$	$1000\mathbf{I}$,	$\text{diag}(1, 1, 1, .1, .1, .1)$	$\mathbf{I}$
Terminal weights	$\mathbf{P}$	DARE*	$10^5\mathbf{I}$	DARE*

*Solution to the discrete-time algebraic Riccati equation (DARE) based on the `dare` function in MATLAB.

The measurement noises in the installed INS sensors are considered additive white Gaussian noise. Two scenarios are studied for conditions with and without tidal currents.

4.2.4.2 Test without Ocean Current

In the absence of current, the simulation results are presented in Fig. 4.2. All three predictive controllers achieve the desired position and orientation at steady state. Compared to the benchmark MPC2, the proposed MPC1 is less sensitive to measurement noise and provides reduced output peaks and control input oscillations. MPC3 tends to show reduced sensitivity to measurement noise, which can be explained by the fact that the computed input signals are not directly dependent

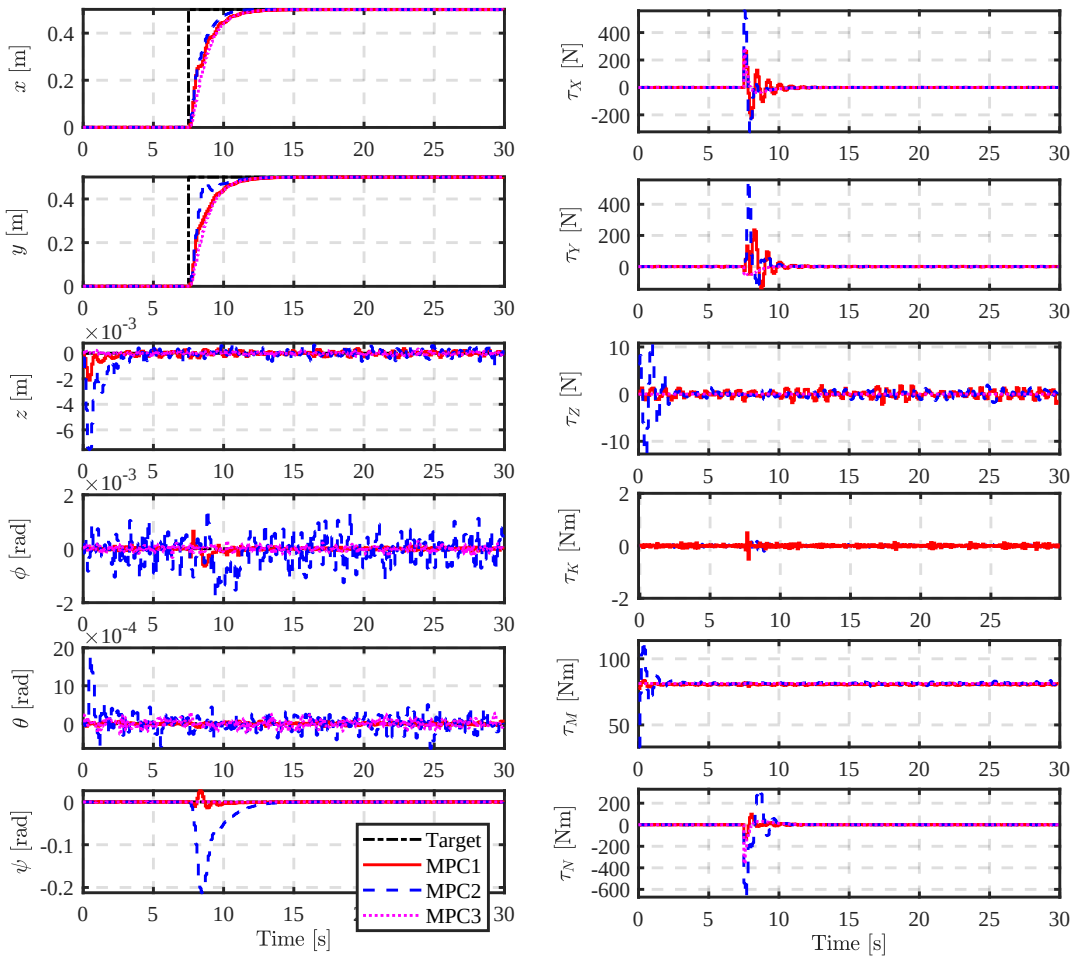

Fig. 4.2: No current test: controlled output (left) and manipulated variables (right) of the AUV.

on the measured states but on the optimal velocities computed by an intermediate control law.

4.2.4.3 Test under Ocean Current

The results under the time-varying tidal current are shown in Fig. 4.3. At steady-state, MPC1 removes tracking error and shows minimal oscillations due to time-varying tidal disturbances. MPC2 also minimises tracking error but yields significant oscillations due to the disturbances. MPC3 fails to eliminate the tracking error and shows the largest oscillations among the three controllers. It is worth noting that

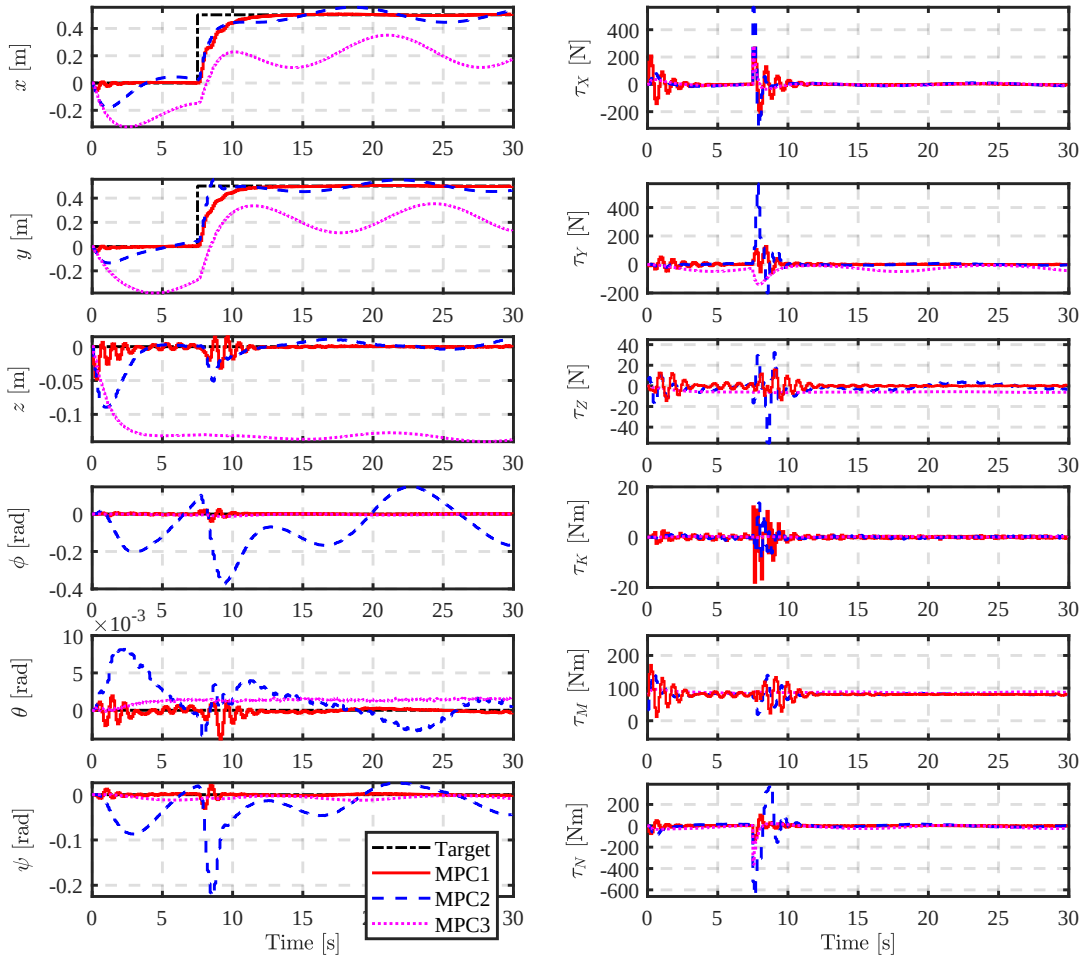

Fig. 4.3: Tidal current test: controlled output (left) and manipulated variables (right) of the AUV.

MPC1 performance under the influence of ocean current is close to the no-current test results in Section 4.2.4.2, which demonstrates the effectiveness of the proposed scheme in handling tidal currents.

The three controllers are compared for both maximum current and no current conditions. The results are shown in Table 4.2 using the root-mean-square-error (RMSE), calculated based on the difference between the controlled output and the desired values. A smaller RMSE value means a smaller accumulated tracking error over the simulation time range. The results show that the proposed MPC1 provides smaller RMSE values than MPC2 for all outputs in both scenarios. Whereas MPC3

generally gives the competitive RMSE values among the three controllers under the no-current test, its performance deteriorates greatly under the maximum current test. For MPC2, the variables z, ϕ and θ show large oscillations. Thus, the reliance on Kalman filter by MPC2 for disturbance rejection is not effective for time-varying disturbances and tends to increase the controller's sensitivity to measurement noise. It can be concluded that, under the influence of time-varying ocean current disturbances, the developed MPC1 show superior performance over MPC2 and MPC3 by providing smaller tracking errors in the AUV position and orientation and smoother control activities.

Table 4.2: RMSE-based performance comparison of predictive controllers.

	MPC1		MPC2		MPC3	
Output/ Unit	No Current	Maximum Current	No Current	Maximum Current	No Current	Maximum Current
x/mm	70.6	71.9	71.5	84.2	69.5	302.2
y/mm	69.1	69.3	68.9	73.2	68.3	304.6
z/mm	0.6	3.1	0.7	14.7	0.1	129.6
ϕ/mrad	0.09	5.4	0.2	55.2	0.1	4.4
θ/mrad	0.2	1.2	0.3	2.8	0.05	1.3
ψ/mrad	1.1	4.2	19.5	33.0	0.1	7.4

4.3 Combined Trajectory Tracking and Dynamic Positioning of an AUV

This section introduces the velocity LPVMPC designed for combined trajectory tracking and dynamic positioning. This algorithm is denoted LPVMPC2. This section includes a description of the system constraints including velocity and input constraints, a statement of the control problem, the MPC design and simulation results.

4.3.1 AUV Dynamics and Constraints

The 6-DoF AUV motion model given in (2.14) with ocean current and wave disturbances is considered. The generated forces and moments generated by the vehicle's thrusters are defined in a 6-DoF vector as $\boldsymbol{\tau} = [\tau_X \ \tau_Y \ \tau_Z \ \tau_K \ \tau_M \ \tau_N]^\top \in \mathbb{R}^{6\times 1}$. Their constraint sets are defined as follows:

$$\boldsymbol{\tau}_1 = [\tau_X \ \tau_Y \ \tau_Z \ ]^\top \in \mathcal{T}_1 \subseteq \mathbb{R}^3, \tag{4.20}$$

$$\boldsymbol{\tau}_2 = [\tau_K \ \tau_M \ \tau_N \ ]^\top \in \mathcal{T}_2 \subseteq \mathbb{R}^3, \tag{4.21}$$

for which the following is defined

$$\mathcal{T}_1 := \left\{ \boldsymbol{\tau}_1 \in \mathbb{R}^3 : |\tau_X|, |\tau_Y|, |\tau_Z| \leq \boldsymbol{\tau}_{1,\max} \right\}, \tag{4.22}$$

$$\mathcal{T}_2 := \left\{ \boldsymbol{\tau}_2 \in \mathbb{R}^3 : |\tau_K|, |\tau_M|, |\tau_N| \leq \boldsymbol{\tau}_{2,\max} \right\}. \tag{4.23}$$

Here $\boldsymbol{\tau}_{1,\max}$ and $\boldsymbol{\tau}_{2,\max}$ denote upper bounds on the input forces and moments, respectively. The constraint set is

$$\mathcal{T} := \left\{ \boldsymbol{\tau} \in \mathbb{R}^6 : |\boldsymbol{\tau}| \leq \boldsymbol{\tau}_{\max} \right\}, \tag{4.24}$$

where $\boldsymbol{\tau} = [\boldsymbol{\tau}_1^\top \ \boldsymbol{\tau}_2^\top]^\top$, $\tau_{\max} = [\boldsymbol{\tau}_{1,\max}^\top \ \boldsymbol{\tau}_{2,\max}^\top]^\top$.

Note that $\mathbf{J}(\boldsymbol{\eta})$ is singular for $\theta = \pm\pi/2$. Hence, the constraint $|\theta| < \pi/2$ is implemented to prevent this singularity problem. Moreover, it is desired that the translational velocities of the underwater vehicle have an upper bound since most tasks are performed at relatively low speeds [22]. Hence, the constraint set $\mathcal{X}$ for the state vector is defined as

$$\mathcal{X} := \left\{ \mathbf{x} \in \mathbb{R}^{12} : |\mathbf{x}| \leq \mathbf{x}_{\max} \right\}, \tag{4.25}$$

where $\mathbf{x}_{\max}$ defines a hard constraint on the state vector.

4.3.2 Problem Statement

Assume a smooth time-dependent desired trajectory defined by

$$\mathbf{y}_d(k) = \begin{bmatrix} x_d(k) & y_d(k) & z_d(k) & \phi_d & \theta_d & \psi_d \end{bmatrix}^\top. \tag{4.26}$$

After tracking (4.26), the AUV is required to accurately dock at the position with the specified orientation defined by

$$\mathbf{y}_{d,ss} = \begin{bmatrix} x_{d,ss} & y_{d,ss} & z_{d,ss} & \phi_d & \theta_d & \psi_d \end{bmatrix}^\top. \tag{4.27}$$

Note that although (4.26) is smooth, there may be a jump discontinuity between its final position and the desired docking position (4.27). The problem considered in this work includes two tasks:

1. 3D tracking. Steer the AUV, modelled by the nonlinear, coupled model for $x(k)$, $y(k)$ and $z(k)$ to follow $[x_d(k)\, y_d(k)\, z_d(k)]^\top$ until the AUV reaches the docking vicinity. The orientation variables, $\phi(k)$, $\theta(k)$ and $\psi(k)$, do not need to accurately track the desired orientation during this task period.

2. Dynamic positioning. When the AUV reaches the docking vicinity, the objective here is to maintain the vehicle at the desired position and orientation, $\mathbf{y}_{d,ss}$.

These two control objectives need to be achieved while ensuring

- the smooth transition from the 3D trajectory to the desired docking location;
- the capability to minimise the impact of environmental disturbances and model mismatch during trajectory tracking;
- the AUV can achieve, with minimum error, the desired position and orientation for docking via the integral action in the MPC controller;

- the physical limitations in the form of input saturation for forces and moments and state constraints for pitch angle and translational velocities are satisfied;
- the vehicle can track both reachable and unreachable reference signals.

4.3.3 Predictive Control Design

In this section, the design of a predictive controller is presented based on the LPV model of the AUV.

4.3.3.1 Prediction Model Formulation

The discretised model in (4.16) - (4.17) is used by ignoring the disturbance term, i.e., $\mathbf{d}(k) = \mathbf{0}$, as follows:

$$\begin{aligned} \mathbf{x}(k+1) &= \mathbf{A}_{\mathbf{x}}\mathbf{x}(k) + \mathbf{B}\boldsymbol{\tau}(k), \\ \mathbf{y}(k) &= \mathbf{G}\mathbf{x}(k), \end{aligned} \tag{4.28}$$

To reduce the impact of the modelling errors and external disturbances, the velocity form of MPC is considered. Specifically, a new formulation of the optimisation problem is employed where the state augmentation can be avoided. First, write the increment form of the LTV model as

$$\begin{aligned} \Delta\mathbf{x}(k+1) &= \mathbf{A}_{\mathbf{x}}\Delta\mathbf{x}(k) + \mathbf{B}\Delta\boldsymbol{\tau}(k), \\ \mathbf{y}(k) &= \mathbf{G}\Delta\mathbf{x}(k) + \mathbf{y}(k-1), \end{aligned} \tag{4.29}$$

where $\Delta\mathbf{x}(k) = \mathbf{x}(k) - \mathbf{x}(k-1)$, $\Delta\boldsymbol{\tau}(k) = \boldsymbol{\tau}(k) - \boldsymbol{\tau}(k-1)$, and there is an implicit velocity term $\Delta\nu(k) = \nu(k) - \nu(k-1)$.

The following assumptions are made for the LPV model.

Assumption 2.

1. *The sets defined by the constraints $\mathcal{X}$ in (4.25) and $\mathcal{T}$ in (4.24) are convex sets containing the origin.*

2. Model (4.28) is locally stabilisable for all $\mathbf{x}(k) \in \mathcal{X}$.

The second item in Assumption 2 implies that the pair $(\mathbf{A}_{\mathbf{x}}, \mathbf{B})$ is point-wise stabilisable in the linear sense for all $\mathbf{x} \in \mathcal{X}$.

4.3.3.2 Velocity Form LPVMPC2 Design

It is worth noting that trajectory generation algorithms typically produce smooth paths for navigation [6]. However, the transition towards the docking point specified by $\mathbf{y}_{d,ss}$ may result in a jump discontinuous reference signal. This can be addressed by parameterising the straight line joining the final point of the trajectory to the docking position. This may be done by defining $\mathbf{p}_t = [x_t \ y_t \ z_t]^\top$ as the tail of the smooth trajectory (4.26) and $\mathbf{p}_{d,ss} = [x_{d,ss} \ y_{d,ss} \ z_{d,ss}]^\top$. The transition must be performed at a low resultant speed defined as $U_s = \sqrt{u^2 + v^2 + w^2}$. Based on this, the transition time t_s can then be approximated as

$$t_s = \frac{\| \mathbf{p}_t - \mathbf{p}_{d,ss} \|}{U_s}. \tag{4.30}$$

Assuming the desired trajectory is sampled at T_s like the AUV model, it is important to clarify that t_s, measured in seconds is a continuous-time variable that should be divided by T_s to obtain its discrete equivalent in the discrete-time implementation of the controller. Define $h = m/t_s$ with $m = 1, 2, 3 \ldots$, then, the parameterisation is obtained as

$$\mathbf{p}_{d,ss}(k) = \begin{cases} (h-1)\mathbf{p}_t + h\mathbf{p}_{d,ss}, & \text{if } h \leq 1 \\ \mathbf{p}_{d,ss}, & \text{Otherwise} \end{cases} \tag{4.31}$$

where $\mathbf{p}_{d,ss}(k) = [x_{d,ss}(k) \ y_{d,ss}(k) \ z_{d,ss}(k)]^\top$.

Through (4.31), a smooth transition from the end of the 3D trajectory to the docking point can be achieved since $\mathbf{y}_{d,ss}$ is replaced by the time-parameterised reference signal defined by $\mathbf{y}_{d,ss}(k) = [x_{d,ss}(k) \ y_{d,ss}(k) \ z_{d,ss}(k) \ \phi_d \ \theta_d \ \psi_d]^\top$.

Several velocity/increment MPC algorithms have been developed for linear and nonlinear systems [234, 235, 273, 275]. The nonlinear method in [235] leads to a

quasi-LPV MPC, where the state vector increment is augmented with the system's output vector and used as the prediction model. Applying such a method in AUV control would increase the dimension of the state prediction model from $\mathbb{R}^{12}$ to $\mathbb{R}^{18}$, leading to increased computational cost. Moreover, the stabilisability of the augmented model may not be locally guaranteed even when the original system $(\mathbf{A_x}, \mathbf{B})$ is locally stabilisable since there would be a need to ensure that the original system has no zeros at the origin. In this work, a different approach is proposed in the implementation of the velocity form MPC, with the aim to achieve the tracking capability without applying state augmentation.

Define the set of reachable states in N steps as

$$\begin{aligned}\mathcal{R}_{\mathcal{X}}^{N} = \{\mathbf{x}_r(k) \mid \exists(\Delta\boldsymbol{\tau}(k|k), \ldots, \Delta\boldsymbol{\tau}(N-1|k) : \\ \Delta\mathbf{x}(k+j|k) = \mathbf{A_x}\Delta\mathbf{x}(k|k) + \sum_{i=0}^{j-1} \mathbf{A_x^i}\mathbf{B}\Delta\boldsymbol{\tau}(k+i|k), \\ \mathbf{x}(k+N|k) = \mathbf{x}_r(k),\ \mathbf{x}(k+j|k) \in \mathcal{X}, \\ \boldsymbol{\tau}(k+j-1|k) = \boldsymbol{\tau}(k-1) + \sum_{i=0}^{j-1} \Delta\boldsymbol{\tau}(k+i|k) \in \mathcal{U}, \\ \Delta\boldsymbol{\nu}(k+N|k) = \mathbf{0},\ j = 1, \ldots, N\}\,.\end{aligned}$$

The corresponding reachable output set is denoted by $\mathcal{R}_{\mathcal{Y}}^{N}$. For workspace constrained AUV operation, the translational position variables, (x, y, z), may become unreachable. To avoid this, define $\mathbf{r} \in \mathcal{Y}_r$, in which $\mathcal{Y}_r \subseteq \mathcal{Y}$ denotes the set that incorporate the workspace positional constraints. Then, the set for reachable output reference signal is defined as

$$\mathcal{R}_{\mathcal{Y}} = \left\{\mathbf{r} \in \mathcal{R}_{\mathcal{Y}}^{N} \mid \lambda\mathbf{r} + (1-\lambda)\mathbf{y}(k) \in \mathcal{R}_{\mathcal{Y}}^{N}, \mathbf{r} \in \mathcal{Y}_r\right\},$$

where $0 \leq \lambda \leq 1$ is a constant coefficient, ensuring $\mathbf{r}$ and $\mathbf{y}(k)$ belong to the same convex set of $\mathcal{R}_{\mathcal{Y}}^{N}$. Then, the reachable reference trajectory in every time step $\mathbf{r}(k)$,

is computed by solving the problem

$$\mathbf{r}(k) = \arg\min_{\mathbf{r}\in\mathcal{R}_{\mathcal{Y}}} \parallel \mathbf{r} - \mathbf{y}_d(k) \parallel^2_{\mathbf{P}_r}, \tag{4.32}$$

with $\mathbf{P}_r \succ \mathbf{0}$. Given the desired trajectory $\mathbf{y}_d(k)$ in (4.26), determine $\mathbf{r}(k)$ based on which the output error is defined as $\mathbf{y}_e(k+j|k) = \mathbf{r}(k+j|k) - \mathbf{y}(k+j|k)$. Then, the following cost function is considered:

$$V(\mathbf{r}(k), \mathbf{Y}_e(k), \Delta\mathbf{U}(k)) = \sum_{j=1}^{N-1} \parallel \mathbf{y}_e(k+j|k) \parallel^2_{\mathbf{Q}} + \sum_{i=0}^{N-1} \parallel \Delta\boldsymbol{\tau}(k+i|k) \parallel^2_{\mathbf{R}}, \tag{4.33}$$

where

$$\Delta\mathbf{U}(k) = [\Delta\boldsymbol{\tau}(k|k)^\top \ \ldots \ \Delta\boldsymbol{\tau}(k+N_u-1|k)^\top]^\top,$$

$$\mathbf{Y}_e(k) = [\mathbf{y}_e(k+1|k)^\top \ \ldots \ \mathbf{y}_e(k+N-1|k)^\top]^\top,$$

$\mathbf{Q} \succ 0$ and $\mathbf{R} \succ 0$ are the weighting matrices for output tracking and control activities, respectively.

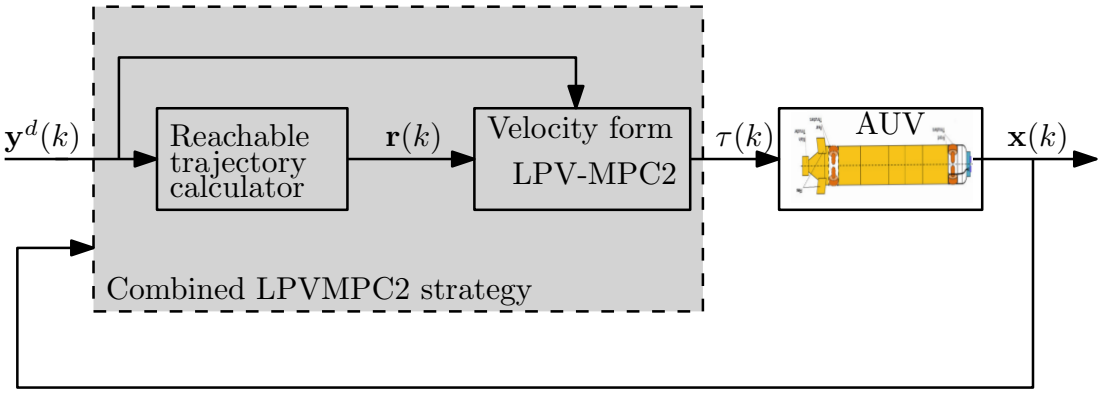

Fig. 4.4: Control strategy leveraging reachable references and velocity dynamics.

The proposed MPC is formulated as a finite-horizon constrained optimal control problem using the velocity form prediction model (4.29). Considering a quadratic

cost function, the novel velocity form LPVMPC2 problem is formulated as

$$
\begin{aligned}
\Delta\mathbf{U}^*(k) = \underset{\Delta\mathbf{U}(k)}{\arg\min}\ & V(\mathbf{r}(k), \mathbf{Y}_e(k), \Delta\mathbf{U}(k)) \\
\text{s.t}: \\
& \mathbf{y}(k+j|k) = \mathbf{C}\Delta\mathbf{x}(k+j|k) + \mathbf{y}(k+j|k-1), \\
& \Delta\mathbf{x}(k+j|k) = \mathbf{A}_{\mathbf{x}}^{j}\Delta\mathbf{x}(k|k) + \sum_{i=0}^{j-1}\mathbf{A}_{\mathbf{x}}^{i}\mathbf{B}\Delta\boldsymbol{\tau}(k+i|k), \\
& \mathbf{x}(k+j|k) \in \mathcal{X},\ j = 1, \ldots, N, \\
& \boldsymbol{\tau}(k+i|k) \in \mathcal{T},\ i = 0, \ldots, N-1, \\
& \Delta\mathbf{x}(k|k) = \Delta\mathbf{x}(k), \\
& \mathbf{y}(k+j|k-1) = \mathbf{y}(k-1), \\
& \mathbf{y}(k+N|k) = \ \mathbf{r}(k),\ \Delta\boldsymbol{\nu}(k+N|k) = \mathbf{0},
\end{aligned}
\tag{4.34}
$$

where N is the prediction horizon, and $\Delta\mathbf{U}^*(k) = \{\Delta\boldsymbol{\tau}^*(k|k), \ldots, \Delta\boldsymbol{\tau}^*(k+N_u-1|k)\}$ is the optimal control sequence. It is noted that obtaining the control sequence by solving (4.34) satisfies the reachable set requirement and assures that the AUV's prescribed trajectory does not exceed the workspace boundary.

Furthermore, the constraints defined as $\mathbf{y}(k+N|k) = \mathbf{r}(k)$ and $\Delta\boldsymbol{\nu}(k+N|k) = \mathbf{0}$ are enforced to impose stability. For every time step k, the stability constraint ensures that the reachable state is given as $\mathbf{x}_r(k) = [\mathbf{r}(k)^\top\ \boldsymbol{\nu}(k+N-1|k)^\top]^\top$. They are set up to assure that the terminal state in each N-window, $\mathbf{x}(k+N|k)$, is a forced equilibrium when the reference $\mathbf{r}(k)$ is constant during point stabilisation task as the AUV navigates at a constant speed. For time-varying reference signal $\mathbf{r}(k)$, these constraints ensure $\mathbf{x}(k+N|k)$ is always feasible because $\mathbf{r}(k)$ is defined within the reachable set according to (4.32).

Based on the receding horizon strategy, the optimal input increment at k is

$\Delta\boldsymbol{\tau}^*(k|k)$ and the corresponding control input applied is

$$\boldsymbol{\tau}^*(k) = \boldsymbol{\tau}(k-1) + \Delta\boldsymbol{\tau}^*(k|k). \tag{4.35}$$

The control strategy leveraging the concept of reachable set is depicted in Fig. 4.4.

Algorithm 2: MPC for 3D trajectory tracking and point stabilisation (LPVMPC2)

Input: AUV LPV model, $\mathbf{Q}$, $\mathbf{R}$ and the prediction horizon, N.
Define the transition resultant speed U_s.
Implement (4.31) to assure a smooth transition from trajectory tracking to point stabilisation.
for $k \geq 0 \in \mathbb{N}$ **do**
  if ${}^{\Delta\mathbf{y}_d(k)}/_{T_s} = \mathbf{0}$ **then**
    $\mathbf{Q} = \mathbf{Q}_2$
  else
    $\mathbf{Q} = \mathbf{Q}_1$
  end
  Solve (4.32) to obtain $\mathbf{r}(k)$
  Get $\Delta\mathbf{x}(k)$ and $\mathbf{y}(k-1)$; then, solve (4.34).
  Obtain the optimal input $\boldsymbol{\tau}^*(k)$ based on (4.35).
  Apply input to the AUV to obtain $\mathbf{x}(k+1)$
  $k \leftarrow k+1$
end

Denote $\mathbf{Q}_1 \in \mathbb{R}^{6\times6}$ and $\mathbf{Q}_2 \in \mathbb{R}^{6\times6}$ as two diagonal matrices on the output error weighting, used for the 3D trajectory tracking and the point stabilisation for docking, respectively. For the trajectory tracking problem, the weighting priorities are put on minimisation of the three error terms on translational positioning

$$e_x(k) = x_d(k) - x(k),\ e_y(k) = y_d(k) - y(k), e_z(k) = z_d(k) - z(k). \tag{4.36}$$

For point stabilisation, the setting of $\mathbf{Q}_2$ needs to cover all 6 DoFs, that is, in addition to the three errors in (4.36), the following three orientation errors

$$\mathbf{e}_\phi(k) = \phi_d - \phi(k),\ e_\theta(k) = \theta_d - \theta(k), e_\psi(k) = \psi_d - \psi(k), \tag{4.37}$$

also need to be minimised so that the specified translational position and orientation are maintained. Switching between the use of $\mathbf{Q_1}$ and $\mathbf{Q_2}$ depends on the nature of the reference signal, $\mathbf{y}_d(k)$. When $\mathbf{y}_d(k)$ is time-varying, $\mathbf{Q} = \mathbf{Q}_1$ holds; when $\mathbf{y}_d(k)$ is time-invariant, $\mathbf{Q} = \mathbf{Q}_2$ is applied. With sampling time of T_s, ${}^{\Delta \mathbf{y}_d(k)}/_{T_s} \neq \mathbf{0}$ for time-varying $\mathbf{y}_d(k)$, and for time-invariant reference, ${}^{\Delta \mathbf{y}_d(k)}/_{T_s} = \mathbf{0}$. The implementation procedure for the developed predictive controller is outlined in Algorithm 2.

Note that the proposed algorithm imposes a computational burden similar to that of a standard MPC problem, with the only extra demand being the solution of (4.32), which constitutes a relatively straightforward quadratic problem. It is noted that the workspace limits, $\mathcal{Y}_r$, can either be a linear or nonlinear constraint which will determine the nature of the problem (4.32). For instance, a linear workspace constraint results in a convex quadratic problem while a circular or spherical constraint gives a quadratically constrained quadratic problem. Consequently, this approach allows us to avoid the need to solve a high-dimensional nonlinear MPC problem having both state and input constraints. Nevertheless, the author acknowledges significant advancements that have been achieved in expediting computations within the realm of nonlinear MPC [276, 277].

Remark 2. *The stability constraint is employed to theoretically demonstrate that the MPC problem (4.34) ensures stability for the discretised model (4.28). Enforcing this constraint typically means using a longer prediction horizon compared to scenarios where the constraint is overlooked.*

4.3.4 Offset-Free Control and Stability Analysis

Let $\mathbf{d}(k)$ represent the lumped unknown disturbances affecting the vehicle, including both constant and time-varying components. The convergence of the system states is a necessary assumption to assure the offset-free property of an MPC controller [278]. The states and outputs of the closed-loop system converge to steady state values as $k \to \infty$, $\mathbf{y}_d(k) \to \mathbf{y}_{d,ss}$.

Remark 3. *Although tracking error may not be eliminated under time-varying disturbances and reference signals, a well-posed optimisation problem can help to minimise the tracking error. Moreover, it is desirable to achieve offset elimination subject to the constant or slowly varying disturbances during docking so as to ensure that the vehicle is driven as close as possible to the desired position and orientation.*

The following theorem summarises the main properties of the proposed control strategy.

Theorem 4.3.1. *Under Assumption 2, the control law $\boldsymbol{\tau}(k)$, obtained by solving (4.34), starting from a feasible initial state increment $\Delta\mathbf{x}(k)$, and applying (4.35), is recursively feasible and (locally) stabilises the system (4.29). As $k \to \infty$, this controller makes the output converge to one of the following: (i) $\mathbf{y}_{d,ss}$ if $\mathbf{y}_{d,ss} \in \mathcal{R}_{\mathcal{Y}}$; (ii) $\mathbf{r}(k)$ if $\mathbf{y}_{d,ss} \notin \mathcal{R}_{\mathcal{Y}}$, where $\mathbf{r}(k)$ is obtained by solving (4.32).*

Proof. This proof is given in three steps. Step I establishes recursive feasibility and Step II shows that the proposed control strategy provides closed-loop stability. In step III, it is shown that offset-free control is ensured for reachable piece-wise constant references. For reference signals that are not reachable, the algorithm converges to a reachable point that minimises the tracking error. The first two steps follow the standard approach in MPC literature with some modifications to suit the current study.

Step I: Given that the initial state increment $\Delta\mathbf{x}(k|k) = \Delta\mathbf{x}(k)$ is feasible, the optimal control sequence from solving (4.34) is

$$\Delta\mathbf{U}^*(k) = \{\Delta\boldsymbol{\tau}^*(k|k), \Delta\boldsymbol{\tau}^*(k+1|k), \ldots, \Delta\boldsymbol{\tau}^*(k+N-1|k)\}$$

and this yields the corresponding output error trajectory

$$\mathbf{Y}_e^*(k) = \{\mathbf{y}_e^*(k+1|k), \mathbf{y}_e^*(k+2|k), \ldots, \mathbf{y}_e^*(k+N|k)\}\,.$$

A feasible but sub-optimal solution given by $\{\Delta\boldsymbol{\tau}^*(k+1|k), \ldots, \Delta\boldsymbol{\tau}^*(k+N-1|k), \mathbf{0}\}$

can be obtained by shifting the current time by 1 so that $k \leftarrow k+1$ and then setting $\Delta\boldsymbol{\tau}^*(k+N|k) = \mathbf{0}$, which also implies $\boldsymbol{\tau}^*(k+N|k) = \boldsymbol{\tau}^*(k+N-1|k)$. The constraint on the terminal output makes it possible to obtain:

$$\mathbf{Y}_e(k+1) = \{\mathbf{y}_e^*(k+2|k), \ldots, \mathbf{y}_e^*(k+N|k), \mathbf{0}\}\,.$$

Based on the constraint $\Delta\boldsymbol{\nu}(k+N|k) = \mathbf{0}$, keeping the input unchanged for a constant reference $\mathbf{y}_{d,ss}$, makes the terminal state $\mathbf{x}(k+N|k) = \mathbf{x}_r(k)$, a forced equilibrium at steady state and is feasible. For curved or time-varying reference signals $\mathbf{y}_d(k)$, the constraint ensures $\mathbf{x}(k+N|k)$ is a feasible state since $\mathbf{r}(k)$ is reachable for all k.

Step II: Let $V(k)$ be equal to the cost function (4.33) evaluated at time k. We note that the cost function is always positive and equal to zero only when $|\mathbf{y}(k+j|k) - \mathbf{r}(k)| = 0$ and $\Delta\boldsymbol{\tau}(k+i|k) = 0$. To guarantee (Lyapunov) stability, we now need to show that $V(k)$ decays monotonously. Considering the feasible input increment sequence at time step $k+1$ constructed in *Step I*, a feasible, possibly suboptimal, value of the cost function $V(k+1)$ is given by

$$\begin{aligned}
V(k+1) &= \sum_{j=1}^{N-1} \| \mathbf{y}_e(k+1+j|k+1) \|_{\mathbf{Q}}^2 + \sum_{i=0}^{N-1} \| \Delta\boldsymbol{\tau}(k+1+i|k+1) \|_{\mathbf{R}}^2 \\
&= \sum_{j=2}^{N} \| \mathbf{y}_e^*(k+j|k) \|_{\mathbf{Q}}^2 + \sum_{i=1}^{N} \| \Delta\boldsymbol{\tau}^*(k+i|k) \|_{\mathbf{R}}^2 \\
&= \sum_{j=1}^{N-1} \| \mathbf{y}_e^*(k+j|k) \|_{\mathbf{Q}}^2 + \sum_{i=0}^{N-1} \| \Delta\boldsymbol{\tau}^*(k+i|k) \|_{\mathbf{R}}^2 \\
&\quad - \| \mathbf{y}_e^*(k+1|k) \|_{\mathbf{Q}}^2 - \| \Delta\boldsymbol{\tau}^*(k|k) \|_{\mathbf{R}}^2 + \| \mathbf{y}_e^*(k+N|k) \|_{\mathbf{Q}}^2 \\
&= V(k) - \| \mathbf{y}_e^*(k+1|k) \|_{\mathbf{Q}}^2 - \| \Delta\boldsymbol{\tau}^*(k|k) \|_{\mathbf{R}}^2 + \| \mathbf{y}_e^*(k+N|k) \|_{\mathbf{Q}}^2
\end{aligned} \tag{4.38}$$

From (4.38), it is straightforward to see that the stability constraint ensures that $\| \mathbf{y}_e^*(k+N|k) \|_{\mathbf{Q}}^2 = 0$. This implies $V(k+1) \leq V(k)$ holds because $\| \mathbf{y}_e^*(k+N|k) \|_{\mathbf{Q}}^2 - \| \mathbf{y}_e^*(k+1|k)(k) \|_{\mathbf{Q}}^2 - \| \Delta\boldsymbol{\tau}^*(k|k) \|_{\mathbf{R}}^2 \leq 0$, and the only condition that will enable

the equality to hold is when the system reaches steady state with $\mathbf{y}_d(k) = \mathbf{y}_{d,ss}$ and $\Delta\boldsymbol{\tau}(k|k) = \mathbf{0}$ as $k \to \infty$. In sum, $V(k)$ is a Lyapunov function that decreases along the prescribed trajectories. Thus, the predictive controller is (locally) asymptotically stable given $\mathbf{r}(k)$ $\forall k$.

Step III Here, we follow an approach similar to that used in [278] where constraints are assumed inactive at steady state which means that the predictive control law can be considered unconstrained. Under the assumption of piece-wise constant reference, $\mathbf{y}_d(\infty) = \mathbf{y}_{d,ss}$ and $\mathbf{d}(k) \to \mathbf{d}(\infty)$ at steady state when the vehicle converges towards the docking point. The stability of the closed-loop system at steady state implies that $\mathbf{x}(k) = \mathbf{x}(\infty)$, $\mathbf{y}(k) = \mathbf{y}(\infty)$ and $\boldsymbol{\tau}(k) = \boldsymbol{\tau}(\infty)$ as $k \to \infty$.

First consider the case where $\mathbf{y}_{d,ss} \in \mathcal{R}_{\mathcal{Y}}$. In this case, the steady state reachable reference $\mathbf{r}(\infty) = \mathbf{y}_{d,ss}$ because it minimises (4.32) and fulfills the properties of $\mathcal{R}_{\mathcal{Y}}$ with $\lambda = 1$. Assume that the predictive controller (4.34) is unconstrained at this steady state. For this unconstrained case, it is evident that the optimal control increment is given by

$$\Delta\boldsymbol{\tau}^*(\infty) = \mathbf{K}_{MPC}(\mathbf{r}(\infty) - \mathbf{y}^0(\infty)) \tag{4.39}$$

where $\mathbf{K}_{MPC}$ is the unconstrained controller gain and $\mathbf{y}^0(\infty)$ is the "free" trajectory which represents the part of $\mathbf{y}(\infty)$ that depend on the past control and the current measurement *i.e.,* without terms in $\Delta\mathbf{U}_k^*$ to be computed. Based on the system convergence, $\Delta\boldsymbol{\tau}^*(\infty) = 0$ which means that $\mathbf{y}^0(\infty) = \mathbf{r}(\infty)$ holds from (4.39). Furthermore, $\mathbf{y}^0(\infty) = \mathbf{y}(\infty)$ because $\mathbf{y}(k-1) = \mathbf{y}(k) = \mathbf{y}(\infty)$ as $k \to \infty$ considering the output vector in (4.29). Therefore, the system converges to $\mathbf{y}_{d,ss}$, *i.e.,* the plant output reaches the reference because $\mathbf{y}^0(\infty) = \mathbf{r}(\infty) \implies \mathbf{y}(\infty) = \mathbf{y}_{d,ss}$ at steady state and this ensures offset-free control.

For the second case in which $\mathbf{y}_{d,ss} \notin \mathcal{R}_{\mathcal{Y}}$, The vector $\mathbf{r}(\infty)$ that minimises (4.32) is not exactly equal to $\mathbf{y}_{d,ss}$, that is, $\mathbf{r}(\infty) \neq \mathbf{y}_{d,ss}$. However, $\mathbf{r}(\infty)$ can take any arbitrary reachable output that minimises (4.32) while ensuring it remains in the

same set $\mathcal{R}_y$ as the current steady state reachable output $\mathbf{y}(\infty)$. Following similar procedure under the assumption of unconstrained law as in the first case, it follows that the closed-loop system converges with $\mathbf{y}(k) = \mathbf{r}(k) \neq \mathbf{y}_{d,ss}$ as $k \to \infty$. Hence, completing the proof. □

4.3.5 Simulated Results

The Naminow-D dynamic model is considered. A state constraint is implemented on the pitch angle such that $|\theta| < \pi/2$ always holds. Since in many underwater tasks AUVs are required to move at relatively low speeds [22], the upper bounds on the translational velocities are defined as follows: $u_{\max} = 1.5$ m/s, $v_{\max} = 1$ m/s and $w_{\max} = 0.5$ m/s. The input forces and moments are constrained as follows: $\boldsymbol{\tau}_{1,\max} = [600\ 600\ 600]^\top$ N and $\boldsymbol{\tau}_{2,\max} = [300\ 300\ 300]^\top$ Nm.

Table 4.3: Tuned parameters of the proposed MPC4 (LPVMPC2).

Parameter	N	N_u	$\mathbf{R}$	$\mathbf{Q}_1$	$\mathbf{Q}_2$	$\mathbf{P}_r$
Value	20	2	$0.05\mathbf{I}$	$\texttt{diag}(2,2,2,1,1,1) \times 1000$	$1000\mathbf{I}$	$\mathbf{I}$

The parameter setting for the proposed MPC (4.34) (MPC4) is shown in Table 4.3. The weights on the translational position terms in $\mathbf{Q}_1$ are selected to be twice those in $\mathbf{Q}_2$ to prioritise minimisation of the translational position errors during trajectory tracking control. The simulation experiment was set up in `MATLAB` environment where (4.32) and (4.34) are solved using `quadprog` to obtain the control signals applied to the nonlinear model (2.14).

4.3.5.1 Comparison of Controllers Performance in Dynamic Positioning

Denote the developed LPVMPC2 algorithm as MPC4. First its performance in dynamic positioning is compared with the proposed algorithm LPVMPC1 (MPC1). The results from tracking the constant reference under the sinusoidal ocean current, as detailed in Section 4.2.4, using MPC1 and MPC4 are presented in Fig. 4.5. It is

evident that MPC1 tends to result in higher variations in the forces and moments required to perform the dynamic positioning task.

Table 4.4 summarises the performance of the two velocity form MPC algorithms. It is observed that both algorithms offer similar performance in terms of minimising the outputs RMSEs with MPC1 showing a slightly better performance. However, MPC4 outperforms MPC1 in reducing the peak tracking error, as measured by the absolute maximum error (MAX Error). Additionally, MPC4 requires significantly smaller input forces and moments than MPC1, underscoring the former's superiority in providing good tracking performance with reduced thruster force variations necessary for mitigating mechanical wear in the system. A possible explanation for the differences in the performance of the controllers, despite both being of the velocity form MPC type, lies in the way they incorporate the increment of the position vector into the prediction model. While LPVMPC1 adds the output vector increment to the state prediction model (4.7), which uses the state vector, $\boldsymbol{\xi}(k)$, containing only the vehicle velocity increment, LPVMPC2 employs a prediction model (4.29) with the state increment, $\Delta\mathbf{x}(k)$, incorporating both the position and velocity vector increments. For the remainder of this simulation study in this subsection, the focus will be on MPC4, showcasing its capabilities.

Table 4.4: A comparative results of the two proposed velocity form MPC algorithms under tidal ocean current.

	RMS Error		**MAX Error**			**RMS Value**	
Output/unit	MPC1	MPC4	MPC1	MPC4	**Input/unit**	MPC1	MPC4
x/mm	71.9	73.4	500	496.6	τ_X/N	79.7	26.5
y/mm	69.3	70.1	495.2	477.9	τ_Y/N	36	14.9
z/mm	3.2	2.8	47.9	37.6	τ_Z/N	9.8	1.6
ϕ/mrad	5.4	4.9	38.4	37.6	τ_K/Nm	2.3	0.42
θ/mrad	1.2	3.1	3.9	3.5	τ_M/Nm	87.2	82.5
ψ/mrad	4.2	5.8	30.4	28.6	τ_N/Nm	83.4	26.6

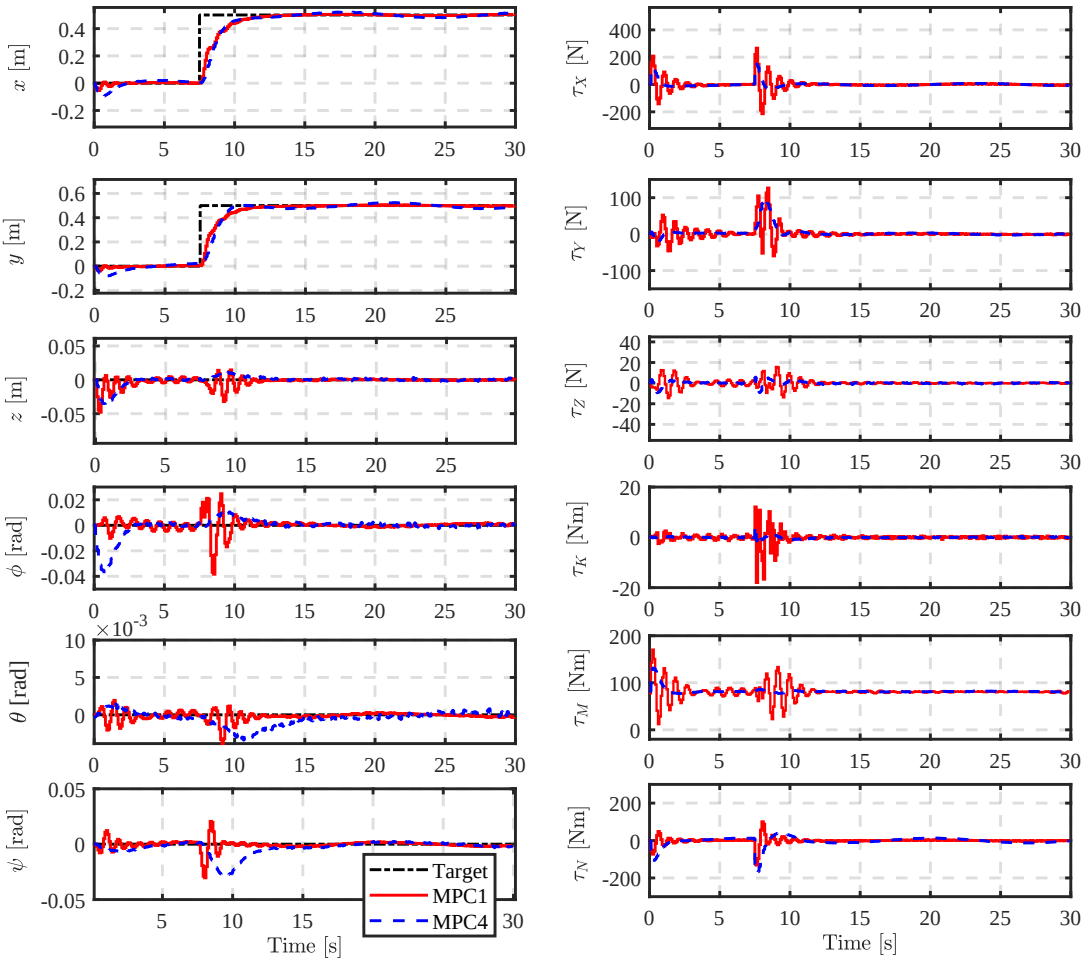

Fig. 4.5: A comparative results of velocity form MPC algorithms, LPVMPC1 and LPVMPC2, under tidal current test: controlled output (left) and manipulated variables (right) of the AUV.

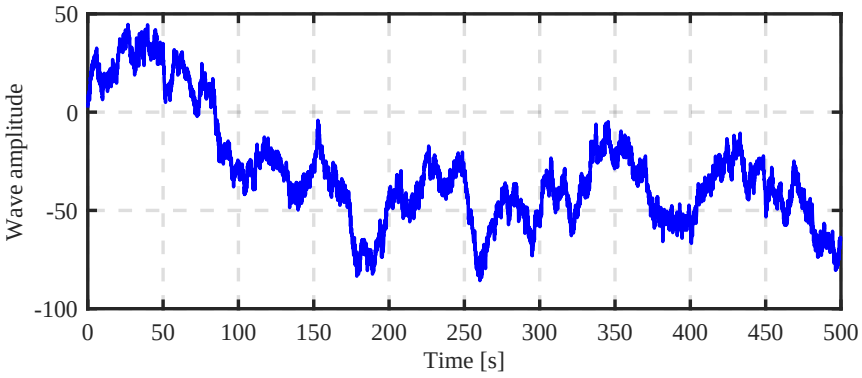

Fig. 4.6: Wave signal produced using modified Pierson–Moskowitz Spectrum.

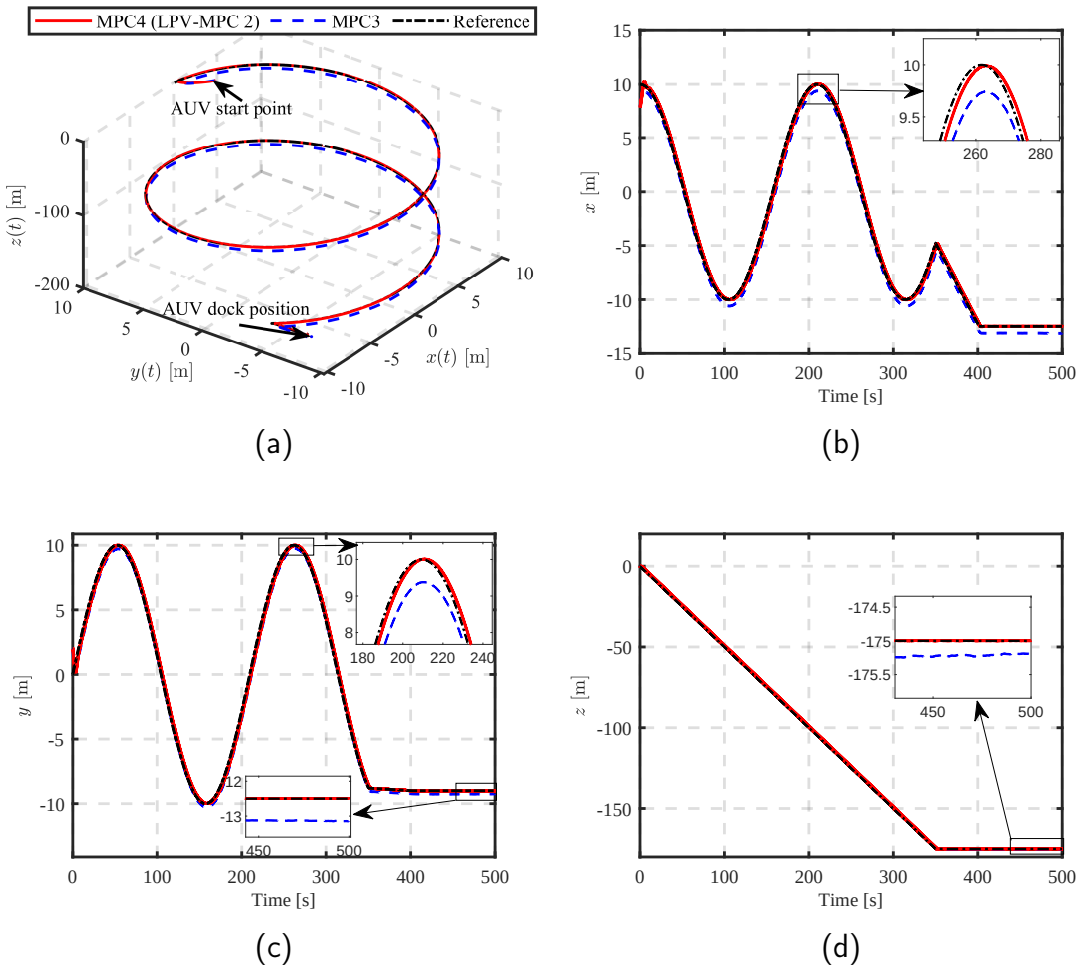

Fig. 4.7: Case 1: (a) AUV 3D closed-loop response for combined trajectory tracking and point stabilisation control (b) Motion in the $x-$direction (c) Motion in the $y-$direction (d) Motion in the $z-$direction.

4.3.5.2 Case 1: Combined 3D Trajectory Tracking and Dynamic Positioning

The wave model in (2.8) and (2.9) is considered in approximating the effects of ocean waves on the vehicle's motion. Here, the modified Pierson–Moskowitz Spectrum [6] is employed with $\xi_i = 0.2573$ and $\omega_{e,i} = 0.8$ rad/s under beam sea condition. The gain $K_{w,i} = 1.5$ and w_i is modelled as a white process noise with zero mean and standard deviation of 0.15. Furthermore, d_i is modelled as a standard Wiener process in the range $[-100, 100]$. These parameters are assumed to hold for $i = X,\ Y,\ Z,\ K,\ M,\ N$, i.e., the wave is considered the same in all 6 DoFs.

The ocean current is modelled in the Cartesian plane with $u_c = 0.2$ m/s, $v_c = 0.15$ m/s, $w_c = 0.1$ m/s. In the studied scenario, the dynamics of the AUV are considered to be affected by both ocean currents and waves according to (4.15). The wave signal impacting the six DoFs of the AUV dynamics is shown in Fig. 4.6.

The 3D reference trajectory considered in Case 1 is defined as

$$\mathbf{y}_d(t) = [10\sin 0.03t\ \ 10\cos 0.03t\ \ -0.5t\ \ 0\ \ 0\ \ \pi/6]^\top, t \leq 350 \text{ s} \tag{4.40}$$

and the final docking position is

$$\mathbf{y}_{d,ss} = [-9.0\ \ -12\ \ -175\ \ 0\ \ 0\ \ \pi/6]^\top, t > 350 \text{ s}, \tag{4.41}$$

where $t = kT_s$. Notice that the AUV needs to perform the task with a 30° heading angle. Also, it is generally desired to always keep roll motion, $(\phi,\ p)$, minimal for improved stability of marine vehicles [279]. Since the final point $\mathbf{p}_t = [-8.797\ \ -4.755\ \ -175]^\top$ on the trajectory (4.40) is significantly distant along the $y-$axis from the docking position $\mathbf{p}_{d,ss} = [-9\ \ -12\ \ -175]^\top$ in (4.41), the straight line joining these points is parameterised by considering a resultant AUV speed of $U_s = 0.15$ m/s. When the vehicle approaches the docking point defined at $t \geq 350$s, it is essential to control the AUV's translational and angular positions such that the

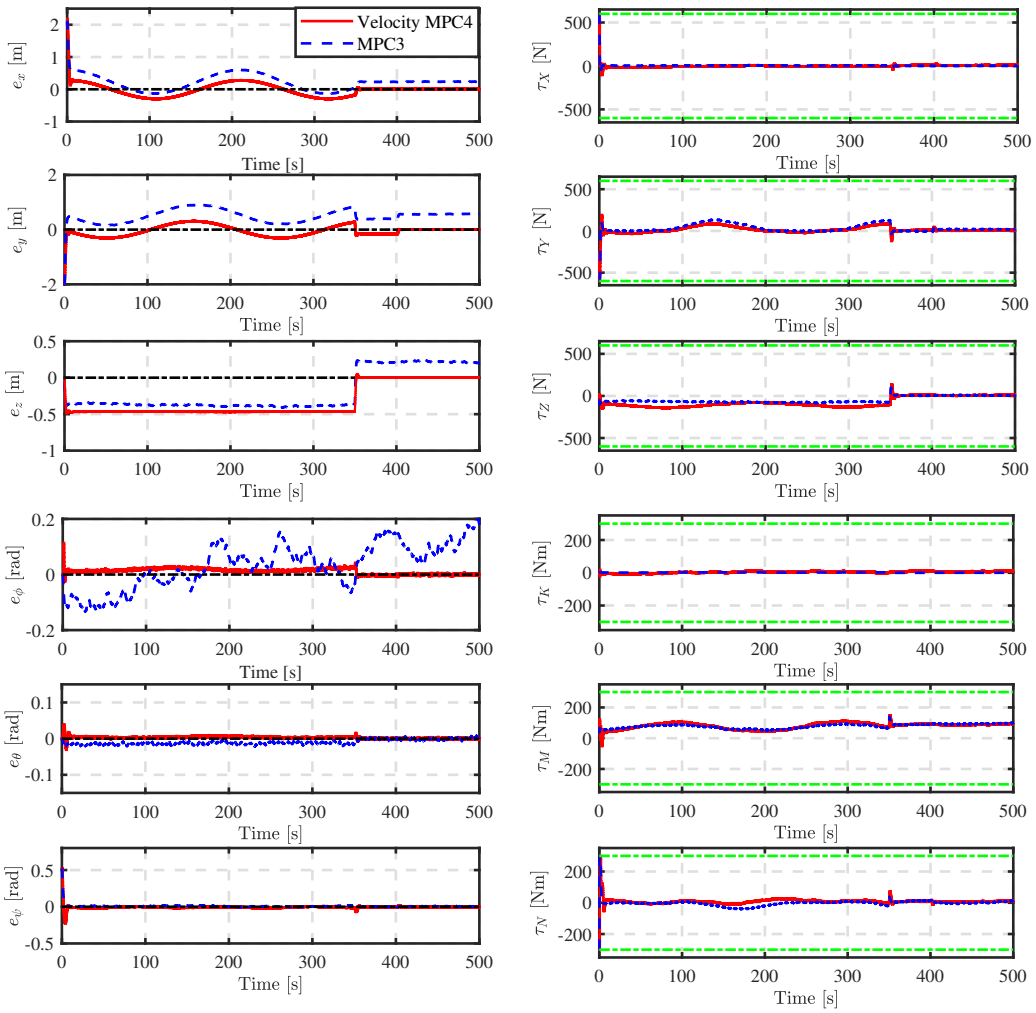

Fig. 4.8: Case 1: Evolution of errors (left) and input forces and moments (right). The green lines in the selected input plot show their constraints.

errors in the 6 outputs are as small as possible for effective docking operation.

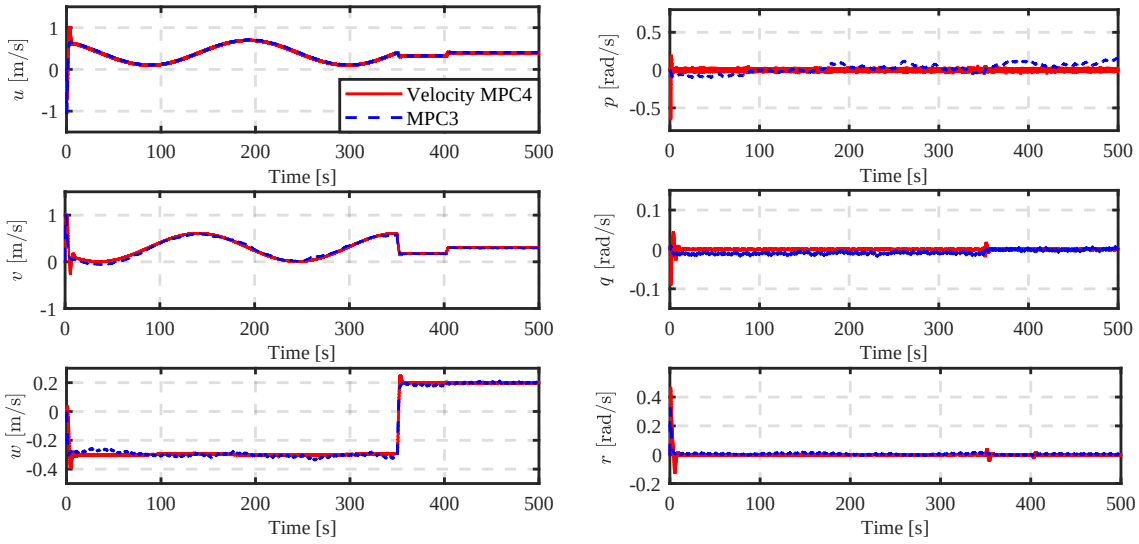

Fig. 4.9: Case 1: Evolution of translational (left) and angular (right) velocities of the AUV.

The AUV's initial position is $\boldsymbol{\eta}(0) = [2\ 8\ 0\ 0\ 0\ \pi/5]^\top$. The 3D motion profiles of the Naminow-D AUV along with the defined trajectory for the two predictive controllers are shown in Fig. 4.7. Fig. 4.8 shows the time profiles of the position tracking errors and input signals for both control methods, from which it is seen that the proposed controller provides better tracking performance. In the second phase when the vehicle is driven towards the docking position, the merit of the proposed controller, LPVMPC2 (MPC4), is even more evident. With MPC3 in [25], steady state errors are maintained due to the persistent non-zero disturbances, whereas the proposed MPC4 achieves the docking position with close-to-zero errors in all 6 DoFs. The translational and angular velocities of the AUV are shown in Fig. 4.9. A salient point worthy of note is that the translational velocities do not converge to zeros at the docking point because the AUV needs to maintain speeds that counter the effects of the non-zero translational velocities of ocean currents $\boldsymbol{\nu}_c$. Compared to the results from MPC3, the proposed MPC4 offers improved stabilisation of roll motion by reducing the sensitivity of the roll angular error e_ϕ and roll velocity p to environmental disturbances, as shown in Figs. 4.8 and 4.9, respectively. Therefore,

the results show the superiority of the proposed MPC4 in 3D trajectory tracking and point stabilisation control tasks.

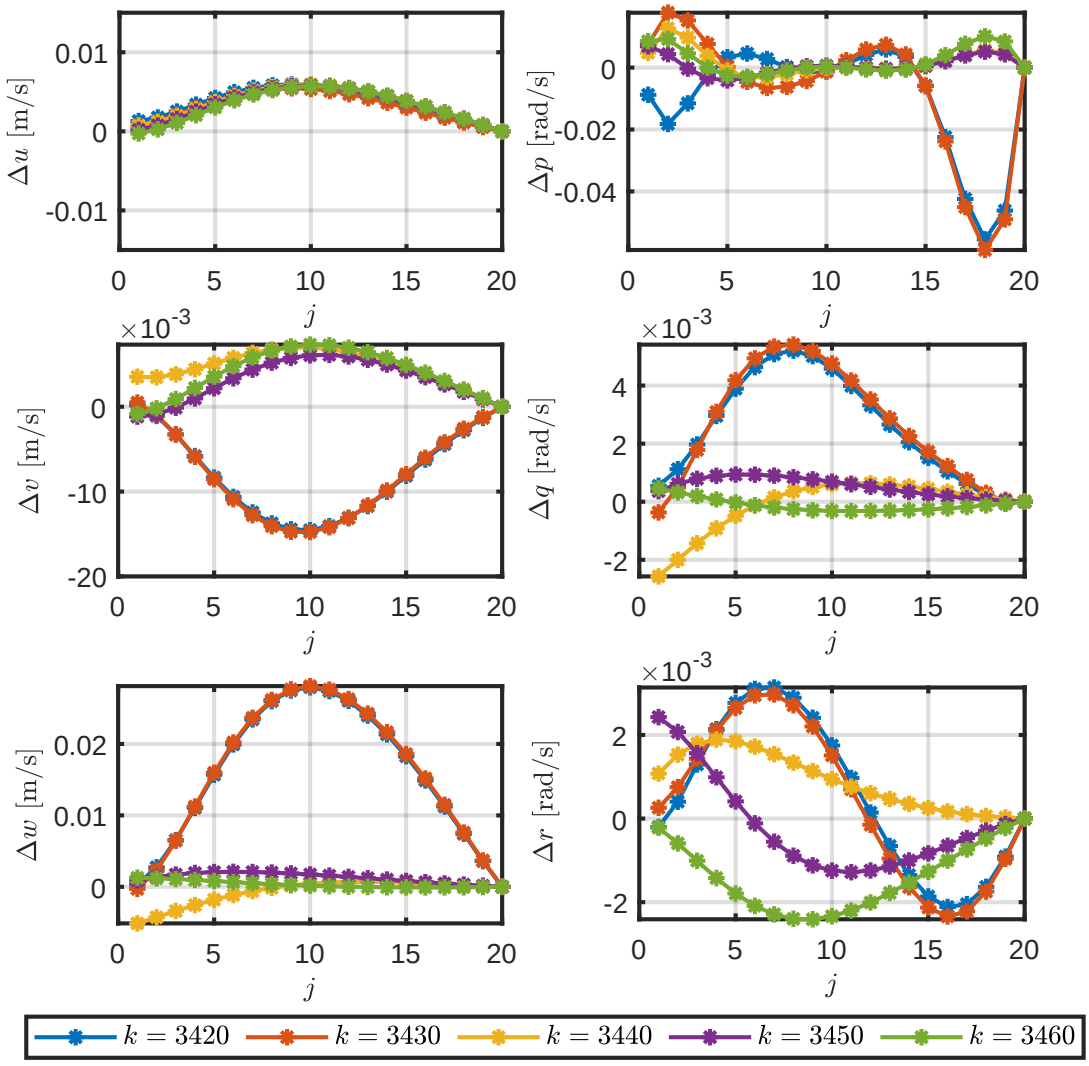

Fig. 4.10: Case 1: Predicted velocity increment trajectories at selected time instants.

Furthermore, in Fig. 4.10, the predicted velocity changes of the AUV at time steps during the transition from the spiral trajectory to the straight-line trajectory, specifically at $t = [342, 346]$ s, are depicted to capture the predictions during the spiral trajectory tracking and the transition towards the docking station. The

graph illustrates that the stability constraint is satisfied by guaranteeing that the predictions converge to zero at the end of the prediction horizon.

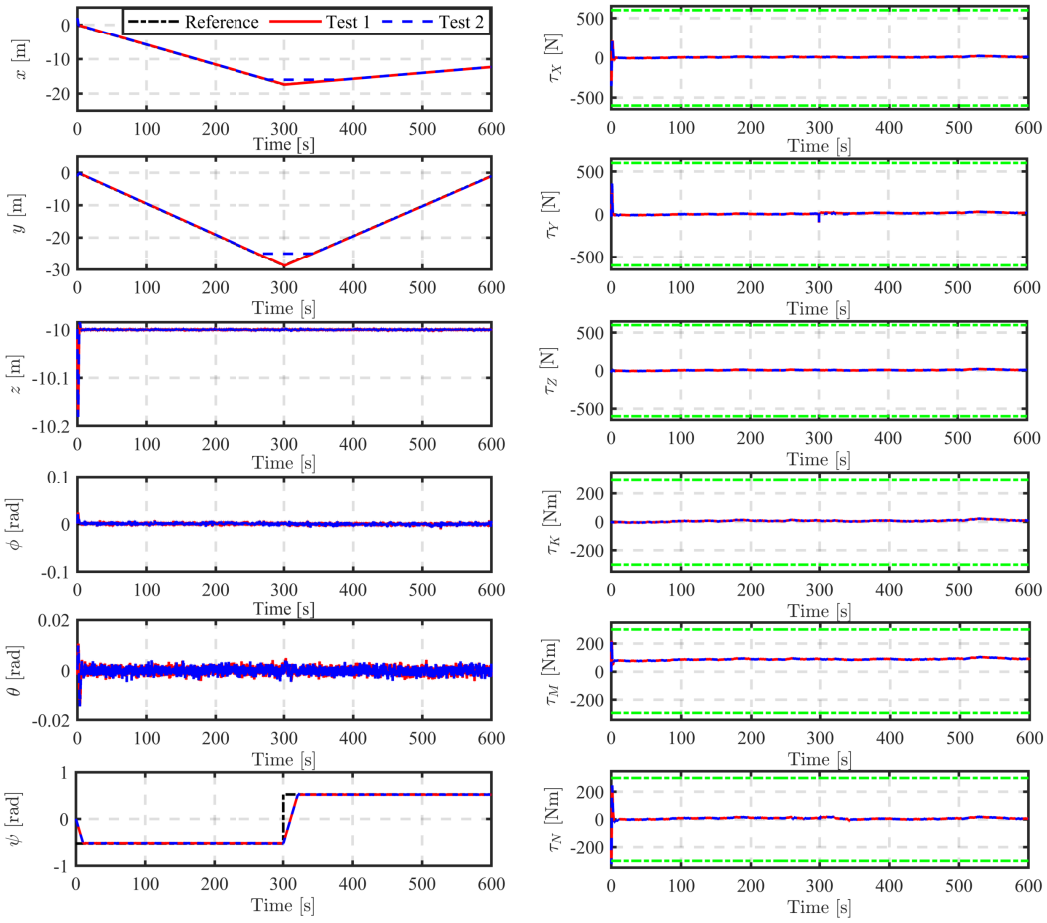

Fig. 4.11: Case 2: Evolution of position variables (left) and input forces and moments (right) under Test 1 and Test 2. The green lines represent input constraints.

4.3.5.3 Case 2: Tracking in Constrained Workspace

In Case 2, two test scenarios are considered to demonstrate the capability of the proposed controller to track trajectories containing unreachable points due to workspace constraint and the limits of the AUV dynamics. The reference trajectory $\mathbf{y}^d(k)$ is defined by two straight lines with a sharp turn, in the $xy-$plane, with no changes in the $z-$direction. The rate at which the AUV can change its direction is constrained, making such a sharp turn infeasible. Hence, in addition to the translational velocity

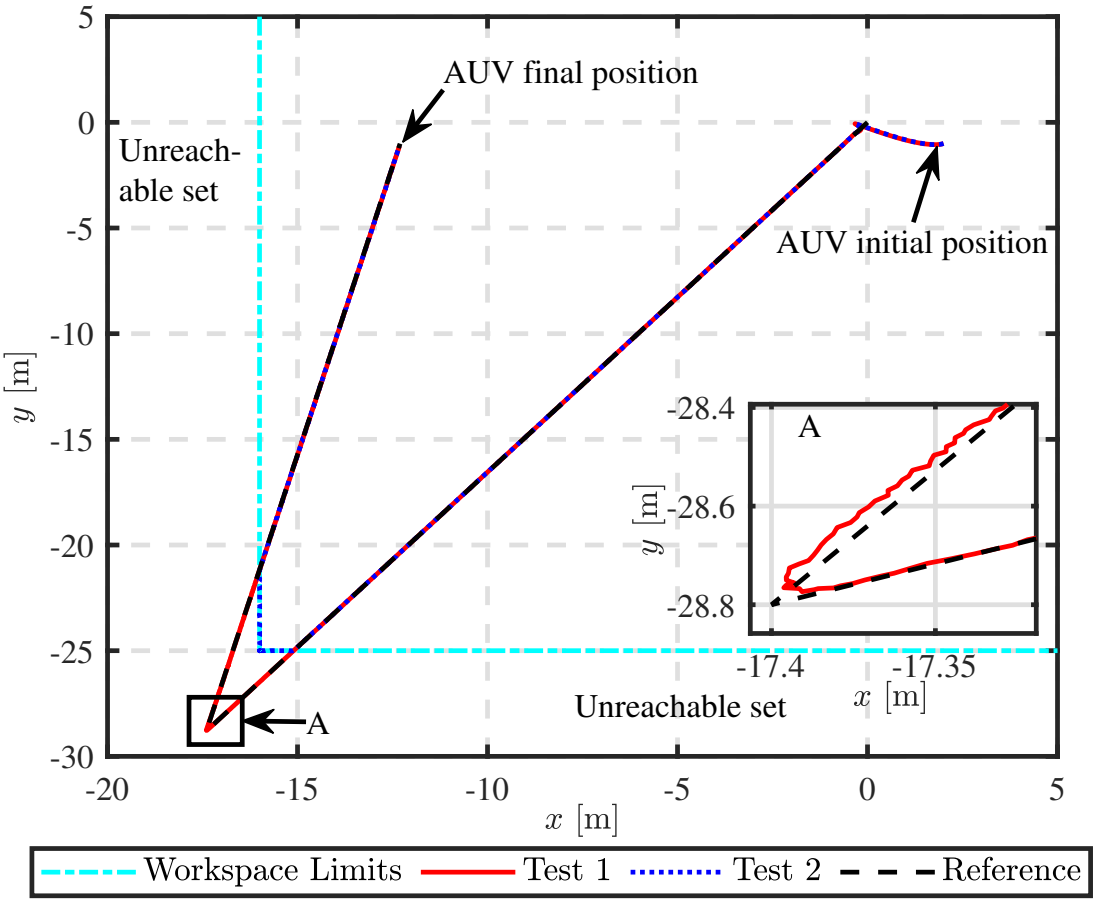

Fig. 4.12: Case 2: Closed-loop motion of the AUV in the $x-y$ plane with the impact of unreachable reference signals demonstrated.

constraints considered in Case 1, the yaw velocity of the AUV is constrained by $|r| \leq 0.05$ rad/s. In Test 1 of Case 2, no vehicle positional workspace constraints are applied; therefore, the reference trajectory $\mathbf{y}^d(k)$ is regarded as reachable but may be infeasible at points requiring sharp turns. In Test 2, the workspace is constrained by $|x| \leq 16$ and $|y| \leq 25$, which makes part of the reference stay outside the constrained region.

The time profiles of the position outputs and control inputs in both Test 1 and Test 2 are shown in Fig. 4.11. To make the convergence properties of the proposed MPC visible, the response in the $xy-$plane is shown in Fig. 4.12 along with the implemented workspace constraints. Evidently, the result of Test 1 is

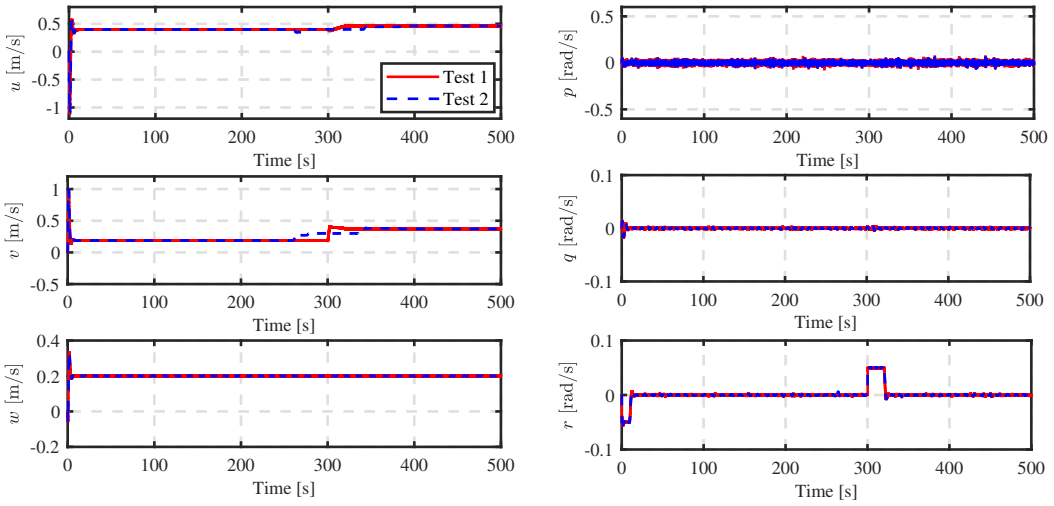

Fig. 4.13: Case 2: Evolution of translational (left) and angular (right) velocities of the AUV.

as expected because the outputs tracked the desired trajectories throughout the simulation range, avoiding the instantaneous sharp turn due to the limits on the rate of heading change that makes it dynamically infeasible for the AUV. In Fig. 4.13, the velocities of the AUV are shown, and it can be observed that the yaw velocity is saturated around $t = [300, 320]$ s that corresponds to the time when the trajectory has a sharp turn, ensuring that the physical limits imposed by the AUV dynamics are not violated. In Test 2, there are unreachable points along the defined trajectories due to the workspace constraints, which deviates the AUV movement from the reference until the desired trajectories become reachable. Based on the reference calculation in (4.32), it is expected that the AUV will converge to the optimum values within the reachable set $\mathcal{R}_{\mathcal{Y}}$, *i.e.,* the optimum points that correspond to the boundaries defined by the intersecting vertical and horizontal constraint lines.

In this scenario, the velocity increments at specific time steps are displayed in Fig. 4.14. The time steps $t = [301, 305]$ seconds are shown to demonstrate that the velocities converge to zero, as required by the stability constraint. It is noted that this occurs despite the abrupt change in orientation after $t = 300$ seconds and the

vehicle's need to navigate the sharp edge at the intersection of the x and y axes.

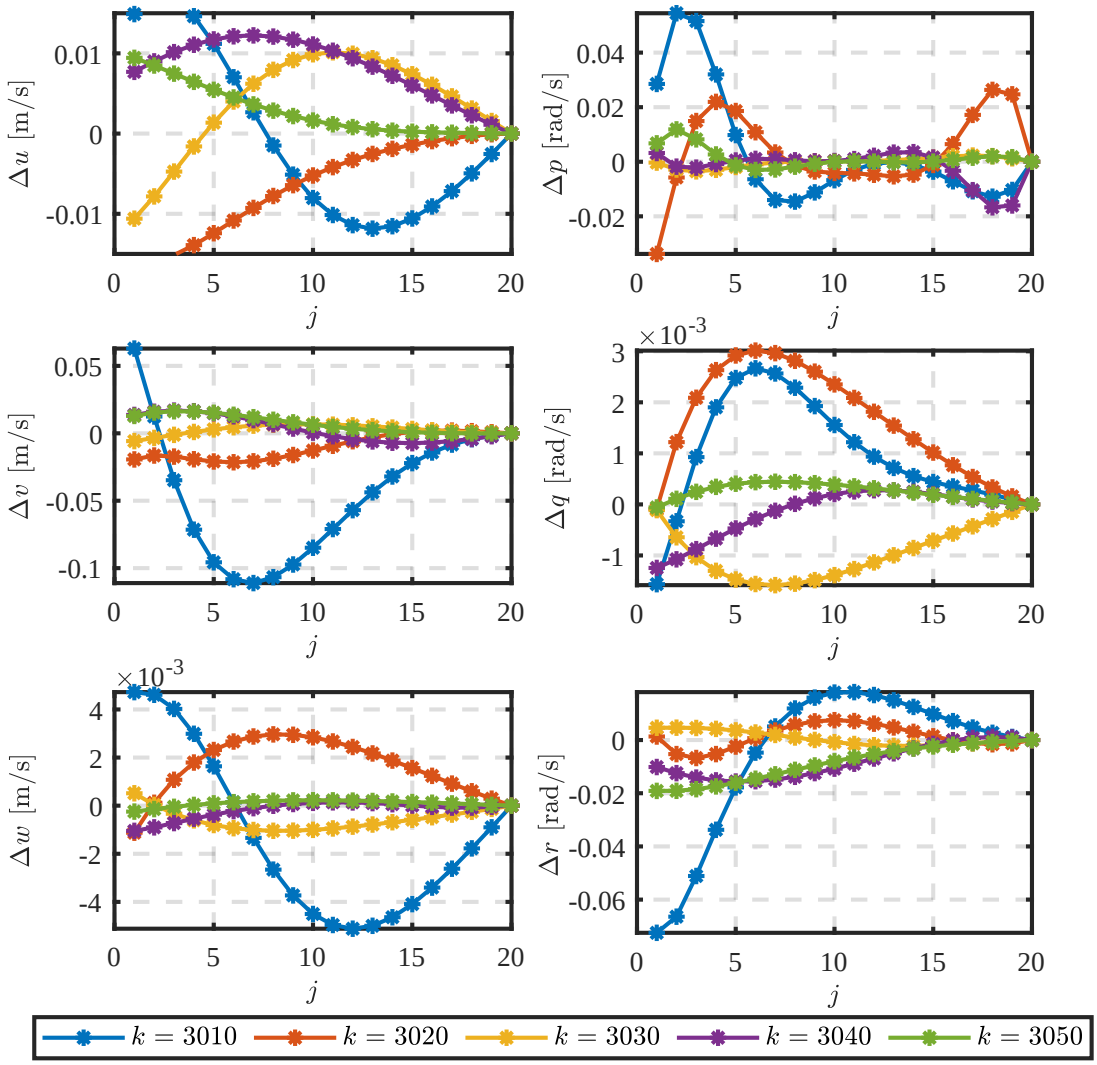

Fig. 4.14: Case 2: Predicted velocity increment trajectories at selected time instants.

4.4 Summary

The design of the first LPVMPC1 strategy for the positioning control of an AUV is investigated considering the influence of slowly varying current disturbance. The interdependence of the kinematic and dynamic models of the vehicle is exploited to

formulate a velocity form LPVMPC1 to facilitate accurate position tracking at the steady state. The algorithm relies on a prediction model that mitigates constant or time-varying disturbance effects via the increments of vehicle velocities. Compared to the benchmark controller (MPC2) and a partial velocity form MPC (MPC3), the proposed complete velocity form LPVMPC1 does not require an estimator yet eliminates steady state error effectively. Simulation experiments demonstrate the advantages of the proposed scheme under current disturbance.

However, the input signals from the LPVMPC1 show significant oscillations, which also negatively impacts the transient performance, especially when step changes occur in the reference signals. This was made evident when LPVMPC1 is compared to the alternate LPVMPC2 designed for combined trajectory tracking and dynamic positioning. The LPVMPC2 showed minimal oscillations in control signals and also reduced the peak deviation of the AUV's track from the reference. This LPVMPC2 was formulated with input and state constraints considered in the optimisation design. The designed predictive controller also achieves close-to-zero errors in the 6 DoFs of the vehicle in dynamic positioning, as required for effective docking operation. The constraint on the pitch angle is imposed to prevent the rotation matrix from becoming singular. The control input constraints are a result of the limits on the forces and moments that the vehicle can generate, and the velocity bounds are usually required for a variety of underwater tasks. The closed-loop stability of LPVMPC2 is guaranteed by enforcing a terminal equality constraints. Additionally, offset-free tracking is shown under the assumption of asymptotically constant reference and disturbance which is essential for effective docking operations. Further simulation results are presented under different operating conditions to demonstrate the effectiveness of the proposed LPVMPC2 algorithm for combined trajectory tracking and positioning control.

The works presented in this chapter have been published. Algorithm 1 was featured at the 2023 IFAC World Congress [280], while Algorithm 2 has been accepted for publication in the IEEE Journal of Oceanic Engineering [281].

Chapter 5

Tube-based Model Predictive Control of an Autonomous Underwater Vehicle using 3D Line-of-Sight Re-planning

5.1 Introduction

The tube-based MPC (TMPC) design presented in this chapter is a robust control strategy developed to ensure the system response stays within a tube around a desired nominal trajectory [282]. As highlighted in the critical review of the literature in Chapter 3, TMPC has the potential to provide robustness against environmental disturbances in AUV control. However, the difficulty associated with determining a local linear controller poses a significant challenge for trajectory tracking problems. Moreover, existing techniques are either focused on local plane motion [264] or rely on simplified AUV models for control design [17, 22]. Additionally, these techniques are computationally expensive, making them less suitable for real-time applications.

Furthermore, AUVs typically rely on thrusters to generate input forces. In the

aforementioned MPC-based motion controllers, thrust limits are usually considered as input constraints. However, this approach overlooks how quickly rapid input variations may degrade control performance. As a result, the work in [18] emphasised the necessity of developing MPCs that incorporate realistic input constraints, including both input magnitude and rate limitations. In advanced nonlinear time-invariant control strategies, this problem has been extensively investigated. For instance, a strategy for adaptive adjustment of the desired trajectory was proposed to obtain region tracking in the presence of input magnitude and rate saturation [283]. A fuzzy re-planning scheme was proposed to obtain a local trajectory to mitigate input saturation that causes chattering in SMC when an AUV's initial position significantly deviates from the desired trajectory [41].

The literature review shows the benefits of TMPC in AUV motion control, showing the need to include realistic constraints in controller design and the challenging issue of determining tubes for nonlinear AUV trajectory tracking. This chapter seeks to develop a robust discrete-time TMPC for AUVs using the full-order model while considering realistic input constraints, including both magnitude and rate limits. The primary contributions of this chapter can be summarised as follows.

1. A 3D LOS local replanner is proposed to tackle the problem of input saturation in the MPC-based trajectory tracking controller. The scheme is developed by modifying a conventional enclosure-based LOS strategy [6] used for path-following control. It constrains the error signal to a user-defined spherical region, thereby preventing excessive variations in the input signals that would otherwise be induced by a substantial tracking error. To provide an informed guess of the spherical error limit, a technique is developed that considers the average distance between consecutive points along the desired trajectory. For a smooth path, this technique may generally provide a suitable value, but the value may need to be tuned for non-smooth trajectories.

2. A discrete-time TMPC framework is developed for 3D trajectory tracking con-

trol of an AUV whose coupled model is approximated by an LPV model. This results in solving a convex quadratically constrained quadratic optimisation (QCQP) problem that can be efficiently solved online. To further strengthen the computational effectiveness of the algorithm, we circumvent the need to solve a nonlinear optimisation problem [264] or a SD-DARE [17] by deriving a state-dependent feedback gain to stabilise the AUV error dynamics. The feedback gain is obtained from the analytical solution of a finite-horizon optimal control problem. The AUV error model can be locally asymptotically stabilised by the derived state-feedback control law. Furthermore, theoretical results on the input-to-state stability of the TMPC law are presented under the stated assumptions.

3. In addition to the conventional performance metrics on tracking accuracy and input chattering, a performance metric on the rate of energy consumption in Watt-hour (Wh) is introduced to assess the effectiveness of the proposed control law.

The rest of this chapter is organised as follows. Section 5.2 defines the control problem that is tackled in this chapter. In Section 5.3, the LOS guidance system used for local trajectory generation is presented while Section 5.4 presents the robust tracking LPV TMPC design. Simulation results are presented in Section 5.5. Finally, concluding remarks are given in Section 5.6.

5.2 Problem Formulation

The LPV system (4.16) is considered and given as follows:

$$\mathbf{x}(k+1) = \mathbf{A}(\mathbf{x}(k))\mathbf{x}(k) + \mathbf{B}\mathbf{u}(k) + \mathbf{w}(k), \tag{5.1}$$

where k is the time index.

In (5.1), the states and the control inputs (both magnitude and rate of change) have bounded constraints. The state constraint is applied to the pitch angle, θ, to avoid the singularity of the transformation matrix. Define the compact set for the states with constraints $\mathbf{x}_{\max}$ as

$$\mathcal{X} = \left\{ \mathbf{x}(k) \in \mathbb{R}^{12} : |\mathbf{x}(k)| \leq \mathbf{x}_{\max} \right\}. \tag{5.2}$$

Thus, the state constraint defined by this set can be rewritten as

$$\mathbf{x}(k) \in \mathcal{X} = \left\{ \mathbf{x}(k) \in \mathbb{R}^{12} : \mathbf{G}_x \mathbf{x}(k) \leq \mathbf{h}_x \right\}, \tag{5.3}$$

in which

$$\mathbf{G}_x = \begin{bmatrix} \mathbf{I} \\ -\mathbf{I} \end{bmatrix}, \ \mathbf{h}_x = \begin{bmatrix} \mathbf{x}_{\max} \\ -\mathbf{x}_{\max} \end{bmatrix}.$$

Also, the compact sets that define the control input and its rate constraints are given by

$$\begin{aligned} \mathbf{u}(k) \in \mathbb{U} &= \left\{ \mathbf{u}(k) \in \mathbb{R}^6 : |\mathbf{u}(k)| \leq \mathbf{u}_{\max} \right\}, \\ \Delta\mathbf{u}(k) \in \Delta\mathbb{U} &= \left\{ \Delta\mathbf{u}(k) \in \mathbb{R}^6 : |\Delta\mathbf{u}(k)| \leq \Delta\mathbf{u}_{\max} \right\}, \end{aligned} \tag{5.4}$$

where $\Delta\mathbf{u}(k) = \mathbf{u}(k) - \mathbf{u}(k-1)$. The two constraints in (5.4) can be combined into a single compact set:

$$\mathbf{u} \in \mathcal{U} = \left\{ \mathbf{u}(k) \in \mathbb{R}^6 : \mathbf{G}_u \mathbf{u}(k) \leq \mathbf{h}_u \right\}, \tag{5.5}$$

where

$$\mathbf{G}_u = \begin{bmatrix} \mathbf{I} \\ -\mathbf{I} \\ \mathbf{I} \\ -\mathbf{I} \end{bmatrix}, \ \mathbf{h}_u = \begin{bmatrix} \mathbf{u}_{\max} \\ \mathbf{u}_{\max} \\ \Delta\mathbf{u}_{\max} \\ \Delta\mathbf{u}_{\max} \end{bmatrix} + \begin{bmatrix} \mathbf{0} \\ \mathbf{0} \\ \mathbf{I} \\ -\mathbf{I} \end{bmatrix} \mathbf{u}(k-1).$$

Let the desired position and attitude of the AUV be defined as

$$\boldsymbol{\eta}_d(k) = [x_d(k)\ y_d(k)\ z_d(k)\ \phi_d(k)\ \theta_d(k)\ \psi_d(k)]^\top.$$

Denote the desired translational 3D trajectory at time k as $\mathbf{p}_d(k) = [x_d(k)\ y_d(k)\ z_d(k)]^\top$. When the 3D tracking error is large, a local desired 3D trajectory, denoted by $\mathbf{p}_{los}(k) = [x_{los}(k)\ y_{los}(k)\ z_{los}(k)]^\top$ is re-planned using a LOS guidance system approach. The reference position trajectory to be used for control implementation is written as

$$\begin{aligned} \mathbf{r}(k) &= [r_x(k)\ r_y(k)\ r_z(k)\ \ \phi_d(k)\ \theta_d(k)\ \psi_d(k)]^\top, \\ [r_x(k)\ r_y(k)\ r_z(k)]^\top &= \mathbf{H} \cdot \left[\mathbf{p}_d(k)^\top\ \mathbf{p}_{los}(k)^\top\right]^\top, \end{aligned} \tag{5.6}$$

where $\mathbf{H} \in \mathbb{R}^{3\times 6}$ is constructed to choose the reference between $\mathbf{p}_d(k)$ and $\mathbf{p}_{los}(k)$ depending on the current AUV position, $\mathbf{p}(k) = [x(k)\ y(k)\ z(k)]^\top$.

The following assumptions are made on the LPV model.

Assumption 3.

1. *The state and input constraint sets $\mathcal{X}$ and $\mathcal{U}$ are convex sets.*

2. *The unknown lumped disturbance $\mathbf{w}(k)$ is bounded and belongs to the polytopic set $\mathcal{W}$ defined as*

$$\mathcal{W} = \left\{\mathbf{w}(k) \in \mathbb{R}^{12} : |\mathbf{w}(k)| \leq \mathbf{w}_{\max}\right\}, \tag{5.7}$$

   where $\mathbf{w}_{\max}$ is the disturbance upper limit.

3. *The LPV model $(\mathbf{A}(\mathbf{x}(k)), \mathbf{B})$ is locally or pointwise stabilisable in the linear sense for all $\mathbf{x}(k) \in \mathcal{X}$.*

In Assumption 3, the first item implies that the state and input limits can be expressed as linear inequality constraints. The second item implies that if the upper bound $\mathbf{w}_{\max}$ is known, then the worst-case scenario of the disturbance can be

considered when designing an input $\mathbf{u}(k) = \boldsymbol{\tau}(k)$ that stabilises the LPV model (5.1).

The objective of the controller design is to drive the LPV system (5.1) to track the reference trajectory $\mathbf{r}(k)$ in (5.6) such that: (i) when $\| \mathbf{p}(k) - \mathbf{p}_d(k) \|_2 \leq R_a$, $\mathbf{r}(k) = \boldsymbol{\eta}_d(k)$; (ii) when $\| \mathbf{p}(k) - \mathbf{p}_d(k) \|_2 > R_a$, $\mathbf{r}(k)$ is temporarily formed by replacing $\boldsymbol{p}_d(k)$ with $\boldsymbol{p}_{los}(k)$ via a LOS re-planner. The radius R_a is the user-defined sphere of acceptance for local replanning. This switching is meant to mitigate input saturation and ensure robust tracking performance under disturbance.

5.3 LOS Based Local Trajectory Generation

Traditionally, the LOS guidance system is used to generate trajectories between two waypoints in motion planning [6] and is commonly deployed in path-following control of marine vehicles [284]. Here, we apply the technique to local re-planning in 3D trajectory tracking problem. Given the AUV current position, $(x(k), y(k), z(k))$, the reference position, $(x_d(k), y_d(k), z_d(k))$, and a sphere of acceptance defined by radius R_a, if the vehicle's position is within the acceptance sphere around the desired trajectory, i.e.

$$(x_d(k) - x(k))^2 + (y_d(k) - y(k))^2 + (z_d(k) - z(k))^2 \leq R_a^2, \tag{5.8}$$

the selector matrix in (5.6) is chosen as $\mathbf{H} = [\mathbf{I}_3 \ \mathbf{0}_3]$ meaning $\mathbf{P}_d$ is selected, otherwise, $\mathbf{H} = [\mathbf{0}_3 \ \mathbf{I}_3]$ meaning the re-planned local trajectory $\mathbf{p}_{los}(k)$ is selected. In the latter, $\mathbf{p}_{los}(k)$ will be computed such that it lies on the surface of a sphere with radius R_a. When the AUV lies outside the sphere of radius R_a, the re-planned local trajectory is employed instead of the original reference trajectory until the tracking error is controlled back to the sphere defined by (5.8).

The re-planned reference trajectory can be obtained by solving the following set

of equations:

$$(x_{los}(k) - x(k))^2 + (y_{los}(k) - y(k))^2 + (z_{los}(k) - z(k))^2 = R_a^2, \tag{5.9a}$$

$$(y_{los}(k) - y(k)) = \left(\frac{y_d(k) - y(k)}{x_d(k) - x(k)}\right)(x_{los}(k) - x(k)), \tag{5.9b}$$

$$(z_{los}(k) - z(k)) = \left(\frac{z_d(k) - z(k)}{x_d(k) - x(k)}\right)(x_{los}(k) - x(k)). \tag{5.9c}$$

The first equation (5.9a) is the standard sphere of acceptance used in the LOS approach [6] and it implies that the local trajectory lies on the sphere defined by R_a. In a conventional LOS strategy, a constant slope is maintained between two successive reference positions, which is not suitable for the problem under study as the reference in this chapter is considered not to have jump discontinuity. Hence, Equations (5.9b) and (5.9c) are formulated to ensure that a constant slope between the AUV's position and the desired trajectory is maintained in the (x, y)-plane and the (x, z)-plane, respectively.

The selection of radius R_a can be challenging and is typically influenced by the nature of the reference trajectory. For smooth paths, a good choice for R_a is to determine the parameter as the average distance between two consecutive points in the desired trajectory as

$$R_a = \frac{1}{N_d}\sqrt{\left(\sum_{i=1}^{N_d}|\delta x_d(i)|\right)^2 + \left(\sum_{i=1}^{N_d}|\delta y_d(i)|\right)^2 + \left(\sum_{i=1}^{N_d}|\delta z_d(i)|\right)^2}, \tag{5.10}$$

where $\delta x_d(i) = x_d(i) - x_d(i-1)$, $\delta y_d(i) = y_d(i) - y_d(i-1)$, $\delta z_d(i) = z_d(i) - z_d(i-1)$ and N_d represents the number of data points obtained from sampling the desired trajectory. In practice, the desired trajectory is not always smooth[1], such as a Dubins' path composed of a series of straight lines and curves [285]. Despite this, a suitable estimate of R_a can be obtained by (5.10), giving a useful starting point for

[1]A smooth trajectory refers to a path with a continuous velocity profile, ensuring no jerks or sudden changes in velocity or acceleration.

tuning R_a used in the local trajectory generation scheme.

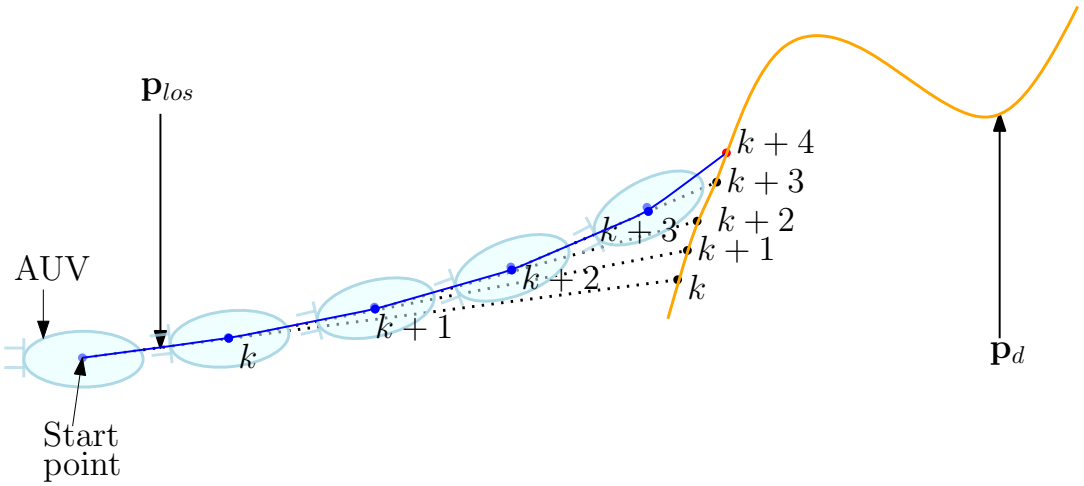

Fig. 5.1: The LOS-based local trajectory re-planning process.

For simplicity, assume the AUV depth coincides with the reference trajectory depth and is constant. An example of the local trajectory re-planning process in (x, y)-plane for the AUV based on the solution of (5.9) is illustrated in Fig. 5.1, in which the solid orange curve denotes the reference trajectory, the blue curve represents the generated re-planned local trajectory and the dotted lines correspond to the constant slope line described by (5.9b) at each time step. The local trajectory converges to the desired trajectory at $k+4$ because the desired trajectory lies within the circle of acceptance, *i.e.,* condition (5.8) is satisfied at time $k+3$. The explicit solution to (5.9) is analytically determined and given in Appendix A, including the unique case of $|x_d(k) - x(k)| = 0$. It is important to note that the proposed LOS replanning is implemented so that the direction of the LOS changes at the same rate as the reference trajectory, making it somewhat similar to the proportional navigation system commonly used in missile technology.

5.4 Tube-Based Control System Design

For the LPV system in (5.1), its prediction model defined over the prediction horizon is written as

$$\mathbf{x}(k+1+j|k) = \mathbf{A}(\mathbf{x}(k+j|k))\mathbf{x}(k+j|k) + \mathbf{B}\mathbf{u}(k+j|k) + \mathbf{w}(k+j|k), \tag{5.11}$$

for all $j = 0, \ldots, N-1$, with $\mathbf{x}(k+j|k)$ denoting the j-th prediction of $\mathbf{x}$, at time k. To reduce the computational load on updating the model at each prediction step, consider the following assumption to freeze the state-dependent system matrix over the prediction interval.

Assumption 4. *At each sampling instant,* $\mathbf{A}_\mathbf{x} = \mathbf{A}(\mathbf{x}(k+j|k)) = \mathbf{A}(\mathbf{x}(k|k))$ *for all* $j = 0, \ldots, N-1$.

Consider $\mathbf{z}(k+j|k)$ as the nominal state of the AUV model and $\mathbf{v}(k+j|k)$ as the nominal input signal, when $\mathbf{w}(k) = 0$ in (5.1). Then, the nominal prediction model is written as

$$\mathbf{z}(k+1+j|k) = \mathbf{A}_\mathbf{z}\mathbf{z}(k+j|k) + \mathbf{B}\mathbf{v}(k+j|k), \tag{5.12}$$

where $\mathbf{A}_\mathbf{z} = \mathbf{A}(\mathbf{z}(k|k))$ and $\mathbf{z}(k|k) = \mathbf{x}(k|k)$.

The difference between the nominal prediction model (5.12) and the actual prediction model (5.11) can be characterised by the state prediction error,

$$\mathbf{x}_e(k+j|k) = \mathbf{x}(k+j|k) - \mathbf{z}(k+j|k) = \mathbf{A}_\mathbf{x}\mathbf{x}_e(k+j|k) + \mathbf{B}\mathbf{u}_e(k+j|k), \tag{5.13}$$

where $\mathbf{u}_e(k+j|k) = \mathbf{u}(k+j|k) - \mathbf{v}(k+j|k)$. The control law for (5.1) with disturbances is designed to include two components, the nominal (zero disturbance) model control and the disturbance controller, that is,

$$\mathbf{u}(k+j|k) = \mathbf{v}(k+j|k) + \mathbf{K}\mathbf{x}_e(k+j|k), \tag{5.14}$$

where $\mathbf{K} \in \mathbb{R}^{6\times 12}$ is a stabilising feedback controller, referred to as the disturbance controller [282]. Given that $\mathbf{K}$ is assumed to stabilise the system $(\mathbf{A_z}, \mathbf{B})$, the evolution of the stabilised state prediction error satisfies

$$\mathbf{x}_e(k+j+1|k) = \Phi_K \mathbf{x}_e(k+j|k) + \mathbf{w}(k+j|k), \tag{5.15}$$

where $\Phi_K = (\mathbf{A_z} + \mathbf{BK})$. Since $\mathbf{w}(k+j|k)$ is assumed to be bounded, it follows that the evolution of the stabilised state error $\mathbf{x}_e(k+j|k)$ is bounded.

At any prediction step j, let $\mathbf{x}_e(k+j|k) \in \mathcal{X}_e(k)$, where $\mathcal{X}_e(k)$ is a polytope containing the origin, defined as

$$\mathcal{X}_e(k) = \{\mathcal{X}_e(k|k), \mathcal{X}_e(k+1|k), \ldots, \mathcal{X}_e(k+N|k)\}. \tag{5.16}$$

This implies $\mathbf{x}_e(k|k) = \mathbf{0}$ and the non-zero entries of $\mathcal{X}_e(k)$ are given by

$$\mathcal{X}_e(k+j|k) = \mathcal{W} \oplus \Phi_K \mathcal{X}_e(k+j|k), \;\; j = 1, \ldots, N. \tag{5.17}$$

The notation $\oplus$ represents the Minkowski set addition.

Given that the state prediction error evolves according to (5.13), the state trajectory over the horizon N evolves as inside a constrained tube with varying shape and cross-section defined by the set $\mathcal{X}_e(k)$. This phenomenon is illustrated in Fig. 5.2.

5.4.1 MPC Design with Tightened Constraint Sets

For the tube-base MPC design [274, 282], it is noted that if the nominal state and input variables, $\mathbf{z}(k+j|k)$ and $\mathbf{v}(k+j|k)$, are chosen to satisfy $\mathbf{z}(k+j|k) \oplus \mathcal{X}_e(k) \subset \mathcal{X}$ and $\mathbf{v}(k+j|k) \oplus \mathbf{K}\mathcal{X}_e(k) \subset \mathcal{U}$, respectively, then the state and input signal constraints are satisfied, that is, $\mathbf{x}(k+j|k) \in \mathcal{X}$ and $\mathbf{u}(k+j|k) \in \mathcal{U}$. This means that the nominal state and input signals can be restricted to tightened constraints

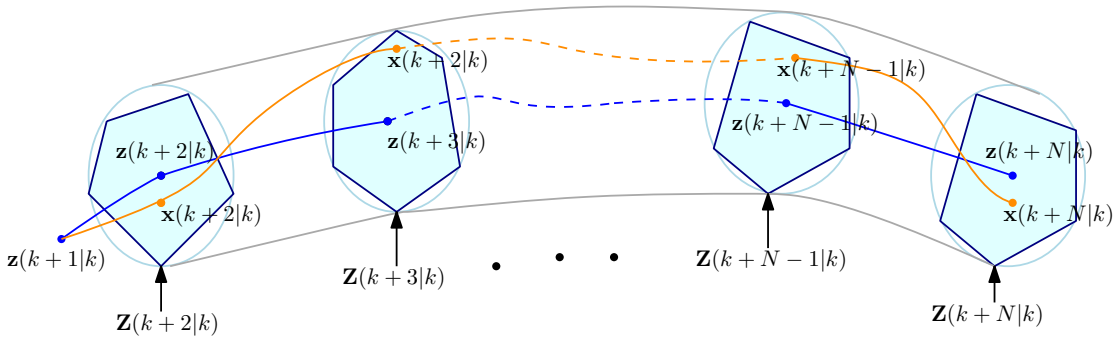

Fig. 5.2: State tube illustration: the actual state $\mathbf{x}(k+j|k)$ evolves in the tube centred along the trajectory of the nominal state $\mathbf{z}(k+j|k)$ with shape and cross section determined by the polytope $\{\mathcal{X}_e(k+j|k)\}$, $j = 1, \ldots, N$.

to ensure that for any unknown disturbance $\mathbf{w}(k+j|k) \in \mathcal{W}$, the actual state and control input satisfy the system constraints.

Denote the nominal position by $\bar{\boldsymbol{\eta}}(k+j|k)$, which is related to the nominal state prediction by

$$\bar{\boldsymbol{\eta}}(k+j|k) = \mathbf{G}_p \mathbf{z}(k+j|k), \tag{5.18}$$

where $\mathbf{G}_p = [\mathbf{I}_6 \ \mathbf{0}_6]$. Denote $\tilde{\mathbf{z}}(k+j|k)$ as the nominal state predictions at k, which rely on the optimal input sequence from $k-1$, written as follows:

$$\begin{aligned}
&\tilde{\mathbf{z}}(k+1+j|k) = \mathbf{A}_{\mathbf{z}} \tilde{\mathbf{z}}(k+j|k) + \mathbf{B}\mathbf{v}(k-1+j|k-1), j = 0, \cdots, N-2, \\
&\tilde{\mathbf{z}}(k+N|k) = \mathbf{A}_{\mathbf{z}} \tilde{\mathbf{z}}(k+N-1|k) + \mathbf{B}\mathbf{v}(k+N-1|k), \\
&\tilde{\boldsymbol{\eta}}(k+j|k) = \mathbf{G}_p \tilde{\mathbf{z}}(k+j|k), \\
&\tilde{\mathbf{z}}(k|k) = \mathbf{z}(k|k).
\end{aligned} \tag{5.19}$$

Remark 4. *Although $\bar{\boldsymbol{\eta}}(k+j|k)$ and $\tilde{\boldsymbol{\eta}}(k+j|k)$ both represent nominal position vectors, they differ in that the former may depend on an unknown input variable, $\mathbf{v}(k+j|k)$, at the current time step k. In contrast, the latter depends solely on known previous input variables, $\mathbf{v}(k+j|k-1)$.*

To minimise the nominal system's tracking error, the cost function is defined as

$$J(k) = \sum_{j=1}^{N-1} \| \bar{\boldsymbol{\eta}}(k+j|k) - \mathbf{r}(k+j|k) \|^2_{\mathbf{Q}} + \sum_{j=0}^{N_u-1} \| \Delta\mathbf{v}(k+j|k) \|^2_{\mathbf{R}} \\ \| \bar{\boldsymbol{\eta}}(k+N|k) - \mathbf{r}(k+N|k) \|^2_{\mathbf{P}}, \tag{5.20}$$

where N_u is the control horizon, $\Delta\mathbf{v}$ is the input variation between k and $k-1$, $\mathbf{Q}$ and $\mathbf{R}$ are positive definite weighting matrices for the output and input, respectively. At any time k, obtain $\mathbf{x}(k)$ and define $\mathbf{z}(k|k) = \mathbf{x}(k)$, based on which the nominal state $\mathbf{z}(k+j|k)$ is predicted using an optimally selected control sequence $\mathbf{v}(k+j|k)$ for $j = 0, \ldots, N-1$. The controller design is achieved in two steps.

In the first step, the nominal optimal control signal sequence is defined as: $\mathbf{V}(k) = \{\mathbf{v}(k|k), \mathbf{v}(k+1|k), \ldots, \mathbf{v}(k+N_u-1|k)\}$. The high-level MPC design for the nominal system is obtained from the QCQP:

$$\mathbb{Q}(\mathbf{z}(k)): \ \mathbf{V}^*(k) = \arg\min_{\mathbf{V}(k)} J(k) \tag{5.21a}$$

$$\text{s.t. } \mathbf{z}(k+j|k) \in \mathcal{Z}, \ j > 0, \tag{5.21b}$$

$$\mathbf{v}(k+j|k) \in \mathcal{V}, \ j \geq 0, \tag{5.21c}$$

$$\mathbf{v}(k+j|k) = \mathbf{v}(k-1) + \sum_{i=0}^{j} \Delta\mathbf{v}(k+i|k), \tag{5.21d}$$

$$\mathbf{v}(k-1) = \mathbf{u}(k-1), \tag{5.21e}$$

$$\| \tilde{\boldsymbol{\eta}}(k+N-1|k) - \mathbf{r}(k+N-1|k) \|^2_{\mathbf{Q}} \\ + \| \Delta\mathbf{v}(k+N_u-1|k) \|^2_{\mathbf{R}} \leq \mu, \tag{5.21f}$$

$$\mathbf{z}(k|k) = \mathbf{x}(k), \tag{5.21g}$$

where $\mathcal{Z} = \mathcal{X} \ominus \mathcal{X}_e(k+j|k)$ and $\mathcal{V} = \mathcal{U} \ominus \mathbf{K}\mathcal{X}_e(k+j|k)$ are the tightened state and input constraint sets. The notation $\ominus$ represents the Minkowski set subtraction. The solution to the quadratic program $\mathbb{Q}(\mathbf{z}(k))$ provides $\mathbf{v}^*(k+j|k)$ for $j = 0, \ldots, N_u-1$, representing the optimal input sequence. It is assumed that for $N_u < N$, $\mathbf{v}^*(k+$

$j|k) = \mathbf{v}(k+j-1|k)$ for $j = N_u, \ldots, N$ which means $\Delta\mathbf{v}(k+j|k) = \mathbf{0}$ for $j = N_u, \ldots, N$. Based on the receding horizon principle, $\mathbf{v}^*(k) = \mathbf{v}^*(k|k)$. Constraints (5.21f) is used to impose a stability condition where μ is given as

$$\begin{aligned}\mu = & \parallel \bar{\boldsymbol{\eta}}(k-1|k-1) - \mathbf{r}(k-1) \parallel^2_{\mathbf{Q}} + \parallel \Delta\mathbf{v}(k-1|k-1) \parallel^2_{\mathbf{R}} \\ & - \sum_{j=1}^{N-2} \parallel \tilde{\boldsymbol{\eta}}(k+j|k) - \bar{\boldsymbol{\eta}}(k+j|k-1) \parallel^2_{\mathbf{Q}} - \varepsilon,\end{aligned} \tag{5.22}$$

where $\varepsilon > 0$.

In the second step, to ensure the actual states of the AUV follow the reference tube trajectory, the low-level disturbance control is computed by

$$\mathbf{u}^*(k) = \mathbf{v}^*(k) + \mathbf{K}\left(\mathbf{x}(k|k) - \mathbf{z}^*(k|k)\right). \tag{5.23}$$

The control signal in (5.23) represents the actual control signal to be applied to the nonlinear AUV model (2.14) for robust tracking of the desired trajectory $\mathbf{r}(k)$. The optimal control problem ($\mathbb{Q}$) is a convex QCQP because $\mathbf{Q}$ and $\mathbf{R}$ are positive definite matrices which means the problem is computationally tractable [286]. The framework of this proposed robust tube-based MPC is shown in Fig. 5.3.

By setting the initial state error to zero, $\mathbf{x}_e(k|k) = \mathbf{0}$, the state error prediction terms are written as

$$\mathbf{x}_e(k+j|k) = \sum_{i=0}^{j-1} \Phi_K^i \mathbf{w}(k+j-1-i|k), j = 1, \ldots, N. \tag{5.24}$$

To implement the tightened constraint in (5.21), it is necessary to determine $\mathbf{w}(k+j|k) \in \mathcal{W}$ for $j = 1, \ldots, N-1$. Based on the definition of the state constraint set in (5.3), the tightened nominal state can be formulated as

$$\mathbf{G}_x \mathbf{z}(k+j|k) \leq \mathbf{h}_x - \Theta_\infty, \tag{5.25}$$

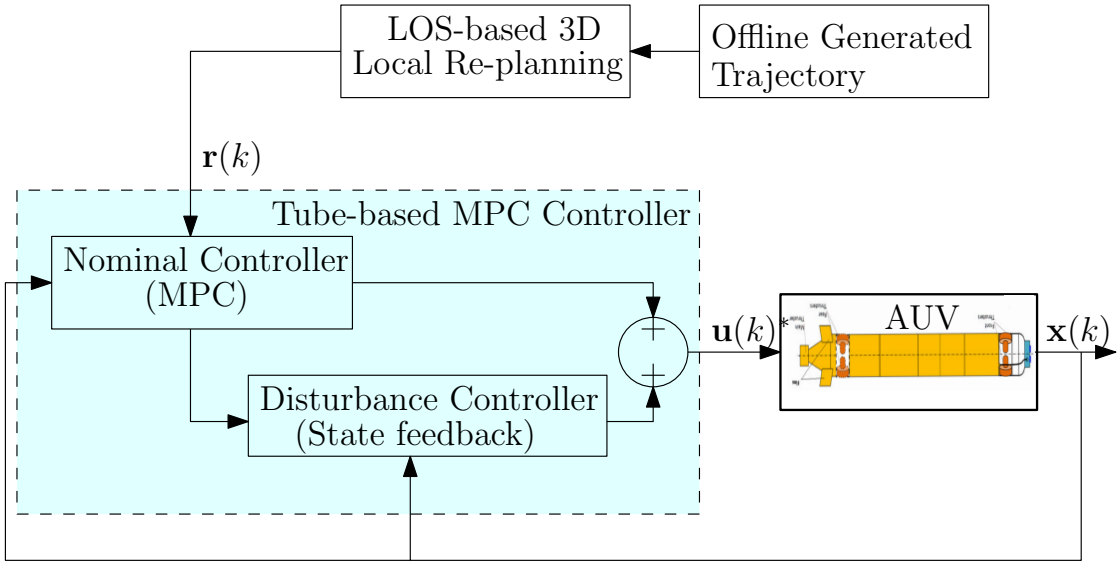

Fig. 5.3: Robust tube-based model predictive control framework for AUV.

where Θ_∞ can be obtained from $\max_{\mathbf{x}_e(k+j|k)} \{\mathbf{G}_x \mathbf{x}_e(k+j|k) : \mathbf{x}_e(k+j|k) \in \mathcal{X}_e(k)\}$, and $\mathbf{x}_e(k+j|k)$ is calculated by (5.24). The exact knowledge of Θ_∞ is not required to satisfy the system constraints, instead, an outer approximation of the parameter would be sufficient. Define $\Theta_\infty \leq (1-\lambda)^{-1}\Theta_N$ with $\lambda \in (0,1)$, Θ_N can be computed from the linear programming problem

$$\mathbb{L}: \ \Theta_N = \arg \max_{\mathbf{w}(k+j|k)\in\mathcal{W}} \left\{ \mathbf{G}_x \sum_{j=0}^{N-1} \Phi_K^i \mathbf{w}(k+j|k) \right\}. \tag{5.26}$$

It is noted that $\mathbf{w}(k|k) = \mathbf{0}$ in (5.26) because of the definition of $\mathcal{X}_e(k+j|k)$ in (5.17). Therefore, the tightened state constraint set is given by

$$\mathcal{Z} = \left\{ \mathbf{z}(k+j|k) \in \mathbb{R}^{12} : \mathbf{G}_x \mathbf{z}(k+j|k) \leq \mathbf{h}_x - \rho\Theta_N \right\}, \tag{5.27}$$

where $\rho = (1-\lambda)^{-1}$. Similarly, the tightened input constraint set is approximated by

$$\mathcal{V} = \left\{ \mathbf{v}(k+j|k) \in \mathbb{R}^{6} : \mathbf{G}_u \mathbf{v}(k+j|k) \leq \mathbf{h}_u - \rho\mathbf{K}\Theta_N \right\}. \tag{5.28}$$

At each k, the optimisation problem $\mathbb{L}$ in (5.26) needs to be solved first before

solving $\mathbb{Q}$ in (5.21). The stability condition for the nominal system is summarised in the following theorem.

Theorem 5.4.1. *Consider that the lumped disturbance is negligible and Assumptions 3 holds. Given the nominal system (5.12) and the MPC law (5.21) with the tightened constraints defined by $\mathcal{Z}$ and $\mathcal{V}$ for state and input, respectively, the closed-loop system $\phi_n(\mathbf{z}(k)) = \mathbf{A_z z}(k) + \mathbf{B v}^*(k)$ is (locally) asymptotically stable.*

Proof. If $\mathbf{K}$ is a stabilising gain for the error model (5.13), the tightened sets $\mathcal{Z}$ and $\mathcal{V}$ are convex. Under negligible lumped disturbance $\mathbf{w}(k)$, for $j = 0$, the nominal system (5.12) is equivalent to the actual AUV system (5.1). Hence, the proof of the theorem follows from the results in [287]. □

Definition 5.4.2 ([288])**.** The closed-loop of the perturbed AUV system $\phi_p(\mathbf{x}(k)) = (\mathbf{A_x x}(k) + \mathbf{B u}^*(k)) + \mathbf{w}(k)$ is called input-to-state stable (ISS) if there exist a $\mathcal{KL}-$function $\beta(\cdot)$ and a $\mathcal{K}-$function $\gamma(\cdot)$ such that, for every $\mathbf{x}(k) \in \mathcal{X}$ and $\mathbf{w}(k) \in \mathcal{W}$ for all k, the state trajectories satisfy

$$\| \phi_p(\mathbf{x}(k)) \| \leq \beta(\| \mathbf{x}(k) \|, k) + \gamma(\| \mathbf{w}(k) \|). \tag{5.29}$$

Definition 5.4.2 is the local version of discrete-time ISS and it is similar to the robust asymptotic stability (RAS) property in [289].

Theorem 5.4.3. *Suppose Assumption 3 holds; then the closed-loop system $\phi_p(\mathbf{x}(k))$ is ISS under the tube-based control law (5.23).*

Proof. The asymptotic stability of the nominal system (5.12) based on Theorem 5.4.1 guarantees the existence of a $\mathcal{KL}-$function $\beta(\cdot)$ such that the closed-loop system, $\phi_n(\mathbf{x}(k))$, satisfies

$$\| \phi_n(\mathbf{x}(k)) \| \leq \beta(\| \mathbf{x}(k) \|, k). \tag{5.30}$$

Considering the effects of disturbances, apply the control input (5.23) to system (5.1), and then adding and subtracting $\mathbf{A_z z}(k|k)$ yields

$$\begin{aligned}\phi_p(\mathbf{x}(k)) &= \mathbf{A_x x}(k) + \mathbf{B v}^*(k|k) + \phi_K(\mathbf{x}(k|k) - \mathbf{z}^*(k|k)) + \mathbf{w}(k), \\ &= \mathbf{z}(k+1|k) + \phi_K(\mathbf{x}(k|k) - \mathbf{z}^*(k|k)) + \mathbf{w}(k), \\ &= \phi_n(\mathbf{x}(k)) + \phi_K \mathbf{x}_e(k|k) + \mathbf{w}(k).\end{aligned} \tag{5.31}$$

From the definition of the set $\mathcal{X}_e(k)$ in (5.17), it follows that $\mathbf{x}_e(k|k) = \mathbf{0}$, therefore

$$\phi_p(\mathbf{x}(k)) = \phi_n(\mathbf{x}(k)) + \mathbf{w}(k). \tag{5.32}$$

Combining (5.32) and (5.30), it can be concluded that there exist a $\mathcal{KL}-$function $\beta(\cdot)$ and a $\mathcal{K}-$function $\gamma(\cdot)$ that satisfy

$$\| \phi_p(\mathbf{x}(k)) \| \leq \beta(\| \mathbf{x}(k) \|, k) + \gamma(\mathbf{w}(k)). \tag{5.33}$$

Hence, the closed-loop system $\phi_p(\mathbf{x}(k))$ is ISS. □

5.4.2 Optimal State-Dependent Feedback Control Design

Designing the disturbance controller $\mathbf{K}$ is a critical step in implementing the proposed robust MPC controller. However, it is difficult to determine the tube with a local linear feedback gain due to system nonlinearities. An intuitive approach to find $\mathbf{K}$ involves solving an infinite horizon, input affine regulator problem using the SDRE method, which requires solving an SD-DARE numerically online. To avoid the computation load, we consider a finite horizon control problem, with a terminal equality constraint, that can be solved analytically to obtain a state-dependent feedback gain.

Define the cost function to regulate the state prediction error as

$$J_1(k) = \sum_{j=1}^{N_1} \| \mathbf{x}_e(k+j|k) \|_{\mathbf{Q}_1} + \sum_{j=0}^{N_1-1} \| \mathbf{u}_e(k+j|k) \|_{\mathbf{R}_1}, \tag{5.34}$$

where $\mathbf{Q}_1 \in \mathbb{R}^{12\times12}$ is positive semi-definite, $\mathbf{R}_1 \in \mathbb{R}^{6\times6}$ is positive definite and N_1 is the prediction horizon. The state feedback controller is determined by solving the optimisation problem

$$\mathbb{P}: \ \mathbf{U}_e^*(k) = \arg\min \ J_1(k) \tag{5.35a}$$

$$\text{s.t. } \mathbf{x}_e(k+j|k) = \mathbf{A}_\mathbf{x}\mathbf{x}_e(k+j|k) + \mathbf{B}\mathbf{u}_e(k+j|k), \tag{5.35b}$$

$$\mathbf{x}_e(k+N_1|k) = \mathbf{0}, \tag{5.35c}$$

where $\mathbf{U}_e(k) = \{\mathbf{u}_e(k|k), \ldots, \mathbf{u}_e(k+N_1-1|k)\}$. Under Assumption 4, the gain matrix $\mathbf{K}_{MPC} \in \mathbb{R}^{6N_1\times12(N_1-1)}$ obtained from (5.35) satisfies

$$\begin{bmatrix} \mathbf{u}_e(k|k) \\ \mathbf{u}_e(k+1|k) \\ \vdots \\ \mathbf{u}_e(k+N_1-1|k) \end{bmatrix} = \mathbf{K}_{MPC} \begin{bmatrix} \mathbf{A}_\mathbf{x} \\ \mathbf{A}_\mathbf{x}^2 \\ \vdots \\ \mathbf{A}_\mathbf{x}^{N_1-1} \end{bmatrix} \mathbf{x}_e(k). \tag{5.36}$$

Based on the receding horizon principle, the gain associated with the first control input is extracted as the state-dependent gain as follows:

$$\mathbf{K} = \mathbf{K}_{MPC}^0 \begin{bmatrix} \mathbf{A}_\mathbf{x} \\ \mathbf{A}_\mathbf{x}^2 \\ \vdots \\ \mathbf{A}_\mathbf{x}^{N-1} \end{bmatrix} \in \mathbb{R}^{6\times12}, \tag{5.37}$$

where $\mathbf{K}_{MPC}^0$ consists of the first 6 rows (dimension of control signal) of $\mathbf{K}_{MPC}$. The steps needed to implement the proposed TMPC law are provided in the pseudo-code

given in Algorithm 3.

Theorem 5.4.4. *Suppose Assumptions 3 and 4 hold, the analytical solution (5.36) obtained from solving* (5.35) *is (locally) asymptotically stabilising for the time-varying error model (5.13).*

Proof. It shows from the cost function in (5.34) that $J_1(k) \geq 0$ for $k > 0$. A sub-optimal solution can be obtained by shifting the error state trajectory at k by 1 to obtain the state trajectory at $k+1$, that is,

$$\begin{aligned}
J_1(k+1) &= \sum_{j=1}^{N_1} \parallel \mathbf{x}_e(k+1+j|k+1) \parallel^2_{\mathbf{Q}_1} + \sum_{j=0}^{N_1-1} \parallel \mathbf{u}_e(k+1+j|k+1) \parallel^2_{\mathbf{R}_1}, \\
&= \sum_{j=2}^{N_1+1} \parallel \mathbf{x}^*_e(k+j|k) \parallel^2_{\mathbf{Q}_1} + \sum_{j=1}^{N_1} \parallel \mathbf{u}^*_e(k+j|k) \parallel^2_{\mathbf{R}_1}, \\
&= \sum_{j=1}^{N_1} \parallel \mathbf{x}^*_e(k+j|k) \parallel^2_{\mathbf{Q}_1} + \sum_{j=0}^{N_1-1} \parallel \mathbf{u}^*_e(k+j|k) \parallel^2_{\mathbf{R}_1} \\
&\quad - \parallel \mathbf{x}^*_e(k+1|k) \parallel^2_{\mathbf{Q}_1} - \parallel \mathbf{u}^*_e(k|k) \parallel^2_{\mathbf{R}_1} + \parallel \mathbf{x}^*_e(k+1+N_1|k) \parallel^2_{\mathbf{Q}_1}, \\
&= J_1(k) - \parallel \mathbf{x}^*_e(k+1|k) \parallel^2_{\mathbf{Q}_1} - \parallel \mathbf{u}^*_e(k|k) \parallel^2_{\mathbf{R}_1} \leq 0.
\end{aligned}$$

Therefore, the cost function in (5.34) is a Lyapunov function, that is, $J_1(k+1) \leq J_1(k)$ holds and $J(k) \geq 0$ for all k. Thus, the error model (5.13) is locally asymptotically stable. □

Remark 5. *The imposition of the zero terminal constraint (5.35c) has the drawback of likely requiring a large control effort to steer the error state to the origin, especially when N_1 is short [290]. Therefore, it is recommended to choose N_1 to be larger than N.*

Algorithm 3: Tube-based MPC with LOS replanning

Input: AUV LPV model, $\mathbf{Q}$, $\mathbf{Q}_1$, $\mathbf{P}$, $\mathbf{R}$, $\epsilon > 0$, $\gamma \in (0,1)$, N and N_u.

$k \leftarrow 0$

Compute the sphere of acceptance radius R_a based on the desired trajectory (x_d, y_d, z_d) using (5.10).

Define the disturbance bound $\mathbf{w}_{\max}$.

Measure current state $\mathbf{x}(k)$ and set $\mathbf{z}(k|k) = \mathbf{x}(k)$.

repeat

  Determine the reference signal such that: (i) $\mathbf{r}(k) = \boldsymbol{\eta}_d(k)$ when $\| \mathbf{p}(k) - \mathbf{p}_d(k) \|_2 \leq R_a$; (ii) $\mathbf{r}(k) = [x_{los}\ y_{los}\ z_{los}\ \phi_d\ \theta_d\ \psi_d]^\top$ when $\| \mathbf{p}(k) - \mathbf{p}_d(k) \|_2 > R_a$.

  Determine the state-dependent feedback gain $\mathbf{K}$ from (5.37) using $\mathbf{x}(k)$.

  Solve (5.26) to obtain Θ_N.

  Compute the tightened constraint sets $\mathcal{Z}$ and $\mathcal{V}$ using (5.27) and (5.28).

  Solve (5.21) to obtain the input sequence $\mathbf{V}^*(k) = \{\mathbf{v}^*(k|k), \ldots, \mathbf{v}^*(k+N_u-1|k)\}$.

  Compute the low-level controller $\mathbf{u}^*(k)$ according to (5.23).

  Implement $\boldsymbol{\tau}(k) = \mathbf{u}^*(k)$ for one sampling period.

  Update the state measurement as $\mathbf{x}(k+1)$

  $k \leftarrow k+1$

until end

5.5 Simulation Results

5.5.1 System Settings and Performance Metrics

The proposed control strategy is numerically validated using the Naminow-D AUV prototype, a scaled version (3 m) of the REMUS AUV. Equipped with an Inertia Navigation System (INS), the position and velocities are measured, allowing real-time calculation of control forces and moments. To avoid excessive thrust forces employed for the navigation task, the input forces and moments are limited to 1000 N and 1000 Nm, respectively. The unknown environmental disturbances τ_X^w, τ_Y^w and τ_Z^w are assumed to be equal and modelled using the modified Pierson–Moskowitz Spectrum as in Chapter 4. However, the offset term d_i is modelled as a standard Wiener process in the range $[-60, 60]$. The wave force-time profile is shown in Fig. 5.4.

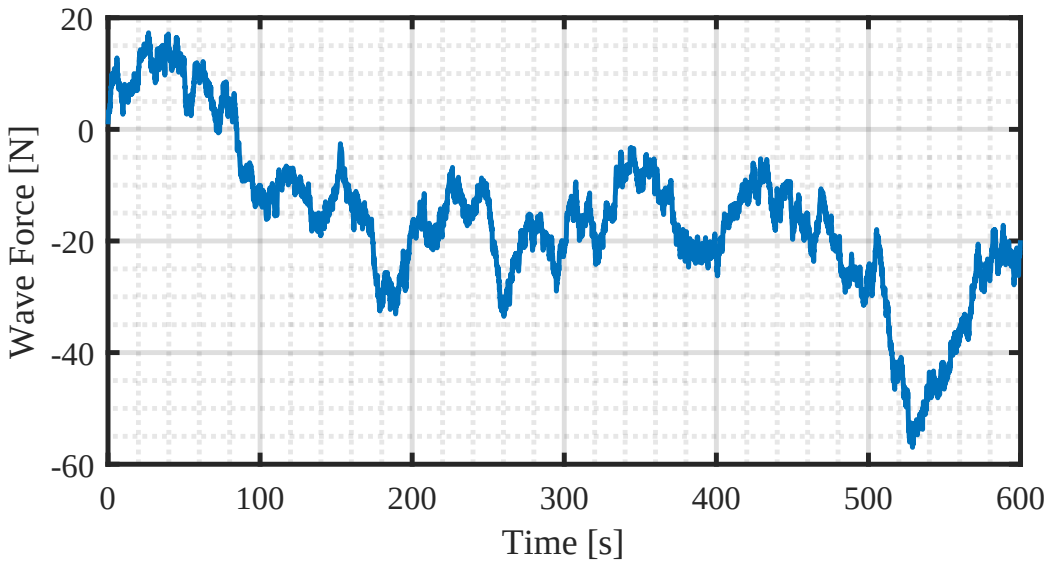

Fig. 5.4: Wave disturbance evolution over time.

In the TMPC design, a sampling time of $T_s = 0.1$ s was used, and the prediction and control horizons were tuned to be $N = 6$, $N_1 = 20$ and $N_u = 2$. The weighting matrices for the proposed TMPC were selected as $\mathbf{Q} = 2\mathbf{I}_6$, $\mathbf{Q}_1 = \mathbf{I}_{12}$, $\mathbf{R} = \mathbf{R}_1 =$

$0.6\mathbf{I}_6$ and $\varepsilon = 0.1$. The lumped disturbance term is bounded by $|\mathbf{w}(k)| \leq \mathbf{0.5}$, and the tightened constraint setting parameter λ is set to be 0.05. Additionally, the input rate constraint is defined by $\delta\mathbf{u}_{\max} \leq 100$, which means that a maximum variation of ± 100 N or Nm is allowed at each control step. The pitch angle θ is bounded by $\theta_{\max} = 2\pi/5$ rad to avoid singularities in the transformation matrix.

The performance of the proposed TMPC in 3D scenarios was compared with an NMPC. For the NMPC design, the input and output weightings were tuned to be $\mathbf{I}_6$ and $600\mathbf{I}_6$, respectively. The input rate constraints were not implemented in the case of NMPC to preserve its feasibility.

The control performance is quantitatively analysed using different metrics. For positioning errors (translational and angular) and input chattering (CT), the integral of absolute error (IAE) and the absolute sum of input variations are used and they are given as follows:

$$\mathrm{IAE}_{\mathrm{pos}} = \sum_{k=1}^{N_d}\sum_{i=1}^{3} |\boldsymbol{\eta}(i,k) - \boldsymbol{\eta}_d(i,k)|,\ \mathrm{IAE}_{\mathrm{ori}} = \sum_{k=1}^{N_d}\sum_{i=4}^{6} |\boldsymbol{\eta}(i,k) - \boldsymbol{\eta}_d(i,k)|, \quad (5.38a)$$

$$\mathrm{CT}_{\mathrm{for}} = \sum_{k=1}^{N_d}\sum_{i=1}^{3} |\delta\boldsymbol{\tau}(i,k)|,\ \mathrm{CT}_{\mathrm{mom}} = \sum_{k=1}^{N_d}\sum_{i=4}^{6} |\delta\boldsymbol{\tau}(i,k)|, \quad (5.38b)$$

where the subscripts 'pos' and 'ori' relate to AUV's position and orientation, CT represents chattering, the subscripts 'for' and 'mom' represent forces and moments, the use of '(i,k)' denotes the i-th entry of a vector at k.

The rate of energy consumption (EC) during navigation is directly related to both the forces and moments applied to the AUV. The following EC metric is formulated:

$$\mathrm{EC}_{\mathrm{tot}} = \sum_{k=1}^{N_d} \left(\underbrace{\sum_{i=1}^{3} |\boldsymbol{\nu}(i,k)\mathbf{u}(i,k)|}_{\mathrm{EC}_{\mathrm{pos}}} + \underbrace{\sum_{i=4}^{6} |\boldsymbol{\nu}(i,k)\mathbf{u}(i,k)|}_{\mathrm{EC}_{\mathrm{ori}}} \right) \times \frac{T_s}{3600}. \quad (5.39)$$

The EC metric defined in (5.39) is in Wh.

Two types of reference trajectories are set up to examine the efficacy of the proposed TMPC with LOS replanning. The first one is a spatial helical trajectory, and the second is a 3D path created using the Dubins method, which includes a mix of straight lines and curves. Simulations are implemented in the MATLAB/Simulink environment using a PC with an Intel Core i7 processor running at 2.2 GHz and 16GB RAM.

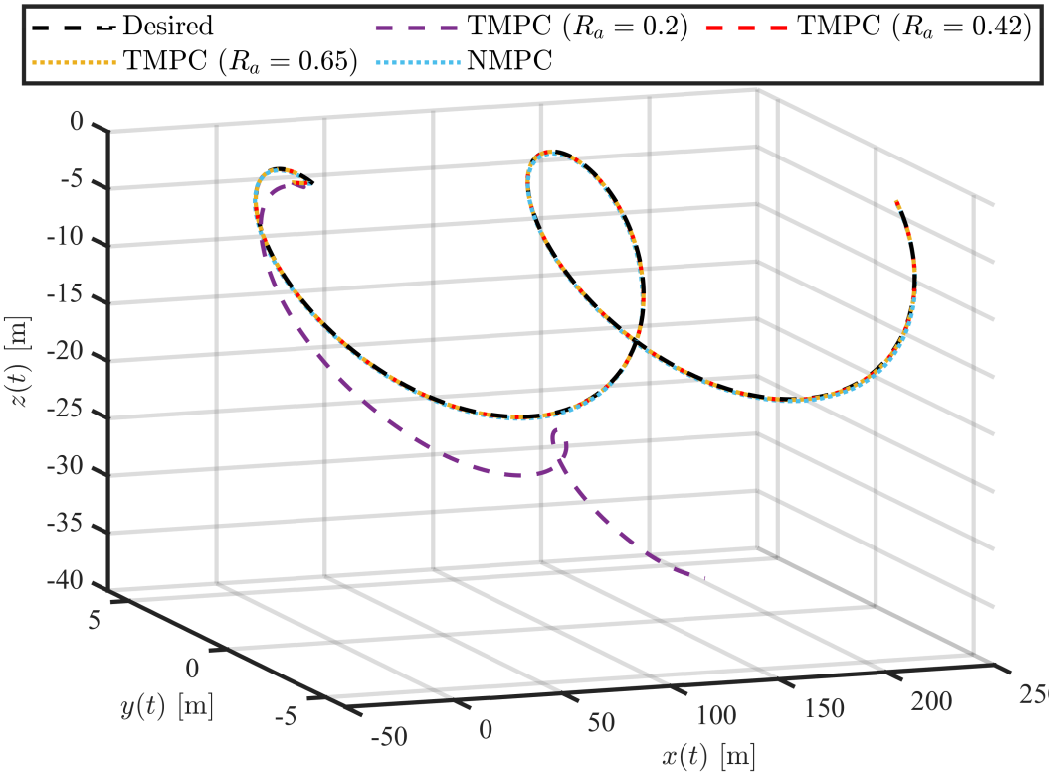

Fig. 5.5: Helical desired trajectory with initial AUV position $\boldsymbol{\eta}_1(0)$: AUV motion in 3D space.

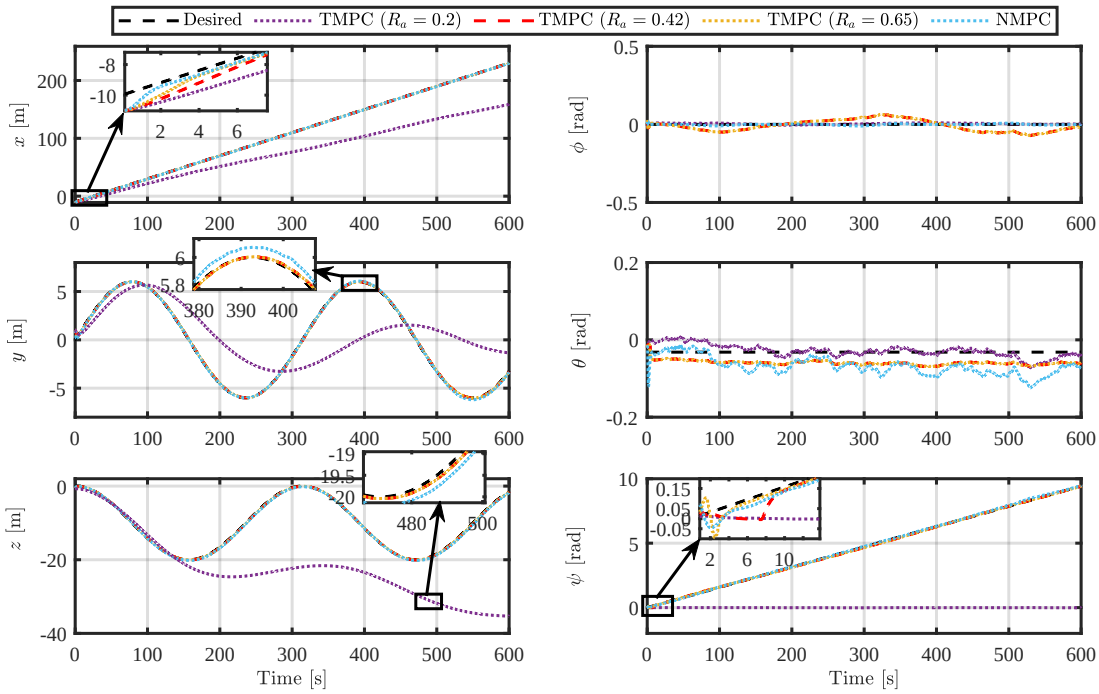

Fig. 5.6: Helical desired trajectory (initial AUV position $\boldsymbol{\eta}_1(0)$): linear (left) and angular (right) position responses.

5.5.2 Helical Trajectory Tracking

The desired helical trajectory is designed following the underwater pipeline inspection task in [22] as follows:

$$\begin{cases} x_d(t) = -10 + 0.04t \text{ m}, \\ y_d(t) = 6\sin(0.02t) \text{ m}, \\ z_d(t) = 10\cos(0.02t) - 10 \text{ m}, \\ \phi_d(t) = 0 \text{ rad}, \\ \theta_d(t) = -\arctan(0.1/\pi) \text{ rad}, \\ \psi_d(t) = 0.005\pi t \text{ rad}. \end{cases} \tag{5.40}$$

Given $\boldsymbol{\eta}_d(0) = [-10\ 0\ 0\ 0\ \ -0.032\ 0]^\top$ as the initial point in the desired trajectory, two different initial AUV positions are considered in the simulation study. The first initial AUV position is set as $\boldsymbol{\eta}_1(0) = [-11\ 1\ \ -0.7\ 0\ 0\ 0]^\top$. Using (5.10) and a

simulation length of 600 s, the sphere of acceptance is calculated to be $R_a = 0.42$ m. To show how the choice of R_a may impact the controller's performance, three values of R_a are used in the simulation: $R_a = 0.2$ m, $R_a = 0.42$ m and $R_a = 0.65$ m. The tracking results obtained from NMPC and the proposed TMPC are presented in Figs. 5.5–5.8. Fig. 5.5 shows the 3D motion of the AUV, while the components of the translational and angular position variables are presented in Fig. 5.6. The AUV velocities are illustrated in Fig. 5.7, and the inputs along with their rates are shown in Fig. 5.8.

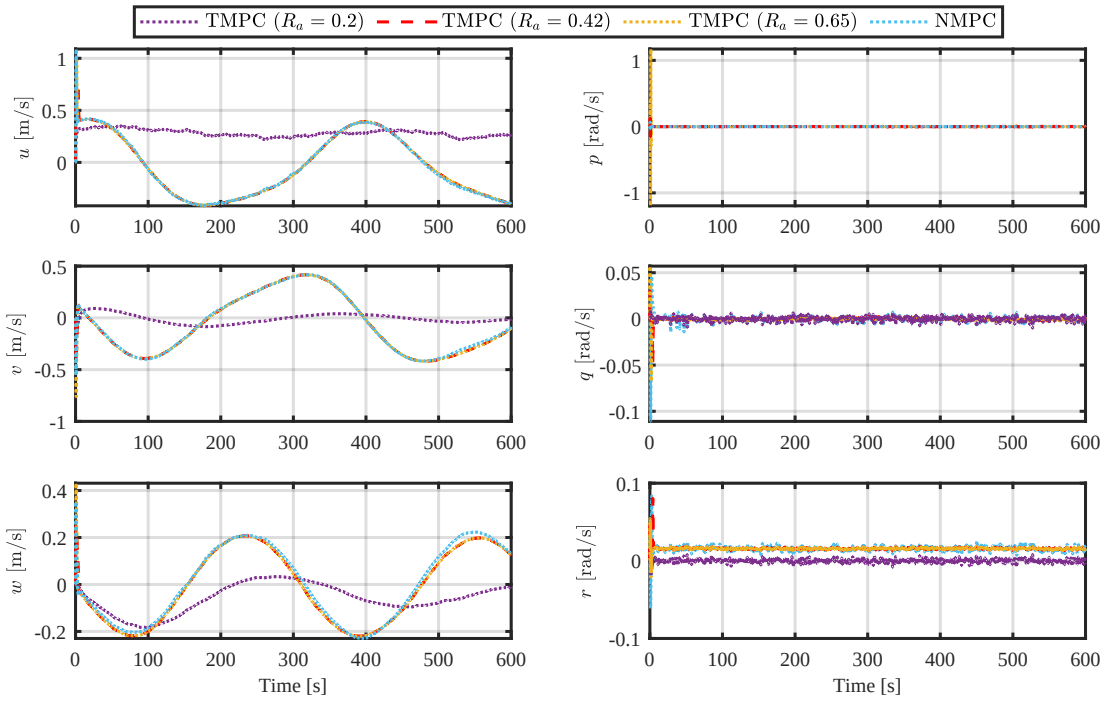

Fig. 5.7: Helical desired trajectory (initial AUV position $\boldsymbol{\eta}_1(0)$): linear (left) and angular (right) velocity responses.

Compared to the NMPC, the two TMPC controllers with $R_a = 0.42$ m and $R_a = 0.65$ m show superior tracking performance by having over 33% reduction in translational position tracking error and 6.2% reduction in angular position tracking error. Although using a larger value of $R_a = 0.65$ m leads to faster convergence in translational position tracking, it also causes higher initial velocity variations,

resulting in higher input saturation as compared to taking $R_a = 0.42$ m. When $R_a = 0.2$ m, which is 52% smaller than the calculated value of 0.42, the proposed TMPC could not achieve the desired control objective (see Fig. 5.6).

Table 5.1 summarises the quantitative performance of the controllers. For the helical trajectory, compared to NMPC, the TMPC ($R_a = 0.42$ m) has lower chattering in the moment input, higher chattering in the force input, and lower energy consumption. This suggests that the proposed TMPC scheme achieves the control objectives with a lower energy cost in control actuation.

To demonstrate the controller's effectiveness, another AUV initial condition, $\boldsymbol{\eta}_2(0) = [-25\ 10\ -8\ 0\ 0\ 0]^\top$, is simulated and the results are given in Figs. 5.9 – 5.12. In this scenario, the distance between $\boldsymbol{\eta}_2(0)$ and $\boldsymbol{\eta}_d(0)$ is large. It took a longer time for the TMPC controllers to converge to the desired path, compared to the case with $\boldsymbol{\eta}_1(0)$, still all the input magnitude and rate constraints were satisfied (see Fig. 5.12). It is noted that NMPC became infeasible in this case despite neglecting the input rate constraints in its implementation.

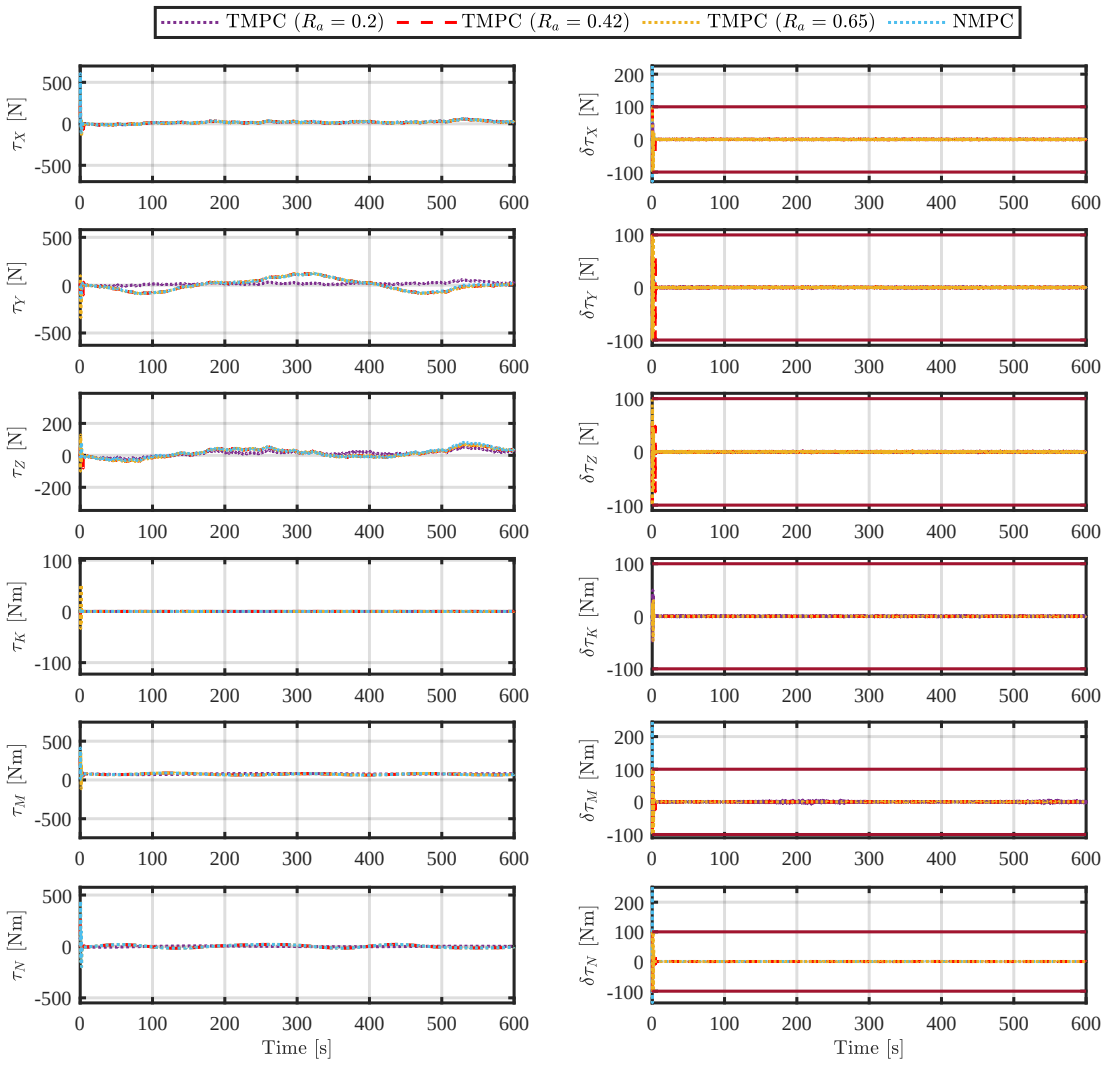

Fig. 5.8: Helical desired trajectory (initial AUV position $\boldsymbol{\eta}_1(0)$): the input forces and moments (left) and their rates of change (right).

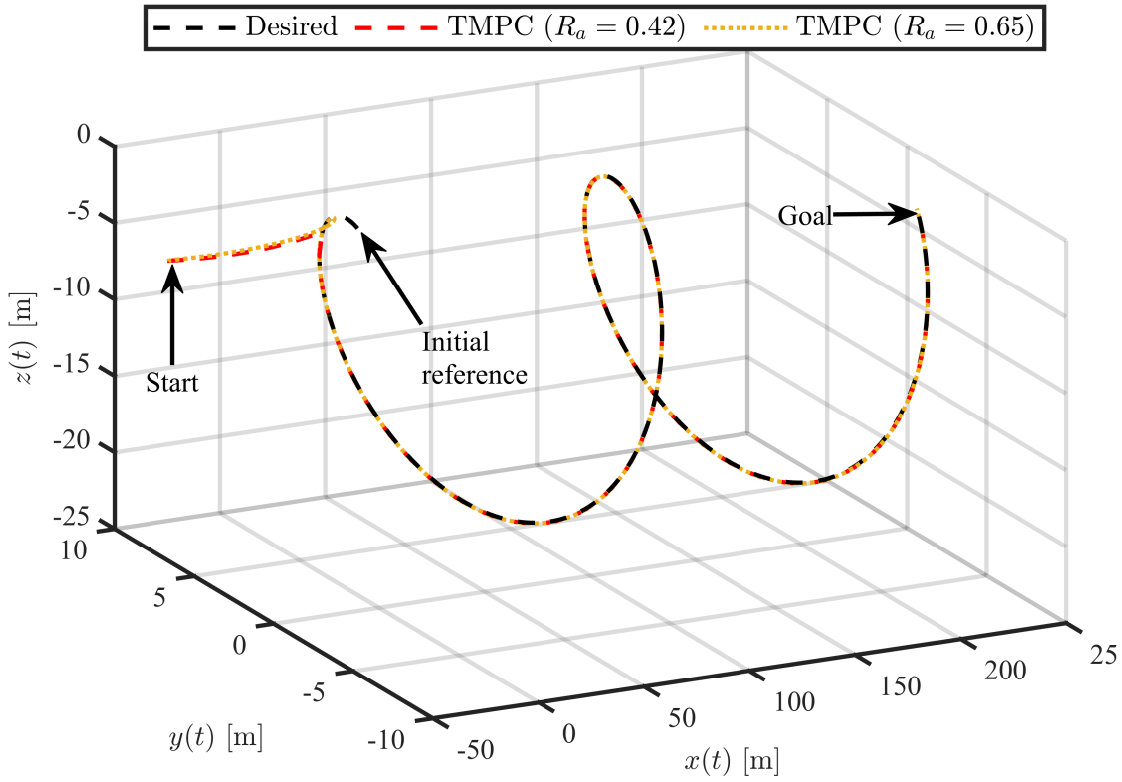

Fig. 5.9: Helical desired trajectory with initial AUV position $\boldsymbol{\eta}_2(0)$: AUV motion in 3D.

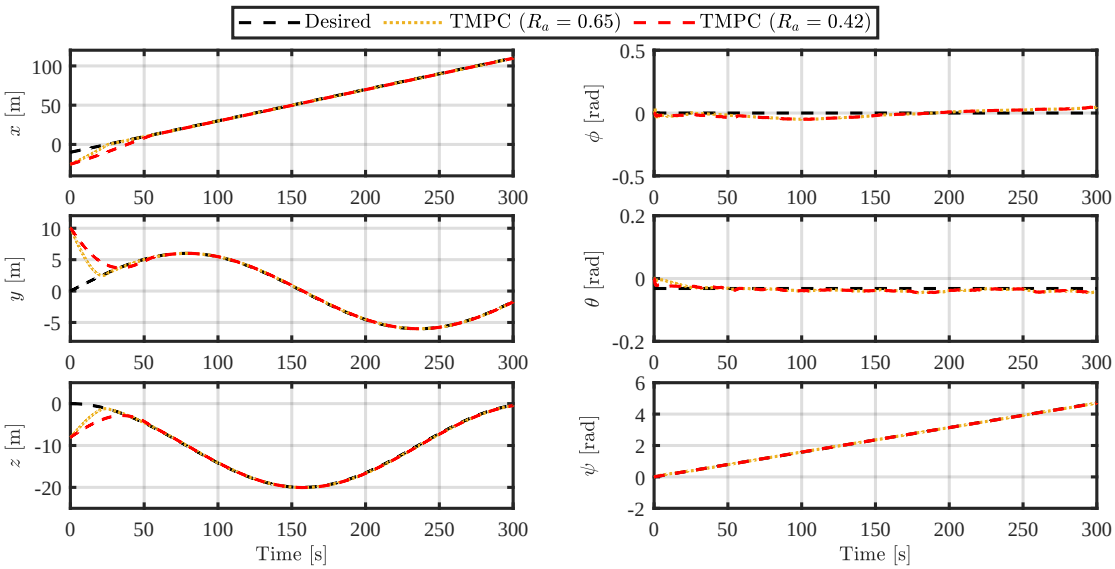

Fig. 5.10: Helical desired trajectory (initial AUV position $\boldsymbol{\eta}_2(0)$): linear (left) and angular (right) position responses.

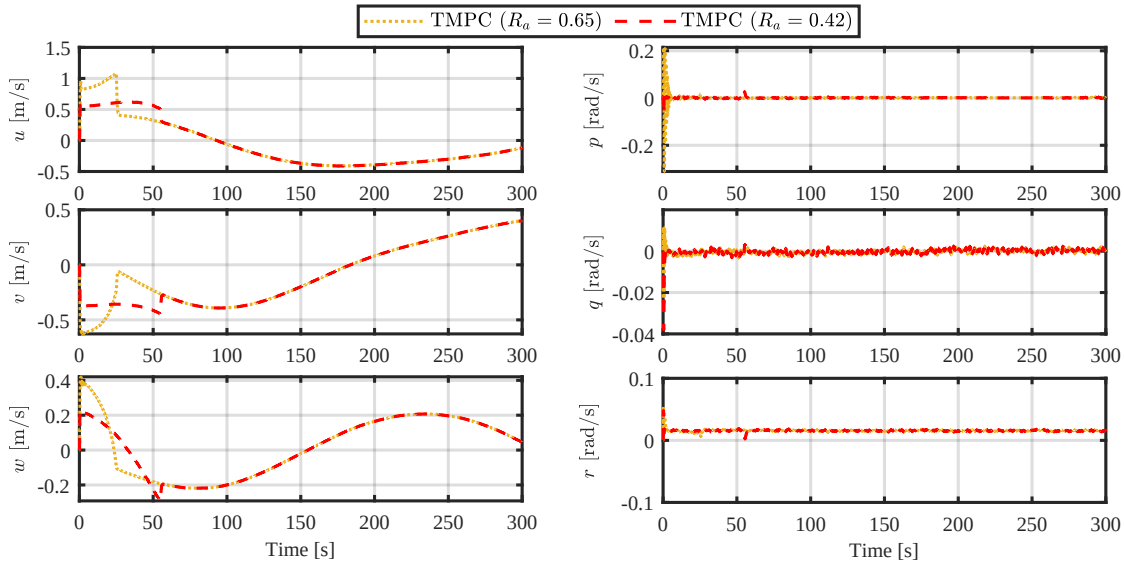

Fig. 5.11: Helical desired trajectory (initial AUV position $\boldsymbol{\eta}_2(0)$): linear (left) and angular (right) velocity responses.

5.5.3 Dubins Trajectory Tracking

The Dubins trajectory is created following the design in [285], but modified to suit the larger size of the Naminow-D AUV in this work compared to the ODIN AUV. The reference path consists of a dive trajectory for 80 s, followed by a horizontal comb-shaped trajectory for 400 s. The desired trajectory is defined as follows:

$$x_d(t) = \begin{cases} 0 \text{ m}, \ 0 \leq t < 80 \text{ s} \\ 1/5t - 16 \text{ m}, \ 80 \leq t < 160 \text{ s} \\ 4\sin((\pi(t/4 - 40))/20) + 16 \text{ m}, \ 160 \leq t < 240 \text{ s} \\ -1/5t + 64 \text{ m}, \ 240 \leq t < 320 \text{ s} \\ -4\sin(\pi(t/4 - 80)/20) \text{ m}, \ 320 < t \leq 400 \text{ s} \\ 1/5t - 80 \text{ m}, \ 400 \leq t < 480 \text{ s} \end{cases} \tag{5.41}$$

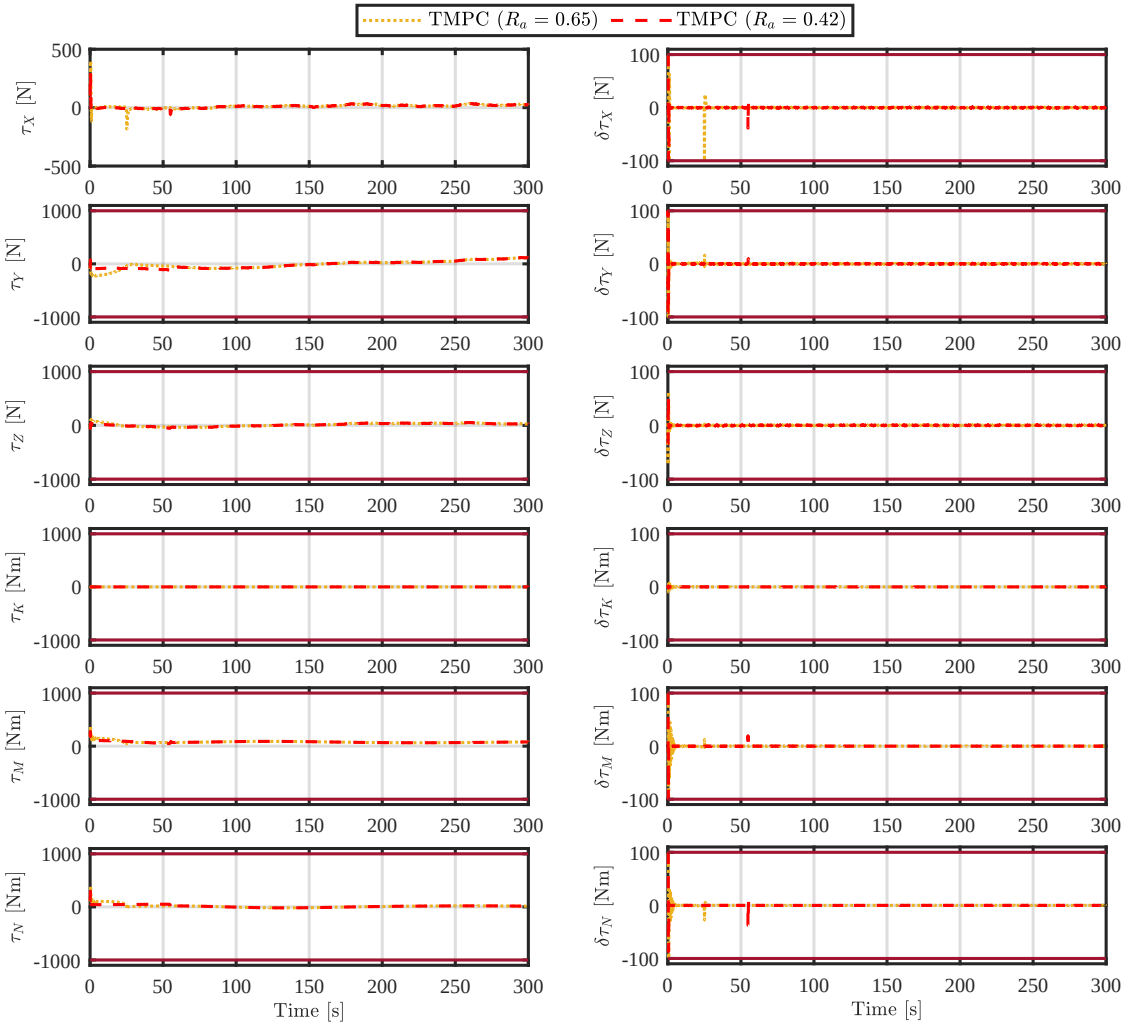

Fig. 5.12: Helical desired trajectory (initial AUV position $\boldsymbol{\eta}_2(0)$): the input forces and moments (left) and their rates of change (right).

$$y_d(t) = \begin{cases} 4 \text{ m}, \ 0 \leq t < 80 \text{ s} \\ 4 \text{ m}, \ 80 \leq t < 160 \text{ s} \\ 8 - 4\cos((\pi(t/4 - 40))/20 \text{ m}, \ 160 \leq t < 240 \text{ s} \\ 12 \text{ m}, \ 240 \leq t < 320 \text{ s} \\ 16 - 4\cos((\pi(t/4 - 80))/20 \text{ m}, \ 320 \leq t < 400 \text{ s} \\ 20 \text{ m}, \ 400 \leq t < 480 \text{ s} \end{cases} \tag{5.42}$$

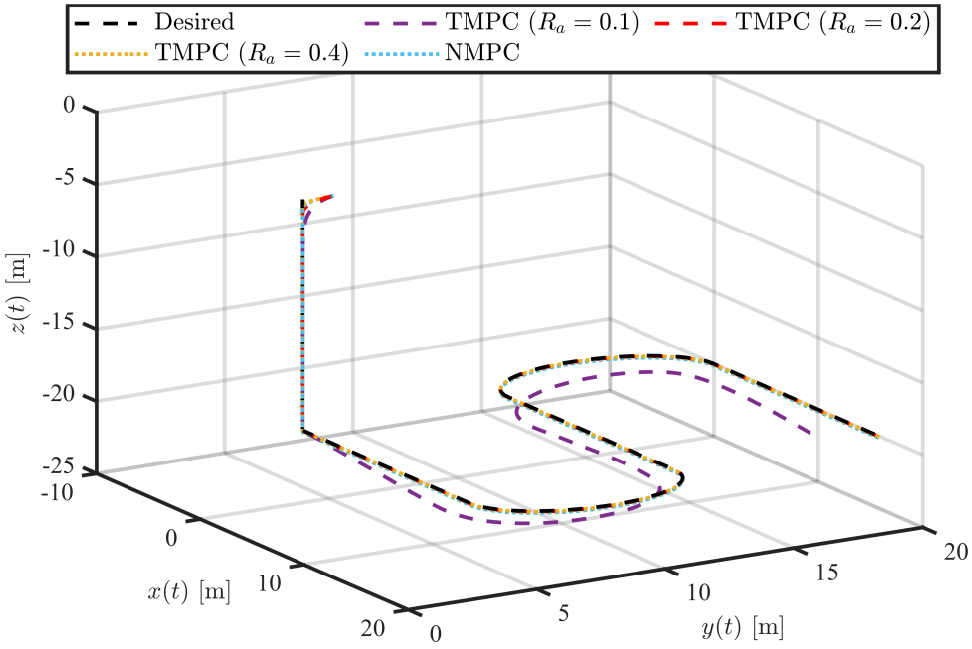

Fig. 5.13: Dubins desired trajectory: AUV motion in 3D space.

$$z_d(t) = \begin{cases} -(t/5+4) \text{ m}, & 0 \leq t < 80 \text{ s} \\ -20 \text{ m}, & 80 \leq t < 480 \text{ s} \end{cases} \tag{5.43}$$

$$\psi_d(t) = \begin{cases} 0 \text{ rad}, & 0 \leq t < 80 \text{ s} \\ 0 \text{ rad}, & 80 \leq t < 160 \text{ s} \\ \pi(t/80 - 2) \text{ rad}, & 160 \leq t < 240 \text{ s} \\ \pi \text{ rad}, & 240 \leq t < 320 \text{ s} \\ \pi - \pi(t/80 - 4) \text{ rad}, & 320 < t \leq 400 \text{ s} \\ 0 \text{ rad}, & 400 \leq t < 480 \text{ s} \end{cases} \tag{5.44}$$

and $\phi_d = \theta_d = 0$ rad for all t. By computing the average velocity in the 3D directions, the parameter R_a is determined using (5.10) to obtain $R_a = 0.14$ m, tuned to be $R_a = 0.2$ m for the non-smooth trajectory. For the simulation, three choices are employed: $R_a = 0.1$ m, $R_a = 0.2$ m, and $R_a = 0.4$ m. The initial position vector is selected as $\boldsymbol{\eta}(0) = [0.5 \ 5 \ -3.9 \ 0 \ 0 \ 0]^\top$. The simulation results for this scenario are presented in Figs. 5.13 - 5.16.

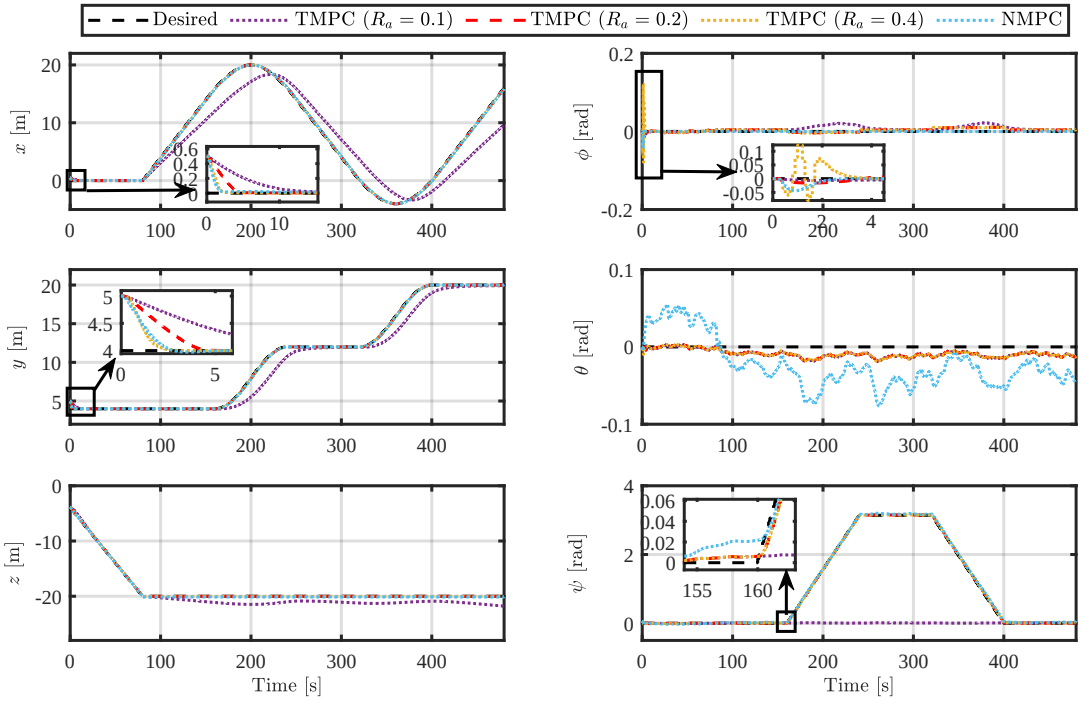

Fig. 5.14: Dubins desired trajectory: translational (left) and angular (right) position responses.

The position tracking time profiles are shown in Fig. 5.14. Since the input forces and moments are directly related to the velocities, spikes are noticed in the input magnitude and changing rate, as shown in Fig. 5.16, and this is more evident in τ_X, τ_K and τ_N and their rates of change when the largest step changes occurred in the AUV translational velocities (see Fig. 5.15). In this case, the TMPC with $R_a = 0.2$ m does not lead to the input saturation, as such the AUV does not suffer from velocity oscillations. It is noted that, compared to NMPC, the proposed TMPC controllers generally show less sensitivity to the effects of disturbances on the AUV velocities, which can be seen in Fig. 5.15. All three choices of R_a ensure that the AUV operational constraints are satisfied.

With the Dubins trajectory, it can be seen from Table 5.1 that, compared to NMPC, the TMPC controllers with $R_a = 0.2$ m and $R_a = 0.4$ m achieved a tracking error reduction of over 42% in translational positioning and over 60%

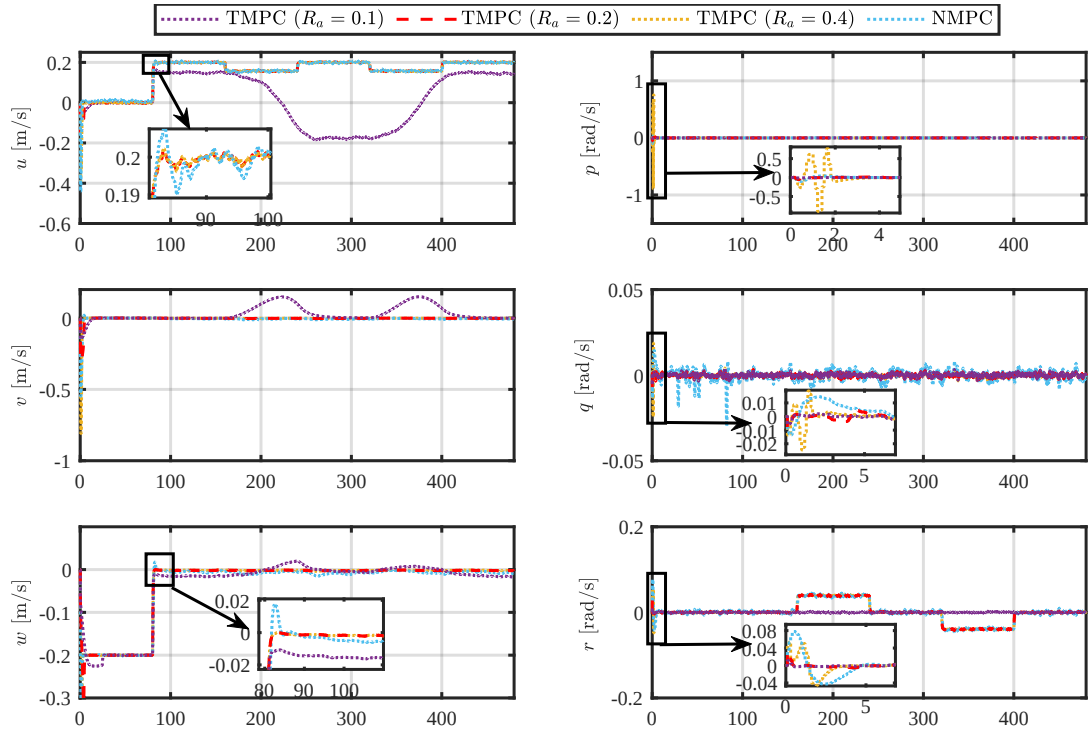

Fig. 5.15: Dubins desired trajectory: translational (left) and angular (right) velocity responses.

reduction in angular position. When $R_a = 0.2$ m, the proposed TMPC reduced moments' chattering by 12.6% but showed a larger force chattering compared to NMPC. When $R_a = 0.4$ m, the TMPC resulted in larger chattering in both input forces and moments compared to the NMPC, as the TMPC experienced significant initial input saturation due to the larger value of R_a. The use of $R_a = 0.2$ m led to an energy saving of 0.05 Wh and 0.08 Wh compared to TMPC ($R_a = 0.4$ m) and NMPC, respectively. Thus, the potential merit that can be obtained from the proposed controller is also strengthened by this scenario.

5.5.4 Remarks on Results

It can be seen from Table 5.1 that TMPC gave significantly larger tracking errors than the other controllers when taking $R_a = 0.1$ m for the Dubins trajectory and $R_a = 0.2$ m for the helical trajectory. This suggests that the choice of R_a should

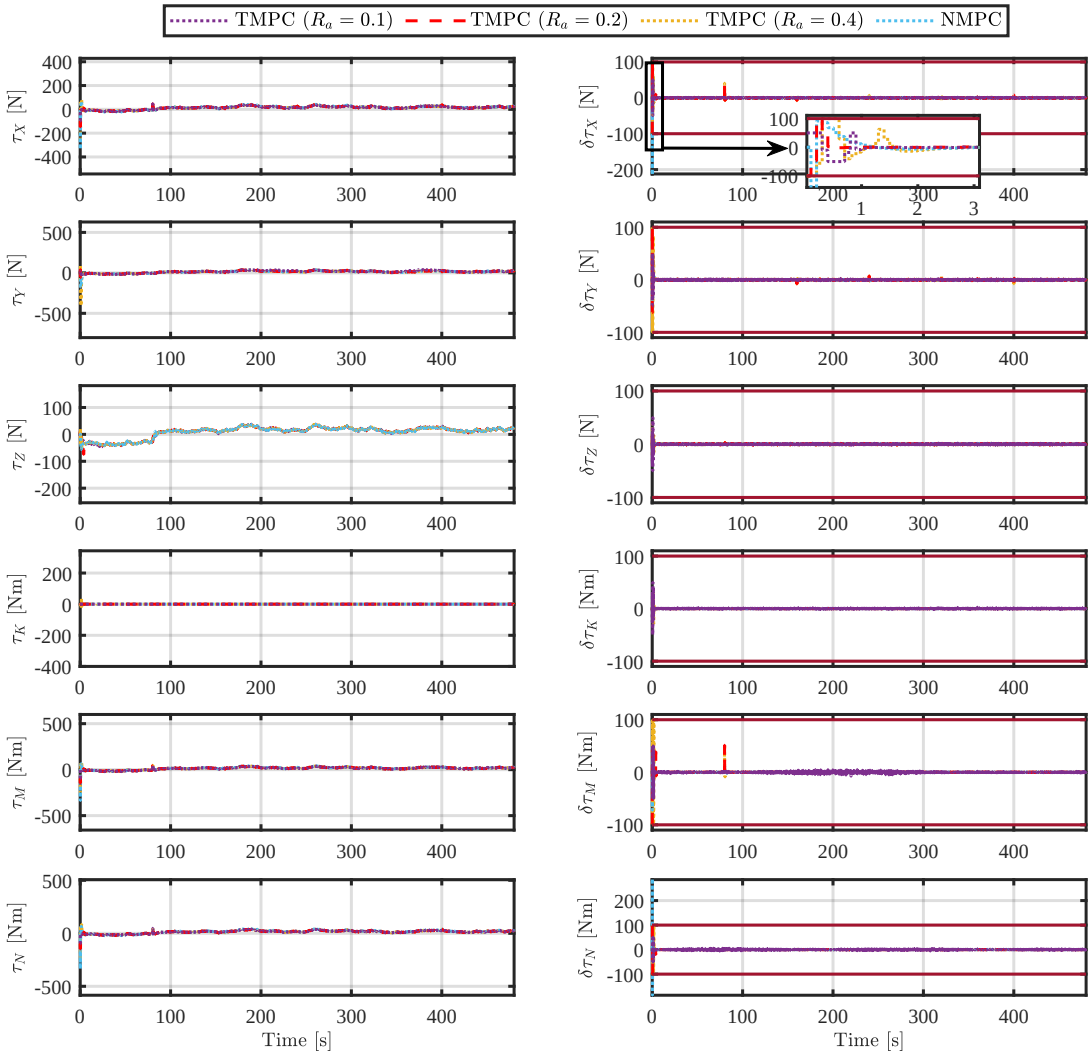

Fig. 5.16: Dubins desired trajectory: The input forces and moments (left) and their rates of change (right).

Table 5.1: Numerical performance comparison of the controllers.

Trajectory	Performance metric	TMPC $R_a = 0.2$	TMPC $R_a = 0.42$	TMPC $R_a = 0.65$	NMPC
Helical	$\text{IAE}_{\text{pos.}}$ 1×10^3 [m]	289.297	2.191	2.174	3.292
	$\text{IAE}_{\text{ori.}}$ 1×10^3 [rad]	28.354	0.300	0.301	0.320
	$\text{CT}_{\text{for.}}$ [kN]	9.777	9.439	10.698	6.551
	$\text{CT}_{\text{mom.}}$ [kNm]	15.896	2.478	4.966	2.718
	$\text{EC}_{\text{tot.}}$ [Wh]	1.201	4.137	4.212	4.20
		$R_a = 0.1$	$R_a = 0.2$	$R_a = 0.4$	
Dubins	$\text{IAE}_{\text{pos.}}$ 1×10^3 [m]	18.25	0.772	0.754	1.352
	$\text{IAE}_{\text{ori.}}$ 1×10^3 [rad]	5.099	0.121	0.122	0.307
	$\text{CT}_{\text{for.}}$ [kN]	8.013	7.564	9.119	5.553
	$\text{CT}_{\text{mom.}}$ [kNm]	12.786	1.721	4.268	1.969
	$\text{EC}_{\text{tot.}}$ [Wh]	0.569	0.579	0.626	0.663

not be too small, that is, the spherical error limit should not be too small when implementing TMPC with a LOS replanner. Additionally, R_a can be chosen to be larger than that computed by (5.10) for faster convergence of the AUV path to the desired trajectory. However, a larger R_a may cause higher input saturation under tight input constraints.

To summarise, the numerical study results demonstrate improved performance of the proposed TMPC as compared to NMPC, in trajectory tracking and energy consumption under disturbances. Moreover, the proposed TMPC avoids the prohibitive computational load associated with NMPC design. For instance, the RMS value of the CPU time for solving the proposed TMPC for the helical trajectory tracking is 17 ms compared to the 523 ms for NMPC. The peak CPU time of the TMPC is 47 ms compared to 822 ms of NMPC. Therefore, the proposed scheme shows better potential to be deployed for real-time applications as the optimisation problems can be solved in a much smaller time than the sampling time of 100 ms.

5.6 Summary

A novel discrete-time tube-based 3D trajectory tracking MPC incorporating a LOS guidance system has been developed for an AUV system. This controller was designed to handle challenges posed by environmental disturbances and input saturation. The re-planned local trajectory converges to the desired trajectory when the AUV tracking error is controlled to satisfy a user-defined spherical error limit defined by a sphere of acceptance. In the tracking MPC design, time-varying tubes were employed to confine the future state evolution. To simplify the tube construction through constraint tightening, the stabilising gain used to characterise the state and input tubes was determined by an analytical solution to an unconstrained MPC based on the nominal state deviation from the actual AUV state.

Simulation results on the Naminow-D AUV dynamic model show that the proposed control strategy has the potential to effectively track smooth and non-smooth trajectories, limit input saturation and reduce energy consumption under environmental disturbances. It was shown that the proposed tuning mechanism for the LOS-based local re-planning can provide a good estimate of the sphere of acceptance necessary to avoid substantial input signals to guide the vehicle towards the reference trajectory.

Future investigations will extend the control strategy to enable real-time collision avoidance capability. The computation of a state-dependent feedback gain for the state-dependent, time-varying AUV model will also be explored in future work.

The findings presented in this chapter have been published in Ocean Engineering journal [291]. In addition, the methodology was extended to integrated speed and power control of DFIG (doubly-fed induction generator) based wind turbines, where the adaptiveness of the strategy was improved through Kalman filtering-based disturbance bounds estimation, which is published in IEEE Transactions on Sustainable Energy [292].

Chapter 6

Accelerated Min-Max MPC for Path-Following of an Autonomous Underwater Vehicle in Uncertain Environments

6.1 Introduction

Advances in navigation, guidance and control systems have a significant role in the progress of improved AUV autonomy [293]. Typically, guidance systems and control systems are developed independently. Popular guidance laws such as proportional navigation guidance (PNG), Lyapunov-based guidance, and line-of-sight (LOS) guidance systems were reviewed in [294]. In guidance systems, it is a common practice to split the desired AUV path into different waypoints that the vehicle needs to go through in order to reach the final destination. Thus, waypoint guidance refers to the process of steering the vehicle from one waypoint to the next [295]. LOS strategy is the most popular guidance system in marine vehicles guidance [6].

A commonly employed method for path-following (PF) is LOS guidance. The

LOS vector, which connects the marine vehicle to either the next waypoint or a point along the path between two waypoints, may be utilised for both heading and course control [6]. Guidance systems based on the LOS strategy are traditionally implemented by generating reference heading angles between waypoints that are then tracked using a suitable heading autopilot. This approach applies to marine surface vehicles and AUV horizontal motion control which has been the main focus of many PF control strategies [220, 296, 297]. For some AUVs whose roll, pitch and heave motions can be assumed decoupled with negligible roll and pitch angles [22, 215], their 3D guidance systems can readily be designed using methods similar to those used for marine surface vehicles [295]. For the 3D case, in addition to the heading angle, the corresponding depth reference is also determined and tracked to achieve the 3D PF task [298]. However, these guidance and control schemes cannot be directly applied to achieve accurate waypoint following for AUVs with coupled motion.

While previous research has focused on 3D PF for smooth and continuous paths [228–230], limited attention has been given to paths defined by 3D waypoints as investigated in [295]. AUVs encounter uncertainties such as environmental obstacles, making waypoint tracking challenging for control engineers due to incomplete knowledge of the ocean environment during waypoint planning [22]. Consequently, real-time collision avoidance with detected obstacles is crucial for demanding marine industry tasks [195, 299]. In [227], a 3D waypoint following MPC-SMC controller was designed based on the LOS approach for error model formulation, albeit without considering disturbances. Nevertheless, the study incorporated a real-time collision avoidance strategy that analytically determines the path to avoid detected obstacles.

In this chapter, a robust PF control strategy is proposed for coupled AUVs operating in uncertain environments with environmental disturbances and obstacles. The guidance and control system presented in this chapter comprises two main components: reference computation and reference tracking.

For reference computation, the enclosure-based LOS strategy is employed to

determine the horizontal 2D coordinate, from which the corresponding depth coordinate is analytically derived. The resulting 3D LOS coordinate is then used to design a PF control system. In the proposed design, the heading and depth control problems are reformulated as a 3D LOS path-tracking problem to eliminate the need for a kinematic error model. This approach is important as it avoids the necessity for motion decoupling or the assumption of negligible roll motion [218]. However, this straightforward approach does not account for situations where the vehicle must avoid newly detected obstacles. To address this limitation, the conventional enclosure-based LOS guidance strategy is leveraged to develop a multi-objective LOS guidance system (MO-LOSGS) that enables both PF and online collision avoidance of detected obstacles.

The reference tracking objective is achieved by formulating a min-max MPC (MM-MPC) to ensure robust performance under time-varying environmental disturbances. To prevent excessive velocity fluctuations during PF control, the objective function minimises increments in vehicle velocity. A duality-inspired method is used to transform the MM-MPC problem into a convex quadratic minimisation problem to obtain the accelerated MM-MPC algorithm, allowing for more efficient online computations. The robust MPC requires a disturbance bound, which is adaptively determined by employing a time-varying Kalman filtering strategy, mitigating the conservatism associated with the use of a constant disturbance bound.

Simulations are conducted using the high-fidelity Naminow-D AUV model under environmental disturbances. The main contributions of this chapter are summarised below.

- A LOS guidance system is proposed, which redefines the conventional heading and depth control problems into a 3D LOS path-tracking problem. This approach circumvents the need to develop a kinematic error model.
- A novel MO-LOSGS is developed to enable online collision avoidance with newly detected obstacles in PF control of AUVs.

- A MPC-based control system is developed, aiming to mitigate fluctuations in the AUV velocity vector. This is achieved by employing velocity increment as the optimisation control variable. To ensure robustness against external disturbances, the controller is formulated as a convex min-max control problem.
- A duality-inspired transformation method is developed to convert the min-max optimisation problem into a convex minimisation quadratic problem (QP) that can be solved more efficiently.
- A time-varying Kalman filtering strategy is proposed to adaptively determine the disturbance upper bounds required for implementing the MM-MPC scheme.

The rest of this chapter is organised as follows. Section 6.2 describes the problem statement to be addressed. The 3D LOS guidance is presented in Section 6.3 while the MO-LOSGS is developed in Section 6.4. Section 6.5 presents the accelerated robust MM-MPC controller. The simulation study and results are presented in Section 6.6. Conclusions are given in Section 6.7.

6.2 Problem Statement

Due to its simplicity and ease of implementation, the LOS method is used by most guidance laws [294]. This work avoids the need to formulate an error model which often relies on simplifying assumptions such as negligible roll motion [218] by directly determining the LOS coordinates $(x_{los}, y_{los}, z_{los})$ and the desired orientation vector $(\phi_d, \theta_d, \psi_d)$ required for PF.

We consider that the AUV operates in a workspace $\mathcal{W} \subset \mathbb{R}^3$ containing scattered obstacles. Based on the translational position vector $\boldsymbol{\eta}_1$ of the AUV, define $\mathcal{B}(\boldsymbol{\eta}_1, r_{AUV})$ and $\mathcal{B}(\boldsymbol{\eta}_1, r_s)$ as the closed balls covering the entire volume of the vehicle and the sensing area of its onboard sensors, respectively, with $r_s > r_{AUV}$. Furthermore, the $\mathcal{Q}$ static obstacles are defined by the closed balls $o_q = \mathcal{B}(\mathbf{p}_{o_q}, r_{o_q})$,

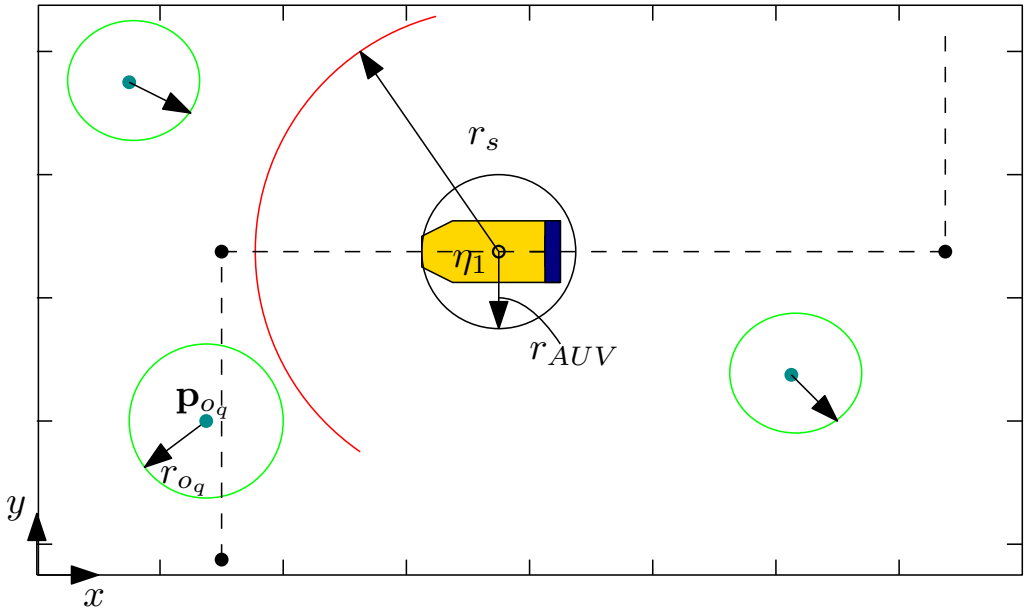

Fig. 6.1: Illustration of the PF task in an uncertain environment with an AUV active sensing radius of r_s. Three obstacles are illustrated by central dots and circles with green circumference.

where $q \in \{1, \ldots, \mathcal{Q}\}$, $\mathbf{p}_{o_q}$ is the obstacle centre coordinate, and r_{o_q} is the obstacle's radius. A graphical illustration of this concept is shown in Fig. 6.1. Based on the spherical world property [300], it is assumed that for each pair of obstacles q and q' with $q \neq q'$, we have $\| o_q - o_{q'} \| > 2r_{AUV} + r_{o_q} + r_{o_{q'}}$. This implies that obstacles q and q' are disjoint, ensuring that the entire AUV volume can pass through the free space between them.

Consider an AUV denoted by (2.1) and (2.2) operating in the environment $\mathcal{W}$ with input and state constraints imposed by sets $\mathcal{T}$ and $\mathcal{X}$, respectively, and whose motion is affected by unknown environmental disturbances, $\boldsymbol{\tau}^w$. The AUV waypoint following control task involves the following aspects:

1. LOS Guidance: compute the reference translational and angular position based on LOS guidance strategy to achieve waypoint following.

2. Collision Avoidance: For newly identified obstacles that were not factored into the predefined waypoints, dynamically re-plan the path to avoid collision.

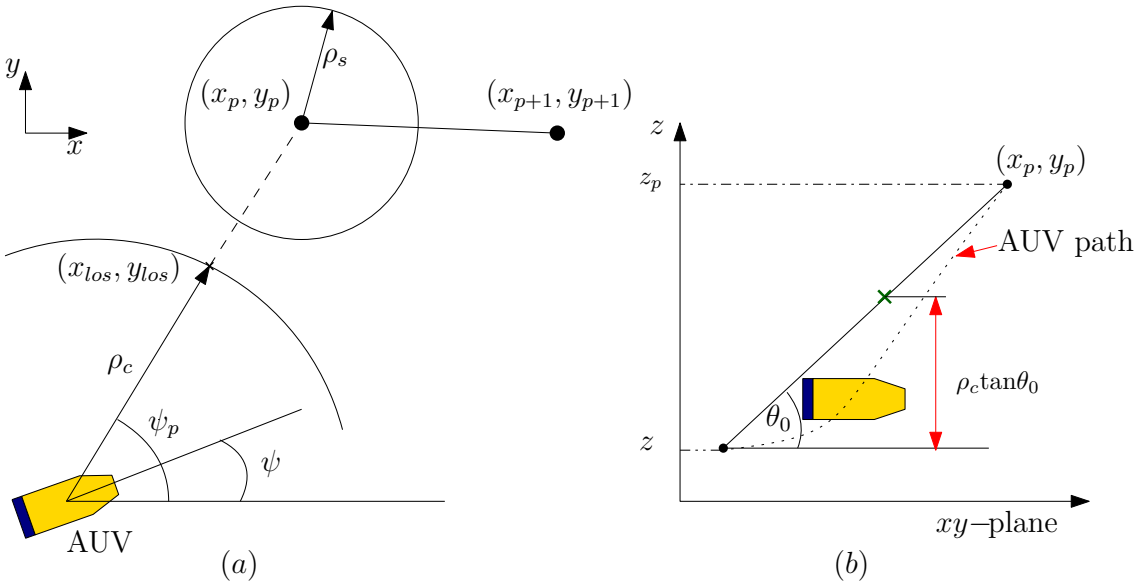

Fig. 6.2: LOS guidance system for waypoints following.

3. Robust Path Tracking: Based on the computed reference, design MM-MPC that achieves robust tracking in the presence of environmental disturbances. This should be done such that input and state constraints are satisfied.

6.3 Line-of-Sight Guidance System

Due to its simplicity and ease of implementation, the LOS method is used by most guidance laws [294]. In 3D motion control, the roll angle, ϕ, and pitch angle, θ, and the corresponding angular velocities p and q are often assumed to be negligible. This assumption applies mostly to under-actuated AUVs. This work avoids such assumptions by directly determining the LOS coordinates and the orientation vector needed for the desired waypoints following task.

With the 2D horizontal plane, as illustrated in Fig. 6.2(a), given the current AUV position as $(x(k), y(k))$ at time k, the desired heading angle is given as [294]:

$$\psi_d = \tan^{-1}\left(\frac{y_p - y(k)}{x_p - x(k)}\right), \tag{6.1}$$

where (x_p, y_p) with $p = 1, 2, ..., m$ are the coordinates of the m waypoints in the horizontal plane. Since the waypoint position may be significantly distant from the AUV position, the LOS coordinate $(x_{los}(k), y_{los}(k))$ is defined by the so-called circle of acceptance as follows:

$$(x_{los}(k) - x(k))^2 + (y_{los}(k) - y(k))^2 = \rho_c^2, \tag{6.2a}$$

$$(y_{los}(k) - y(k)) = (x_{los}(k) - x(k)) \tan\psi_d. \tag{6.2b}$$

Here ρ_c is the radius of the circle of acceptance which the LOS coordinate should not exceed. It is evident that the desired yaw angle ψ_d will be maintained by the LOS coordinates obtained from (6.2) and the LOS point will lie on the circumference of the circle of acceptance.

The value of ρ_c directly impacts the speed of the AUV along the prescribed horizontal path since it determines the average distance between successive LOS coordinates. To see this, from (6.2a) and (6.2b), there is

$$\begin{aligned} x_{los}(k) &= x(k) \pm \frac{\rho_c}{(1 + \tan^2\psi_d)^{1/2}}, \\ &= x(k) \pm \rho_c \cos\psi_d. \end{aligned} \tag{6.3}$$

In (6.3), the positive sign corresponds to $(x_p - x(k)) \geq 0$ while $(x_p - x(k)) < 0$ is related to the negative sign. Subtract $x_{los}(k-1)$ from both sides of (6.3) and then divide by the sampling time, T_s, to obtain:

$$u_{los}(k) = \frac{x(k) - x_{los}(k-1)}{T_s} \pm \frac{\rho_c \cos\psi_d}{T_s}, \tag{6.4}$$

where $u_{los}(k) = \frac{x_{los}(k) - x_{los}(k-1)}{T_s}$ represents the discrete-time approximation of the LOS surge speed. This equation reveals that the LOS surge speed is directly influenced by the circle of acceptance used. When following a straight-line path where ψ_d remains constant, the speed is mainly dictated by ρ_c. A significant speed change may

occur when the vehicle adjusts its heading ψ_d to track the next waypoint (x_{p+1}, y_{p+1}). Indeed, opting for $\rho_c < L$, where L is the length of the AUV, ensures that the AUV maintains a relatively low speed along the path, which is often desirable for underwater tasks, as it limits the effects of coupling. This is due to the fact that coupling effects are stronger at higher speeds [6].

Since the target LOS depth is not necessarily equal to the desired depth, we compute the LOS depth to be proportional to the distance between the LOS horizontal coordinate and the AUV position. Consider the angle θ_0, defined by the line joining the vehicle's depth, z, on the $z-$axis to the waypoint (x_p, y_p) on the horizontal plane, as shown in Fig. 6.2(b). This angle is computed as

$$\theta_0 = \tan^{-1} \frac{z_p - z(k)}{\sqrt{(x_p - x(k))^2 + (y_p - y(k))^2}}. \tag{6.5}$$

To keep this angle for any current depth $z(k)$, the desired depth of AUV is given by

$$z_{los}(k) = z(k) + \tan\theta_0 \cdot \rho_c. \tag{6.6}$$

Aside from the 3D LOS path to be followed, it is important to define the condition necessary for switching from one waypoint, (x_p, y_p, z_p), to follow to the next waypoint, $(x_{p+1}, y_{p+1}, z_{p+1})$. This is achieved by defining the "sphere of acceptance ρ_s" around each waypoint in the 3D environment (see Fig. 6.2). The $(x_{p+1}, y_{p+1}, z_{p+1})$ is chosen when the following inequality is satisfied.

$$(x_p - x(k))^2 + (y_p - y(k))^2 + (z_p - z(k))^2 \leq \rho_s^2. \tag{6.7}$$

Furthermore, there is a need to define the reference orientation for the AUV while moving along the path. Consider the straight line path P_k starting at the waypoint (x_p, y_p, z_p) and terminates at the next waypoint $(x_{p+1}, y_{p+1}, z_{p+1})$. The yaw and pitch angles from the path coordinates at (x_p, y_p, z_p) with respect to the

inertia frame is given as

$$\begin{aligned}\psi_d(k) &= \arctan2\left(y_{los}(k) - y_p, x_{los}(k) - x_p\right), \\ \theta_d(k) &= -\tan^{-1}\frac{z_{los}(k) - z_p}{\sqrt{(x_{los}(k) - x_p)^2 + (y_{los}(k) - y_p)^2}},\end{aligned} \tag{6.8}$$

where arctan2 is the four quadrant inverse function used to ensure $-\pi \leq \psi_p \leq \pi$. Next, the set of equations in (6.2) forms the basis of the developed MO-LOSGS for PF in the presence of obstacles.

6.4 Multi-Objective LOS Guidance System

Consider a single obstacle with the centre position denoted $\mathbf{p}_{o_q} = (x_o(k), y_o(k), z_o(k))$. The MO-LOSGS problem is presented as follows.

- Formulate a multi-objective optimisation problem to compute the LOS coordinate $(x^*_{los}, y^*_{los}, z^*_{los})$ such that:
  - the coordinate exactly satisfies the set of equations (6.2) and (6.6) in an obstacle-free scenario, that is, $(x^*_{los}, y^*_{los}, z^*_{los}) = (x_{los}, y_{los}, z_{los})$;
  - for obstacle constrained scenarios, the coordinate is modified to ensure collision avoidance, that is, $(x^*_{los}, y^*_{los}, z^*_{los}) \neq (x_{los}, y_{los}, z_{los})$.

The obstacle can potentially result in a collision if

$$\left(x(k) - x_o(k)\right)^2 + \left(y(k) - y_o(k)\right)^2 + \left(z(k) - z_o(k)\right)^2 \leq r_s^2 \tag{6.9}$$

is satisfied. When (6.9) holds, the reference position $(x_{los}, y_{los}, z_{los})$ needs to be generated to lie outside the unsafe region defined by the sphere of radius r_{o_q}. The safety-critical constraint to be satisfied by the generated horizontal LOS coordinate is defined as

$$h_s := \left(x_{los}(k) - x_o(k)\right)^2 + \left(y_{los}(k) - y_o(k)\right)^2 > r_{o_q}^2. \tag{6.10}$$

Note that z_{los} does not need to be included to avoid the obstacle since the modification of the horizontal coordinate is sufficient to avoid the detected obstacle. This follows from the fact that the LOS coordinate will be along the horizontal circle around the detected obstacle.

For the obstacle-free scenario, the desired LOS horizontal coordinate can be obtained from (6.2) as follows:

Case 1: $|x_p - x(k)| > 0$ we have

$$x_{los} = \frac{-b \pm \sqrt{b^2 - 4ac}}{2a}, \tag{6.11}$$

where $a = 1+d^2,\ b = 2(dg-dy(k)-x(k)),\ c = x(k)^2+y(k)^2+g^2-2gy(k)-\rho_c^2,\ g = y(k) - dx(k)$ and

$$d = \frac{y_d(k) - y(k)}{x_d(k) - x(k)}.$$

For this case, the positive sign in (6.11) is adopted if $x_p - x(k) > 0$ while the negative sign is used when $x_p - x(k) < 0$. Based on the computed $x_{los}(k)$, the $y_{los}(k)$ is calculated as:

$$y_{los}(k) = d(x_{los}(k) - x(k)) + y(k). \tag{6.12}$$

Case 2: If $|x_p - x(k)| = 0$, then (6.2b) becomes invalid so we have $x_{los}(k) = x(k)$ and

$$y_{los}(k) = y(k) \pm \sqrt{\rho_c^2 - (x_{los} - x(k))^2}, \tag{6.13}$$

where the positive sign is adopted if $y_p - y(k) > 0$ while the negative sign is adopted for $y_p - y(k) < 0$.

To maintain the flexibility between obstacle-constrained and obstacle-free conditions, a multi-objective optimisation problem is formulated. The following objective function is defined:

$$J_{mo}(k) = [J_{los}(k)\ J_{oa}(k)]^\top, \tag{6.14}$$

where

$$J_{los}(k) = (x^*_{los}(k))^2 + (y^*_{los}(k))^2,$$

$$J_{oa}(k) = (x^*_{los}(k) - x_{los}(k))^2 + (y^*_{los}(k) - y_{los}(k))^2 + s_v^2.$$

Based on the cost (6.14), the guidance system is implemented by solving the optimisation problem, called MO-LOSGS, as follows:

$$(x^*_{los}(k),\, y^*_{los}(k),\, s_v) = \arg \min_{x^*_{los}(k), y^*_{los}(k), s_v} a_c^\top J_{mo}(k) \tag{6.15a}$$

s.t.

$$x_{los}(k) - x^*_{los}(k) = 0, \tag{6.15b}$$

$$y_{los}(k) - y^*_{los}(k) + \alpha s_v = 0, \tag{6.15c}$$

$$\alpha((x^*_{los}(k) - x_o(k))^2 + (y^*_{los}(k) - y_o(k))^2 - (r_{o_q} + \epsilon_s)^2) \geq 0, \tag{6.15d}$$

$$\epsilon_s = k_p d_o,\ s_v \geq 0, \tag{6.15e}$$

where $a_c^\top = [1, \alpha]^\top$ with $\alpha = 0$ or 1, s_v is a slack variable used to impose a soft constraint on the LOS coordinate in the y axis and $k_p > 0$ is a design gain and

$$d_o = \left((x(k) - x_o(k))^2 + (y(k) - y_o(k))^2\right)^{\frac{1}{2}}$$

is the distance of the AUV to the obstacle. The margin of safety ϵ_s, added to the radius of the unsafe region defined by r_{o_q}, dynamically reduces as the AUV approaches the obstacle. This adjustment ensures smoother navigation around obstacles by preventing a sudden need to turn around a circle with a constant radius. Notice that the constraint (6.15b) ensures that $x^*_{los}(k)$ is equal to $x_{los}(k)$ obtained from the solution of (6.2a) while constraint (6.15c) makes it posible to make $y^*_{los}(k)$ different from $y_{los}(k)$ via the slack variable s_v.

Remark 6. *The MO-LOSGS (6.15) is implemented with $\alpha = 1$ if inequality (6.9) holds, and $\alpha = 0$ otherwise. This maintains consistency with Cases 1 and 2 in*

the absence of obstacles. The LOS coordinate is modified to satisfy the obstacle constraint (6.15d) when obstacles are detected.

Based on the horizontal LOS coordinate, the goal is to design a robust MPC law such that the AUV position vector $\boldsymbol{\eta}$, under unknown environmental disturbances, robustly tracks the desired position $\boldsymbol{\eta}_d(k) = [x^*_{los}(k)\ y^*_{los}(k)\ z^*_{los}(k)\ \phi_d(k)\ \theta_d(k)\ \psi_d(k)]^\top$, with the orientation angles given by

$$\begin{aligned} \psi_d(k) &= \arctan2\left(y^*_{los}(k) - y_p, x^*_{los}(k) - x_p\right), \\ \theta_d(k) &= -\tan^{-1}\frac{z^*_{los}(k) - z_p}{\sqrt{(x^*_{los}(k) - x_p)^2 + (y^*_{los}(k) - y_p)^2}}, \end{aligned} \tag{6.16}$$

The desired roll angle is chosen as, $\phi_d(k) = 0$ in order to keep it small for the stability of the vehicle.

6.5 Accelerated Min-Max MPC Design

6.5.1 Robust MM-MPC Design

The AUV kinematic model is formulated as a discrete-time system to obtain:

$$\boldsymbol{\eta}(k+1) = \boldsymbol{\eta}(k) + \mathbf{J}(k)\boldsymbol{\nu}(k), \tag{6.17}$$

where $\mathbf{J}(k) = \mathbf{J}(\boldsymbol{\eta})T_s$. The AUV increment velocity is defined as

$$\Delta\boldsymbol{\nu}(k) = \boldsymbol{\nu}(k) - \boldsymbol{\nu}(k-1). \tag{6.18}$$

Combine (6.17) and (6.18) to obtain:

$$\begin{aligned} \mathbf{x}(k+1) &= \mathbf{A}(\boldsymbol{\eta}(k))\mathbf{x}(k) + \mathbf{B}(\boldsymbol{\eta}(k))\Delta\boldsymbol{\nu}(k), \\ \boldsymbol{\eta}(k) &= \mathbf{G}_p\mathbf{x}(k), \end{aligned} \tag{6.19}$$

in which $\mathbf{G}_p = [\mathbf{I}_6 \ \mathbf{0}_6]$, and

$$\mathbf{A}(\boldsymbol{\eta}(k)) = \begin{bmatrix} \mathbf{I} & \mathbf{J}(k) \\ \mathbf{0} & \mathbf{I} \end{bmatrix}, \ \mathbf{B}(\boldsymbol{\eta}(k)) = \begin{bmatrix} \mathbf{J}(k) \\ \mathbf{I} \end{bmatrix}.$$

Here $\mathbf{I}$ and $\mathbf{0}$ represent identity and zero matrices of appropriate dimensions, respectively.

Define the reference state as $\mathbf{x}_d(k) = [\boldsymbol{\eta}_d^\top(k) \ \boldsymbol{\nu}_d^\top(k)]^\top$, where $\boldsymbol{\nu}_d(k)$ is the desired velocity vector. Define the stacked versions of the predicted future state, state reference and velocity increment as

$$\begin{aligned} \mathbf{X}(k) &= \begin{bmatrix} \mathbf{x}(k+1|k)^\top & \dots & \mathbf{x}(k+N|k)^\top \end{bmatrix}^\top, \\ \mathbf{X}_d(k) &= \begin{bmatrix} \mathbf{x}_d(k+1|k)^\top & \dots & \mathbf{x}_d(k+N|k)^\top \end{bmatrix}^\top, \\ \mathbf{Y}(k) &= \begin{bmatrix} \boldsymbol{\eta}(k+1|k)^\top & \dots & \boldsymbol{\eta}(k+N|k)^\top \end{bmatrix}^\top, \\ \mathbf{U}(k) &= \begin{bmatrix} \Delta\boldsymbol{\nu}(k|k)^\top & \dots & \Delta\boldsymbol{\nu}(k+N_u-1|k)^\top \end{bmatrix}^\top. \end{aligned} \tag{6.20}$$

The state prediction model can be written as

$$\mathbf{X}(k) = \tilde{\mathbf{A}}\mathbf{x}(k|k) + \tilde{\mathbf{B}}\mathbf{U}(k), \tag{6.21}$$

where $\tilde{\mathbf{A}} \in \mathbb{R}^{12N\times 12}$ and $\tilde{\mathbf{B}} \in \mathbb{R}^{12N\times 6N_u}$ are defined below.

Remark 7. *It is evident that the augmented matrices $\tilde{\mathbf{A}}$ and $\tilde{\mathbf{B}}$ can be computed online using only the current state measurement $\mathbf{x}(k)$, with the position and velocity vectors updated according to (6.17) and (6.18), respectively.*

To robustly handle the effects of disturbance on the AUV state, the same bounded disturbance, $\mathbf{w}(k) \in \mathcal{W} \subset \mathbb{R}^{12}$, as in (5.8) is considered in this model. Considering this disturbance, the state space representation of the AUV model becomes

$$\mathbf{x}(k+1) = \mathbf{A}(\boldsymbol{\eta}(k))\mathbf{x}(k) + \mathbf{B}(\boldsymbol{\eta}(k))\Delta\boldsymbol{\nu}(k) + \mathbf{w}(k). \tag{6.22}$$

$$\tilde{\mathbf{A}} = \begin{bmatrix} \mathbf{A}(\boldsymbol{\eta}(k)) \\ \mathbf{A}(\boldsymbol{\eta}(k+1))\mathbf{A}(\boldsymbol{\eta}(k)) \\ \vdots \\ \mathbf{A}(\boldsymbol{\eta}(k+N-1))\dots\mathbf{A}(\boldsymbol{\eta}(k+1))\mathbf{A}(\boldsymbol{\eta}(k)) \end{bmatrix},$$

$$\tilde{\mathbf{B}} = \begin{bmatrix} \mathbf{B}(\boldsymbol{\eta}(k)) & \mathbf{0} & \cdots \\ \mathbf{A}(\boldsymbol{\eta}(k+1))\mathbf{B}(\boldsymbol{\eta}(k)) & \mathbf{B}(\boldsymbol{\eta}(k+1)) & \cdots \\ \vdots & \vdots & \cdots \\ \mathbf{A}(\boldsymbol{\eta}(k+N-1))\dots\mathbf{A}(\boldsymbol{\eta}(k+1))\mathbf{B}(\boldsymbol{\eta}(k)) & \mathbf{A}(\boldsymbol{\eta}(k+N-1))\dots\mathbf{A}(\boldsymbol{\eta}(k+1))\mathbf{B}(\boldsymbol{\eta}(k)) & \cdots \end{bmatrix}.$$

Let $\mathbf{W}(k) = [\mathbf{w}(k+1|k)^\top \ \dots \ \mathbf{w}(k+N|k)^\top]^\top$, the prediction model (6.21) with additive external disturbance yields

$$\mathbf{X}(k) = \tilde{\mathbf{A}}\mathbf{x}(k|k) + \tilde{\mathbf{B}}\mathbf{U}(k) + \mathbf{W}(k). \tag{6.23}$$

With the defined upper bounds on the disturbances, the objective of robust control is to minimise the worst-case scenario, *i.e.,* minimise the tracking error under maximum uncertainties subject to input constraints. The MM-MPC approach is employed because it offers a straightforward method to address this problem without requiring an intermediate control law.

The objective function of the finite horizon MM-MPC problem is defined to minimise the PF error which involves the difference between the AUV state vector and the reference $\mathbf{x}_d(k)$ as

$$\begin{aligned} V\left(\mathbf{U}(k), \mathbf{x}(k)\right) =& \frac{1}{2}\sum_{j=1}^{N} \parallel \mathbf{x}(k+j|k) - \mathbf{x}_d(k+j|k) \parallel^2_{\mathbf{Q}_x} \\ &+ \frac{1}{2}\sum_{j=0}^{N_u-1} \parallel \Delta\boldsymbol{\nu}(k+j|k) \parallel^2_{\mathbf{R}}, \end{aligned} \tag{6.24}$$

where $\mathbf{Q}_x \in \mathbb{R}^{12\times12}$ and $\mathbf{R} \in \mathbb{R}^{6\times6}$ are positive definite matrices, and N_u ($N_u < N$) is the control horizon in MPC. The control law can be structured by assuming that there is no variation in the control signal beyond N_u [301], *i.e.,* $\Delta\boldsymbol{\nu}(k+j|k) = \mathbf{0}$ for $j = N_u, \dots, N-1$. In this case, the dimension of the MPC problem is reduced

from $6N$ to $6N_u$. Employing (6.24) as the performance index, the MM-MPC is formulated as

$$\begin{aligned}
\mathbf{U}^*(k) = & \arg\min_{\mathbf{U(k)}} \max_{\mathbf{W}(k)} V\left(\mathbf{U}(k), \mathbf{x}(k)\right) \\
& \text{s. t. : (6.23)} \\
& \mathbf{x}(k+j|k) \in \ \mathcal{X}, \ j > 0, \\
& \boldsymbol{\tau}(k+j|k) \in \ \mathcal{T}, \ j \geq 0, \\
& \mathbf{w}(k+j|k) \in \ \mathcal{D}, \ j \geq 0. \\
& \mathbf{x}(k|k) = \ \mathbf{x}(k).
\end{aligned} \tag{6.25}$$

It is noted that the dimension of the tracking objective in (6.25) can be reduced by using the output position vector in the cost function instead of the state vector. The output prediction of the AUV system is given by

$$\mathbf{Y}(k) = \tilde{\mathbf{G}}\mathbf{X}(k), \tag{6.26}$$

with $\tilde{\mathbf{G}} = \text{diag}(\mathbf{G}, \ldots, \mathbf{G})$. The cost function is then defined to minimise the path following error which is the difference between the AUV position and the reference $\mathbf{y}_d$ as

$$\begin{aligned}
V\left(\mathbf{U}(k), \mathbf{Y}(k)\right) = & \sum_{j=1}^{N} \parallel \boldsymbol{\eta}(k+j|k) - \boldsymbol{\eta}_d(k+j|k) \parallel^2_{\mathbf{Q}} \\
& + \sum_{j=0}^{N_u-1} \parallel \Delta\boldsymbol{\nu}(k+j|k) \parallel^2_{\mathbf{R}} .
\end{aligned} \tag{6.27}$$

Based on the cost function (6.27), an alternative MM-MPC problem can be formu-

lated as follows:

$$\begin{aligned}
\mathbf{U}^*(k) = \ & \arg\min_{\mathbf{U(k)}} \max_{\mathbf{W}(k)} V\left(\mathbf{U}(k), \mathbf{Y}(k)\right) \\
& \text{s. t. : (6.23) \& (6.26)}, \\
& \mathbf{x}(k+j|k) \in \ \mathcal{X}, \ j > 0, \\
& \boldsymbol{\tau}(k+j|k) \in \ \mathcal{T}, \ j \geq 0, \\
& \mathbf{w}(k+j|k) \in \ \mathcal{D}, \ j \geq 0, \\
& \mathbf{x}(k|k) = \ \mathbf{x}(k).
\end{aligned} \tag{6.28}$$

Remark 8. *Although obtaining the solution to (6.28) may offer computational speed advantage due to the reduced dimensionality of the tracking objective, the min-max problem in (6.25) is used for the remainder of the analysis in this chapter. This ensures that the developed accelerated optimisation problem is well-conditioned for numerical solvers. The computational effort of the accelerated MPC problem is benchmarked using the problem (6.28).*

Note that to enforce constraints on input forces and moments, the variable $\boldsymbol{\tau}(k+j|k)$ must be expressed in terms of the optimisation variable $\Delta\boldsymbol{\nu}(k+j|k)$. Hence, the AUV dynamic model (2.2) is re-written in the compact form

$$\boldsymbol{\tau} = \mathbf{M}\dot{\boldsymbol{\nu}} + \boldsymbol{\Xi}(\boldsymbol{\nu}), \tag{6.29}$$

in which $\Xi(\boldsymbol{\nu}) = \mathbf{C}(\boldsymbol{\nu})\boldsymbol{\nu} + \mathbf{D}(\boldsymbol{\nu})\boldsymbol{\nu} + \mathbf{g}(\boldsymbol{\eta})$.

Given the optimal velocity increment, $\Delta\boldsymbol{\nu}^*(k) = \Delta\boldsymbol{\nu}^*(k|k)$, the discrete-time approximation of (6.29) as follows:

$$\boldsymbol{\tau}^*(k) = \bar{\mathbf{M}}\Delta\boldsymbol{\nu}^*(k) + \Xi(\boldsymbol{\nu}(k-1)), \tag{6.30}$$

where $T_s\bar{\mathbf{M}} = \mathbf{M}$. The desired velocity used to implement the MM-MPC in the next time step is defined in terms of the optimal velocity increment as

$$\boldsymbol{\nu}_d(k) = \Delta\boldsymbol{\nu}^*(k) + \boldsymbol{\nu}(k-1). \tag{6.31}$$

The constraints on the generalised input forces and moments can be enforced over N_u, using (6.30), as

$$\boldsymbol{\tau}(k+j|k) = \bar{\mathbf{M}}\Delta\boldsymbol{\nu}^*(k+j|k) + \Xi(\boldsymbol{\nu}(k-1)). \tag{6.32}$$

Remark 9. *Compared to the formulation by [262], which leads to nonlinear optimisation, the formulation (6.25) is a quadratic problem with linear constraints because the system* $(\mathbf{A}(\boldsymbol{\eta}(k)), \mathbf{B}(\boldsymbol{\eta}(k)))$ *is linear parameter-dependent. The convex optimisation problem (6.25) can readily be solved using standard min-max solvers.*

6.5.2 Duality-based Transformation of the MM-MPC

Here, a duality-based approach is proposed to convert the MM-MPC problem in (6.25) into a minimisation problem. First, the problem (6.25) can be rewritten as

$$\min_{\mathbf{U(k)}} \max_{\mathbf{W}(k)} \frac{1}{2} \begin{bmatrix} \mathbf{U}(k) \\ \mathbf{W}(k) \end{bmatrix}^\top \mathbf{H}_q \begin{bmatrix} \mathbf{U}(k) \\ \mathbf{W}(k) \end{bmatrix} + \begin{bmatrix} \mathbf{h}_1 \\ \mathbf{h}_2 \end{bmatrix}^\top \begin{bmatrix} \mathbf{U}(k) \\ \mathbf{W}(k) \end{bmatrix} \tag{6.33a}$$

$$\text{s. t.} : \mathbf{G}_1\mathbf{U}(k) \leq \mathbf{g}_1,\ \mathbf{G}_2\mathbf{W}(k) \leq \mathbf{g}_2, \tag{6.33b}$$

where $\tilde{\mathbf{Q}} = \text{diag}(\mathbf{Q}_x, \ldots, \mathbf{Q}_x) \in \mathbb{R}^{12N\times 12N}$ and $\tilde{\mathbf{R}} = \text{diag}(\mathbf{R}, \ldots, \mathbf{R}) \in \mathbb{R}^{6N_u\times 6N_u}$, and

$$\mathbf{H}_q = \begin{bmatrix} \tilde{\mathbf{B}}^\top\tilde{\mathbf{Q}}\tilde{\mathbf{B}} + \tilde{\mathbf{R}} & \tilde{\mathbf{B}}^\top\tilde{\mathbf{Q}} \\ \tilde{\mathbf{Q}}\tilde{\mathbf{B}} & \tilde{\mathbf{Q}} \end{bmatrix} = \begin{bmatrix} \mathbf{H}_{11} & \mathbf{H}_{12} \\ \mathbf{H}_{21} & \mathbf{H}_{22} \end{bmatrix},$$
$$\mathbf{h}_1 = \tilde{\mathbf{B}}^\top\tilde{\mathbf{Q}}(\tilde{\mathbf{A}}\mathbf{x}(k) - \mathbf{X}_d),$$
$$\mathbf{h}_2 = \tilde{\mathbf{Q}}(\tilde{\mathbf{A}}\mathbf{x}(k) - \mathbf{X}_d),$$

$$\mathbf{G}_1 = \begin{bmatrix} \tilde{\mathbf{B}} \\ -\tilde{\mathbf{B}} \\ \tilde{\bar{\mathbf{M}}} \\ -\tilde{\bar{\mathbf{M}}} \end{bmatrix},\ \mathbf{g}_1 = \begin{bmatrix} \mathbf{X}_{\max} - \tilde{\mathbf{A}}\mathbf{x}(k) - \mathbf{W}(k) \\ -\mathbf{X}_{\min} + \tilde{\mathbf{A}}\mathbf{x}(k) + \mathbf{W}(k) \\ \mathbf{T}_{\max} - \tilde{\Xi} \\ -\mathbf{T}_{\min} + \tilde{\Xi} \end{bmatrix},$$

$$\mathbf{G}_2 = \begin{bmatrix} \mathbf{I} \\ -\mathbf{I} \end{bmatrix}, \ \mathbf{g}_1 = \begin{bmatrix} \mathbf{W}_{\max} \\ -\mathbf{W}_{\min} \end{bmatrix},$$

$$\tilde{\bar{\mathbf{M}}} = \text{diag}(\bar{\mathbf{M}}, \ldots, \bar{\mathbf{M}}) \in \mathbb{R}^{6N_u \times 6N_u}, \ \tilde{\Xi} = \mathbf{1}_{N_u \times 1} \otimes \Xi,$$

$$\mathbf{T}_{\max} = [\boldsymbol{\tau}_{\max}{}^{\top} \ \ldots \ \boldsymbol{\tau}_{\max}{}^{\top}]^{\top} \in \mathbb{R}^{6N_u}, \ \mathbf{T}_{\max} = -\mathbf{T}_{\min},$$

$$\mathbf{W}_{\max} = [\mathbf{w}_{\max}{}^{\top} \ \ldots \ \mathbf{w}_{\max}{}^{\top}]^{\top} \in \mathbb{R}^{12N}, \ \mathbf{W}_{\max} = -\mathbf{W}_{\min},$$

$$\mathbf{X}_{\max} = [\mathbf{x}_{\max}{}^{\top} \ \ldots \ \mathbf{x}_{\max}{}^{\top}]^{\top} \in \mathbb{R}^{12N},$$

$$\mathbf{X}_{\min} = [\mathbf{x}_{\min}{}^{\top} \ \ldots \ \mathbf{x}_{\min}{}^{\top}]^{\top} \in \mathbb{R}^{12N}.$$

Although the optimization problem (6.25) is convex, min-max problems are computationally expensive due to the need to account for all possible worst-case disturbance scenarios [290].

To achieve the accelerated optimisation problem, re-write the cost function (6.33a) as:

$$\begin{aligned} V(\mathbf{U}(k), \mathbf{W}(k)) = &\frac{1}{2}\mathbf{U}(k)^{\top}\mathbf{H}_{11}\mathbf{U}(k) + \mathbf{U}(k)^{\top}\mathbf{H}_{12}\mathbf{W}(k) \\ &+ \frac{1}{2}\mathbf{W}(k)^{\top}\mathbf{H}_{22}\mathbf{W}(k) + \mathbf{h}_1^{\top}\mathbf{U}(k) + \mathbf{h}_2^{\top}\mathbf{W}(k). \end{aligned} \tag{6.34}$$

First, focus on the maximisation objective of the min-max problem to obtain the following QP:

$$\max_{\mathbf{W}(k)} V_1(\mathbf{W}(k)) \tag{6.35a}$$

$$\text{s. t. : } \mathbf{G}_2\mathbf{W}(k) \leq \mathbf{g}_2, \tag{6.35b}$$

where

$$V_1(k) = \frac{1}{2}\mathbf{W}(k)^{\top}\mathbf{H}_{22}\mathbf{W}(k) + (\mathbf{H}_{12}^{\top}\mathbf{U}(k)(k) + \mathbf{h}_2)^{\top}\mathbf{W}(k).$$

The objective here is to determine the disturbance realisation $\mathbf{W}(k)$ that maximises (6.35) based on which the original problem (6.33) can be solved as a minimisation

problem given as:

$$\min_{\mathbf{U}(k)} V(\mathbf{U}(k), \mathbf{W}(k)) \tag{6.36a}$$

$$\text{s. t. : } \mathbf{G}_1\mathbf{U}(k) \leq \mathbf{g}_1. \tag{6.36b}$$

To proceed, define the dual function of (6.35) as:

$$\begin{aligned}\mathbf{g}_d(\boldsymbol{\lambda}) =& \max_{\mathbf{W}(k)} \frac{1}{2}\mathbf{W}(k)^\top \mathbf{H}_{22}\mathbf{W}(k) \\ &+ \left(\mathbf{H}_{12}^\top \mathbf{U}(k) + \mathbf{h}_2 + \mathbf{G}_2^\top \boldsymbol{\lambda}\right)^\top \mathbf{W}(k) - \mathbf{g}_2^\top \boldsymbol{\lambda},\end{aligned} \tag{6.37}$$

in which $\boldsymbol{\lambda} \geq \mathbf{0}$ is the Lagrange multiplier for the constraints defined on $\mathbf{W}(k)$. Then, the Lagrangian is:

$$\begin{aligned}\mathcal{L}(\mathbf{W}(k), \boldsymbol{\lambda}) = &\frac{1}{2}\mathbf{W}^\top \mathbf{H}_{22}\mathbf{W} + (\mathbf{H}_{12}^\top \mathbf{U}(k) + \mathbf{h}_2)^\top \mathbf{W} \\ &+ \boldsymbol{\lambda}^\top(\mathbf{G}_2\mathbf{W} - \mathbf{g}_2).\end{aligned} \tag{6.38}$$

The gradient of the Lagrangian with respect to $\mathbf{W}(k)$ is

$$\nabla_{\mathbf{W}}\mathcal{L} = \mathbf{H}_{22}\mathbf{W}(k) + \mathbf{H}_{12}^\top \mathbf{U}(k) + \mathbf{h}_2 + \boldsymbol{\lambda}. \tag{6.39}$$

By setting the gradient to zero, the unconstrained maximisation problem (6.37) is convex for every $\boldsymbol{\lambda}$ because $\mathbf{H}_{22}$ is positive definite. The optimal disturbance realisation satisfies:

$$\mathbf{W}^*(k) = -\mathbf{H}_{22}^{-1}\left(\mathbf{H}_{12}^\top \mathbf{U}(k) + \mathbf{h}_2 + \mathbf{G}_2^\top \boldsymbol{\lambda}\right). \tag{6.40}$$

Substitute $\mathbf{W}^*(k)$ into the problem (6.36) to obtain:

$$\min_{\mathbf{U}(k),\boldsymbol{\lambda}} V(\mathbf{U}(k), \mathbf{W}^*(k)) \tag{6.41a}$$

$$\text{s. t. } \mathbf{G}_3 \begin{bmatrix} \mathbf{U}(k) \\ \boldsymbol{\lambda} \end{bmatrix} \leq \mathbf{g}_3, \tag{6.41b}$$

$$\boldsymbol{\lambda} \geq \mathbf{0}, \tag{6.41c}$$

where

$$\mathbf{G}_3 = \begin{bmatrix} \tilde{\mathbf{B}} - \mathbf{H}_{22}^{-1}\mathbf{H}_{12}^{\top} & -\mathbf{H}_{22}^{-1}\mathbf{G}_2^{\top} \\ -\tilde{\mathbf{B}} + \mathbf{H}_{22}^{-1}\mathbf{H}_{12}^{\top} & \mathbf{H}_{22}^{-1}\mathbf{G}_2^{\top} \\ \tilde{\tilde{\mathbf{M}}} & \mathbf{0} \\ -\tilde{\tilde{\mathbf{M}}} & \mathbf{0} \end{bmatrix},$$

$$\mathbf{g}_3 = \begin{bmatrix} \mathbf{X}_{\max} - \tilde{\mathbf{A}}\mathbf{x}(k) + \mathbf{H}_{22}^{-1}\mathbf{h}_2 \\ -\mathbf{X}_{\min} + \tilde{\mathbf{A}}\mathbf{x}(k) - \mathbf{H}_{22}^{-1}\mathbf{h}_2 \\ \mathbf{T}_{\min} - \tilde{\Xi} \\ -\mathbf{T}_{\max} + \tilde{\Xi} \end{bmatrix}.$$

Note that the value of $\mathbf{W}^*(k)$ from (6.40) can only be assumed to satisfy (6.35b) in the convex maximisation problem if the dual problem of (6.35) is solved to find the optimal value of the Lagrangian $\boldsymbol{\lambda}^*$. We clarify that (6.41) is not the dual problem of (6.35). To ensure that the optimal value $\boldsymbol{\lambda}^*$ obtained from solving (6.41) satisfies the disturbance bound, the additional constraint defined in (6.35b) is introduced to get the final optimisation problem:

$$\mathbf{U}^*(k) = \arg\min_{\mathbf{U}(k),\boldsymbol{\lambda}} V(\mathbf{U}(k), \mathbf{W}^*(k)) \tag{6.43a}$$

$$\text{s. t. } \begin{bmatrix} \mathbf{G}_3 \\ \mathbf{G}_4 \end{bmatrix} \begin{bmatrix} \mathbf{U}(k) \\ \boldsymbol{\lambda} \end{bmatrix} \leq \begin{bmatrix} \mathbf{g}_3 \\ \mathbf{g}_4 \end{bmatrix}, \ \boldsymbol{\lambda} \geq \mathbf{0}, \tag{6.43b}$$

where

$$\mathbf{G}_4 = \begin{bmatrix} -\mathbf{G}_2\mathbf{H}_{22}^{-1}\mathbf{H}_{12}^{\top} & -\mathbf{G}_2\mathbf{H}_{22}^{-1}\mathbf{G}_2^{\top} \end{bmatrix},$$

$$\mathbf{g}_4 = \mathbf{g}_2 + \mathbf{G}_2\mathbf{H}_{22}^{-1}\mathbf{h}_2.$$

The proposed accelerated MM-MPC strategy implementation procedure is outlined in Algorithm 4.

Remark 10. *The problem (6.43) can generally be solved as a QP in* $\begin{bmatrix} \mathbf{U}(k) \\ \boldsymbol{\lambda} \end{bmatrix}$ *using conventional quadratic solvers.*

Next, the determination of the disturbance bound $\mathbf{w}_{\max}$ required for the MM-MPC implementation is discussed.

6.5.3 Disturbance Bounds Estimation

In the development of the MM-MPC, the disturbance upper bound $\mathbf{w}_{\max}$ is assumed to be known. However, in practice, obtaining this bound is challenging [6], and using an arbitrary constant bound can result in a conservative performance by the min-max controller [302]. To mitigate the conservatism associated with a constant disturbance bound, a time-varying Kalman filtering technique is used to estimate the disturbance bounds [292]. Unlike the prediction model (6.21), which is formulated based on the AUV kinematics, the state estimation model incorporates both the kinematics and dynamics as in (4.16):

$$\mathbf{x}(k+1) = \mathbf{A}_{\mathbf{x}}\mathbf{x}(k) + \mathbf{B}\boldsymbol{\tau}(k) + \mathbf{w}(k). \tag{6.44}$$

Here, $\mathbf{w}(k) \in \mathbb{R}^{12}$ has two components defined as

$$\mathbf{w}(k) = \mathbf{w}^{u}(k) + \mathbf{w}^{n}(k), \tag{6.45}$$

in which $\mathbf{w}^{u}(k)$ denotes the unknown environmental disturbance and modelling

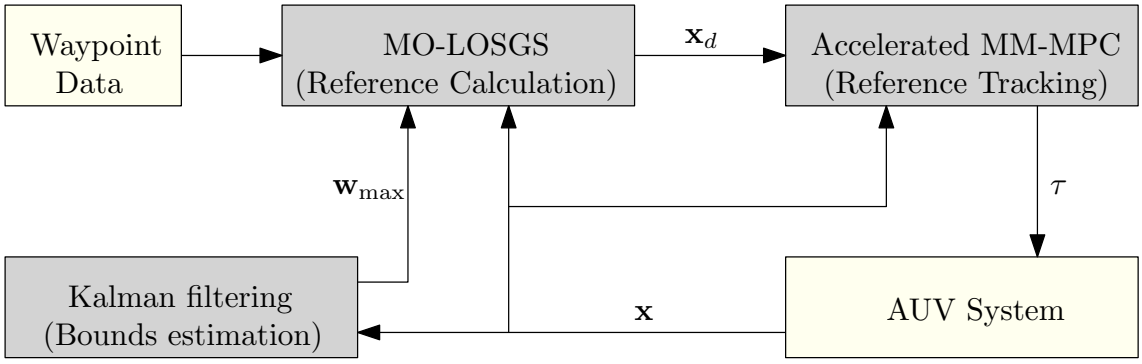

Fig. 6.3: Schematic diagram of the proposed accelerated robust control framework.

errors, $\mathbf{w}^n(k)$ is known and given as

$$\mathbf{w}^n(k) = \begin{bmatrix} \mathbf{0} \\ -\mathbf{M}^{-1}\mathbf{g}(\boldsymbol{\eta})T_s \end{bmatrix}. \tag{6.46}$$

The estimated state is given by the time-varying Kalman filter as

$$\hat{\mathbf{x}}(k+1) = \underbrace{\mathbf{A}(\mathbf{x}(k))\hat{\mathbf{x}}(k) + \mathbf{B}\boldsymbol{\tau}(k) + \mathbf{w}^n(k)}_{\text{nominal prediction}} + \underbrace{\mathbf{L}(k)(\mathbf{x}(k) - \hat{\mathbf{x}}(k))}_{\text{correction term}}, \tag{6.47}$$

where $\hat{\mathbf{x}}(k)$ is the state estimate and $\mathbf{L}(k)$ is the standard time-varying Kalman gain. Since the disturbance bound needs to be known before solving the control problem (6.43), the input signal $\boldsymbol{\tau}(k)$ is an unknown that must be determined at the current time step. Therefore, to approximate the disturbance, the measured states at time steps k and $k-1$ are employed to capture the dynamics of the disturbances between two consecutive steps. The disturbance estimate $\mathbf{w}^u(k)$ is given by

$$\mathbf{w}^u(k) = \hat{\mathbf{x}}(k) - [\mathbf{A}(\mathbf{x}(k-1))\hat{\mathbf{x}}(k-1) + \mathbf{B}\boldsymbol{\tau}(k-1) + \mathbf{w}^n(k-1)]. \tag{6.48}$$

The disturbance bound estimated as $\mathbf{w}_{\max} = |\mathbf{w}^u(k)|$ is used to solve (6.43). The proposed accelerated MM-MPC strategy implementation procedure is outlined in Algorithm 4. Fig. 6.3 illustrates the interconnections between the main components of the control framework.

Algorithm 4: Accelerated Min-max LPV MPC

Input: AUV LPV model, $\mathbf{Q}$, $\mathbf{R}$, N and N_u.

$k \leftarrow 0$
Measure current state $\mathbf{x}(k)$ comprising $\boldsymbol{\eta}(k)$ and $\boldsymbol{\nu}(k)$.
repeat
  Compute $\mathbf{w}_{\max} = |\mathbf{w}^u(k)|$, where $\mathbf{w}^u(k)$ is defined in (6.48).
  Iteratively compute $\tilde{\mathbf{A}}$ and $\tilde{\mathbf{B}}$ from $j = 1$ to $j = N$ using (6.17) and (6.18).
  Define $\mathbf{W}^*(k)$ as a function of $\boldsymbol{\lambda}$ according to (6.40).
  Solve (6.43) with $\mathbf{x}(k|k) = \mathbf{x}(k)$.
  The optimal solution is $\mathbf{U}^*(k) = \{\Delta\boldsymbol{\nu}^*(k|k), \ldots, \Delta\boldsymbol{\nu}^*(k + N_u - 1|k)\}$
  Employ $\Delta\boldsymbol{\nu}^*(k|k)$ to compute $\boldsymbol{\tau}^*(k)$ using (6.30).
  Implement $\boldsymbol{\tau}^*(k)$ for one sampling period.
  Update the state measurement as $\mathbf{x}(k + 1)$
  Update reference velocity, $\boldsymbol{\nu}_d$, according to (6.31).
  $k \leftarrow k + 1$
until end

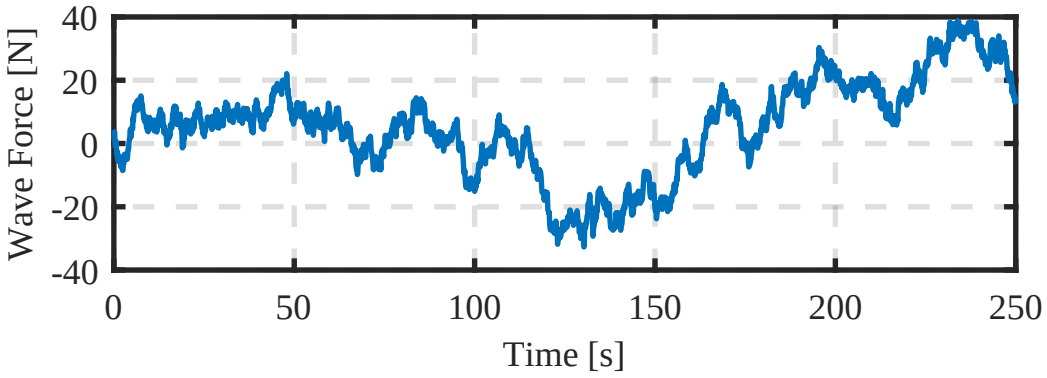

Fig. 6.4: Environmental disturbance based on modified Pierson–Moskowitz Spectrum.

6.6 Simulation Results

The simulation study considers the dynamic model of the Naminow-D AUV whose parameters are presented in Table 2.3. The length of the AUV including installed sensors is 3.0 m. The control objective is for the guidance and control system to guide the AUV to follow a set of waypoints determined offline. The input forces and

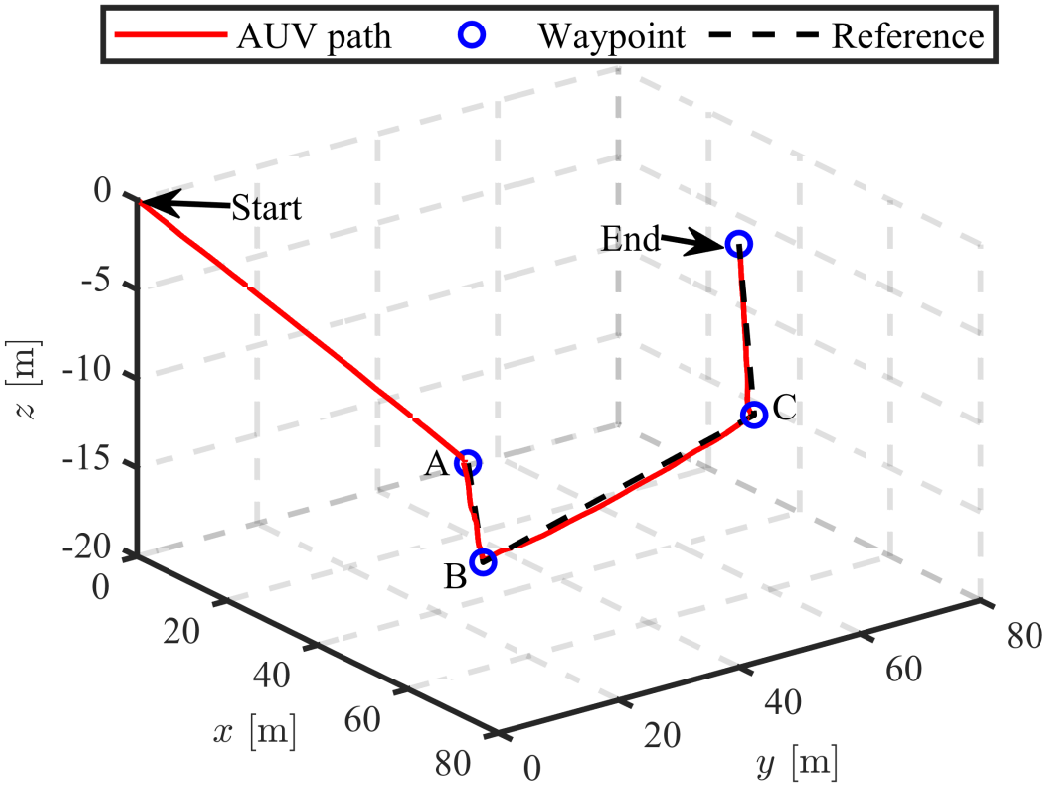

Fig. 6.5: Obstacle-free scenario: closed-loop AUV 3D PF using the accelerated MM-MPC.

moments are constrained to ±2 kN and ±2 kNm, respectively. The surge, sway and heave velocities are constrained as 0 m/s $\leq u_{\max} \leq$ 1.5 m/s, $|v_{\max}| \leq$ 1 m/s and $|w_{\max}| \leq$ 0.5 m/s, respectively while the pitch angle is constrained by $\pm 2\pi/5$ rad to avoid singularity problem in the rotation matrix.

Similar to Chapters 4 and 5, this chapter considered the effects of ocean disturbance modelled according to (2.8)-(2.9) using the modified Pierson–Moskowitz Spectrum [6] but with d_i is modelled as a Wiener process that lie in the range $[-50, 50]$. The ocean waves disturbance is modelled such that $\boldsymbol{\tau}_u^w = \boldsymbol{\tau}_v^w = \boldsymbol{\tau}_w^w$. The evolution of environmental disturbance over time is illustrated in Fig. 6.4.

An underwater waypoint-following mission at varying depths is considered for the simulation. The waypoints for the PF mission are defined as $A = (20, 40, -16)$,

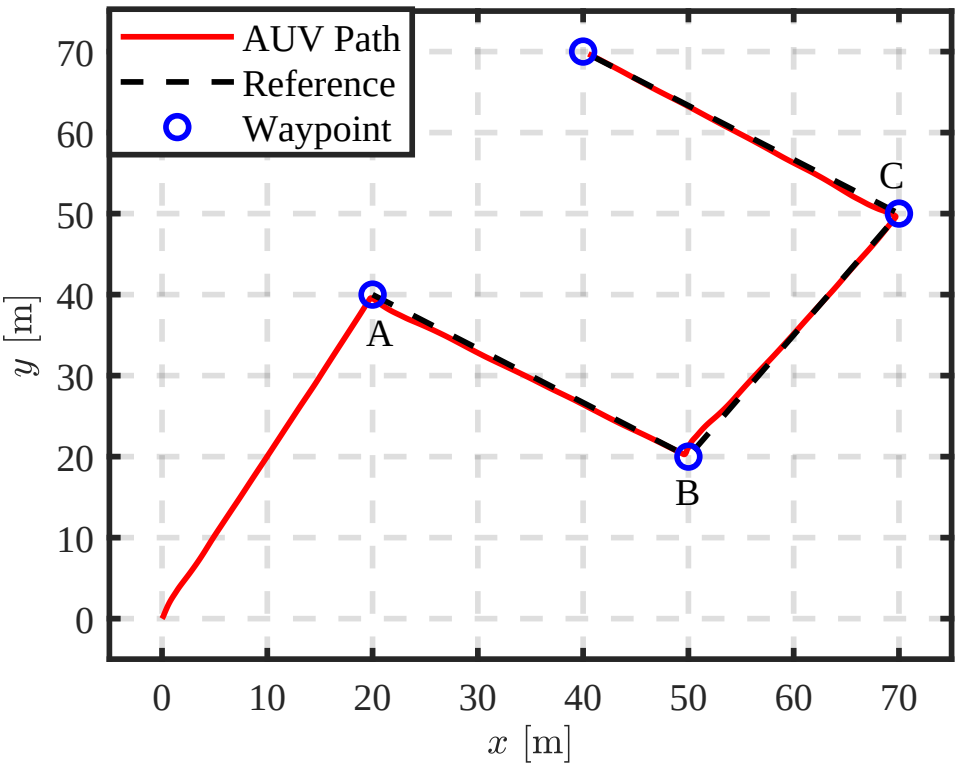

Fig. 6.6: Obstacle-free scenario: Closed-loop AUV 2D PF using the accelerated MM-MPC.

$B = (50, 20, -16)$, and $C = (70, 50, -8)$. The start and end waypoints are located at $(0, 0, 0)$ and $(40, 70, -4)$, respectively. The tuned parameters for the guidance and control system are given as follows: $\mathbf{R} = \text{diag}([27, 27, 27, 27, 27, 36])$, $N_u = 2$, $N = 14$, $\mathbf{Q} = \text{diag}([4, 4, 4, 0.4, 0.1, 0.1, 0.01, 0.01, 0.01, 0.01, 0.01, 0.01])$, and $\rho_c = \rho_s = L/5$ and $k_p = 1.5$. The sampling period $T_s = 0.1$ s is maintained.

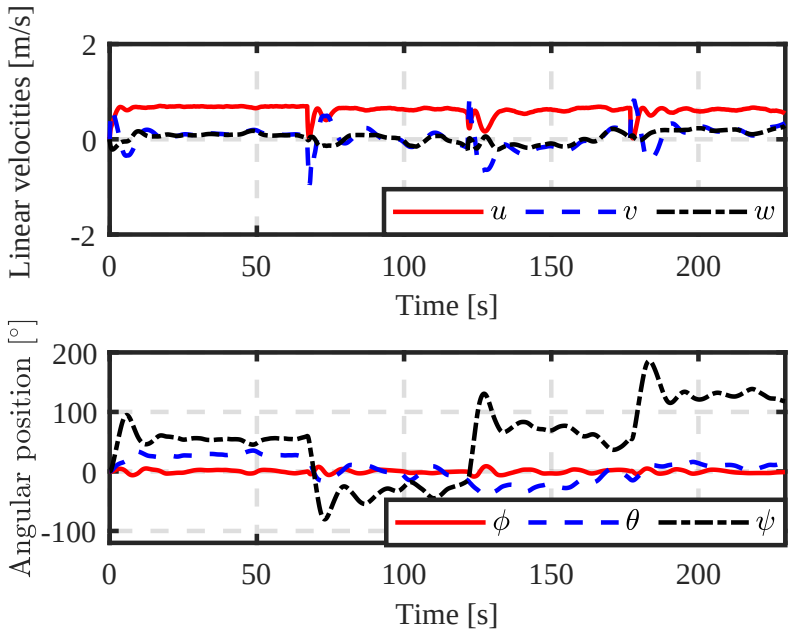

Fig. 6.7: Obstacle-free scenario: closed-loop AUV translational velocities (top) and angular position using the accelerated MM-MPC.

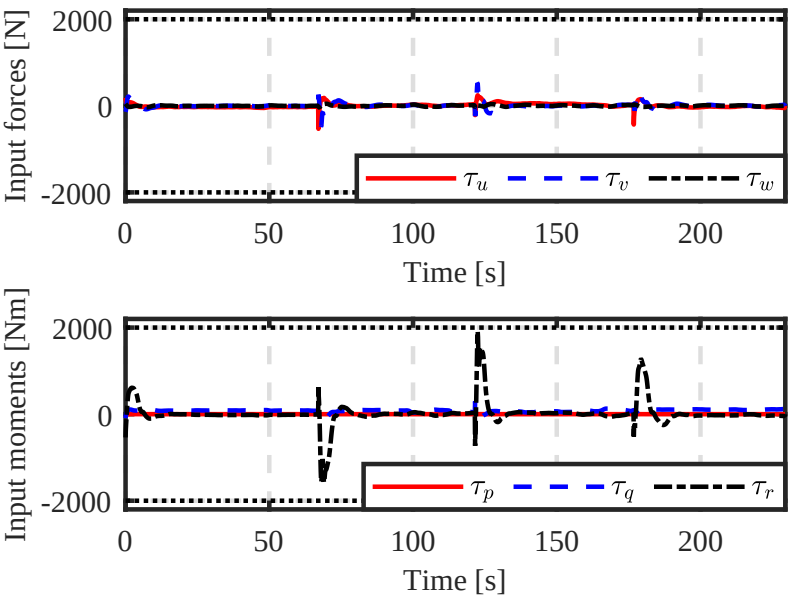

Fig. 6.8: Obstacle-free scenario: closed-loop input forces and moments of the AUV using the accelerated MM-MPC.

6.6.1 Path-Following in Obstacle-Free Scenario

The results for the scenario are depicted in Figs. 6.5 - 6.8. It can be observed that the AUV successfully navigates through the specified waypoints, as illustrated in Figs. 6.5 and 6.6, despite the influence of environmental disturbances. The velocity plot in Fig. 6.7 indicates that the AUV maintains a roughly constant surge speed of approximately $u \approx 0.8$ m/s. Although not depicted here, a surge speed of 1 m/s is achieved when $\rho_c = L/4$ is used in the simulation. The input forces and moments, displayed in Fig. 6.8, adhere to the specified constraints.

The importance of penalising the velocity increment rather than the actual input forces and moments in the cost function (6.24) is highlighted by performing the same simulation using the LPVMPC2 scheme. This LPVMPC2 controller in Chapter 4, which effectively mitigates disturbances, directly penalises the input forces and moments in its cost function. The outcomes, presented in Figs. 6.9 - 6.12, reveal that unlike the proposed MM-MPC, which stabilises the travel velocities, the translational velocities under the LPVMPC2 control approach exhibit oscillatory behaviour, and as a result, the surge velocity was not constrained by $0 \leq u \leq 1.5$ m/s. The task under the LPVMPC2 controller took over 630 seconds to complete, which is three times longer than with the proposed MM-MPC.

Table 6.1: The accelerated MM-MPC performance benchmarked by LPVMPC2. EC = Energy Consumed.

Controller	Task Duration [s]	Improvement [%]	EC [Wh]	Improvement [%]
MM-MPC	229.4	60	5.35	47
LPVMPC2	634.7	–	10.19	–

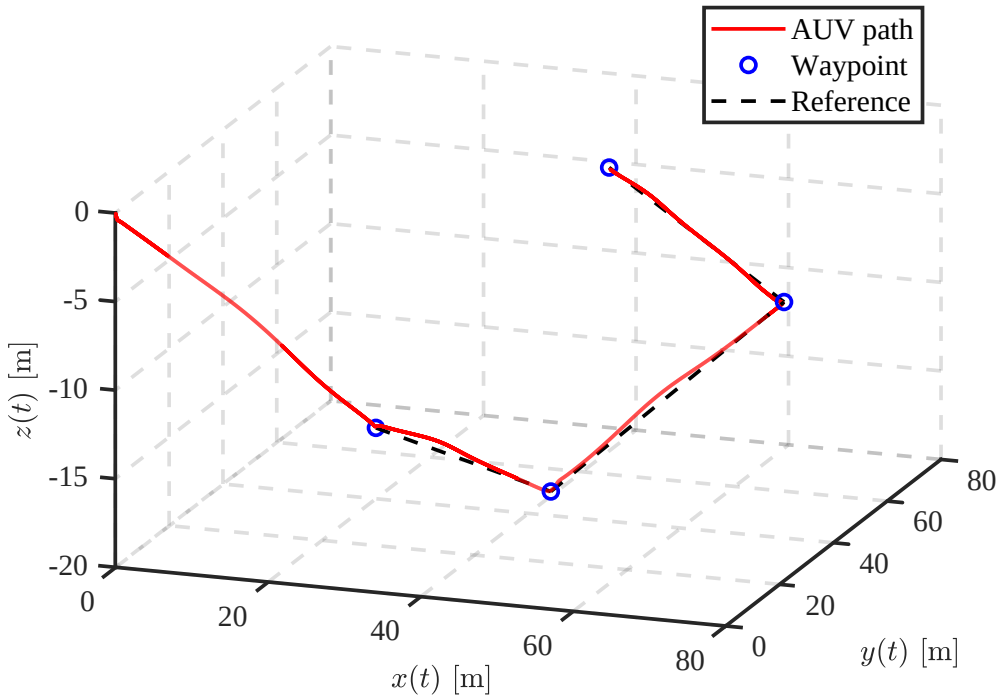

Fig. 6.9: Obstacle-free scenario: closed-loop AUV 3D PF using the LPVMPC2.

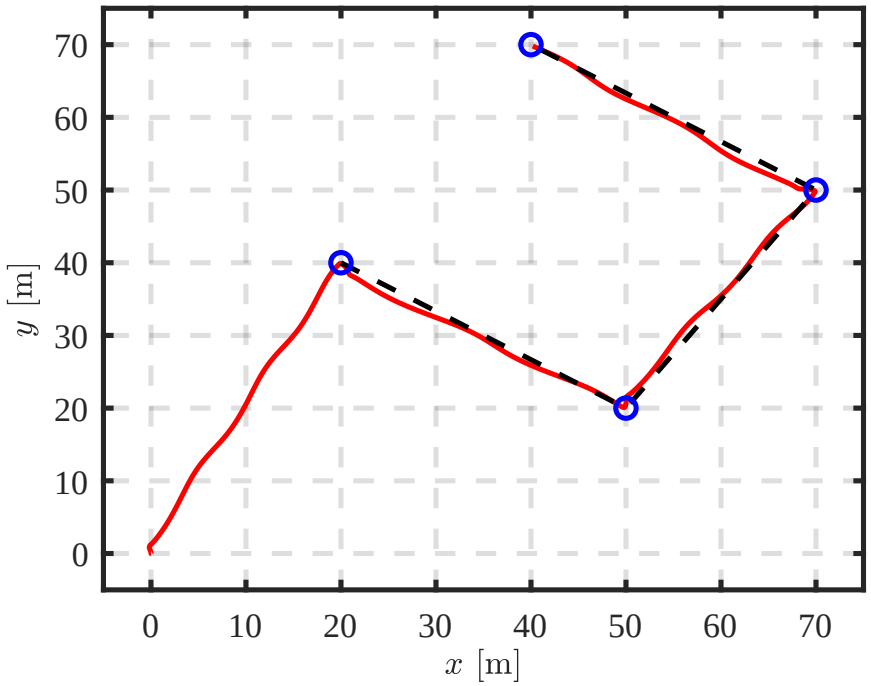

Fig. 6.10: Obstacle-free scenario: closed-loop AUV 2D PF using the LPVMPC2.

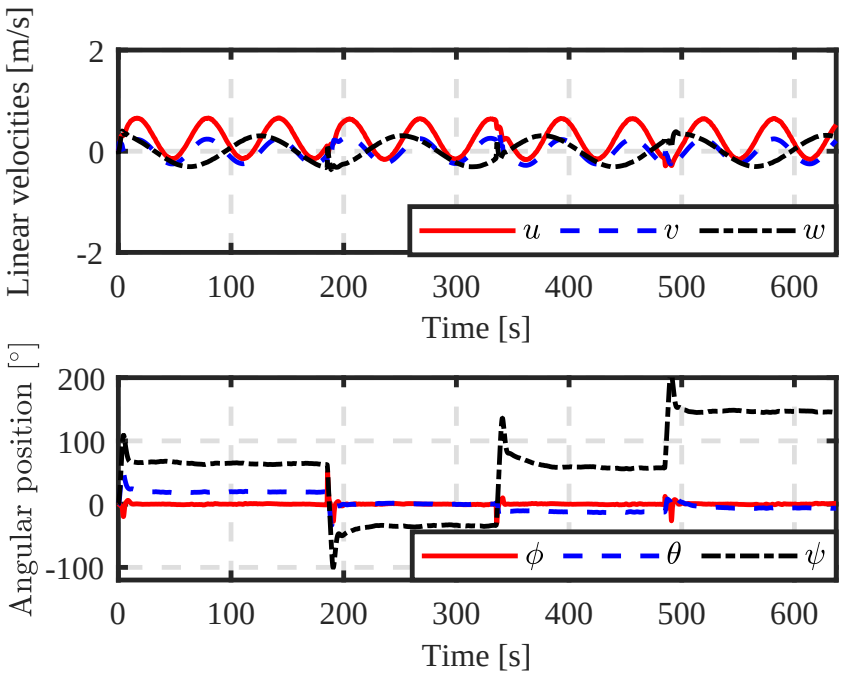

Fig. 6.11: Obstacle-free scenario: closed-loop translational velocities (top) and angular position (bottom) using the LOS guidance and LPVMPC 2.

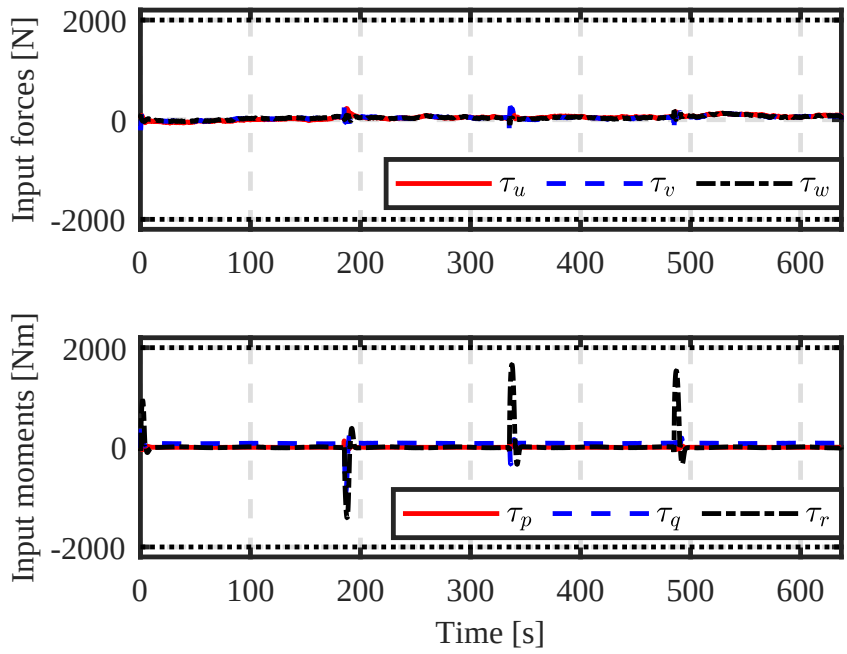

Fig. 6.12: Obstacle-free scenario: closed-loop input forces and moments of the AUV using the LOS guidance and LPVMPC2.

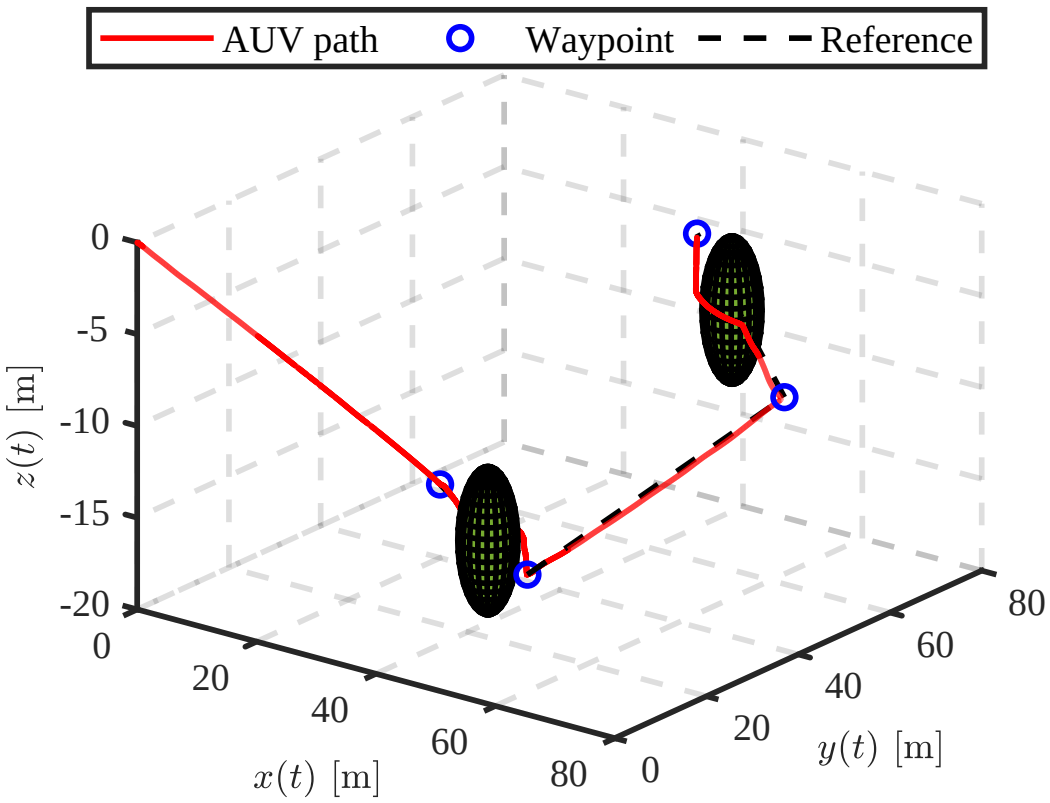

Fig. 6.13: Obstacle-constrained scenario: closed-loop AUV 3D PF task using the accelerated MM-MPC.

6.6.2 Path-Following in Obstacle-Constrained Scenario

In this scenario, static obstacles obstruct direct routes between waypoints A and B, as well as between C and the goal, making them impractical. Specifically, obstacle 1 is located at coordinates $(38, 30, -16)$, and obstacle 2 at $(55, 60, -6.2)$. The unsafe region is defined by the radius $r_{o_q} = 4.5$ m, encompassing an obstacle with a radius of 3 and a safe margin of 1.5 m. Note that the safe margin is set to half the total length of the vehicle to ensure it does not collide with the obstacle when the AUV's centre position coincides with the boundary of the unsafe region. The useful sensing range of the AUV onboard sensor is assumed to be $r_s = 6$ m.

The results are depicted in Figs. 6.13 - 6.16. From Figs. 6.13 and 6.14, it is

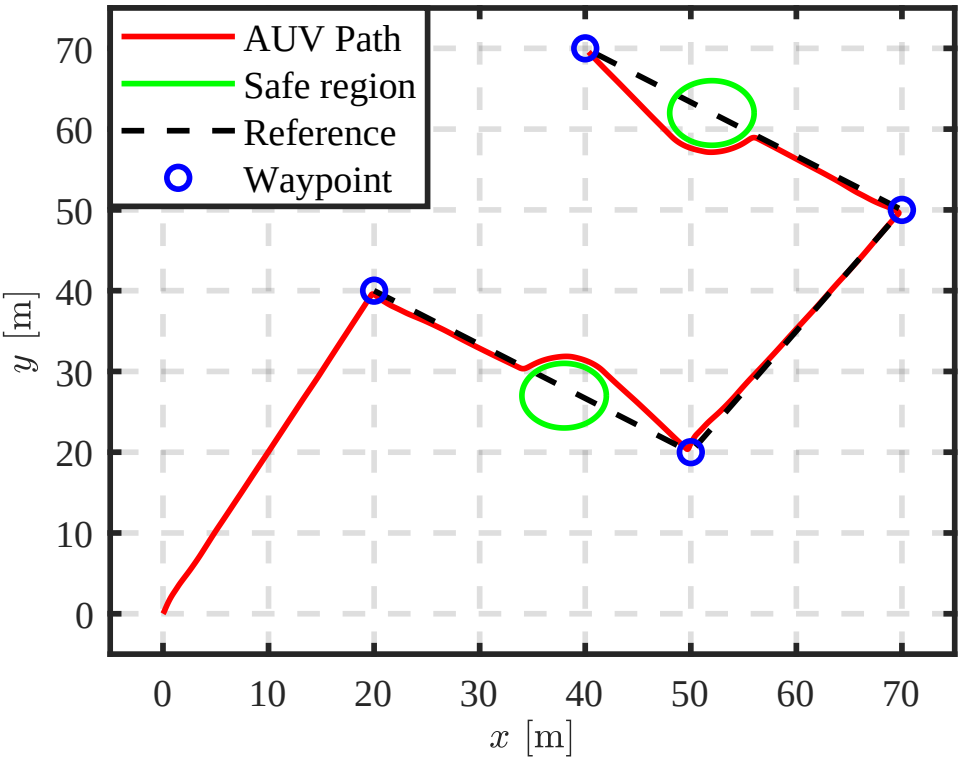

Fig. 6.14: Obstacle-constrained scenario: closed-loop AYV 2D PF task using the accelerated MM-MPC.

evident that the AUV's trajectory entirely avoids collision with the obstacles represented by the spheres. As seen in the horizontal plane in Fig. 6.14, after avoiding the obstacles, the AUV follows an approximate straight line from its position to the waypoint, rather than retracing the original straight line between the two successive waypoints. This approach guarantees that the AUV travels the shortest distance between its current position and the waypoint. Fig. 6.15 illustrates that the surge velocity (u) of the vehicle decreases during the collision avoidance task. Regarding the input forces and moments, as shown in Fig. 6.16, the resulting changes caused by path modification for collision avoidance are modest compared to when the vehicle alters its course from one waypoint to another.

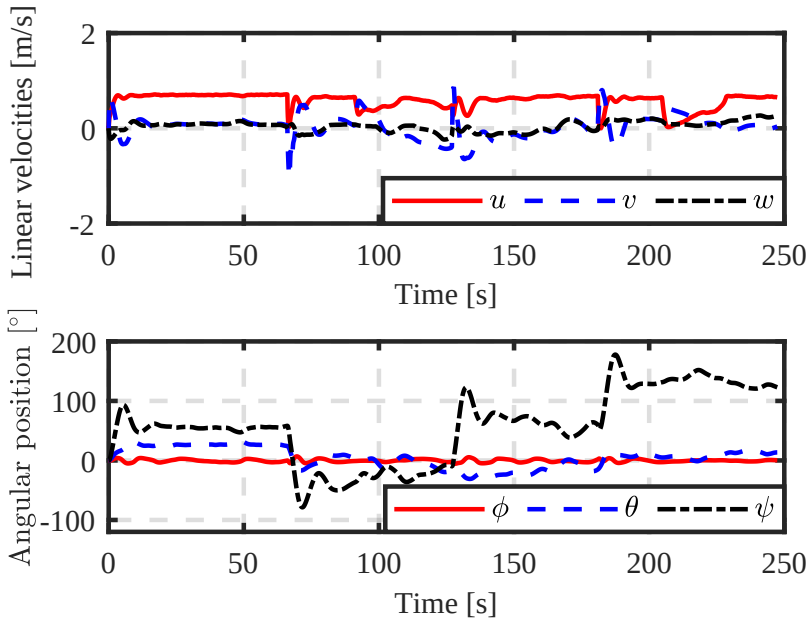

Fig. 6.15: Obstacle-constrained scenario: closed-loop translational velocities (top) and angular position (bottom) using the accelerated MM-MPC.

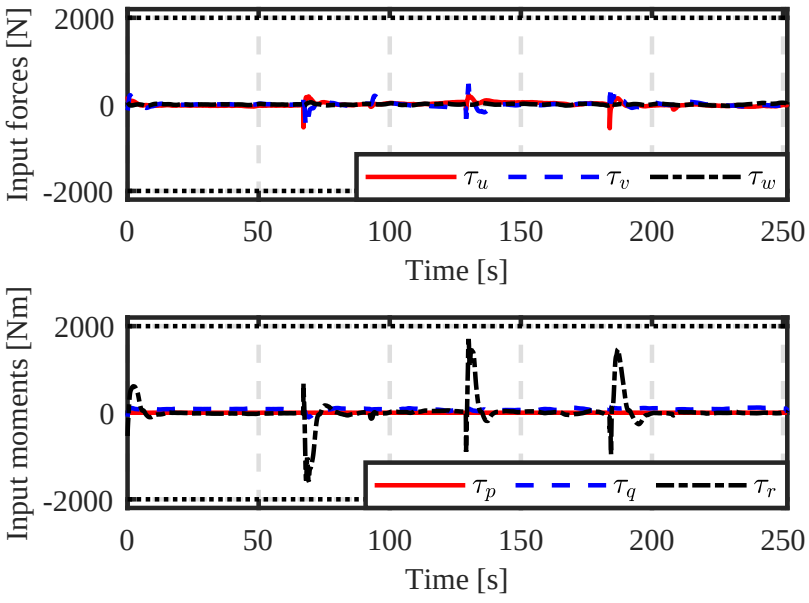

Fig. 6.16: Obstacle-constrained scenario: closed-loop input forces and moments of the AUV using the accelerated MM-MPC.

The transformation of the min-max problem (6.33) into the minimization problem (6.43) offers significant benefits in reducing computational effort. The results were obtained using an Intel Core i7 processor running at 2.2 GHz with 16 GB of RAM. The transformed problem (6.43) was solved using `quadprog` via the `sdpvar` and `optimize` functions of YALMIP [303], while the min-max problem (6.33) was solved using `fminimax` solver. Both solvers were employed because they are standard MATLAB solvers for quadratic and min-max problems, respectively.

For the solution of problem (6.33), we considered only $N = 12$ and $N_u = 2$ to benchmark the computational efficiency of the proposed method. The RMS value of the solver time for the problem (6.33) was 3405 ms, and this is decreased by more than fourfold to 826 ms by solving the output tracking alternative given in (6.25). The problem-building time was 14.26 ms, including the time to solve (6.15) and compute the matrices $(\tilde{\mathbf{A}}, \tilde{\mathbf{B}})$ in (6.23). Note that this formulation assumed constant prediction matrices at each time step [304], avoiding the need to update prediction matrices over the horizon N. Here, the more computationally efficient output tracking formulation of the min-max problem (6.25) was used to benchmark the proposed accelerated MM-MPC in (6.43).

Fig. 6.17 illustrates how the solver time for obtaining the solution to (6.43) varies for different N and N_u. In general, the total computation time (solver plus building time) required by the transformed problem (6.43) was approximately ten times shorter than that needed for the min-max problem. The total computation time for the transformed problem remained under 100 ms (the control sampling time), except in three cases: $(N_u = 3,\ N = 18)$, $(N_u = 6,\ N = 16)$ and $(N_u = 6,\ N = 18)$ as seen in Fig. 6.17. It is pertinent to note that using commercial solvers like MOSEK or Gurobi can enhance computation speed, increasing the likelihood of applying the controller in real-time applications.

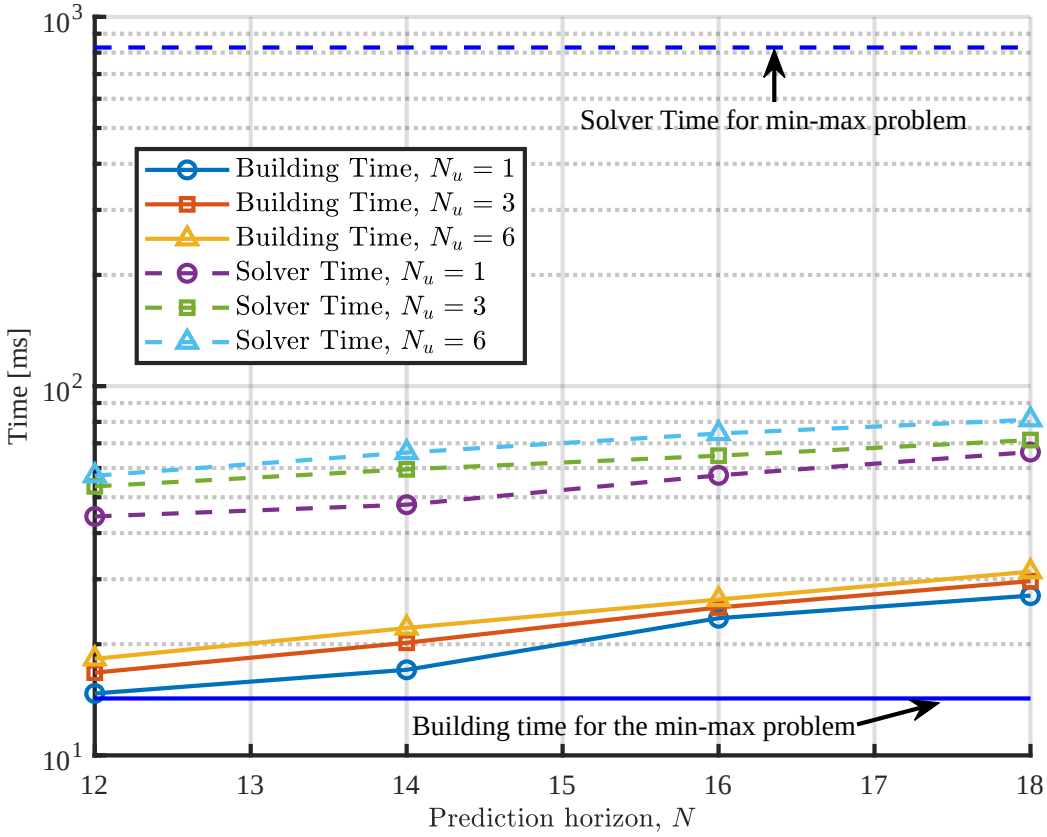

Fig. 6.17: Accelerated MM-MPC computational time for different prediction and control horizons benchmarked by the min-max problem (blue lines) with $N_u = 2$, $N = 12$.

6.7 Summary

This chapter presented a guidance and control framework for waypoint-following tasks by a coupled AUV. The system is designed to enable an AUV to follow 3D waypoints even in the presence of unknown environmental disturbances. The proposed guidance system operates without relying on simplifying assumptions such as negligible roll motion or decoupled motion. It uses the desired heading angle to determine the LOS horizontal coordinate, and the depth reference is proportional to the distance of AUV's current position to the LOS position in the horizontal plane.

In the presence of detected obstacles, a collision avoidance strategy is developed to adjust the reference position to ensure collision-free motion of the vehicle. This is achieved by exploiting the simplicity of the enclosure-based LOS guidance system to develop a MO-LOSGS that facilitates both PF and online collision avoidance of detected obstacles. The proposed MO-LOSGS computed the desired horizontal LOS coordinates, which are then used to determine the desired corresponding depth coordinate and orientation vector.

To track the reference generated by MO-LOSGS, an MM-MPC strategy is developed to ensure robust performance under time-varying environmental disturbances. The MM-MPC strategy used the velocity increment as the optimisation variable to mitigate excessive velocity fluctuations. The significant computational demand associated with the MM-MPC problem is addressed by developing a duality-based approach to transform the min-max problem into a convex quadratic optimisation control problem that off-the-shelf-solvers can solve efficiently.

Simulation results demonstrated the effectiveness of the proposed strategy in both PF and collision avoidance. The robust MM-MPC stabilised the AUV's surge velocity, reducing PF task duration and enhancing energy efficiency. Additionally, the transformed MM-MPC problem achieved a tenfold increase in computation speed. Future work will aim to provide theoretical guarantees on feasibility and stability.

The main results in this Chapter were presented at the 2024 IFAC CAMS conference and published in IFAC-Papers Online [304]. Additionally, the accelerated MM-MPC strategy has been submitted for consideration in a top-tier journal.

Chapter 7

Conclusions and Future Works

This concluding chapter summarises the research findings presented in the previous chapters on 6-DoF MPC design for AUVs in various motion control problems. It offers a comprehensive summary of the primary research findings and outlines potential avenues for future investigation.

7.1 Conclusions

This thesis presented MPC-based controllers for 3D motion control of AUVs. The three fundamental motion control problems, namely, dynamic positioning, trajectory tracking and path-following are investigated and novel control frameworks are provided considering environmental disturbances. Chapter 3 presented a critical review of the existing literature on MPC-based motion controllers for AUVs. It discusses the main limitations of existing works and forms the basis for the research questions presented in Chapter 1. Thus, the subsequent chapters focused on contributing towards addressing these limitations.

In a bid to address the first research question, "*How can effective and computationally efficient MPC-based motion controllers be designed without relying on traditional controllers like PID to stabilise some AUV dynamics?*", all the developed control algorithms are based on the LPV model formulation, where the state vector

is used as the updated parameter for the state matrix. This approach avoids solving the computationally prohibitive NMPC problem for high-order AUV models. Additionally, the need for simple controllers like PID is eliminated, as full-order models are used in the controllers' design to stabilise the 6 DoF of the vehicle.

To address the shortcomings of the partial velocity form MPC and the disturbance modelling approaches in AUV dynamic positioning, two complete velocity MPC algorithms were proposed in Chapter 4. These algorithms eliminate the necessity for an estimator and offer substantial mitigation of disturbance effects, thereby ensuring more accurate positioning of the vehicle. The first velocity MPC algorithm denoted LPVMPC1, is developed for dynamic positioning, incorporating a prediction model that utilises velocity increment to counteract the impacts of disturbances. The dynamic model serves as the state space equation, while the kinematic model is utilised as the output equation. The interrelation between these equations is leveraged to prevent an increased state dimension. The simulation results obtained for this controller compared to existing strategies showed that the tracking accuracy of MPC in dynamic positioning is significantly improved via the use of the velocity MPC approach. Therefore, LPVMPC1 addresses Research Question 2: "*How can the tracking accuracy of MPC-based motion controllers be enhanced under disturbances, especially for dynamic positioning, which is critical for successful docking operations?*" In addition, it contributes to achieving the first research objective outlined in Chapter 1.

To provide more efficient use of input forces, an alternative velocity MPC algorithm denoted as LPVMPC2 is developed for combined dynamic positioning and trajectory tracking. This algorithm incorporates both position and velocity increments in the formulation of the prediction model. This approach entirely avoids the need for model augmentation, thereby averting an increase in state dimensionality. It is applicable to a broad spectrum of linear time-invariant and time-varying systems. In this formulation, the MPC problem is framed as a reachable set problem, enabling the tracking of trajectories that contain unreachable positions for AUVs

operating in a constrained workspace. Additionally, a time parameterisation of the path followed by the AUV during the transition from trajectory tracking to dynamic positioning is formulated. The LPVMPC2 demonstrates comparable performance to LPVMPC1 in dynamic positioning, yet it requires significantly less input consumption to accomplish the same task. The LPVMPC2 algorithm stability and capability for offset-free tracking are established under the stated assumptions in Chapter 4. The LPVMPC2 controller contributed to addressing both the second, "*How can the tracking accuracy of MPC-based motion controllers be enhanced under disturbances, especially for dynamic positioning that is critical for successful docking operations?*" and third, "*How can trajectory tracking and dynamic positioning be integrated to enable an AUV to transition seamlessly from executing tracking missions to safe docking?*", research questions of this thesis. This is due to the fact the LPVMPC2 improves AUV position and orientation accuracy for docking operations and offers a seamless strategy for combined trajectory tracking and dynamic positioning. This also implies that the second research objective was achieved through this controller.

The fifth chapter investigates robust trajectory tracking for an AUV subject to input saturation using a tube-based approach to predictive control design. The input saturation problem was addressed by formulating a LOS local replanning strategy to limit the error signal encountered by the tracking controller, thereby avoiding excessive variations in the generated input forces. To characterise the time-varying tubes of the TMPC controller, an unconstrained finite-horizon control problem is analytically solved to obtain a state-dependent feedback gain. This approach eliminates the need to solve a nonlinear optimization problem or an SDRE, further reducing the controller's online computational requirements. The chapter also provided closed-loop stability results for the TMPC law. Finally, extensive simulation results demonstrated the effectiveness of this scheme over an NMPC controller, both in terms of tracking performance and efficient energy consumption by the AUV. By requiring only the online solution of a convex quadratically constrained quadratic problem, which can be efficiently solved online, this demonstrated the feasibility

of a computationally efficient robust MPC law, as required by the fourth research question: "*Can robust predictive control be designed for a high-dimensional AUV system without prohibitive computational requirements for real-time applications?*" By extension, the TMPC law helped achieve the third research objective.

In Chapter 6, the path-following control problem is investigated for an AUV operating in uncertain environments containing obstacles. The path to be followed is described by a series of waypoints. The developed framework comprised reference calculation and tracking subsystems. To compute the reference signals, the enclosure-based LOS strategy is utilised to calculate the horizontal 2D coordinate, from which the corresponding depth coordinate is determined analytically. In the proposed framework, the heading and depth control problems are transformed into a 3D LOS path-tracking formulation, eliminating the need for a kinematic error model. However, this technique does not address scenarios where the vehicle needs to avoid newly detected obstacles. This limitation is addressed by formulating a multi-objective LOS guidance system capable of facilitating both path-following and real-time collision avoidance of detected obstacles. The fourth research objective is achieved via the developed multi-objective LOS guidance system.

To achieve the tracking objective, a robust MPC strategy employing min-max optimistion is developed. During the AUV's motion from one waypoint to the next, maintaining a constant speed is desired for efficient task completion and minimal input energy consumption [6, 223]. The developed min-max controller penalises velocity increments in the optimisation cost function rather than the input forces and moments to enhance task completion efficiency by minimising variations in AUV speed. The use of MM-MPC helps to ensure robustness through the consideration of the disturbance upper bounds but results in prohibitive computational requirements. To mitigate the computational complexity associated with solving the min-max problem, a duality-based transformation strategy is employed to reformulate the problem into a quadratic minimisation control problem. This resulted in the so-called accelerated MM-MPC scheme. Simulation results indicated that

the proposed robust controller can yield over 40% reduction in energy consumption while completing the path-following task in a considerably shorter duration. Additionally, the reformulated minimisation problem yields a tenfold improvement in online computational speed compared to the original min-max problem. Hence, the results presented in Chapter 6 contributed to addressing both the fourth research question, "*Can robust predictive control be designed for a high-dimensional AUV system without prohibitive computational requirements for real-time applications?*" and fifth research question, "*How can robust optimal path-following be achieved in a time-efficient manner when tracking 3D waypoints in uncertain environments including obstacles?*" Also, the final research objective was achieved via the developed accelerated MM-MPC.

7.2 Recommendation for Future Works

The MPC-based motion controllers outlined in this thesis rely on a 6-DoF model of an AUV, approximated as a linear time-varying system to ensure computational tractability in solving the control optimisation problem online. While this thesis presents promising results that support the deployment of advanced MPC algorithms for 3D motion control of AUVs, several intriguing areas for future research have been identified and are outlined below.

1. *Data-aided MPC design for AUVs.* The AUV model used in this thesis is a well-established model for marine vehicles. However, accurately determining the model parameters is challenging, and effective underwater navigation is often compromised by unpredictable environmental disturbances. Given the advancements in artificial intelligence, which have led to the development of data-driven models showing promising results for AUV applications [254–256], it is believed that investigating data-driven methods to enhance the performance of mathematical model-based approaches is worthwhile. These data-aided, model-based strategies can significantly enhance the adaptability of

advanced control systems for AUVs by developing AI models for predicting disturbances and their bounds.

2. *6-DoF MPC design for multiple AUVs.* The cooperative control of multiple marine vehicles has garnered significant interest in recent years [232]. MPC can be a powerful tool for developing coordination control laws for AUVs. However, most existing studies primarily focus on motion control in local planes [18] due to the high computational demands associated with the 6-DoF model-based MPC design. Based on the speed at which the optimal control problems can be solved for the MPC laws developed in this thesis, future work can focus on extending these strategies, and their variants, to the use of the 6-DoF AUV model for distributed MPC in coordinating the motion of multiple AUVs.

3. *Radius of acceptance determination.* In Chapter 5, we presented a method to estimate the sphere of acceptance R_a and this tends to provide a generally good performance of the TMPC controller. Hence, it would be interesting to develop a method to determine the value of the radius of acceptance, ρ_c, used in the implementation of the MO-LOSGS presented in Chapter 6.

4. *Intelligent tuning methods for MPC parameters.* In the developed robust schemes, namely the tube-based MPC and the accelerated MM-MPC, the weighting matrices, control and prediction horizons, as well as parameters such as the radius of acceptance, sphere of acceptance, and (ideal) safe region, are manually tuned. Advances in machine learning can be exploited to develop intelligent techniques for the automatic tuning of these parameters based on predefined performance criteria and the physical limits of the vehicle.

5. *Collision avoidance with dynamic obstacles.* The guidance and control system presented in Chapter 6 considers only static obstacles, which are realistic as they could represent underwater rocks, seamounts, sandbanks, fixed structures used for oil and gas extraction (such as oil rigs and offshore platforms)

and shipwrecks. However, dynamic obstacles are also prevalent, such as moving sea animals and other marine vehicles. Future work may investigate the consideration of collision avoidance with dynamic obstacles.

6. *Stability results.* Although Chapter 6 provides a framework that may encourage the deployment of min-max MPC due to the accelerated computational speed, theoretical guarantees on closed-loop stability remain an open area of research for the developed strategy. Therefore, future work could focus on establishing theoretical guarantees for the closed-loop performance of the AUV system under this control law. Additionally, the tube-based MPC in Chapter 5 relies on a locally stabilising gain, so further investigations are needed to develop a stabilising feedback controller for the unfrozen AUV model and extend the stability properties of the overall tube-based controller.

7. *Experimental validation of MPC-based motion controllers.* This research is based on simulation studies for control validation, leaving experimental validation of the algorithms as an open area of research interest. Furthermore, existing experimental studies primarily focus on local planes, such as depth control problems. Hence, investigations focused on 3D motion represent an intriguing area for future work. Experimental validation in real-world scenarios, particularly in 3D motion contexts, would significantly enhance the applicability of the developed algorithms.

Appendix A

Fourth-order Runge Kutta Method for AUV Simulation

For the nonlinear AUV model $\dot{\mathbf{x}} = f(\mathbf{x}, \boldsymbol{\tau})$ given in (2.14), the Fourth-order Runge Kutta method is used to solve the differential equation as follows: (2.14) as

$$\mathbf{x}(k+1) = \mathbf{x}(k) + \frac{T_s}{6}(k_1 + 2k_2 + 2k_3 + k_4) \tag{A.1}$$

with

$$\begin{aligned} k_1 &= f(\mathbf{x}(k), \boldsymbol{\tau}(k)) \\ k_2 &= f\left(\mathbf{x}(k) + \frac{T_s}{2}k_1, \boldsymbol{\tau}(k)\right) \\ k_3 &= f\left(\mathbf{x}(k) + \frac{T_s}{2}k_2, \boldsymbol{\tau}(k)\right) \\ k_4 &= f(\mathbf{x}(k) + T_s k_3, \boldsymbol{\tau}(k)) \end{aligned}$$

Appendix B

Numerical Solution to the LOS Re-planning Scheme

The set of equations (5.9) is analytically solved for two scenarios. To simplify the notation, the time index k is dropped in the rest of this analytical solution.

Case 1: $|x_d - x| > 0$. For brevity, let

$$d_1 = \left(\frac{y_d - y}{x_d - x}\right), \; d_2 = \left(\frac{z_d - z}{x_d - x}\right)$$

and $g_1 = y - d_1 x$ and $g_2 = z - d_2 x$. It is trivial to show that

$$x_{los} = \frac{-b \pm \sqrt{b^2 - 4ac}}{2a}. \tag{B.1}$$

where

$$a = 1 + d_1^2 + d_2^2$$

$$b = 2(d_1 g_1 + d_2 g_2 - d_1 y - d_2 z - x)$$

$$c = x^2 + y^2 + z^2 + g_1^2 + g_2^2 - 2g_1 y - 2g_2 z - R_a^2$$

The positive sign is used if $x_d - x > 0$ while for $x_d - x < 0$, the negative sign is adopted in (B.1). Based on the calculated x_{los}, the values of y_{los} and z_{los} can readily be determined: $y_{los} = d_1 (x_{los} - x) + y = d_1 x_{los} + g_1$, $z_{los} = d_2 (x_{los} - x) + z = d_2 x_{los} + g_2$.

Appendix B. Numerical Solution to the LOS Re-planning Scheme

Notice that $y_{los} = y$ and $z_{los} = z$ if $y_d - y = 0$ and $z_d - z = 0$, respectively.
Case 2: $|x_d - x| = 0$, We have that $x_{los} = x$. In this scenario, only (5.9a) is valid and the equation reduces to a circle in the yz-plane, *i.e.,*

$$(y_{los} - y)^2 + (z_{los} - z)^2 = R_a^2. \tag{B.2}$$

It is noted that there are multiple values of y_{los} and z_{los} that satisfy (B.2). To obtain a solution that suite our application, define $\alpha \in [0, 1]$, based on which we obtain:

$$y_{los} = y \pm R_a\sqrt{\alpha},\ z_{los} = z \pm R_a\sqrt{(1-\alpha)} \tag{B.3}$$

where α can adaptively be determined as

$$\alpha = \frac{|y_d - y|}{|y_d - y| + |z_d - z|} \tag{B.4}$$

Notice that $\alpha \to 0$ as $|y_d - y| \to 0$ in which case $y_{los} \to y$. Conversely, $\alpha \to 1$ as $|z_d - z| \to 0$ in which case $z_{los} \to z$. We also remark that α is always defined because the solution to (5.9) is not required when $|x_d - x| = |y_d - y| = |z_d - z| = 0$ as the condition (5.8) will be fulfilled in such scenario. In (B.3), if $(y_d - y) > 0$ then $y_{los} = y + R_a\sqrt{\alpha}$, if $(y_d - y) < 0$ then $y_{los} = y - R_a\sqrt{\alpha}$. Furthermore, if $(z_d - z) > 0$ then $z_{los} = z + R_a\sqrt{(1-\alpha)}$ and if $(z_d - z) < 0$ then $z_{los} = z - R_a\sqrt{(1-\alpha)}$.

Bibliography

[1] H. Uchihori, L. Cavanini, M. Tasaki, P. Majecki, Y. Yashiro, M. J. Grimble, I. Yamamoto, G. M. van der Molen, A. Morinaga, and K. Eguchi, "Linear parameter-varying model predictive control of AUV for docking scenarios," *Applied Sciences*, vol. 11, no. 10, p. 4368, 2021. https://doi.org/10.3390/app11104368.

[2] K. Teo, E. An, and P.-P. J. Beaujean, "A robust fuzzy autonomous underwater vehicle (AUV) docking approach for unknown current disturbances," *IEEE Journal of Oceanic Engineering*, vol. 37, no. 2, pp. 143–155, 2012. https://doi.org/10.1109/JOE.2011.2180058.

[3] A. Sahoo, S. K. Dwivedy, and P. Robi, "Advancements in the field of autonomous underwater vehicle," *Ocean Engineering*, vol. 181, pp. 145–160, 2019. https://doi.org/10.1016/j.oceaneng.2019.04.011.

[4] D. Ribas, P. Ridao, A. Turetta, C. Melchiorri, G. Palli, J. J. Fernández, and P. J. Sanz, "I-AUV mechatronics integration for the TRIDENT FP7 project," *IEEE/ASME Transactions on Mechatronics*, vol. 20, no. 5, pp. 2583–2592, 2015. https://doi.org/10.1109/TMECH.2015.2395413.

[5] Y.-H. Lin, S.-M. Wang, L.-C. Huang, and M.-C. Fang, "Applying the stereo-vision detection technique to the development of underwater inspection task with pso-based dynamic routing algorithm for autonomous underwater vehicles," *Ocean Engineering*, vol. 139, pp. 127–139, 2017. https://doi.org/10.1016/j.oceaneng.2017.04.051.

[6] T. I. Fossen, *Handbook of marine craft hydrodynamics and motion control.* John Wiley & Sons, 2011. [Online]. Available: https://doi.org/10.1002/9781119994138

[7] H. Deng and T. Ohtsuka, "A parallel newton-type method for nonlinear model predictive control," *Automatica*, vol. 109, p. 108560, 2019. https://doi.org/10.1016/j.automatica.2019.108560.

[8] A. B. Martinsen, A. M. Lekkas, and S. Gros, "Reinforcement learning-based NMPC for tracking control of ASVs: Theory and experiments," *Control Engineering Practice*, vol. 120, p. 105024, 2022. https://doi.org/10.1016/j.conengprac.2021.105024.

[9] W. Wang, T. Shan, P. Leoni, D. Fernández-Gutiérrez, D. Meyers, C. Ratti, and D. Rus, "Roboat II: A novel autonomous surface vessel for urban environments," in *2020 IEEE/RSJ International Conference on Intelligent Robots and Systems (IROS)*. IEEE, 2020. pp, 1740–1747, https://doi.org/10.1109/IROS45743.2020.9340712.

[10] R. M. Saback, A. G. S. Conceicao, T. L. M. Santos, J. Albiez, and M. Reis, "Nonlinear model predictive control applied to an autonomous underwater vehicle," *IEEE Journal of Oceanic Engineering*, vol. 45, no. 3, pp. 799–812, 2019. https://doi.org/10.1109/JOE.2019.2919860.

[11] W. Wang, L. A. Mateos, S. Park, P. Leoni, B. Gheneti, F. Duarte, C. Ratti, and D. Rus, "Design, modeling, and nonlinear model predictive tracking control of a novel autonomous surface vehicle," in *2018 IEEE International Conference on Robotics and Automation (ICRA)*. IEEE, 2018. https://doi.org/10.1109/ICRA.2018.8460632, pp. 6189–6196.

[12] H. Wei and Y. Shi, "MPC-based motion planning and control enables smarter and safer autonomous marine vehicles: Perspectives and a tutorial survey," *IEEE/CAA Journal of Automatica Sinica*, 2022. https://doi.org/10.1109/JAS.2022.106016.

[13] C. Shen, "Motion control of autonomous underwater vehicles using advanced model predictive control strategy," Ph.D. dissertation, University of Victoria, 2018. http://hdl.handle.net/1828/9144.

[14] Y. Shi and K. Zhang, "Advanced model predictive control framework for autonomous intelligent mechatronic systems: A tutorial overview and perspectives," *Annual Re-*

views in Control, vol. 52, pp. 170–196, 2021. https://doi.org/10.1016/j.arcontrol.2021.10.008.

[15] K. Shi, X. Wang, H. Xu, Z. Chen, and H. Zhao, "Integrated approach to AUV docking based on nonlinear offset-free model predictive control," *Measurement and Control*, vol. 56, no. 3-4, pp. 733–750, 2023. https://doi.org/10.1177/00202940221106568.

[16] W. Gan, D. Zhu, and D. Ji, "QPSO-model predictive control-based approach to dynamic trajectory tracking control for unmanned underwater vehicles," *Ocean Engineering*, vol. 158, pp. 208–220, 2018. https://doi.org/10.1016/j.oceaneng.2018.03.078.

[17] Z. Yan, J. Yan, S. Cai, Y. Yu, and Y. Wu, "Robust MPC-based trajectory tracking of autonomous underwater vehicles with model uncertainty," *Ocean Engineering*, vol. 286, p. 115617, 2023. https://doi.org/10.1016/j.oceaneng.2023.115617.

[18] Y. Shi, C. Shen, H. Wei, and K. Zhang, *Advanced Model Predictive Control for Autonomous Marine Vehicles*. Springer International Publishing, 2023. https://doi.org/10.1007/978-3-031-19354-5.

[19] M. Ebrahimi, A. Kamali, and M. Abbaspour, "Enhancing the roll dynamics of an auv by contra-rotating-propellers," *Ships and Offshore Structures*, vol. 16, no. 7, pp. 787–796, 2021. https://doi.org/10.1080/17445302.2020.1786233.

[20] A. A. R. Al Makdah, N. Daher, D. Asmar, and E. Shammas, "Three-dimensional trajectory tracking of a hybrid autonomous underwater vehicle in the presence of underwater current," *Ocean Engineering*, vol. 185, pp. 115–132, 2019. https://doi.org/10.1016/j.oceaneng.2019.05.030.

[21] N. Yang, C. Shen, Z. Song, M. Johnson-Roberson, and J. Sun, "Robust energy-optimal control for 3-D path-following of autonomous underwater vehicles under ocean currents," *IEEE Transactions on Control Systems Technology*, 2023. https://doi.org/10.1109/TCST.2023.3315602.

[22] S. Heshmati-Alamdari, A. Nikou, and D. V. Dimarogonas, "Robust trajectory tracking control for underactuated autonomous underwater vehicles in uncertain environments," *IEEE Transactions on Automation Science and Engineering*, vol. 18, no. 3, pp. 1288–1301, 2020. https://doi.org/10.1109/TASE.2020.3001183.

[23] X. Cao, L. Ren, and C. Sun, "Dynamic target tracking control of autonomous underwater vehicle based on trajectory prediction," *IEEE Transactions on Cybernetics*, vol. 53, no. 3, pp. 1968–1981, 2023. https://doi.org/10.1109/TCYB.2022.3189688.

[24] Z. Yan, P. Gong, W. Zhang, and W. Wu, "Model predictive control of autonomous underwater vehicles for trajectory tracking with external disturbances," *Ocean Engineering*, vol. 217, p. 107884, 2020. https://doi.org/10.1016/j.oceaneng.2020.107884.

[25] Y. Zhang, X. Liu, M. Luo, and C. Yang, "MPC-based 3-D trajectory tracking for an autonomous underwater vehicle with constraints in complex ocean environments," *Ocean Engineering*, vol. 189, p. 106309, 2019. https://doi.org/10.1016/j.oceaneng.2019.106309.

[26] C. Shen and Y. Shi, "Distributed implementation of nonlinear model predictive control for AUV trajectory tracking," *Automatica*, vol. 115, p. 108863, 2020. https://doi.org/10.1016/j.automatica.2020.108863.

[27] P. Haghi, M. Naraghi, and S. A. S. Vanini, "Adaptive position and attitude tracking of an AUV in the presence of ocean current disturbances," in *2007 IEEE International Conference on Control Applications*. IEEE, 2007, pp. 741–746. https://doi.org/10.1109/CCA.2007.4389321.

[28] Z. Dong, L. Wan, Y. Li, T. Liu, J. Zhuang, and G. Zhang, "Point stabilization for an underactuated AUV in the presence of ocean currents," *International Journal of Advanced Robotic Systems*, vol. 12, no. 7, p. 100, 2015. https://doi.org/10.5772/61037.

[29] X. Liang, X. Qu, Y. Hou, and Q. Ma, "Three-dimensional trajectory tracking control of an underactuated autonomous underwater vehicle based on ocean current

observer," *International Journal of Advanced Robotic Systems*, vol. 15, no. 5, p. 1729881418806811, 2018. https://doi.org/10.1177/1729881418806811.

[30] H. Joe, M. Kim, and S.-c. Yu, "Second-order sliding-mode controller for autonomous underwater vehicle in the presence of unknown disturbances," *Nonlinear Dynamics*, vol. 78, no. 1, pp. 183–196, 2014. https://doi.org/10.1007/s11071-014-1431-0.

[31] C. P. Bechlioulis, G. C. Karras, S. Heshmati-Alamdari, and K. J. Kyriakopoulos, "Trajectory tracking with prescribed performance for underactuated underwater vehicles under model uncertainties and external disturbances," *IEEE Transactions on Control Systems Technology*, vol. 25, no. 2, pp. 429–440, 2016. https://doi.org/10.1109/TCST.2016.2555247.

[32] Y. Xia, K. Xu, Y. Li, G. Xu, and X. Xiang, "Improved line-of-sight trajectory tracking control of under-actuated AUV subjects to ocean currents and input saturation," *Ocean Engineering*, vol. 174, pp. 14–30, 2019. https://doi.org/10.1016/j.oceaneng.2019.01.025.

[33] Q. Yang, H. Su, and G. Tang, "Approximate optimal tracking control for near-surface AUVs with wave disturbances," *Journal of Ocean University of China*, vol. 15, no. 5, pp. 789–798, 2016. https://doi.org/10.1007/s11802-016-2986-9.

[34] J. Kim, H. Joe, S.-c. Yu, J. S. Lee, and M. Kim, "Time-delay controller design for position control of autonomous underwater vehicle under disturbances," *IEEE Transactions on Industrial Electronics*, vol. 63, no. 2, pp. 1052–1061, 2015. https://doi.org/10.1109/TIE.2015.2477270.

[35] G. V. Lakhekar, L. M. Waghmare, and R. G. Roy, "Disturbance observer-based fuzzy adapted s-surface controller for spatial trajectory tracking of autonomous underwater vehicle," *IEEE Transactions on Intelligent Vehicles*, vol. 4, no. 4, pp. 622–636, 2019. https://doi.org/10.1109/TIV.2019.2938082.

[36] M. Kim, H. Joe, J. Kim, and S.-c. Yu, "Integral sliding mode controller for precise manoeuvring of autonomous underwater vehicle in the presence of unknown

environmental disturbances," *International Journal of Control*, vol. 88, no. 10, pp. 2055–2065, 2015. https://doi.org/10.1080/00207179.2015.1031182.

[37] E. Fredriksen and K. Y. Pettersen, "Global κ-exponential way-point maneuvering of ships: Theory and experiments," *Automatica*, vol. 42, no. 4, pp. 677–687, 2006. https://doi.org/10.1016/j.automatica.2005.12.020.

[38] E. Borhaug, A. Pavlov, and K. Y. Pettersen, "Integral LOS control for path following of underactuated marine surface vessels in the presence of constant ocean currents," in *Proceedings of the 47th IEEE Conference on Decision and Control*. IEEE, 2008. https://doi.org/10.1109/CDC.2008.4739352, pp. 4984–4991.

[39] W. Caharija, K. Y. Pettersen, J. T. Gravdahl, and E. Børhaug, "Integral LOS guidance for horizontal path following of underactuated autonomous underwater vehicles in the presence of vertical ocean currents," in *2012 American Control Conference (ACC)*. IEEE, 2012, pp. 5427 – 5434. https://doi.org/10.1109/ACC.2012.6315607.

[40] T. I. Fossen, *Guidance and Control of Ocean Vehicles*. John Wiley & Sons, Chichester, England, 1994.

[41] X. Liu, M. Zhang, and E. Rogers, "Trajectory tracking control for autonomous underwater vehicles based on fuzzy re-planning of a local desired trajectory," *IEEE Transactions on Vehicular Technology*, vol. 68, no. 12, pp. 11 657–11 667, 2019. https://doi.org/10.1109/TVT.2019.2948153.

[42] K. Vickery, "Acoustic positioning systems. a practical overview of current systems," in *Proc. of the 1998 Workshop on AUVs (Cat. No. 98CH36290)*. IEEE, 1998, pp. 5–17. [Online]. Available: https://doi.org/10.1109/AUV.1998.744434

[43] Y. Chen, D. Zheng, P. A. Miller, and J. A. Farrell, "Underwater inertial navigation with long baseline transceivers: A near-real-time approach," *IEEE Trans. Control Systems Technol.*, vol. 24, no. 1, pp. 240–251, 2015. [Online]. Available: https://doi.org/10.1109/TCST.2015.2429613

[44] National Oceanic and Atmospheric Administration, "Ocean exploration and its importance [Retrieved 31 March 2022]," 2022. [Online]. Available: https://oceanexplorer.noaa.gov/backmatter/whatisexploration.html#:~:text=Findings

[45] C. Von Alt, "Autonomous underwater vehicles," in *Autonomous Underwater Lagrangian Platforms and Sensors Workshop*, vol. 3, 2003, pp. 1–4. https://data.coaps.fsu.edu/eric_pub/RSMAS/transfer/AutonomousUnderwaterVehicles.pdf.

[46] W. Nodland, T. Ewart, W. Bendiner, J. Miller, and E. Aagaard, "SPURV II-an unmanned, free-swimming submersible developed for oceanographic research," in *OCEANS 81*. IEEE, 1981, pp. 92–98. https://doi.org/10.1109/OCEANS.1981.1151607.

[47] S. Bryant, "Advanced unmanned search system (AUSS) performance analysis," Naval Ocean Center, San Diego, California, Tech. Rep., 1979. https://archive.org/details/DTIC_ADA267909/page/6/mode/2up.

[48] S. McPhail, "Development of a simple navigation system for the autosub autonomous underwater vehicle," in *OCEANS'93*. IEEE, 1993. https://doi.org/10.1109/OCEANS.1993.326148, pp. II504–II509.

[49] S. M. Smith, P. E. An, K. Holappa, J. Whitney, A. Burns, K. Nelson, E. Heatzig, O. Kempfe, D. Kronen, T. Pantelakis *et al.*, "The morpheus ultramodular autonomous underwater vehicle," *IEEE Journal of Oceanic Engineering*, vol. 26, no. 4, pp. 453–465, 2001. https://doi.org/10.1109/48.972078.

[50] H. Singh, A. Can, R. Eustice, S. Lerner, N. McPhee, and C. Roman, "Seabed AUV offers new platform for high-resolution imaging," *EOS, Transactions American Geophysical Union*, vol. 85, no. 31, pp. 289–296, 2004. https://doi.org/10.1029/2004EO310002.

[51] R. Madhan, E. Desa, S. Prabhudesai, L. Sebastião, A. Pascoal, E. Desa, A. Mascarenhas, P. Maurya, G. Navelkar, S. Afzulpurkar *et al.*, "Mechanical design and development aspects of a small AUV-maya," in *7th IFAC Conference MCMC2006*.

IFAC, 2006. https://citeseerx.ist.psu.edu/document?repid=rep1&type=pdf&doi=55c5c30076373b5174b11a75a9187d2fd1792004.

[52] C. Osterloh, M. Litza, and E. Maehle, "Hard-and software architecture of a small autonomous underwater vehicle for environmental monitoring tasks," in *Advances in Robotics Research*. Springer, 2009. https://doi.org/10.1007/978-3-642-01213-6_31, pp. 347–356.

[53] E. A. de Barros, L. O. Freire, and J. L. Dantas, "Development of the Pirajuba AUV," *IFAC Proceedings Volumes*, vol. 43, no. 20, pp. 102–107, 2010. https://doi.org/10.3182/20100915-3-DE-3008.00063.

[54] A. Sousa, L. Madureira, J. Coelho, J. Pinto, J. Pereira, J. B. Sousa, and P. Dias, "LAUV: The man-portable autonomous underwater vehicle," *IFAC Proceedings Volumes*, vol. 45, no. 5, pp. 268–274, 2012. https://doi.org/10.3182/20120410-3-PT-4028.00045.

[55] H. Singh, T. Maksym, J. Wilkinson, and G. Williams, "Inexpensive, small AUVs for studying ice-covered polar environments," *Science Robotics*, vol. 2, no. 7, p. eaan4809, 2017. https://doi.org/10.1126/scirobotics.aan4809.

[56] T. Wu, C. Tao, J. Zhang, A. Wang, G. Zhang, J. Zhou, and X. Deng, "A hydrothermal investigation system for the Qianlong-II autonomous underwater vehicle," *Acta Oceanologica Sinica*, vol. 38, no. 3, pp. 159–165, 2019. https://doi.org/10.1007/s13131-019-1408-4.

[57] Y. Chardard and T. Copros, "Swimmer: final sea demonstration of this innovative hybrid AUV/ROV system," in *International Symposium on Underwater Technology*. IEEE, 2002, pp. 17–23. https://doi.org/10.1109/UT.2002.1002371.

[58] D. Loebis, F. Dalgleish, R. Sutton, S. Tetlow, J. Chudley, and R. Allwood, "An integrated approach in the design of a navigation system for an AUV," *IFAC-Papers Online*, vol. 36, no. 21, pp. 281–286, 2003. https://doi.org/10.1016/S1474-6670(17)37821-7.

[59] MIT Sea Grant, "A history of the odyssey-class of autonomous underwater vehicles [Retrieved 25 Feb. 2022]," 2022. [Online]. Available: https://seagrant.mit.edu/auv-odyssey-class/

[60] D. Goldberg, "Huxley: A flexible robot control architecture for autonomous underwater vehicles," in *OCEANS 2011 IEEE-Spain*. IEEE, 2011, pp. 1–10. https://doi.org/10.1109/Oceans-Spain.2011.6003512.

[61] General Dynamics Mission Systems, "Bluefin robotics unmanned underwater vehicles [Retrieved 24 Feb. 2022]," 2022. [Online]. Available: https://gdmissionsystems.com/underwater-vehicles/bluefin-robotics

[62] G. Griffiths, *Technology and applications of autonomous underwater vehicles*. Taylor & Francis, 2002, vol. 2. https://doi.org/10.1201/9780203522301.

[63] A. Shukla and H. Karki, "Application of robotics in offshore oil and gas industry—a review part II," *Robotics and Autonomous Systems*, vol. 75, pp. 508–524, 2016. https://doi.org/10.1016/j.robot.2015.09.013.

[64] HM Government, "Net zero strategy: Build back greener," Presented to Parliament pursuant to Section 14 of the Climate Change Act 2008, Tech. Rep., 2021. [Online]. Available: https://assets.publishing.service.gov.uk/government/uploads/system/uploads/attachment_data/file/1033990/net-zero-strategy-beis.pdf

[65] Zagreb, "Submission by Croatia and the European Commission on behalf of the European Union and its member states [Retrieved 31 March 2024]," 2020. [Online]. Available: https://unfccc.int/sites/default/files/resource/HR-03-06-2020%20EU%20Submission%20on%20Long%20term%20strategy.pdf

[66] J. Kerry and G. McCarthy, "The long-term strategy of the united states - pathways to net-zero greenhouse gas emissions by 2050 [Retrieved 31 March 2022]," 2021. [Online]. Available: https://www.whitehouse.gov/wp-content/uploads/2021/10/US-Long-Term-Strategy.pdf

[67] Canadian Government, "Net-zero emissions by 2050 [Retrieved 31 March 2022]," 2022. [Online]. Available: https://www.canada.ca/en/services/environment/weather/climatechange/climate-plan/net-zero-emissions-2050.html

[68] R. Danovaro, J. Aguzzi, E. Fanelli, D. Billett, K. Gjerde, A. Jamieson, E. Ramirez-Llodra, C. Smith, P. Snelgrove, L. Thomsen *et al.*, "An ecosystem-based deep-ocean strategy," *Science*, vol. 355, no. 6324, pp. 452–454, 2017. https://doi.org/10.1126/science.aah7178.

[69] M. Sibenac, T. Podder, W. Kirkwood, and H. Thomas, "Autonomous underwater vehicles for ocean research: Current needs and state of the art technologies," *Marine Technology Society Journal*, vol. 38, no. 2, pp. 63–72, 2004. https://doi.org/10.4031/002533204787522848.

[70] R. H. Littlefield, K. Soenen, G. Packard, and J. Kaeli, "Seafloor cable based navigation and monitoring with autonomous underwater vehicles," in *OCEANS'19*. IEEE, 2019, pp. 1–5. https://doi.org/10.23919/OCEANS40490.2019.8962587.

[71] A. Carrera, N. Palomeras, D. Ribas, P. Kormushev, and M. Carreras, "An intervention-AUV learns how to perform an underwater valve turning," in *Oceans'14*. IEEE, 2014, pp. 1–7. https://doi.org/10.1109/OCEANS-TAIPEI.2014.6964483.

[72] N. Palomeras, A. Peñalver, M. Massot-Campos, P. L. Negre, J. J. Fernández, P. Ridao, P. J. Sanz, and G. Oliver-Codina, "I-AUV docking and panel intervention at sea," *Sensors*, vol. 16, no. 10, p. 1673, 2016. https://doi.org/10.3390/s16101673.

[73] M. Prats, J. Garcia, S. Wirth, D. Ribas, P. Sanz, P. Ridao, N. Gracias, and G. Oliver, "Multipurpose autonomous underwater intervention: A systems integration perspective," in *2012 20th Mediterranean Conference on Control & Automation (MED)*. IEEE, 2012, pp. 1379–1384. https://doi.org/10.1109/MED.2012.6265831.

[74] P. J. Sanz, P. Ridao, G. Oliver, G. Casalino, Y. Petillot, C. Silvestre, C. Melchiorri, and A. Turetta, "TRIDENT an european project targeted to increase the autonomy levels for underwater intervention missions," in *2013 OCEANS-San Diego*. IEEE, 2013, pp. 1–10. https://doi.org/10.23919/OCEANS.2013.6741370.

[75] P. Ridao, M. Carreras, D. Ribas, P. J. Sanz, and G. Oliver, "Intervention AUVs: the next challenge," *Annual Reviews in Control*, vol. 40, pp. 227–241, 2015. https://doi.org/10.1016/j.arcontrol.2015.09.015.

[76] Hydro International, "49% growth in AUV demand by 2020 [Retrieved 24 Feb. 2022]," 2021. [Online]. Available: https://www.hydro-international.com/content/news/auv-demand-to-grow-49-by-2020?output=pdf

[77] P. J. B. Sánchez, M. Papaelias, and F. P. G. Márquez, "Autonomous underwater vehicles: Instrumentation and measurements," *IEEE Instrumentation & Measurement Magazine*, vol. 23, no. 2, pp. 105–114, 2020. https://doi.org/10.1109/MIM.2020.9062680.

[78] Data Bridge Market Research, "Global autonomous underwater vehicle (AUV) market – industry trends and forecast to 2028 [Retrieved 23 Feb. 2022]," 2021. [Online]. Available: https://www.databridgemarketresearch.com/reports/global-autonomous-underwater-vehicle-auv-market

[79] R. A. George, L. A. Gee, A. W. Hill, J. A. Thomson, and P. Jeanjean, "High-resolution AUV surveys of the eastern sigsbee escarpment," in *Offshore Technology Conference*. OnePetro, 2002, pp. 1–12, https://doi.org/10.4043/14139-MS.

[80] N. Tito and E. Rambaldi, "SWIMMER: Innovative IMR AUV," in *Offshore Technology Conference*. OnePetro, 2009. https://doi.org/10.4043/19930-MS.

[81] B. Chemisky, F. Menna, E. Nocerino, and P. Drap, "Underwater survey for oil and gas industry: A review of close range optical methods," *Remote Sensing*, vol. 13, no. 14, p. 2789, 2021. https://doi.org/10.3390/rs13142789.

[82] W. Naeem, R. Sutton, and S. Ahmad, "Pure pursuit guidance and model predictive control of an autonomous underwater vehicle for cable/pipeline tracking," *IMarEST Journal of marine Science and Environment*, vol. C(1), pp. 15–25, Mar. 2004. https://pure.qub.ac.uk/en/publications/pure-pursuit-guidance-and-model-predictive-control-of-an-autonomo.

[83] X. Xiang, B. Jouvencel, and O. Parodi, "Coordinated formation control of multiple autonomous underwater vehicles for pipeline inspection," *International Journal of Advanced Robotic Systems*, vol. 7, no. 1, p. 3, 2010. https://doi.org/10.5772/7242.

[84] M. Jacobi and D. Karimanzira, "Multi sensor underwater pipeline tracking with AUVs," in *OCEANS'14*. IEEE, 2014, pp. 1–6. https://doi.org/10.1109/OCEANS.2014.7003013.

[85] Y. Tipsuwan and P. Hoonsuwan, "Design and implementation of an AUV for petroleum pipeline inspection," in *7th International Conference on Information Technology and Electrical Engineering (ICITEE*. IEEE, 2015, pp. 382–387. https://doi.org/10.1109/ICITEED.2015.7408976.

[86] H. Zhang, S. Zhang, Y. Wang, Y. Liu, Y. Yang, T. Zhou, and H. Bian, "Subsea pipeline leak inspection by autonomous underwater vehicle," *Applied Ocean Research*, vol. 107, p. 102321, 2021. https://doi.org/10.1016/j.apor.2020.102321.

[87] A. G. Rumson, "The application of fully unmanned robotic systems for inspection of subsea pipelines," *Ocean Engineering*, vol. 235, p. 109214, 2021. https://doi.org/10.1016/j.oceaneng.2021.109214.

[88] F. Maurelli, M. Carreras, J. Salvi, D. Lane, K. Kyriakopoulos, G. Karras, M. Fox, D. Long, P. Kormushev, and D. Caldwell, "The PANDORA project: A success story in AUV autonomy," in *OCEANS 2016-Shanghai*. IEEE, 2016. https://doi.org/10.1109/OCEANSAP.2016.7485618, pp. 1–8.

[89] D. M. Lane, F. Maurelli, P. Kormushev, M. Carreras, M. Fox, and K. Kyriakopoulos, "Persistent autonomy: the challenges of the PANDORA project," *IFAC Proceedings Volumes*, vol. 45, no. 27, pp. 268–273, 2012. https://doi.org/10.3182/20120919-3-IT-2046.00046.

[90] J. Albiez, S. Joyeux, C. Gaudig, J. Hilljegerdes, S. Kroffke, C. Schoo, S. Arnold, G. Mimoso, P. Alcantara, R. Saback *et al.*, "FlatFish-a compact subsea-resident inspection AUV," in *OCEANS 2015-MTS/IEEE Washington*. IEEE, 2015, pp. 1–8. url=https://doi.org/10.23919/OCEANS.2015.7404442.

[91] P. Ridao, M. Carreras, D. Ribas, P. J. Sanz, and G. Oliver, "Intervention AUVs: the next challenge," *IFAC Proceedings Volumes*, vol. 47, no. 3, pp. 12 146–12 159, 2014. https://doi.org/10.1016/j.arcontrol.2015.09.015.

[92] N. Palomeras, A. Penalver, M. Massot-Campos, G. Vallicrosa, P. L. Negre, J. J. Fernández, P. Ridao, P. J. Sanz, G. Oliver-Codina, and A. Palomer, "I-AUV docking and intervention in a subsea panel," in *2014 IEEE/RSJ International Conference on Intelligent Robots and Systems*. IEEE, 2014. pp. 2279–2285, https://doi.org/10.1109/IROS.2014.6942870.

[93] G. Alendal, "Cost efficient environmental survey paths for detecting continuous tracer discharges," *Journal of Geophysical Research: Oceans*, vol. 122, no. 7, pp. 5458–5467, 2017. https://doi.org/10.1002/2016JC012655.

[94] N. Kato, M. Choyekh, R. Dewantara, H. Senga, H. Chiba, E. Kobayashi, M. Yoshie, T. Tanaka, and T. Short, "An autonomous underwater robot for tracking and monitoring of subsea plumes after oil spills and gas leaks from seafloor," *Journal of Loss Prevention in the Process Industries*, vol. 50, pp. 386–396, 2017. https://doi.org/10.1016/j.jlp.2017.03.006.

[95] M. Buffagni, F. Gasparoni, N. H. Bergseth, E. Bjornbom, and P. Broccia, "Development and test of an AUV for environmental monitoring and asset integrity in offshore o&g scenarios: CLEAN SEA project," in *SPE International Conference on Health, Safety, and Environment*. OnePetro, 2014. https://doi.org/10.2118/168471-MS.

[96] F. Gasparoni, F. Bruni, R. Chomicz, V. Ciccarelli, M. Favaretto, M. Filippini, F. Furlan, T. Grasso, N. H. Bergseth, E. Bjornbom *et al.*, "Development and test of an AUV for asset integrity and environmental monitoring in offshore oil and gas scenarios," in *The Twenty-third International Offshore and Polar Engineering Conference*. OnePetro, 2013, pp. 388–396. https://onepetro.org/ISOPEIOPEC/proceedings/ISOPE13/All-ISOPE13/ISOPE-I-13-268/15319.

[97] R. Pi, P. Cieślak, P. Ridao, and P. J. Sanz, "TWINBOT: autonomous underwater cooperative transportation," *IEEE Access*, vol. 9, pp. 37 668–37 684, 2021. https://doi.org/10.1109/ACCESS.2021.3063669.

[98] R. P. Stokey, A. Roup, C. von Alt, B. Allen, N. Forrester, T. Austin, R. Goldsborough, M. Purcell, F. Jaffre, G. Packard *et al.*, "Development of the REMUS 600 autonomous underwater vehicle," in *Proceedings of OCEANS 2005 MTS/IEEE*. IEEE, 2005, pp. 1301–1304. https://doi.org/10.1109/OCEANS.2005.1639934.

[99] B. Butler and V. den Hertog, "Theseus: a cable-laying AUV," in *OCEANS'93*. IEEE, 1993, pp. I210–I213. https://doi.org/10.1109/OCEANS.1993.326046.

[100] J. S. Ferguson, "The theseus autonomous underwater vehicle. two successful missions," in *Proceedings of 1998 International Symposium on Underwater Technology*. IEEE, 1998, pp. 109–114. https://doi.org/10.1109/UT.1998.670072.

[101] J. Thorleifson, T. Davies, M. Black, D. Hopkin, R. Verrall, A. Pope, I. Monteith, V. Den Hertog, and B. Butler, "The theseus autonomous underwater vehicle. A canadian success story," in *Oceans' 97*, vol. 2. IEEE, 1997, pp. 1001–1006. https://doi.org/10.1109/OCEANS.1997.624127.

[102] A. Balasuriya and T. Ura, "Vision-based underwater cable detection and following using AUVs," in *OCEANS'02*, vol. 3. IEEE, 2002, pp. 1582–1587. https://doi.org/10.1109/OCEANS.2002.1191871.

[103] Hydro International, "AUV capability widened to include cable and pipeline tracking [Retrieved 01 Mar. 2022]," 2017. [Online]. Available: https://www.hydro-international.com/content/news/auv-capability-widened-to-include-cable-and-pipeline-tracking

[104] N. Palomeras, G. Vallicrosa, A. Mallios, J. Bosch, E. Vidal, N. Hurtos, M. Carreras, and P. Ridao, "AUV homing and docking for remote operations," *Ocean Engineering*, vol. 154, pp. 106–120, 2018. https://doi.org/10.1016/j.oceaneng.2018.01.114.

[105] A. Inzartsev and A. Pavin, *AUV application for inspection of underwater communications*. In-Tech Publishers, 2009. https://doi.org/10.5772/6704.

[106] J. G. Northcutt, A. A. Kleiner, T. S. Chance, and J. Lee, "Cable route surveys utilizing autonomous underwater vehicles (AUVs)," *Marine Technology Society. Marine Technology Society Journal*, vol. 34, no. 3, p. 11, 2000. https://doi.org/10.4031/MTSJ.34.3.3.

[107] M. E. Furlong, D. Paxton, P. Stevenson, M. Pebody, S. D. McPhail, and J. Perrett, "Autosub long range: A long range deep diving AUV for ocean monitoring," in *2012 IEEE/OES Autonomous Underwater Vehicles (AUV)*. IEEE, 2012, pp. 1–7. https://doi.org/10.1109/AUV.2012.6380737.

[108] B. Chen, R. Li, W. Bai, J. Li, Y. Zhou, and R. Guo, "Application analysis of autonomous underwater vehicle in submarine cable detection operation," in *Proceedings of the 2018 International Conference on Robotics, Control and Automation Engineering*, 2018, pp. 71–75. https://doi.org/10.1145/3303714.3303729.

[109] G. Marani, S. K. Choi, and J. Yuh, "Underwater autonomous manipulation for intervention missions AUVs," *Ocean Engineering*, vol. 36, no. 1, pp. 15–23, 2009. https://doi.org/10.1016/j.oceaneng.2008.08.007.

[110] A. Ajdin, "Kongsberg unveils new HUGIN AUV [Retrieved 28 Feb. 2022]," 2022. [Online]. Available: https://www.offshore-energy.biz/kongsberg-unveils-new-hugin-auv/

[111] W. O'Halloran and J. Elvander, "AUVs and ROVs: Supporting offshore renewable technologies," in *Offshore Technology Conference*. OnePetro, 2013. https://doi.org/10.4043/24243-MS.

[112] E. Lubofsky, "A new way of seeing offshore wind power cables. source: Woods hole oceanographic institution. [Retrieved 4 Mar. 2022]," 2022. [Online]. Available: https://www.whoi.edu/oceanus/feature/a-new-way-of-seeing-offshore-wind-power-cables/

[113] T. Fong, "Robotics and autonomous systems in O&M removing the barriers to BVLOS operations," ORE Catapult, Tech. Rep., 2019. [Online]. Available: http://bit.ly/4hUFj4H

[114] A. W. Stoner, C. H. Ryer, S. J. Parker, P. J. Auster, and W. W. Wakefield, "Evaluating the role of fish behavior in surveys conducted with underwater vehicles," *Canadian Journal of Fisheries and Aquatic Sciences*, vol. 65, no. 6, pp. 1230–1243, 2008. https://doi.org/10.1139/F08-032.

[115] T. M. Grothues, A. E. Newhall, J. F. Lynch, K. S. Vogel, and G. G. Gawarkiewicz, "High-frequency side-scan sonar fish reconnaissance by autonomous underwater vehicles," *Canadian Journal of Fisheries and Aquatic Sciences*, vol. 74, no. 2, pp. 240–255, 2017. https://doi.org/10.1139/cjfas-2015-0301.

[116] R. K. Katzschmann, J. DelPreto, R. MacCurdy, and D. Rus, "Exploration of underwater life with an acoustically controlled soft robotic fish," *Science Robotics*, vol. 3, no. 16, p. eaar3449, 2018. https://doi.org/10.1126/scirobotics.aar3449.

[117] S. N. M. Yusof, H. A. Kadir, K. Isa, R. Ambar, and M. S. M. Shamshuri, "An analysis of acoustics fish surveys module for autonomous underwater vehicle (AUV)," in *Proceedings of the 12th National Technical Seminar on Unmanned System Technology 2020*. Springer, 2022, pp. 153–160. https://doi.org/10.1007/978-981-16-2406-3_13.

[118] C. F. White, Y. Lin, C. M. Clark, and C. G. Lowe, "Human vs robot: Comparing the viability and utility of autonomous underwater vehicles for the acoustic telemetry tracking of marine organisms," *Journal of Experimental Marine Biology and Ecology*, vol. 485, pp. 112–118, 2016. https://doi.org/10.1016/j.jembe.2016.08.010.

[119] D. R. Yoerger, M. Curran, J. Fujii, C. R. German, D. Gomez-Ibanez, A. F. Govindarajan, J. C. Howland, J. K. Llopiz, P. H. Wiebe, B. W. Hobson *et al.*, "Mesobot: An autonomous underwater vehicle for tracking and sampling midwater targets," in *2018 IEEE/OES autonomous underwater vehicle workshop (AUV)*. IEEE, 2018, pp. 1–7. https://doi.org/10.1109/AUV.2018.8729822.

[120] L. Hawkes, O. Exeter, S. Henderson, C. Kerry, A. Kukulya, J. Rudd, S. Whelan, N. Yoder, and M. Witt, "Autonomous underwater videography and tracking of basking sharks," *Animal Biotelemetry*, vol. 8, no. 1, pp. 1–10, 2020. https://doi.org/10.1186/s40317-020-00216-w.

[121] F. Caratori Tontini, B. Davy, C. De Ronde, R. Embley, M. Leybourne, and M. Tivey, "Crustal magnetization of brothers volcano, new zealand, measured by autonomous underwater vehicles: Geophysical expression of a submarine hydrothermal system," *Economic Geology*, vol. 107, no. 8, pp. 1571–1581, 2012. https://doi.org/10.2113/econgeo.107.8.1571.

[122] Y. Sato, T. Maki, T. Matsuda, and T. Sakamaki, "Detailed 3D seafloor imaging of kagoshima bay by AUV Tri-TON2," in *2015 IEEE Underwater Technology (UT)*. IEEE, 2015, pp. 1–6. https://doi.org/10.1109/UT.2015.7108314.

[123] Ø. Sture, M. Ludvigsen, L. M. S. Aas *et al.*, "Autonomous underwater vehicles as a platform for underwater hyperspectral imaging," in *Oceans 2017-Aberdeen*. IEEE, 2017, pp. 1–8. https://doi.org/10.1109/OCEANSE.2017.8084995.

[124] M. A. Moline, S. M. Blackwell, C. Von Alt, B. Allen, T. Austin, J. Case, N. Forrester, R. Goldsborough, M. Purcell, and R. Stokey, "Remote environmental monitoring units: An autonomous vehicle for characterizing coastal environments," *Journal of Atmospheric and Oceanic Technology*, vol. 22, no. 11, pp. 1797–1808, 2005. https://doi.org/10.1175/JTECH1809.1.

[125] J. A. Farrell, S. Pang, and W. Li, "Chemical plume tracing via an autonomous underwater vehicle," *IEEE Journal of Oceanic Engineering*, vol. 30, no. 2, pp. 428–442, 2005. https://doi.org/10.1109/JOE.2004.838066.

[126] J. Villa, J. Paez, C. Quintero, E. Yime, and J. Cabrera, "Design and control of an unmanned surface vehicle for environmental monitoring applications," in *2016 IEEE Colombian Conference on Robotics and Automation (CCRA)*. IEEE, 2016, pp. 1–5. https://doi.org/10.1109/CCRA.2016.7811411.

[127] A. Vasilijević, Đ. Nađ, F. Mandić, N. Mišković, and Z. Vukić, "Coordinated navigation of surface and underwater marine robotic vehicles for ocean sampling and environmental monitoring," *IEEE/ASME Transactions on Mechatronics*, vol. 22, no. 3, pp. 1174–1184, 2017. https://doi.org/10.1109/TMECH.2017.2684423.

[128] C. Roman and R. Mather, "Autonomous underwater vehicles as tools for deep-submergence archaeology," *Proceedings of the institution of mechanical engineers, Part M: Journal of Engineering for the Maritime Environment*, vol. 224, no. 4, pp. 327–340, 2010. https://doi.org/10.1243/14750902JEME202.

[129] B. Bingham, B. Foley, H. Singh, R. Camilli, K. Delaporta, R. Eustice, A. Mallios, D. Mindell, C. Roman, and D. Sakellariou, "Robotic tools for deep water archaeology: Surveying an ancient shipwreck with an autonomous underwater vehicle," *Journal of Field Robotics*, vol. 27, no. 6, pp. 702–717, 2010. https://doi.org/10.1002/rob.20350.

[130] B. Allotta, R. Costanzi, A. Ridolfi, O. Salvetti, M. Reggiannini, M. Kruusmaa, T. Salumae, D. M. Lane, G. Frost, N. Tsiogkas *et al.*, "The ARROWS project: robotic technologies for underwater archaeology," in *IOP Conference Series: Materials Science and Engineering*, vol. 364, no. 1. IOP Publishing, 2018, p. 012088. https://doi.org/10.1088/1757-899X/364/1/012088.

[131] G. Vallicrosa, M. J. Fumas, F. Huber, and P. Ridao, "Sparus II AUV as a sensor suite for underwater archaeology: Falconera cave experiments," in *2020 IEEE/OES Autonomous Underwater Vehicles Symposium (AUV)*. IEEE, 2020, pp. 1–5. https://doi.org/10.1109/AUV50043.2020.9267935.

[132] J. Jalbert, J. Baker, J. Duchesney, P. Pietryka, W. Dalton, D. Blidberg, S. Chappell, R. Nitzel, and K. Holappa, "A solar-powered autonomous underwater vehicle," in *Oceans 2003. Celebrating the Past... Teaming Toward the Future (IEEE Cat. No. 03CH37492)*, vol. 2. IEEE, 2003, pp. 1132–1140. https://doi.org/10.1109/OCEANS.2003.178503.

[133] S. Shome, S. Nandy, D. Pal, S. Das, S. Vadali, J. Basu, and S. Ghosh, "Development of modular shallow water AUV: Issues & trial results," *Journal of The Institution of Engineers (India): Series C*, vol. 93, no. 3, pp. 217–228, 2012. https://doi.org/10.1007/s40032-012-0026-0.

[134] S. Bauk, N. Kapidani, J.-P. Boisgard, and Ž. Lukšić, "Key features of the autonomous underwater vehicles for marine surveillance missions," in *The 1st Inter-*

national Conference on Maritime Education and Development. Springer, 2021. https://doi.org/10.1007/978-3-030-64088-0_7, pp. 69–82.

[135] R. Stokey, T. Austin, B. Allen, N. Forrester, E. Gifford, R. Goldsborough, G. Packard, M. Purcell, and C. von Alt, "Very shallow water mine countermeasures using the REMUS AUV: a practical approach yielding accurate results," in *MTS/IEEE Oceans 2001 (IEEE Cat. No. 01CH37295)*, vol. 1. IEEE, 2001, pp. 149–156. https://doi.org/10.1109/OCEANS.2001.968696.

[136] L. Freitag, M. Grund, C. Von Alt, R. Stokey, and T. Austin, "A shallow water acoustic network for mine countermeasures operations with autonomous underwater vehicles," *Underwater Defense Technology (UDT)*, pp. 1–6, 2005. https://www.cse.psu.edu/~buu1/teaching/fall06/uuv/papers/Networks/Acoustic_Network_for_MCM.pdf.

[137] G. Slocombe, "Autonomous underwater vehicles: Roles in future maritime warfare?" *Asia-Pacific Defence Reporter (2002)*, vol. 47, no. 3, pp. 18–19, 2021. https://search.informit.org/doi/abs/10.3316/informit.899096780282715.

[138] B. Anderson and J. Crowell, *Workhorse AUV-a cost-sensible new autonomous underwater vehicle for surveys/soundings, search & rescue, and research*. IEEE, 2005. https://doi.org/10.1109/OCEANS.2005.1639923.

[139] A. Murphy, M. Landamore, and R. Birmingham, "The role of autonomous underwater vehicles for marine search and rescue operations," *Underwater Technology*, vol. 27, no. 4, pp. 195–205, 2008. https://doi.org/10.3723/ut.27.195.

[140] M. Purcell, D. Gallo, G. Packard, M. Dennett, M. Rothenbeck, A. Sherrell, and S. Pascaud, "Use of REMUS 6000 AUVs in the search for the air france flight 447," in *OCEANS'11*. IEEE, 2011, pp. 1–7. https://doi.org/10.23919/OCEANS.2011.6107253.

[141] L. D. Stone, C. Keller, T. Kratzke, and J. Strumpfer, "Search analysis for the location of the AF447 underwater wreckage," Metron Scientific Solution,

Tech. Rep., 2011. https://citeseerx.ist.psu.edu/document?repid=rep1&type=pdf&doi=46e50e6e6a3875f17a0ea4daa78486271755f503.

[142] S. Venkatesan, "AUV for search & rescue at sea-an innovative approach," in *2016 IEEE/OES Autonomous Underwater Vehicles (AUV)*. IEEE, 2016, pp. 1–9. https://doi.org/10.1109/AUV.2016.7778711.

[143] J. Wu, C. Song, J. Ma, J. Wu, and G. Han, "Reinforcement learning and particle swarm optimization supporting real-time rescue assignments for multiple autonomous underwater vehicles," *IEEE Transactions on Intelligent Transportation Systems*, 2021. https://doi.org/10.1109/TITS.2021.3062500.

[144] M. Kaess, H. Johannsson, B. J. Englot, F. S. Hover, and J. J. Leonard, "Towards autonomous ship hull inspection using the Bluefin HAUV," in *Proceedings of the 9th International Symposium on Technology and the Mine Problem series: Unmanned Systems, Technologies, Concepts, and Applications*, 2010, pp. 1–10. http://hdl.handle.net/1721.1/64472.

[145] T. Ura, Y. Kurimoto, H. Kondo, Y. Nose, T. Sakamaki, and Y. Kuroda, "Observation behavior of an AUV for ship wreck investigation," in *Proceedings of OCEANS 2005*. IEEE, 2005, pp. 2686–2691. https://doi.org/10.1109/OCEANS.2005.1640179.

[146] J. Albiez, D. Cesar, C. Gaudig, S. Arnold, R. Cerqueira, T. Trocoli, G. Mimoso, R. Saback, and G. Neves, "Repeated close-distance visual inspections with an AUV," in *OCEANS'16*. IEEE, 2016, pp. 1–8. https://doi.org/10.1109/OCEANS.2016.7761099.

[147] R. Eldred, J. Lussier, and A. Pollman, "Design and testing of a spherical autonomous underwater vehicle for shipwreck interior exploration," *Journal of Marine Science and Engineering*, vol. 9, no. 3, p. 320, 2021. https://doi.org/10.3390/jmse9030320.

[148] J.-L. Michel and H. Le Roux, "Epaulard:-deep bottom surveys now with acoustic remote controlled vehicle-first operational experience," in *OCEANS 81*. IEEE, 1981, pp. 99–103. https://doi.org/10.1109/OCEANS.1981.1151610.

[149] J. Ferguson, "Under-ice seabed mapping with AUVs," in *OCEANS 2009-EUROPE*. IEEE, 2009, pp. 1–6. https://doi.org/10.1109/OCEANSE.2009.5278204.

[150] C. Kaminski, T. Crees, J. Ferguson, A. Forrest, J. Williams, D. Hopkin, and G. Heard, "12 days under ice–an historic AUV deployment in the canadian high arctic," in *2010 IEEE/OES Autonomous Underwater Vehicles*. IEEE, 2010, pp. 1–11. https://doi.org/10.1109/AUV.2010.5779651.

[151] K. Kim, T. Ura, K. Nagahashi, T. Asanuma, T. Matsuzawa, K. Nakane, T. Obata, H. Koyama, Y. Ooyabu, and R. Nagata, "Towards AUV-based iceberg profiling and gouging survey in arctic sea: the first japanese under-ice AUV deployment in okhotsk sea," in *2013 IEEE International Underwater Technology Symposium (UT)*. IEEE, 2013, pp. 1–5. https://doi.org/10.1109/UT.2013.6519870.

[152] B. McCarter, S. Portner, W. L. Neu, D. J. Stilwell, D. Malley, and J. Mims, "Design elements of a small AUV for bathymetric surveys," in *2014 IEEE/OES Autonomous Underwater Vehicles (AUV)*. IEEE, 2014, pp. 1–5. https://doi.org/10.1109/AUV.2014.7054428.

[153] S. B. Williams, O. R. Pizarro, M. V. Jakuba, C. R. Johnson, N. S. Barrett, R. C. Babcock, G. A. Kendrick, P. D. Steinberg, A. J. Heyward, P. J. Doherty *et al.*, "Monitoring of benthic reference sites: using an autonomous underwater vehicle," *IEEE Robotics & Automation Magazine*, vol. 19, no. 1, pp. 73–84, 2012. https://doi.org/10.1109/MRA.2011.2181772.

[154] P. Bénet, F. Novella, M. Ponchart, P. Bosser, and B. Clement, "State-of-the-art of standalone accurate AUV positioning-application to high resolution bathymetric surveys," in *OCEANS 2019-Marseille*. IEEE, 2019, pp. 1–10. https://doi.org/10.1109/OCEANSE.2019.8867041.

[155] A. E. Johnson and M. Hebert, "Seafloor map generation for autonomous underwater vehicle navigation," *Autonomous Robots*, vol. 3, no. 2, pp. 145–168, 1996. https://doi.org/10.1007/BF00141152.

[156] M. Grasmueck, G. P. Eberli, D. A. Viggiano, T. Correa, G. Rathwell, and J. Luo, "Autonomous underwater vehicle (AUV) mapping reveals coral mound distribution, morphology, and oceanography in deep water of the straits of florida," *Geophysical Research Letters*, vol. 33, no. 23, 2006. https://doi.org/10.1029/2006GL027734.

[157] C. Morice, S. Veres, and S. McPhail, "Terrain referencing for autonomous navigation of underwater vehicles," in *Oceans 2009-Europe*. IEEE, 2009, pp. 1–7. https://doi.org/10.1109/OCEANSE.2009.5278257.

[158] P. W. Kimball and S. M. Rock, "Mapping of translating, rotating icebergs with an autonomous underwater vehicle," *IEEE Journal of Oceanic Engineering*, vol. 40, no. 1, pp. 196–208, 2014. https://doi.org/10.1109/JOE.2014.2300396.

[159] D. L. Bongiorno, M. Bryson, T. C. Bridge, D. G. Dansereau, and S. B. Williams, "Coregistered hyperspectral and stereo image seafloor mapping from an autonomous underwater vehicle," *Journal of Field Robotics*, vol. 35, no. 3, pp. 312–329, 2018. https://doi.org/10.1002/rob.21713.

[160] D. Thompson, D. Caress, H. Thomas, and D. Conlin, "MBARI mapping AUV operations in the gulf of california 2015," in *OCEANS 2015-MTS/IEEE Washington*. IEEE, 2015, pp. 1–7. https://doi.org/10.23919/OCEANS.2015.7401816.

[161] E. Riddell-Dixon, "Meeting the deadline: Canada's arctic submission to the commission on the limits of the continental shelf," *Ocean Development & International Law*, vol. 42, no. 4, pp. 368–382, 2011. https://doi.org/10.1080/00908320.2011.619376.

[162] E. Simetti, G. Casalino, S. Torelli, A. Sperinde, and A. Turetta, "Floating underwater manipulation: Developed control methodology and experimental validation within the trident project," *Journal of Field Robotics*, vol. 31, no. 3, pp. 364–385, 2014. https://doi.org/10.1002/rob.21497.

[163] Y. Wu, "Coordinated path planning for an unmanned aerial-aquatic vehicle (UAAV) and an autonomous underwater vehicle (AUV) in an underwater target strike mission," *Ocean Engineering*, vol. 182, pp. 162–173, 2019. https://doi.org/10.1016/j.oceaneng.2019.04.062.

[164] R. Been, D. T. Hughes, J. R. Potter, and C. Strode, "Cooperative anti-submarine warfare at nurc moving towards a net-centric capability," in *OCEANS'10*. IEEE, 2010, pp. 1–10. https://doi.org/10.1109/OCEANSSYD.2010.5603637.

[165] K. T. Hjelmervik and H. Berg, "Automatic target classification for low-frequency anti-submarine warfare sonars," in *OCEANS'13*. IEEE, 2013, pp. 1–3. [Online]. Available: https://doi.org/10.1109/OCEANS-Bergen.2013.6608190

[166] K. D. LePage, R. Goldhahn, J. Alves, C. Strode, P. Braca, G. Ferri, A. Munafò, M. Oddone, J. Sildam, F. Baralli *et al.*, "Autonomous networked anti-submarine warfare research and development at CMRE," in *OCEANS'15*. IEEE, 2015, pp. 1–6. https://doi.org/10.1109/OCEANS-Genova.2015.7271777.

[167] G. Ferri, P. Stinco, G. De Magistris, A. Tesei, and K. D. LePage, "Cooperative autonomy and data fusion for underwater surveillance with networked AUVs," in *2020 IEEE ICRA*. IEEE, 2020, pp. 871–877. https://doi.org/10.1109/ICRA40945.2020.9197367.

[168] US Navy, "Navy unmanned undersea vehicle (uuv) master plan," Department of the Navy, USA, Tech. Rep., 2004. [Online]. Available: https://higherlogicdownload.s3.amazonaws.com/AUVSI/958c920a-7f9b-4ad2-9807-f9a4e95d1ef1/UploadedImages/UUVMPPubRelease.pdf

[169] A. A. Al Makdah, E. Shammas, N. Daher, and I. ElHajj, "Modeling and optimal three-dimensional trajectory tracking for an autonomous underwater vehicle," in *2016 IEEE International Conference on Advanced Intelligent Mechatronics (AIM)*. IEEE, 2016, pp. 172–177. https://doi.org/10.1109/AIM.2016.7576762.

[170] Y. Liu, J. Liu, Q.-G. Wang, and J. Yu, "Adaptive command filtered backstepping tracking control for auvs considering model uncertainties and input saturation," *IEEE Transactions on Circuits and Systems II: Express Briefs*, vol. 70, no. 4, pp. 1475–1479, 2022. https://doi.org/10.1109/TCSII.2022.3221082.

[171] J. Cervantes, W. Yu, S. Salazar, I. Chairez, and R. Lozano, "Output based backstepping control for trajectory tracking of an autonomous underwater vehicle,"

in *American Control Conference (ACC)*. IEEE, 2016, pp. 6423–6428. https://doi.org/10.1109/ACC.2016.7526680.

[172] Y. Li, C. Wei, Q. Wu, P. Chen, Y. Jiang, and Y. Li, "Study of 3 dimension trajectory tracking of underactuated autonomous underwater vehicle," *Ocean Engineering*, vol. 105, pp. 270–274, 2015. https://doi.org/10.1016/j.oceaneng.2015.06.034.

[173] X. Liang, X. Qu, N. Wang, R. Zhang, and Y. Li, "Three-dimensional trajectory tracking of an underactuated AUV based on fuzzy dynamic surface control," *IET Intelligent Transport Systems*, vol. 14, no. 5, pp. 364–370, 2020. https://doi.org/10.1049/iet-its.2019.0347.

[174] B. Huang, B. Zhou, S. Zhang, and C. Zhu, "Adaptive prescribed performance tracking control for underactuated autonomous underwater vehicles with input quantization," *Ocean Engineering*, vol. 221, p. 108549, 2021. https://doi.org/10.1016/j.oceaneng.2020.108549.

[175] I. Astrov and A. Pedai, "Multirate depth control of an AUV by neural network predictive controller for enhanced situational awareness," in *2011 5th International Symposium on Computational Intelligence and Intelligent Informatics (ISCIII)*. IEEE, 2011, pp. 47–52. https://doi.org/10.1109/ISCIII.2011.6069740.

[176] Y. Pan and H. Yu, "Dynamic surface control via singular perturbation analysis," *Automatica*, vol. 57, pp. 29–33, 2015. https://doi.org/10.1016/j.automatica.2015.03.033.

[177] K. D. von Ellenrieder and H. C. Henninger, "Improving the robustness of trajectory tracking dynamic surface control," in *American Control Conference (ACC)*. IEEE, 2019, pp. 4386–4392. https://doi.org/10.23919/ACC.2019.8814886.

[178] T. Xie, Y. Li, Y. Jiang, L. An, and H. Wu, "Backstepping active disturbance rejection control for trajectory tracking of underactuated autonomous underwater vehicles with position error constraint," *International Journal of Advanced Robotic Systems*, vol. 17, no. 2, p. 1729881420909633, 2020. https://doi.org/10.1177/1729881420909633.

[179] Y. Shtessel, C. Edwards, L. Fridman, A. Levant *et al.*, *Sliding mode control and observation*. Springer, 2014. https://doi.org/10.1007/978-0-8176-4893-0.

[180] S. Venkataraman and S. Gulati, "Control of nonlinear systems using terminal sliding modes," *Journal of Dynamic Systems, Measurement and Control*, vol. 115, no. 3, pp. 554–560, 1993. https://doi.org/10.1115/1.2899138.

[181] V. Utkin and H. Lee, "Chattering problem in sliding mode control systems," in *International Workshop on Variable Structure Systems, 2006. VSS'06.* IEEE, 2006, pp. 346–350. https://doi.org/10.1109/VSS.2006.1644542.

[182] Y. Wang, L. Gu, M. Gao, and K. Zhu, "Multivariable output feedback adaptive terminal sliding mode control for underwater vehicles," *Asian Journal of Control*, vol. 18, no. 1, pp. 247–265, 2016. https://doi.org/10.1002/asjc.1013.

[183] L. Qiao and W. Zhang, "Adaptive non-singular integral terminal sliding mode tracking control for autonomous underwater vehicles," *IET Control Theory & Applications*, vol. 11, no. 8, pp. 1293–1306, 2017. https://doi.org/10.1049/iet-cta.2017.0016.

[184] Z. Yan, H. Yu, W. Zhang, B. Li, and J. Zhou, "Globally finite-time stable tracking control of underactuated UUVs," *Ocean Engineering*, vol. 107, pp. 132–146, 2015. https://doi.org/10.1016/j.oceaneng.2015.07.039.

[185] J. Guerrero, J. Torres, V. Creuze, and A. Chemori, "Trajectory tracking for autonomous underwater vehicle: An adaptive approach," *Ocean Engineering*, vol. 172, pp. 511–522, 2019. https://doi.org/10.1016/j.oceaneng.2018.12.027.

[186] J. Guo, F.-C. Chiu, and C.-C. Huang, "Design of a sliding mode fuzzy controller for the guidance and control of an autonomous underwater vehicle," *Ocean Engineering*, vol. 30, no. 16, pp. 2137–2155, 2003. https://doi.org/10.1016/S0029-8018(03)00048-9.

[187] P. S. Londhe and B. Patre, "Adaptive fuzzy sliding mode control for robust trajectory tracking control of an autonomous underwater vehicle," *Intelligent Service Robotics*, vol. 12, no. 1, pp. 87–102, 2019. https://doi.org/10.1007/s11370-018-0263-z.

[188] G. Lakhekar and L. Waghmare, "Adaptive fuzzy exponential terminal sliding mode controller design for nonlinear trajectory tracking control of autonomous underwater vehicle," *International Journal of Dynamics and Control*, vol. 6, no. 4, pp. 1690–1705, 2018. https://doi.org/10.1007/s40435-017-0387-6.

[189] Z. Ding, H. Wang, Y. Sun, and H. Qin, "Adaptive prescribed performance second-order sliding mode tracking control of autonomous underwater vehicle using neural network-based disturbance observer," *Ocean Engineering*, vol. 260, p. 111939, 2022. https://doi.org/10.1016/j.oceaneng.2022.111939.

[190] Z. Zhu, Z. Duan, H. Qin, and Y. Xue, "Adaptive neural network fixed-time sliding mode control for trajectory tracking of underwater vehicle," *Ocean Engineering*, vol. 287, p. 115864, 2023. https://doi.org/10.1016/j.oceaneng.2023.115864.

[191] Y. Jiang, C. Guo, and H. Yu, "Robust trajectory tracking control for an underactuated autonomous underwater vehicle based on bioinspired neurodynamics," *International Journal of Advanced Robotic Systems*, vol. 15, no. 5, p. 1729881418806745, 2018. https://doi.org/10.1177/1729881418806745.

[192] D. Wang, Y. Shen, J. Wan, Q. Sha, G. Li, G. Chen, and B. He, "Sliding mode heading control for AUV based on continuous hybrid model-free and model-based reinforcement learning," *Applied Ocean Research*, vol. 118, p. 102960, 2022. https://doi.org/10.1016/j.apor.2021.102960.

[193] B.-O. H. Eriksen, M. Breivik, E. F. Wilthil, A. L. Flåten, and E. F. Brekke, "The branching-course model predictive control algorithm for maritime collision avoidance," *Journal of Field Robotics*, vol. 36, no. 7, pp. 1222–1249, 2019. https://doi.org/10.1002/rob.21900.

[194] D. K. M. Kufoalor, T. A. Johansen, E. F. Brekke, A. Hepsø, and K. Trnka, "Autonomous maritime collision avoidance: Field verification of autonomous surface vehicle behavior in challenging scenarios," *Journal of Field Robotics*, vol. 37, no. 3, pp. 387–403, 2020. https://doi.org/10.1002/rob.21919.

[195] S. Campbell, W. Naeem, and G. Irwin, "A review on improving the autonomy of unmanned surface vehicles through intelligent collision avoidance manoeuvres," *Annual Reviews in Control*, vol. 36, no. 2, pp. 267–283, 2012. https://doi.org/10.1016/j.arcontrol.2012.09.008.

[196] X. Zhang, C. Wang, L. Jiang, L. An, and R. Yang, "Collision-avoidance navigation systems for maritime autonomous surface ships: A state of the art survey," *Ocean Engineering*, vol. 235, p. 109380, 2021. https://doi.org/10.1016/j.oceaneng.2021.109380.

[197] C. Zhou, S. Gu, Y. Wen, Z. Du, C. Xiao, L. Huang, and M. Zhu, "The review unmanned surface vehicle path planning: Based on multi-modality constraint," *Ocean Engineering*, vol. 200, p. 107043, 2020. https://doi.org/10.1016/j.oceaneng.2020.107043.

[198] A. J. Sørensen, "A survey of dynamic positioning control systems," *Annual reviews in control*, vol. 35, no. 1, pp. 123–136, 2011. https://doi.org/10.1016/j.arcontrol.2011.03.008.

[199] Z. Liu, Y. Zhang, X. Yu, and C. Yuan, "Unmanned surface vehicles: An overview of developments and challenges," *Annual Reviews in Control*, vol. 41, pp. 71–93, 2016. https://doi.org/10.1016/j.arcontrol.2016.04.018.

[200] S. Yu, M. Reble, H. Chen, and F. Allgöwer, "Inherent robustness properties of quasi-infinite horizon nonlinear model predictive control," *Automatica*, vol. 50, no. 9, pp. 2269–2280, 2014. https://doi.org/10.1016/j.automatica.2014.07.014.

[201] J. Gao, C. Liu, and A. Proctor, "Nonlinear model predictive dynamic positioning control of an underwater vehicle with an onboard USBL system," *Journal of Marine Science and Technology*, vol. 21, pp. 57–69, 2016. https://doi.org/10.1007/s00773-015-0332-3.

[202] G. Zhou, X. Xiang, and C. Liu, "Parameter identification and model prediction path following control of underactuated AUV: Methodology and experimen-

tal verification," *Control Engineering Practice*, vol. 141, p. 105729, 2023. https://doi.org/10.1016/j.conengprac.2023.105729.

[203] T. Elmokadem, M. Zribi, and K. Youcef-Toumi, "Control for dynamic positioning and way-point tracking of underactuated autonomous underwater vehicles using sliding mode control," *Journal of Intelligent & Robotic Systems*, vol. 95, pp. 1113–1132, 2019. https://doi.org/10.1007/s10846-018-0830-8.

[204] R. Brocket, "Asymptoticstability and feedback stabilization," *Differential Geometric Control Theory, RW Brockett, RS Milman, and HJ Sussman, eds. Birkhiuser, Basel, Boston*, 1983. https://courses.ece.ucsb.edu/ECE594/594D_W10Byl/hw/Brockett83.pdf.

[205] A. Veksler, T. A. Johansen, F. Borrelli, and B. Realfsen, "Dynamic positioning with model predictive control," *IEEE Transactions on Control Systems Technology*, vol. 24, no. 4, pp. 1340–1353, 2016. https://doi.org/10.1109/TCST.2015.2497280.

[206] C. Shen, Y. Shi, and B. Buckham, "Lyapunov-based model predictive control for dynamic positioning of autonomous underwater vehicles," in *2017 IEEE International Conference on Unmanned Systems (ICUS)*. IEEE, 2017, pp. 588–593. https://doi.org/10.1109/ICUS.2017.8278413.

[207] H. Øveraas, H. S. Halvorsen, O. Landstad, V. Smines, and T. A. Johansen, "Dynamic positioning using model predictive control with short-term wave prediction," *IEEE Journal of Oceanic Engineering*, vol. 48, no. 4, pp. 1065–1077, 2023. https://doi.org/10.1109/JOE.2023.3288969.

[208] H. Li and W. Yan, "Model predictive stabilization of constrained underactuated autonomous underwater vehicles with guaranteed feasibility and stability," *IEEE/ASME Transactions on Mechatronics*, vol. 22, no. 3, pp. 1185–1194, 2016. https://doi.org/10.1109/TMECH.2016.2587288.

[209] A. A. do Nascimento, H. R. Feyzmahdavian, M. Johansson, W. Garcia-Gabin, and K. Tervo, "Tube-based model predictive control for dynamic positioning of marine

vessels," *IFAC-PapersOnLine*, vol. 52, no. 21, pp. 33–38, 2019. https://doi.org/10.1016/j.ifacol.2019.12.279.

[210] H. Zheng, J. Wu, W. Wu, and Y. Zhang, "Robust dynamic positioning of autonomous surface vessels with tube-based model predictive control," *Ocean Engineering*, vol. 199, p. 106820, 2020. https://doi.org/10.1016/j.oceaneng.2019.106820.

[211] K. Shi, X. Wang, and H. Xu, "On the offset-free nonlinear model predictive control for AUV docking," in *WRC Symposium on Advanced Robotics and Automation*. IEEE, 2021, pp. 117–122. https://doi.org/10.1109/WRCSARA53879.2021.9612699.

[212] C. Long, X. Qin, Y. Bian, and M. Hu, "Trajectory tracking control of ROVs considering external disturbances and measurement noises using ESKF-based MPC," *Ocean Engineering*, vol. 241, p. 109991, 2021. https://doi.org/10.1016/j.oceaneng.2021.109991.

[213] A. P. Aguiar and J. P. Hespanha, "Trajectory-tracking and path-following of underactuated autonomous vehicles with parametric modeling uncertainty," *IEEE Transactions on Automatic Control*, vol. 52, no. 8, pp. 1362–1379, 2007. https://doi.org/10.1109/TAC.2007.902731.

[214] Z. Peng, J. Wang, and Q.-L. Han, "Path-following control of autonomous underwater vehicles subject to velocity and input constraints via neurodynamic optimization," *IEEE Transactions on Industrial Electronics*, vol. 66, no. 11, pp. 8724–8732, 2018. https://doi.org/10.1109/TIE.2018.2885726.

[215] H. C. Lamraoui and Z. Qidan, "Path following control of fully-actuated autonomous underwater vehicle in presence of fast-varying disturbances," *Applied Ocean Research*, vol. 86, pp. 40–46, 2019. https://doi.org/10.1016/j.apor.2019.02.015.

[216] B. N. Rath and B. Subudhi, "A robust model predictive path following controller for an autonomous underwater vehicle," *Ocean Engineering*, vol. 244, p. 110265, 2022. https://doi.org/10.1016/j.oceaneng.2021.110265.

[217] R. Skjetne, T. I. Fossen, and P. V. Kokotović, "Adaptive maneuvering, with experiments, for a model ship in a marine control laboratory," *Automatica*, vol. 41, no. 2, pp. 289–298, 2005. https://doi.org/10.1016/j.automatica.2004.10.006.

[218] A. M. Lekkas and T. I. Fossen, "Line-of-sight guidance for path following of marine vehicles," *Advanced in marine robotics*, vol. 5, pp. 63–92, 2013. https://api.semanticscholar.org/CorpusID:45758623.

[219] T. Faulwasser and R. Findeisen, "Constrained output path-following for nonlinear systems using predictive control," *IFAC-Papers Online*, vol. 43, no. 14, pp. 753–758, 2010. https://doi.org/10.3182/20100901-3-IT-2016.00122.

[220] S.-R. Oh and J. Sun, "Path following of underactuated marine surface vessels using line-of-sight based model predictive control," *Ocean Engineering*, vol. 37, no. 2-3, pp. 289–295, 2010. https://doi.org/10.1016/j.oceaneng.2009.10.004.

[221] J. Zhang, T. Sun, and Z. Liu, "Robust model predictive control for path-following of underactuated surface vessels with roll constraints," *Ocean Engineering*, vol. 143, pp. 125–132, 2017. https://doi.org/10.1016/j.oceaneng.2017.07.057.

[222] A. Gonzalez-Garcia, I. Collado-Gonzalez, R. Cuan-Urquizo, C. Sotelo, D. Sotelo, and H. Castañeda, "Path-following and LiDAR-based obstacle avoidance via NMPC for an autonomous surface vehicle," *Ocean Engineering*, vol. 266, p. 112900, 2022. https://doi.org/10.1016/j.oceaneng.2022.112900.

[223] C. Shen, Y. Shi, and B. Buckham, "Path-following control of an AUV: A multiobjective model predictive control approach," *IEEE Transactions on Control Systems Technology*, vol. 27, no. 3, pp. 1334–1342, 2018. https://doi.org/10.1109/TCST.2018.2789440.

[224] Y. Zhang, X. Wang, S. Wang, and J. Miao, "DO-LPV-based robust 3D path following control of underactuated autonomous underwater vehicle with multiple uncertainties," *ISA Transactions*, vol. 101, pp. 189–203, 2020. https://doi.org/10.1016/j.isatra.2020.01.017.

[225] C. Liu, D. Wang, Y. Zhang, and X. Meng, "Model predictive control for path following and roll stabilization of marine vessels based on neurodynamic optimization," *Ocean Engineering*, vol. 217, p. 107524, 2020. https://doi.org/10.1016/j.oceaneng.2020.107524.

[226] J. Pan, H. Li, Z. Zhou, and J. Yu, "3D path-following control of robotic penguin: an ETFLMPC approach," *Nonlinear Dynamics*, vol. 104, pp. 1415–1427, 2021. https://doi.org/10.1007/s11071-021-06365-8.

[227] X. Yao, X. Wang, F. Wang, and L. Zhang, "Path following based on waypoints and real-time obstacle avoidance control of an autonomous underwater vehicle," *Sensors*, vol. 20, no. 3, p. 795, 2020. https://doi.org/10.3390/s20030795.

[228] J. Zhou, Z. Tang, H. Zhang, J. Jiao *et al.*, "Spatial path following for AUVs using adaptive neural network controllers," *Mathematical Problems in Engineering*, vol. 2013, 2013. https://doi.org/10.1155/2013/749689.

[229] C. Yu, X. Xiang, L. Lapierre, and Q. Zhang, "Nonlinear guidance and fuzzy control for three-dimensional path following of an underactuated autonomous underwater vehicle," *Ocean Engineering*, vol. 146, pp. 457–467, 2017. https://doi.org/10.1016/j.oceaneng.2017.10.001.

[230] X. Liang, X. Qu, Y. Hou, and J. Zhang, "Three-dimensional path following control of underactuated autonomous underwater vehicle based on damping backstepping," *International Journal of Advanced Robotic Systems*, vol. 14, no. 4, p. 1729881417724179, 2017. https://doi.org/10.1177/1729881417724179.

[231] J. Wang, C. Wang, Y. Wei, and C. Zhang, "On the fuzzy-adaptive command filtered backstepping control of an underactuated autonomous underwater vehicle in the three-dimensional space," *Journal of Mechanical Science and Technology*, vol. 33, pp. 2903–2914, 2019. https://doi.org/10.1007/s12206-019-0538-0.

[232] Z. Peng, J. Wang, D. Wang, and Q.-L. Han, "An overview of recent advances in coordinated control of multiple autonomous surface vehicles," *IEEE Transactions*

on Industrial Informatics, vol. 17, no. 2, pp. 732–745, 2020. https://doi.org/10.1109/TII.2020.3004343.

[233] A. H. González, E. J. Adam, and J. L. Marchetti, "Conditions for offset elimination in state space receding horizon controllers: A tutorial analysis," *Chemical Engineering and Processing: Process Intensification*, vol. 47, no. 12, pp. 2184–2194, 2008. https://doi.org/10.1016/j.cep.2007.11.011.

[234] I. A. Jimoh, I. B. Küçükdemiral, G. Bevan, and P. E. Orukpe, "Offset-free model predictive control: a study of different formulations with further results," in *28th Mediterranean Conference on Control and Automation (MED2020)*. IEEE, 2020, pp. 671–676. https://doi.org/10.1109/MED48518.2020.9183056.

[235] P. S. Cisneros and H. Werner, "A velocity algorithm for nonlinear model predictive control," *IEEE Transactions on Control Systems Technology*, vol. 29, no. 3, pp. 1310–1315, 2020. https://doi.org/10.1109/TCST.2020.2979386.

[236] K. R. Muske and J. B. Rawlings, "Linear model predictive control of unstable processes," *Journal of Process Control*, vol. 3, no. 2, pp. 85–96, 1993. https://doi.org/10.1016/0959-1524(93)80004-U.

[237] S. Kong, J. Sun, C. Qiu, Z. Wu, and J. Yu, "Extended state observer-based controller with model predictive governor for 3-D trajectory tracking of underactuated underwater vehicles," *IEEE Transactions on Industrial Informatics*, vol. 17, no. 9, pp. 6114–6124, 2020. https://doi.org/10.1109/TII.2020.3036665.

[238] B. Wang, M. Mihalec, Y. Gong, D. Pompili, and J. Yi, "Disturbance observer-based motion control of small autonomous underwater vehicles," in *Dynamic Systems and Control Conference*, vol. 51913. American Society of Mechanical Engineers, 2018, p. V003T35A004. https://doi.org/10.1115/DSCC2018-9200.

[239] Y. Hu, B. Li, B. Jiang, J. Han, and C.-Y. Wen, "Disturbance observer-based model predictive control for an unmanned underwater vehicle," *Journal of Marine Science and Engineering*, vol. 12, no. 1, p. 94, 2024. https://doi.org/10.3390/jmse12010094.

[240] É. L. de Oliveira, D. C. Donha, A. de T Fleury, and E. A. de Barros, "Station-keeping of a ROV under wave disturbance: Modeling and control design," *Proceedings of the Institution of Mechanical Engineers, Part M: Journal of Engineering for the Maritime Environment*, vol. 237, no. 2, pp. 455–477, 2023. https://doi.org/10.1177/14750902221116673.

[241] P. Mhaskar, N. H. El-Farra, and P. D. Christofides, "Predictive control of switched nonlinear systems with scheduled mode transitions," *IEEE Transactions on Automatic Control*, vol. 50, no. 11, pp. 1670–1680, 2005. https://doi.org/10.1109/TAC.2005.858692.

[242] ——, "Stabilization of nonlinear systems with state and control constraints using lyapunov-based predictive control," *Systems & Control Letters*, vol. 55, no. 8, pp. 650–659, 2006. https://doi.org/10.1016/j.sysconle.2005.09.014.

[243] C. Shen, Y. Shi, and B. Buckham, "Trajectory tracking control of an autonomous underwater vehicle using Lyapunov-based model predictive control," *IEEE Transactions on Industrial Electronics*, vol. 65, no. 7, pp. 5796–5805, 2018. https://doi.org/10.1109/TIE.2017.2779442.

[244] H. Wei, C. Shen, and Y. Shi, "Distributed lyapunov-based model predictive formation tracking control for autonomous underwater vehicles subject to disturbances," *IEEE Transactions on Systems, Man, and Cybernetics: Systems*, vol. 51, no. 8, pp. 5198–5208, 2019. https://doi.org/10.1109/TSMC.2019.2946127.

[245] G. Lv, Z. Peng, H. Wang, L. Liu, D. Wang, and T. Li, "Extended-state-observer-based distributed model predictive formation control of under-actuated unmanned surface vehicles with collision avoidance," *Ocean Engineering*, vol. 238, p. 109587, 2021. https://doi.org/10.1016/j.oceaneng.2021.109587.

[246] D. C. Fernández and G. A. Hollinger, "Model predictive control for underwater robots in ocean waves," *IEEE Robotics and Automation letters*, vol. 2, no. 1, pp. 88–95, 2016. https://doi.org/10.1109/LRA.2016.2531792.

[247] K. L. Walker, R. Gabl, S. Aracri, Y. Cao, A. A. Stokes, A. Kiprakis, and F. Giorgio-Serchi, "Experimental validation of wave induced disturbances for predictive station keeping of a remotely operated vehicle," *IEEE Robotics and Automation Letters*, vol. 6, no. 3, pp. 5421–5428, 2021. https://doi.org/10.1109/LRA.2021.3075662.

[248] B. Miao, T. Li, and W. Luo, "A DSC and MLP based robust adaptive nn tracking control for underwater vehicle," *Neurocomputing*, vol. 111, pp. 184–189, 2013. https://doi.org/10.1016/j.neucom.2012.12.026.

[249] B. Seok Park, "Neural network-based tracking control of underactuated autonomous underwater vehicles with model uncertainties," *Journal of Dynamic Systems, Measurement, and Control*, vol. 137, no. 2, p. 021004, 2015. https://doi.org/10.1115/1.4027919.

[250] C. Yang, F. Yao, and M.-J. Zhang, "Adaptive backstepping terminal sliding mode control method based on recurrent neural networks for autonomous underwater vehicle," *Chinese Journal of Mechanical Engineering*, vol. 31, no. 1, pp. 1–16, 2018. https://doi.org/10.1186/s10033-018-0307-5.

[251] J. Zhou, X. Zhao, T. Chen, Z. Yan, and Z. Yang, "Trajectory tracking control of an underactuated AUV based on backstepping sliding mode with state prediction," *IEEE Access*, vol. 7, pp. 181 983–181 993, 2019. https://doi.org/10.1109/ACCESS.2019.2958360.

[252] S. Liu, Y. Liu, X. Liang, and N. Wang, "Uncertainty observation-based adaptive succinct fuzzy-neuro dynamic surface control for trajectory tracking of fully actuated underwater vehicle system with input saturation," *Nonlinear Dynamics*, vol. 98, no. 3, pp. 1683–1699, 2019. https://doi.org/10.1007/s11071-019-05279-w.

[253] H. Bao, H. Zhu, X. Li, and J. Liu, "APSO-MPC and NTSMC cascade control of fully-actuated autonomous underwater vehicle trajectory tracking based on RBF-NN compensator," *Journal of Marine Science and Engineering*, vol. 10, no. 12, p. 1867, 2022. https://doi.org/10.3390/jmse10121867.

[254] J. Yin and N. Wang, "Predictive trajectory tracking control of autonomous underwater vehicles based on variable fuzzy predictor," *International Journal of Fuzzy Systems*, vol. 23, no. 6, pp. 1809–1822, 2021. https://doi.org/10.1007/s40815-020-00898-7.

[255] C. Wu, Y. Dai, L. Shan, and Z. Zhu, "Date-driven tracking control via fuzzy-state observer for auv under uncertain disturbance and time-delay," *Journal of Marine Science and Engineering*, vol. 11, no. 1, p. 207, 2023. https://doi.org/10.3390/jmse11010207.

[256] H. Bao, H. Zhu, and D. Liu, "Improved SSA-RBF neural network-based dynamic 3-D trajectory tracking model predictive control of autonomous underwater vehicles with external disturbances," *Optimal Control Applications and Methods*, vol. 45, no. 1, pp. 138–162, 2024. https://doi.org/10.1002/oca.3050.

[257] D. Limón, T. Alamo, F. Salas, and E. F. Camacho, "Input to state stability of min–max MPC controllers for nonlinear systems with bounded uncertainties," *Automatica*, vol. 42, no. 5, pp. 797–803, 2006. https://doi.org/10.1016/j.automatica.2006.01.001.

[258] D. L. Marruedo, T. Alamo, and E. F. Camacho, "Input-to-state stable MPC for constrained discrete-time nonlinear systems with bounded additive uncertainties," in *Proceedings of the 41st IEEE Conference on Decision and Control, 2002.*, vol. 4. IEEE, 2002, pp. 4619–4624. https://doi.org/10.1109/CDC.2002.1185106.

[259] J. Fleming, B. Kouvaritakis, and M. Cannon, "Robust tube MPC for linear systems with multiplicative uncertainty," *IEEE Transactions on Automatic Control*, vol. 60, no. 4, pp. 1087–1092, 2014. https://doi.org/10.1109/TAC.2014.2336358.

[260] D. Q. Mayne, E. C. Kerrigan, E. Van Wyk, and P. Falugi, "Tube-based robust nonlinear model predictive control," *International Journal of Robust and Nonlinear Control*, vol. 21, no. 11, pp. 1341–1353, 2011. https://doi.org/10.1002/rnc.1758.

[261] G. Pin, D. M. Raimondo, L. Magni, and T. Parisini, "Robust model predictive control of nonlinear systems with bounded and state-dependent uncertainties," *IEEE*

Transactions on Automatic Control, vol. 54, no. 7, pp. 1681–1687, 2009. https://doi.org/10.1109/TAC.2009.2020641.

[262] Z. Yan and J. Wang, "Model predictive control for tracking of underactuated vessels based on recurrent neural networks," *IEEE Journal of Oceanic Engineering*, vol. 37, no. 4, pp. 717–726, 2012. https://doi.org/10.1109/JOE.2012.2201797.

[263] L.-Y. Hao, Z.-J. Wu, C. Shen, Y. Cao, and R.-Z. Wang, "Tube-based model predictive control for constrained unmanned marine vehicles with thruster faults," *IEEE Transactions on Industrial Informatics*, vol. 20, no. 3, pp. 4606–4615, 2023. https://doi.org/10.1109/TII.2023.3326543.

[264] L.-Y. Hao, R.-Z. Wang, C. Shen, and Y. Shi, "Trajectory tracking control of autonomous underwater vehicles using improved tube-based model predictive control approach," *IEEE Transactions on Industrial Informatics*, no. 4, pp. 5647–5657, 2023. https://doi.org/10.1109/TII.2023.3331772.

[265] N. Yang, D. Chang, M. Johnson-Roberson, and J. Sun, "Robust energy-optimal path following control for autonomous underwater vehicles in ocean currents," in *2020 American Control Conference (ACC)*. IEEE, 2020, pp. 5119–5124. https://doi.org/10.23919/ACC45564.2020.9147322.

[266] J. Arcos-Legarda and Á. Gutiérrez, "Robust model predictive control based on active disturbance rejection control for a robotic autonomous underwater vehicle," *Journal of Marine Science and Engineering*, vol. 11, no. 5, p. 929, 2023. https://doi.org/10.3390/jmse11050929.

[267] J.-H. Park, T.-H. Kim, and T. Sugie, "Output feedback model predictive control for LPV systems based on quasi-min–max algorithm," *Automatica*, vol. 47, no. 9, pp. 2052–2058, 2011. https://doi.org/10.1016/j.automatica.2011.06.015.

[268] M. Zhao, N. Li, and S. Li, "Min-max model predictive control for constrained nonlinear systems via multiple LPV embeddings," *Science in China Series F: Information Sciences*, vol. 52, no. 7, pp. 1129–1135, 2009. https://doi.org/10.1007/s11432-009-0129-2.

[269] D. M. Raimondo, T. Alamo, D. Limón, and E. F. Camacho, "Towards the practical implementation of min-max nonlinear model predictive control," in *2007 46th IEEE Conference on Decision and Control*. IEEE, 2007, pp. 1257–1262. https://doi.org/10.1109/CDC.2007.4434980.

[270] X. Xiang, L. Lapierre, C. Liu, and B. Jouvencel, "Path tracking: Combined path following and trajectory tracking for autonomous underwater vehicles," in *2011 IEEE/RSJ International Conference on Intelligent Robots and Systems*. IEEE, 2011, pp. 3558–3563. https://doi.org/10.1109/IROS.2011.6094949.

[271] C. Shen, Y. Shi, and B. Buckham, "Trajectory tracking control of an autonomous underwater vehicle using lyapunov-based model predictive control," *IEEE Transactions on Industrial Electronics*, vol. 65, no. 7, 2017. https://doi.org/10.1109/TIE.2017.2779442.

[272] L. Wang, *Model predictive control system design and implementation using MATLAB®*. Springer Science & Business Media, 2009. https://doi.org/10.1007/978-1-84882-331-0.

[273] I. A. Jimoh, *A novel approach to disturbance rejection in constrained model predictive control*. Master's Thesis, Glasgow Caledonian University, 2019. https://bit.ly/3OfMlDx.

[274] H. S. Abbas, G. Männel, C. H. né Hoffmann, and P. Rostalski, "Tube-based model predictive control for linear parameter-varying systems with bounded rate of parameter variation," *Automatica*, vol. 107, pp. 21–28, 2019. https://doi.org/10.1016/j.automatica.2019.04.046.

[275] G. Betti, M. Farina, and R. Scattolini, "A robust MPC algorithm for offset-free tracking of constant reference signals," *IEEE Transactions on Automatic Control*, vol. 58, no. 9, pp. 2394–2400, 2013. https://doi.org/10.1109/TAC.2013.2254011.

[276] S. Gros, M. Zanon, R. Quirynen, A. Bemporad, and M. Diehl, "From linear to nonlinear MPC: bridging the gap via the real-time iteration," *International Journal*

of Control, vol. 93, no. 1, pp. 62–80, 2020. https://doi.org/10.1080/00207179.2016.1222553.

[277] C. Shen, B. Buckham, and Y. Shi, "Modified C/GMRES algorithm for fast nonlinear model predictive tracking control of AUVs," *IEEE Transactions on Control Systems Technology*, vol. 25, no. 5, pp. 1896–1904, 2016. https://doi.org/10.1109/TCST.2016.2628803.

[278] U. Maeder, F. Borrelli, and M. Morari, "Linear offset-free model predictive control," *Automatica*, vol. 45, no. 10, pp. 2214–2222, 2009. https://doi.org/10.1016/j.automatica.2009.06.005.

[279] I. A. Jimoh, I. B. Küçükdemiral, and G. Bevan, "Fin control for ship roll motion stabilisation based on observer enhanced MPC with disturbance rate compensation," *Ocean Engineering*, vol. 224, p. 108706, 2021. https://doi.org/10.1016/j.oceaneng.2021.108706.

[280] I. A. Jimoh, H. Yue, and I. B. Küçükdemiral, "Autonomous underwater vehicle positioning control - a velocity form LPV-MPC approach," *IFAC-PapersOnLine*, vol. 56, no. 2, pp. 4388–4393, 2023. https://doi.org/10.1016/j.ifacol.2023.10.1820.

[281] I. A. Jimoh and H. Yue, "A velocity form model predictive control of an autonomous underwater vehicle," *Accepted in IEEE Journal of Oceanic Engineering*, 2024. https://doi.org/10.1109/JOE.2024.3519680.

[282] D. Q. Mayne, M. M. Seron, and S. Raković, "Robust model predictive control of constrained linear systems with bounded disturbances," *Automatica*, vol. 41, no. 2, pp. 219–224, 2005. https://doi.org/10.1016/j.automatica.2004.08.019.

[283] M. Zhang, X. Liu, and F. Wang, "Backstepping based adaptive region tracking fault tolerant control for autonomous underwater vehicles," *The Journal of Navigation*, vol. 70, no. 1, pp. 184–204, 2017. https://doi.org/10.1017/S0373463316000370.

[284] L. Lapierre and D. Soetanto, "Nonlinear path-following control of an AUV," *Ocean Engineering*, vol. 34, no. 11-12, pp. 1734–1744, 2007. https://doi.org/10.1016/j.oceaneng.2006.10.019.

[285] L. Qiao and W. Zhang, "Double-loop integral terminal sliding mode tracking control for UUVs with adaptive dynamic compensation of uncertainties and disturbances," *IEEE Journal of Oceanic Engineering*, vol. 44, no. 1, pp. 29–53, 2018. https://doi.org/10.1109/JOE.2017.2777638.

[286] J. E. Mitchell, J.-S. Pang, and B. Yu, "Convex quadratic relaxations of nonconvex quadratically constrained quadratic programs," *Optimization Methods and Software*, vol. 29, no. 1, pp. 120–136, 2014. https://doi.org/10.1080/10556788.2012.749876.

[287] P. Falcone, F. Borrelli, H. E. Tseng, J. Asgari, and D. Hrovat, "Linear time-varying model predictive control and its application to active steering systems: Stability analysis and experimental validation," *International Journal of Robust and Nonlinear Control*, vol. 18, no. 8, pp. 862–875, 2008. https://doi.org/10.1002/rnc.1245.

[288] M. Lazar, W. Heemels, A. Bemporad, and S. Weiland, "Discrete-time non-smooth nonlinear MPC: Stability and robustness," in *Assessment and Future Directions of Nonlinear Model Predictive Control*. Springer, 2007, pp. 93–103. https://doi.org/10.1007/978-3-540-72699-9_7.

[289] G. Grimm, M. J. Messina, S. E. Tuna, and A. R. Teel, "Examples when nonlinear model predictive control is nonrobust," *Automatica*, vol. 40, no. 10, pp. 1729–1738, 2004. https://doi.org/10.1016/j.automatica.2004.04.014.

[290] A. Bemporad and M. Morari, "Robust model predictive control: A survey," in *Robustness in Identification and Control*. Springer, 2007, pp. 207–226. https://doi.org/10.1007/BFb0109870.

[291] I. A. Jimoh, H. Yue, and M. J. Grimble, "Tube-based model predictive control of an autonomous underwater vehicle using line-of-sight re-planning," *Ocean Engineering*, vol. 314, p. 119688, 2024. https://doi.org/10.1016/j.oceaneng.2024.119688.

[292] I. A. Jimoh, T. Zaman, M. Syed, H. Yue, G. Burt, and M. S. E. Moursi, "Tube-based linear parameter-varying model predictive control for wind energy conversion systems," *IEEE Trans. Sustainable Energy*, pp. 1–13, 2024. https://doi.org/10.1109/TSTE.2024.3512997.

[293] Z. Zeng, L. Lian, K. Sammut, F. He, Y. Tang, and A. Lammas, "A survey on path planning for persistent autonomy of autonomous underwater vehicles," *Ocean Eng.*, vol. 110, pp. 303–313, 2015. https://doi.org/10.1016/j.oceaneng.2015.10.007.

[294] W. Naeem, R. Sutton, S. Ahmad, and R. Burns, "A review of guidance laws applicable to unmanned underwater vehicles," *The Journal of Navigation*, vol. 56, no. 1, pp. 15–29, 2003. https://doi.org/10.1017/S0373463302002138.

[295] M. Ataei and A. Yousefi-Koma, "Three-dimensional optimal path planning for waypoint guidance of an autonomous underwater vehicle," *Robotics and Autonomous Systems*, vol. 67, pp. 23–32, 2015. https://doi.org/10.1016/j.robot.2014.10.007.

[296] T. I. Fossen, M. Breivik, and R. Skjetne, "Line-of-sight path following of underactuated marine craft," *IFAC-PapersOnLine*, vol. 36, no. 21, pp. 211–216, 2003. https://doi.org/10.1016/S1474-6670(17)37809-6.

[297] M. Breivik and T. I. Fossen, "Path following of straight lines and circles for marine surface vessels," *IFAC-PapersOnLine*, vol. 37, no. 10, pp. 65–70, 2004. https://doi.org/10.1016/S1474-6670(17)31709-3.

[298] M. H. Khodayari and S. Balochian, "Modeling and control of autonomous underwater vehicle (AUV) in heading and depth attitude via self-adaptive fuzzy pid controller," *Journal of Marine Science and Technology*, vol. 20, no. 3, pp. 559–578, 2015. https://doi.org/10.1007/s00773-015-0312-7.

[299] K. A. Dastgerdi, B. Singh, W. Naeem, N. Athanasopoulos, and B. Lecallard, "Uncertainty aware path planning and collision avoidance for marine vehicles," *IFAC-PapersOnLine*, vol. 58, no. 20, pp. 235–240, 2024. https://doi.org/10.1016/j.ifacol.2024.10.060.

[300] D. E. Koditschek and E. Rimon, "Robot navigation functions on manifolds with boundary," *Advances in Applied Mathematics*, vol. 11, no. 4, pp. 412–442, 1990. https://doi.org/10.1016/0196-8858(90)90017-S.

[301] E. Fernandez-Camacho and C. Bordons, *Model predictive control*, 2nd ed. Springer, 2007. https://doi.org/10.1007/978-0-85729-398-5.

[302] J. Hu, X. Lv, H. Pan, and M. Zhang, "Handling the constraints in min-max MPC," *IEEE Trans. Autom. Sci. Eng.*, vol. 21, no. 1, pp. 296–304, 2022. https://doi.org/10.1109/TASE.2022.3219252.

[303] J. Löfberg, "YALMIP: A toolbox for modeling and optimization in MATLAB," in *In Proceedings of the CACSD Conference*, Taipei, Taiwan, 2004. https://doi.org/10.1109/CACSD.2004.1393890.

[304] I. A. Jimoh and H. Yue, "Path following model predictive control of a coupled autonomous underwater vehicle," *IFAC-PapersOnLine*, vol. 58, no. 20, pp. 183–188, 2024. https://doi.org/10.1016/j.ifacol.2024.10.052.